VOL. 16 NO. 4 APRIL 1968
COMPLETING VOLUME 16
PUBLISHED MONTHLY

JOURNAL OF

ELECTROANALYTICAL CHEMISTRY

AND INTERFACIAL ELECTROCHEMISTRY

International Journal devoted to all Aspects of Electroanalytical Chemistry, Double Layer Studies, Electrokinetics, Colloid Stability, and Electrode Kinetics.

EDITORIAL BOARD:

J. O'M. BOCKRIS (Philadelphia, Pa.)
G. CHARLOT (Paris)
B. E. CONWAY (Ottawa)
P. DELAHAY (New York)
A. N. FRUMKIN (Moscow)
L. GIERST (Brussels)
M. ISHIBASHI (Kyoto)
W. KEMULA (Warsaw)
H. L. KIES (Delft)
J. J. LINGANE (Cambridge, Mass.)
G. W. C. MILNER (Harwell)
R. H. OTTEWILL (Bristol)
J. E. PAGE (London)
R. PARSONS (Bristol)
C. N. REILLEY (Chapel Hill, N.C.)
G. SEMERANO (Padua)
M. VON STACKELBERG (Bonn)
I. TACHI (Kyoto)
P. ZUMAN (Prague)

ELSEVIER

GENERAL INFORMATION

See also Suggestions and Instructions to Authors which will be sent free, on request to the Publishers.

Types of contributions

(a) Original research work not previously published in other periodicals.
(b) Reviews on recent developments in various fields.
(c) Short communications.
(d) Bibliographical notes and book reviews.

Languages

Papers will be published in English, French or German.

Submission of papers

Papers should be sent to one of the following Editors:
Professor J. O'M. Bockris, John Harrison Laboratory of Chemistry, University of Pennsylvania, Philadelphia 4, Pa. 19104, U.S.A.
Dr. R. H. Ottewill, Department of Chemistry, The University, Bristol 8, England.
Dr. R. Parsons, Department of Chemistry, The University, Bristol 8, England.
Professor C. N. Reilley, Department of Chemistry, University of North Carolina, Chapel Hill, N. C. 27514, U.S.A.

Authors should preferably submit two copies in double-spaced typing on pages of uniform size. Legends for figures should be typed on a separate page. The figures should be in a form suitable for reproduction, drawn in Indian ink on drawing paper or tracing paper, with lettering etc. in thin pencil. The sheets of drawing or tracing paper should preferably be of the same dimensions as those on which the article is typed. Photographs should be submitted as clear black and white prints on glossy paper. Standard symbols should be used in line drawings, the following are available to the printers:

All references should be given at the end of the paper. They should be numbered and the numbers should appear in the text at the appropriate places.
A summary of 50 to 200 words should be included.

Reprints

Fifty reprints will be supplied free of charge. Additional reprints (minimum 100) can be ordered at quoted prices. They must be ordered on order forms which are sent together with the proofs.

Publication

The *Journal of Electroanalytical Chemistry and Interfacial Electrochemistry* appears monthly and has four issues per volume and three volumes per year.
Subscription price: $ 52.50 or Sfr. 228.00 per year; $ 17.50 or Sfr. 76.00 per volume; plus postage. Additional cost for copies by air mail available on request. For advertising rates apply to the publishers.

Subscriptions

Subscriptions should be sent to:

ELSEVIER SEQUOIA S.A., P.O. Box 851, 1001 Lausanne 1, Switzerland

ELECTROANALYTICAL CHEMISTRY AND INTERFACIAL ELECTROCHEMISTRY
Elsevier Sequoia S.A., Lausanne – Printed in The Netherlands

THEORY OF THE POTENTIAL STEP–LINEAR SCAN ELECTROLYSIS METHOD WITH A COMPARISON OF RATE CONSTANTS DETERMINED ELECTROCHEMICALLY AND BY CLASSICAL METHODS

JOSEPH T. LUNDQUIST, JR. AND RICHARD S. NICHOLSON
Chemistry Department, Michigan State University, East Lansing, Michigan (U.S.A.)
(Received August 3rd, 1967)

INTRODUCTION

An important application of modern electroanalytical techniques based on diffusion theory is measurement of rates of homogeneous chemical reactions. In spite of the number of such applications, however, there have been few cases where a direct comparison has been made between the rate constants determined electrochemically and those determined by classical kinetic measurements. One reason for this situation is that the time scales of the two approaches usually do not overlap. In general, therefore, to make comparisons an extrapolation of one of the sets of data must be made. For example, SCHWARZ AND SHAIN[1] recently used the Hammett acidity function to extrapolate electrochemically-measured rate constants about two orders of magnitude (toward longer half-lives) to compare them with classical measurements. More recently, REILLEY and co-workers[2] applied dielectric constant corrections to classically-measured rate constants to provide a comparison with an electrochemically-determined constant. Results in both of these cases indicated reasonable agreement between the two approaches. Nevertheless, the uncertainties associated with the various extrapolations leave room for argument that the agreement may have been in part fortuitous.

In the course of studying in detail the reduction of substituted azobenzene compounds, we have measured rate constants for the benzidine rearrangement, and have compared these constants with those determined spectrophotometrically. We have used also an extrapolation of the classical data based on dielectric corrections, but in addition we have repeated some of the spectrophotometric experiments to prove that the extrapolations are valid. Our results show very good agreement between classical and electrochemical measurements; the purpose of this communication is to describe these results.

The electrochemical method we chose for measurement of the homogeneous rate constants was the potential step-linear scan method first described quantitatively by SCHWARZ AND SHAIN[3]. This method was selected because it appeared to combine useful features of both step functional electrolysis[1] and cyclic voltammetry[4]. Thus, the initial step is not influenced by charging current, and also minimizes adsorption effects, whereas the linear scan step has the diagnostic advantages of cyclic voltammetry[4]. Moreover, in principle the method can be applied both to slower and faster reactions than is possible with conventional cyclic voltammetry. However, in actually

applying this method using the theoretical calculations of SCHWARZ AND SHAIN, we encountered difficulties because of the simplifying assumptions these authors were forced to make in their theoretical treatment. As a result of these approximations, application of their results is limited to cases in which duration of the linear scan is small with respect to the half-life of the chemical reaction[3]. This means that scan rates used must be as much as 2 orders of magnitude larger than is actually necessary to detect kinetic effects. Consequently, factors such as charging current and charge transfer kinetics rapidly become limiting. In addition, it always is necessary to measure small changes of large peak currents, and considerable sensitivity is lost. Thus, to use the potential step-linear scan method effectively we found it necessary to repeat the work of SCHWARZ AND SHAIN without introducing any simplifying approximations. The results of these calculations are also reported here. To provide a logical discussion, the calculations are presented first, followed by results of kinetic measurements.

THEORY

The boundary value problem for the potential step-linear scan technique and the following electrolysis mechanism

$$O + ne \rightleftarrows R \qquad (I)$$

$$R \xrightarrow{k} Z$$

is given by SCHWARZ AND SHAIN[3]. We assume that the electron-transfer reaction is Nernstian, and that the chemical reaction initiated by electron transfer is both irreversible and first-order.

Although the boundary value problem cannot be solved analytically without introducing approximations[3], accurate numerical solutions can be obtained. Numerical calculations are less complex if the boundary value problem is converted to integral equation form. The result of such transformations for the present problem leads to the following dimensionless linear integral equation

$$1 - \int_0^{at} \frac{\chi(z)\mathrm{d}z}{\sqrt{(at-z)}} = S_\lambda(at) \int_0^{at} \frac{\exp\{-(k/a)(at-z)\}\chi(z)\mathrm{d}z}{\sqrt{(at-z)}} \qquad (1)$$

The function $S_\lambda(at)$ defines electrode potential as a function of time for the step-scan waveform:

$$\ln[S_\lambda(at)] = \begin{cases} (nF/RT)(E_i - E_{\frac{1}{2}}) & t = 0 \\ (nF/RT)(E_i - E_{\frac{1}{2}} - E_s) & 0 < t \leqslant \lambda \\ at - a\lambda + (nF/RT)(E_i - E_{\frac{1}{2}} - E_s) & t > \lambda \end{cases} \qquad (2)$$

where E_i is the initial potential, $E_{\frac{1}{2}}$ the conventional polarographic half-wave potential, E_s the potential to which the electrode is stepped, λ the time at which the linear scan begins, and a a parameter directly proportional to the scan rate, v, used during the linear scan

$$a = nFv/RT \qquad (3)$$

The solution of eqn. (1), $\chi(at)$, is directly proportional to current

$$i = nFA\sqrt{\pi a D_0}\, C_0^* \chi(at) \qquad (4)$$

Solution of integral equation

The only limiting case for which eqn. (1) yields a direct solution is $t < \lambda$ when $(E_{\frac{1}{2}} - E_s)n$ is large—*i.e.*, a potential step to the limiting current region for reduction of O. Under these conditions the right-hand side of eqn. (1) is negligible and eqn. (1) reduces to

$$\int_0^{at} \frac{\chi(z)\mathrm{d}z}{\sqrt{(at-z)}} = 1 \tag{5}$$

The solution of eqn. (5) is

$$\chi(at) = 1/\pi\sqrt{at} \tag{6}$$

Combination of eqns. (4) and (6) gives the expression for current

$$i = nFA\sqrt{D_0}C_0^*/\sqrt{\pi t} \tag{7}$$

Equation (7) is the familiar equation for purely diffusion-controlled potentiostatic electrolysis under conditions where the surface concentration of substance O can be assumed to be zero. Under these conditions, the current clearly is independent of all kinetic parameters, and also is independent of E_s. Thus, by suitable selection of E_s, interpretation of theoretical calculations can be simplified.

In general, solutions of eqn. (1) including times greater than λ only can be obtained numerically. Equation (1) is readily amenable to numerical solution using methods we have described previously[5]. These numerical solutions of eqn. (1) were obtained with an accuracy of better than 0.5%.

Results of numerical calculations

Typical results of numerical solution of eqn. (1) are shown in Fig. 1. Equation (1) contains several variables and, in principle, the curves of Fig. 1 should be a function of all of them. Fortunately, proper specification of experimental conditions permits elimination of some of the variables. In the following discussion, the effect of each of the variables of eqn. (1) is considered separately.

Effect of E_i. It is expected that curves such as those in Fig. 1 should be independent of initial potential. We found this to be the case whenever $(E_i - E_{\frac{1}{2}})n$ was greater than about 150 mV. All subsequent data reported here (including those of Fig. 1) were calculated for the arbitrary value of $(E_i - E_{\frac{1}{2}})n$ equal to 167 mV, and in this way the parameter E_i was eliminated as a variable.

Effect of E_s. The derivation of eqn. (7) illustrated that if E_s corresponds to the limiting current region, then the current for $t \leqslant \lambda$ is independent of E_s. We found numerical solutions of eqn. (1) for $t \leqslant \lambda$ to be described by eqn. (7) (within better than 1%) provided the quantity $(E_{\frac{1}{2}} - E_s)n$ was greater than about 120 mV. For $t < \lambda$, the curves are only slightly dependent on E_s, but even in this case E_s can be effectively eliminated as a variable in eqn. (1) (see discussion under *Measurement of rate constants*). All calculations reported here were performed with the arbitrary value of $(E_{\frac{1}{2}} - E_s)n$ equal to 167 mV.

Effect of k/a *and* $a\lambda$. In general, both the parameters k/a and $a\lambda$ influence solutions of eqn. (1). For example, Fig. 1 illustrates the effect of the kinetic parameter, k/a, for a fixed value of $a\lambda$. Clearly, for times less than λ, the current is independent

of k/a. This fact is consistent with eqn. (7) and is a result of the stepping potential used. As k/a approaches zero, the linear scan portion of the curve also becomes independent of k/a provided measurements are made to the extension of the current–time curve as a baseline. For measurements made in this way, the linear scan portion of the curves also is independent of $a\lambda$ in a manner analogous with cyclic voltammetry[4].

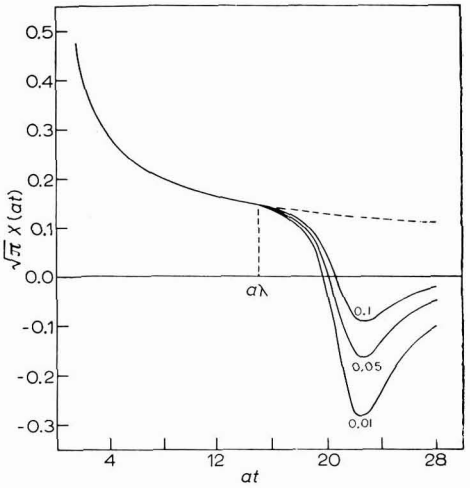

Fig. 1. Variation of current function with k/a (0.1, 0.05, 0.01) at constant $a\lambda$.

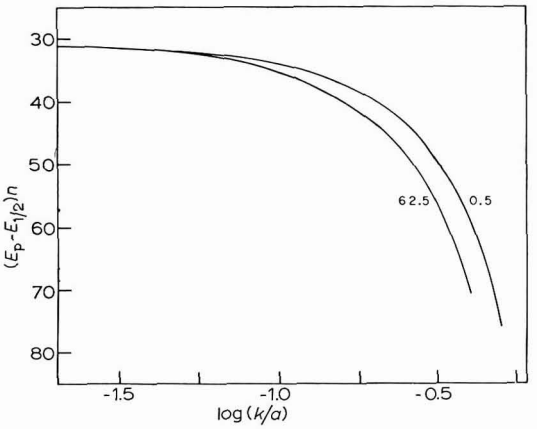

Fig. 2. Variation of anodic peak potential with k/a for $a\lambda = 0.5$ and 62.5.

For example, for small k/a, the value of $\sqrt{\pi}\chi_p$* always approaches 0.446, which is the same value obtained for cyclic voltammetry in the absence of kinetic complications[4].

For finite values of k/a, the linear scan portion of the curve is sensitive to changes of k/a in two ways. First, the peak potential shifts anodically as k/a increases.

* The new subscript refers to the peak value of the function $\sqrt{\pi}\chi(at)$ measured to the extension of the current–time curve.

This behaviour is illustrated in Fig. 2 where $(E_p - E_{\frac{1}{2}})n$ is plotted as a function of k/a for two values of $a\lambda$. Although peak potential clearly depends on both k/a and $a\lambda$, the dependence on $a\lambda$ is not great since the values of $a\lambda$ represented in Fig. 2 correspond to extreme limits.

The second effect of k/a is in terms of anodic peak current, and is illustrated in Figs. 1 and 3. In Fig. 3, $\sqrt{\pi}\chi_p$ is plotted *versus* k/a for several values of $a\lambda$. In general, for fixed $a\lambda$, $\sqrt{\pi}\chi_p$ decreases with increasing k/a. The actual magnitude of the peak, however, is a function of both k/a and $a\lambda$. Thus, for fixed k/a, the size of the anodic peak also decreases with increasing $a\lambda$. The reason for this effect is that with large $a\lambda$ (constant potential step corresponding to long times) and finite k/a, more time is available for the chemical reaction to proceed, and therefore the concentration of unreacted R available for oxidation during the linear scan is less.

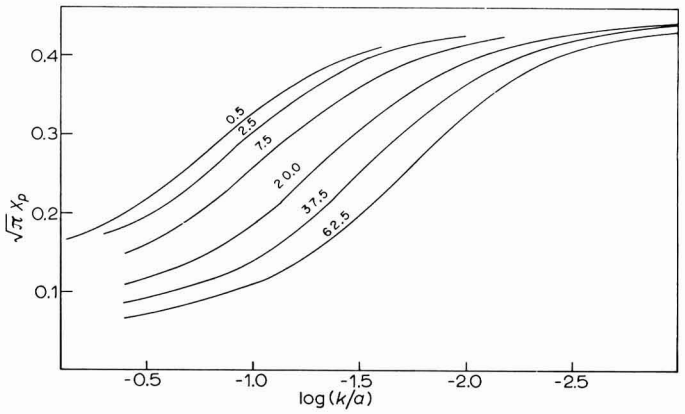

Fig. 3. Variation of peak current function with k/a for $a\lambda$ = 0.5, 2.5, 7.5, 20.0, 37.5, and 62.5.

From an experimental point of view, the fact that $\sqrt{\pi}\chi_p$ is a function of both $a\lambda$ and k/a is particularly important, because this allows adjustment of two experimental parameters, λ and v (or a), in such a way as to optimize the effect of the kinetics. Thus, the study of very fast chemical reactions does not necessarily require large scan rates, because $a\lambda$ can be made small. In this case (see Fig. 3, small $a\lambda$) kinetic effects are measurable for relatively large k/a (*i.e.*, slow scan rates). This situation is in sharp contrast to the work of SCHWARZ AND SHAIN[3] where their theoretical results are restricted to working with values of k/a less than about 0.008. Therefore, to measure the same value of k using the theory of SCHWARZ AND SHAIN requires scan rates approximately 2 orders of magnitude larger than is required using data such as those of Fig. 3. An analogous situation exists for measuring slow chemical reactions, where large values of $a\lambda$ (see Fig. 3) can be selected to provide enhancement of kinetic effects.

Measurement of rate constants. To measure rate constants quantitatively, data such as those of either Figs. 2 or 3 could be used. From an experimental point of view, peak potential shifts are relatively small, and therefore it is preferable to apply the data of Fig. 2 as a diagnostic criterion to ensure that the system under consideration conforms with Mechanism I.

As implied in the preceding section, data such as those of Fig. 3 are most suitable for quantitative measurement of k, but to do this experimental values of $\sqrt{\pi}\chi_p$ must be obtained. This is easily accomplished by recognizing that

$$\sqrt{\pi}\chi_p = (i_p/i_\lambda)\,(1/\sqrt{\pi a\lambda}) \tag{8}$$

where i_p is the experimental peak current (measured to the extension of the current–time curve), i_λ the current at time λ, and the remaining terms already have been defined. Thus, data of Fig. 3 serve as working curves from which experimental values of i_p/i_λ $(1/\sqrt{\pi a\lambda})$ can be converted directly to values of k/a. Since a is known, k can be calculated directly. In addition to its simplicity, this approach has the advantage that experimental parameters such as C_0^*, D_0, A, etc., need not be known. Table 1 contains numerical values from which working curves like those of Fig. 3 can be constructed.

TABLE 1

VARIATION OF $\sqrt{\pi}\chi_p$ WITH k/a AND $a\lambda$

$a\lambda$ 0.5		2.5		7.5		20		37.5		62.5	
k/a	$\sqrt{\pi}\chi_p$	k/a	$\sqrt{\pi}\chi_p$	k/a	$\sqrt{\pi}\chi_p$	k/a	$\sqrt{\pi}\chi_p$	k/a	$\sqrt{\pi}\chi_p$	k/a	$\sqrt{\pi}\chi_p$
0.0250	0.412	0.0100	0.426	0.0067	0.425	0.0010	0.442	0.0010	0.440	0.0010	0.430
0.0400	0.392	0.0200	0.410	0.0133	0.405	0.0030	0.438	0.0027	0.424	0.0024	0.415
0.0600	0.368	0.0400	0.377	0.0267	0.373	0.0050	0.415	0.0100	0.363	0.0050	0.382
0.1000	0.329	0.0600	0.347	0.0400	0.345	0.0100	0.393	0.0160	0.328	0.0075	0.355
0.1600	0.281	0.0800	0.325	0.0670	0.299	0.0200	0.347	0.0267	0.271	0.0100	0.324
0.2000	0.259	0.1200	0.286	0.1000	0.258	0.0300	0.313	0.0400	0.225	0.0150	0.283
0.2500	0.239	0.2000	0.230	0.1330	0.228	0.0500	0.260	0.0533	0.196	0.0250	0.226
0.4000	0.201	0.3200	0.193	0.2000	0.191	0.0750	0.216	0.0800	0.159	0.0500	0.155
0.5000	0.185	0.4000	0.183	0.2670	0.172	0.1400	0.160	0.1000	0.140	0.0800	0.121
0.7500	0.168	0.5000	0.175	0.4000	0.149	0.2500	0.128	0.2000	0.107	0.1500	0.094
						0.4000	0.110	0.4000	0.087	0.4000	0.068

It should be emphasized that the curves of Fig. 3 (and data of Table 1) are strictly applicable only when $(E_{\frac{1}{2}}-E_s)n$ equals 167 mV. Actually, the linear scan portion of the curves is not strongly dependent on E_s, and values of $(E_{\frac{1}{2}}-E_s)n$ within about ± 10 mV of 167 mV are acceptable. Nevertheless, this fact does constitute a limitation of the method, and therefore an alternative approach was sought. This approach consists of realizing that if a stepping potential more cathodic than -167 mV is used, then an effective λ, λ_e, can be defined as the time at which the electrode potential during the anodic scan has reached a value of -167 mV with respect to $E_{\frac{1}{2}}$. This is possible because for any potential more cathodic of $E_{\frac{1}{2}}$ than -167 mV, the electrode potential is always the limiting current region and the curve is described by eqn. (7) regardless of whether the potential is fixed or is a function of time. Because peak potential of the anodic curve is directly proportional to $E_{\frac{1}{2}}$ for $k/a < 0.1$ (see Fig. 2), in this case λ_e is defined as the point $197/n$ mV cathodic of the anodic peak. If values of k/a greater than 0.1 are encountered, the correct estimate of λ_e can be obtained from Fig. 2. Experimentally, then, one simply ensures that $(E_{\frac{1}{2}}-E_s)n$ is greater than or equal to 167 mV, and after the experiment is completed the value of λ_e to be used with Fig. 3 is determined.

Results of calculations described above extend the versatility of the potential step-linear scan method considerably with respect to the results of SCHWARZ AND SHAIN. Because application of the rigorous theory is easier than application of the original theory of SCHWARZ AND SHAIN, the potential step-linear scan method now provides a very attractive means of measuring rate constants of chemical reactions initiated electrochemically.

MEASUREMENT OF RATES OF BENZIDINE REARRANGEMENTS

Recently we have been studying in detail the electrochemistry of substituted azobenzene compounds. Some of this work has involved use of the potential step-linear scan method to evaluate rate constants for the benzidine rearrangements. Results of these measurements for two compounds—azobenzene and *m*-azotoluene (3,3'-dimethylazobenzene)—are reported here. Azobenzene has already been well characterized by several workers[1-3], and results for this compound serve as a check of the theory just described. In the case of the second compound, *m*-azotoluene, we report for the first time rate constants measured at high acid concentrations (short half-lives), and also compare electrochemical results with data obtained by spectrophotometry.

Experimental

Instrumentation. Circuits used were essentially the same as those of SCHWARZ AND SHAIN[1,3]. Two different potentiostats were employed, a commercial instrument (Wenking Potentiostat, model 61RS, Brinkmann Instruments, Westbury, N.Y.), and one constructed from an operational amplifier and booster [Philbrick Researches, Inc., Dedham, Mass., model P45AU and P66A (booster)]. No distinction could be made between results obtained with the two instruments.

The potential step-linear scan waveform was obtained by summing *via* a passive adding network, a delayed triangular wave with a gate of opposite polarity. The triangular wave was obtained from a commercial function generator (Exact Electronics, Inc., Hillsboro, Ore., Model 255). This function generator contains an internal delay mechanism so that it is possible to trigger the function generator with the gate making λ easily variable.

Two recording devices were used depending on the time-scale of the experiment. For λ less than about 1 sec and/or scan rates greater than about 150 mV/sec, a storage oscilloscope (Tektronix, Inc., Beaverton, Ore., type 564 with 2A63 (vertical) and 2B67 (horizontal) plug-in units) with Polaroid camera attachment (Tektronix type C-12) was used. For slower scan rates an X–Y recorder (Honeywell, Inc., San Diego, Calif., Model 520) was used.

For the spectrophotometric measurements a Beckman model DB was employed.

The cell and electrodes were essentially identical with those described by SCHWARZ AND SHAIN[1]. All measurements were made in a constant temperature room at ambient temperature of 24–25°.

Chemicals. Zone-refined azobenzene (Litton Chemicals, Inc., Fernandina Beach, Fla.) was used without further treatment. *m*-Azotoluene was prepared by reduction of *m*-nitrotoluene with zinc dust and sodium hydroxide[6]. The product was purified by eluting it with petroleum ether (30–60°) from an alumina column,

followed by repeated recrystallizations from ethanol. Melting point (54°, uncorrected) and infrared spectra agreed with the literature. (Found: C, 80.06; H, 6.69; N, 13.36. Calcd. for $C_{14}H_{14}N_2$: C, 79.97; H, 6.71; N, 13.32%.) *m*-Hydrazotoluene was prepared by reduction of *m*-azotoluene[7].

Procedures. For electrochemical experiments, procedures and preparation of solutions were identical with those of SCHWARZ AND SHAIN[1,3] except that to avoid air oxidation of *m*-azotoluene, solvents were de-aerated prior to dissolving the *m*-azotoluene. The solvent for all experiments was 50 wt.% ethanol–water. As in the work of SCHWARZ AND SHAIN, no attempt was made to maintain constant ionic strength, because the salt effect in 50% ethanol is small.

In general, for spectrophotometric measurements the procedure of CARLIN AND ODIOSO[7] was followed exactly except that, because the half-life of the reaction being studied was fairly small (*ca.* 70 sec), their quenching procedure could not be used. Our procedure consisted of rapid mixing of a solution of *m*-hydrazotoluene in 50% ethanol with a solution of perchloric acid in 50% ethanol, followed by rapid transfer to the spectrophotometer cell. These operations were easily completed within one half-life of the chemical reaction. Absorbance was then recorded directly as a function of time with a potentiometric recorder. Analysis of these absorbance–time data followed the procedure of CARLIN AND ODIOSO[7].

RESULTS AND DISCUSSION

Reduction of azobenzene

The theoretical calculations for the potential step-linear scan method, can be checked using the azobenzene system because of the extensive electrochemical data already available[1–3]. We arbitrarily selected experimental conditions identical with those of SCHWARZ AND SHAIN[3]. In general, we found the azobenzene system to behave exactly as they described[1,3]. The one exception is that we find gelatin tends to eliminate the anomalous behaviour SCHWARZ AND SHAIN observed when electrolysis times were longer than the half-life of the chemical reaction (presumably because of adsorption of hydrazobenzene[2]). As shown below, the presence of gelatin does not have a significant effect on measured rate constants.

In Fig. 4, theoretical and experimental potential step-linear scan curves for azobenzene are compared. The theoretical currents (circles) were calculated from eqn. (4) using the diffusion coefficient determined by SCHWARZ AND SHAIN[1] (3.4×10^{-6} cm^2/sec). The experimental curve (solid line) actually corresponds to two different experiments, one in which gelatin was employed (0.02%) and another in which gelatin was not used. These two curves are within experimental error and therefore are represented by a single line.

The fact that rate constants determined with the aid of the working curves discussed above (Fig. 3) agree with rate constants determined by an independent electrochemical method, is illustrated in Fig. 5*. In Fig. 5, circles represent rate constants determined with the potential step-linear scan theory developed above. Each circle corresponds to measurements both with and without gelatin; results in

* At high acid concentrations in 50% ethanol, the Hammett acidity function, H_0, must be used as a measure of acidity rather than the molarity of the acid. Values of H_0 in Fig. 5 were obtained from the paper of SCHWARZ AND SHAIN[1].

the two cases are within experimental error. Nevertheless, with gelatin present, much larger values of λ could be used than in the absence of gelatin. The squares of Fig. 5 represent rate constants determined by SCHWARZ AND SHAIN.

With the potential step-linear scan method we have been able to cover as wide a range of rate constants as SCHWARZ AND SHAIN reported for the square-wave technique. Moreover, the range is considerably greater (in the direction of large rate

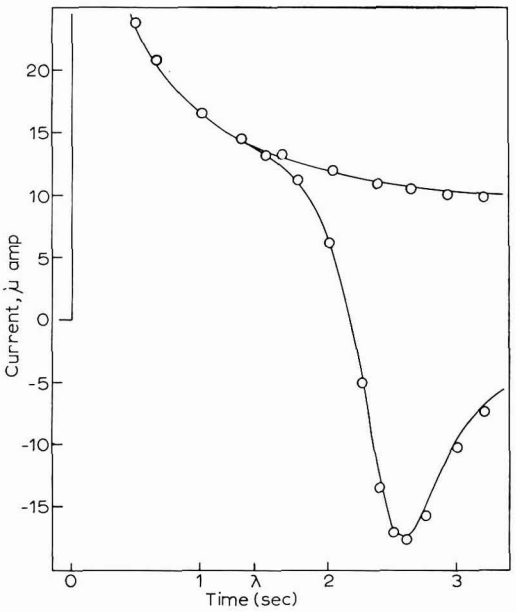

Fig. 4. Comparison of theory and experiment. (○), theory ($a\lambda = 10.4$, $k/a = 0.03$); (—), exptl. for reduction of mM azobenzene in 0.5 M perchloric acid (scan rate, 94 mV/sec).

constants) than SCHWARZ AND SHAIN studied with their potential step-linear scan theory[3] (the largest rate constant they report is $\log(k) = 0.4$). Although not stated explicitly by SCHWARZ AND SHAIN, the reason for this upper limit was no doubt set by the approximations of their theory. Thus, for them to measure larger rate constants and still satisfy the assumptions of their theory would have required prohibitively large scan rates where effects of adsorption, double-layer charging, and charge transfer kinetics become dominant.

Reduction of m-azotoluene

We have also used the potential step-linear scan method to study the reduction of *m*-azotoluene. Qualitatively, this system behaves in the same way as azobenzene. Some differences were observed, however. For example, the anomalous behavior reported by SCHWARZ AND SHAIN for long electrolysis times was even more pronounced than with azobenzene. As with azobenzene, we found that gelatin minimized this effect without affecting the value of measured rate constants. Most of the data reported for *m*-azotoluene were obtained with 0.01% gelatin. Another difference between *m*-azotoluene and azobenzene is reversibility of the electrode reaction. Thus,

under identical experimental conditions (without gelatin) the apparent heterogeneous rate constant for azobenzene is a factor of 2 or 3 larger than for *m*-azotoluene. This effect presumably is related to structural differences in the two compounds and currently is being investigated further. The final major difference between the two compounds is the rate of the benzidine rearrangement. At identical acid concentrations, *m*-azotoluene rearranges roughly 5 times more rapidly than azobenzene.

TABLE 2

RATE CONSTANTS FOR REARRANGEMENT OF *m*-HYDRAZOTOLUENE

Acid concn.[a] *(M)*	k^b *(sec*$^{-1}$*)*	k^d *(sec*$^{-1}$*)*
0.05	0.0067; 0.0059	—
0.06	0.0126[c]	—
0.07	0.0133	—
0.08	0.0177	0.021 (±0.003)
0.10	0.035	0.036 (±0.003)
0.20	—	0.138 (±0.004)
0.30	—	0.329 (±0.007)
0.40	—	0.769 (±0.017)

[a] For rate constants in the second column the acid was hydrochloric (however, see footnote c); in the third column the acid was perchloric.
[b] Extrapolated values of CARLIN AND ODIOSO[7].
[c] For our spectrophotometric measurements, we obtained 0.010 and 0.015 sec^{-1} in perchloric acid.
[d] Rate constants measured by potential step-linear scan. Numbers in parentheses are average deviations of at least 12 expts.

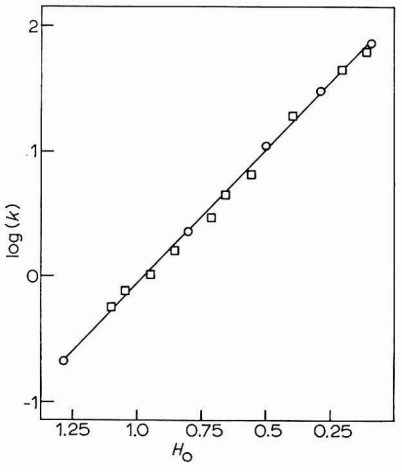

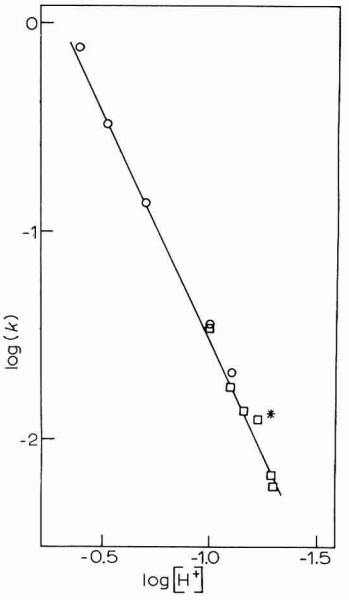

Fig. 5. Variation of k with H_0 for the benzidine rearrangement of hydrazobenzene. (○), potential step-linear scan method; (□), square-wave electrolysis[1].

Fig. 6. Variation of k with perchloric acid concn. for rearrangement of *m*-hydrazotoluene. (○), potential step-linear scan method; (□), spectrophotometric technique[7]; (*), determined spectrophotometrically under electrochemical conditions.

This effect is well known and explained by the inductive influence of the methyl groups.

Rate constants determined for rearrangement of *m*-hydrazotoluene are summarized in Table 2, and are plotted against acid concentration* in Fig. 6 (circles). The slope of the straight line drawn in Fig. 6 is 2.16 which is consistent with the well-known second-order dependence of benzidine rearrangements on acid concentration.

Comparison of rate constants. Rate constants for rearrangement of *m*-hydrazotoluene have been determined spectrophotometrically by CARLIN AND ODIOSO[7], and it is possible to compare these results with the electrochemical results reported above. Unfortunately, the classical measurements were performed under different experimental conditions where the rate of the reaction is slower (lower temperature and lower dielectric constant solvent—95% ethanol rather than the 50% we have used). Nevertheless, the dependence of rate constant on dielectric constant and temperature is known, and therefore it is possible to extrapolate the rate constants of CARLIN AND ODIOSO to experimental conditions identical with ours. This same procedure was used by REILLEY and co-workers[2] who for one specific acid concentration found reasonably good agreement between extrapolated classical and electrochemical measurements. Rate constants of CARLIN AND ODIOSO extrapolated to our experimental conditions are also included in Fig. 6 (squares) and Table 2. The agreement between the two approaches is excellent, and appears to justify the extrapolation. In spite of this, a number of criticisms can be raised against the extrapolation procedure, and it might be argued that the agreement of Fig. 6 is, at least, partly fortuitous. To test this possibility we repeated the measurements of CARLIN AND ODIOSO for one acid concentration, but for the same solvent and other experimental conditions employed for the electrochemical measurements (see discussion under *Experimental*). The rate constant we determined in this way is identical within experimental error with the extrapolated value (see Fig. 6 and Table 2). Thus, the extrapolation is valid, and one concludes that at least for the mechanism and timescale considered here, homogeneous rate constants can be measured electrochemically with complete confidence.

ACKNOWLEDGEMENT

Support of this work by the United States Army Research Office—Durham under Contract No. DA-31-124-ARO-D-308 is gratefully acknowledged. We also thank Professor STANLEY BRUCKENSTEIN for helpful discussions of part of this work.

SUMMARY

Theory for the potential step-linear scan technique for the case of a chemical reaction following reversible electron transfer has been developed without the use of simplifying approximations introduced by previous authors. Results of the theoretical calculations are presented in the form of working curves from which homogeneous kinetic parameters are easily determined. Results of the theory indicate that this technique should be a versatile method for studying electrode processes and

* For these acid concentrations it is unnecessary to use the Hammett acidity function.

measuring homogeneous rate constants. These conclusions are illustrated by measuring rates of benzidine rearrangement of hydrazobenzene and *m*-hydrazotoluene. In the case of the latter compound, a direct comparison is given between rate constants measured electrochemically and by classical kinetic methods, and it is concluded that homogeneous rate constants can be measured electrochemically with complete confidence.

REFERENCES

1 W. M. SCHWARZ AND I. SHAIN, *J. Phys. Chem.*, 69 (1965) 30.
2 D. M. OGLESBY, J. D. JOHNSON AND C. N. REILLEY, *Anal. Chem.*, 38 (1966) 385.
3 W. M. SCHWARZ AND I. SHAIN, *J. Phys. Chem.*, 70 (1966) 845.
4 R. S. NICHOLSON AND I. SHAIN, *Anal. Chem.*, 36 (1964) 706.
5 M. L. OLMSTEAD AND R. S. NICHOLSON, *J. Electroanal. Chem.*, 16 (1968) 145.
6 G. SCHULTZ, *Ber.*, 17 (1884) 473.
7 R. B. CARLIN AND R. C. ODIOSO, *J. Am. Chem. Soc.*, 76 (1954) 2345.

ELECTROANALYTICAL CHEMISTRY AND INTERFACIAL ELECTROCHEMISTRY
Elsevier Sequoia S.A., Lausanne – Printed in The Netherlands

EQUATIONS OF THE POLAROGRAPHIC WAVES OF SIMPLE OR COMPLEXED METAL IONS

I. THE METAL ION IS REDUCED WITH AMALGAM FORMATION AND THE LIGAND IS A NON-HYDROLYSABLE SUBSTANCE

MIHAIL E. MACOVSCHI

Institute of Physical Chemistry of Roumanian Academy of Sciences, Bucharest (Roumania)

(Received May 4th, 1967; in revised form, July 21st, 1967)

LINGANE[1] has shown that during the polarography of a solution of the complex, MX_q, with reversible reduction of the metal, the free ligand concentration at the dropping electrode surface must generally be different from that in the bulk solution, *i.e.*:

$$C_X^0 = C_X + \Delta C_X = C_X + (i/k_X)q \tag{1}$$

LINGANE avoided the calculation of the concentration excess, ΔC_X, by using the simplifying clause that there is a sufficiently high ligand excess; therefore,

$$C_X^0 \approx C_X \tag{2}$$

Using the same simplification, which we shall call "Lingane's approximation", DEFORD AND HUME[2] further developed the theory, solving the problem of the complex series, and later, SCHAAP AND MCMASTERS[3] studied the mixed complex. When the paper of LAITINEN *et al.*[4], dealing with the effect of solution pH is also considered, it can be seen that for Lingane's approximation, the problem of the polarography of the complexes has been practically solved.

But in the determination of stability constants there are many cases when only a slight excess of ligand concentration can be used; in such cases the theory developed on Lingane's approximation is insufficient. Among the methods for fitting the calculation to the cases of small ligand excess, the work of RINGBOM AND ERIKSON[5] is of importance.

The limits of application of Lingane's approximation have been indicated by BUTLER AND KAYE[6]. They showed, theoretically and experimentally, that when only the complex exists in solution, the potential at the dropping electrode surface is a function of $\ln\{i^{q+1}/(i_d - i)\}$, compared with $\ln\{i/(i_d - i)\}$ for the usual case.

Since an equation for the polarographic waves of the complexes which for the condition $C_X^{tot} = 0$ leads to the classical equation of the polarographic wave of the metal ion does not yet exist, the theory in its present stage does not explain completely the polarographic behaviour of the complexed ions.

We have, therefore, tried to find a general equation of the reversible polarographic waves that will represent (as nearly as possible) the real polarographic behaviour of the complexed metal or simple (non-complexed) ions.

The present work is the first stage in this investigation and deals with the case when only the complex MX_q* exists in solution—the metal ion is reduced with amalgam formation and the ligand is a non-hydrolysable compound. For this case, the following special equations can be found in the literature:

(a) The classical equation[7] for polarographic waves of the simple metal ions:

$$E = E^{M}_{\frac{1}{2}} - \frac{RT}{nF} \ln \frac{i}{i_d - i} \tag{3}$$

(b) LINGANE's equation[1] for the case where the complexing agent is present in large excess:

$$E = \varepsilon + \frac{RT}{nF} \ln \frac{\beta_q f_{MX_q} k_{am}}{f_{am} k_{MX_q}} - q \frac{RT}{nF} \ln C_X^{tot} f_X - \frac{RT}{nF} \ln \frac{i}{i_d - i} \tag{4}$$

where β_q is the dissociation constant of the complex MX_q (see eqn. (8)).

(c) BUTLER AND KAYE's equation[6] for the case where there is no excess of complexing agent:

$$E = \varepsilon + \frac{RT}{nF} \ln \frac{\beta_q f_{MX_q} k_{am}}{f_{am} k_{MX_q}} - q \frac{RT}{nF} \ln \frac{\alpha f_{HX} f_X}{C_H f_H f_X + \alpha f_{HX}} - q \frac{RT}{nF} \ln \frac{q}{k_X} - \frac{RT}{nF} \ln \frac{i^{q+1}}{i_d - i} \tag{5}$$

where α is the dissociation constant of the acid, HX, that forms the complex** and C_H is the concentration of H^+ ions in solution; the other symbols have their usual significance.

(d) BUCK's equation[8] for a large excess of complexing agent where the complex is of low stability***:

$$E = \varepsilon + \frac{RT}{nF} \ln \frac{\beta_q f_{MX_q}}{f_{am}} - q \frac{RT}{nF} \ln C_X f_X - \frac{RT}{nF} \ln \left(1 + \frac{\beta_q f_{MX_q}}{C_X^q f_X^q f_M} \right) + \frac{RT}{nF} \ln \frac{i_d - i}{i} \tag{6}$$

* It must be emphasized that MX_q is not the highest complex that could appear, but the simple complex present in the solution under the given conditions; in other words, q is a parameter the value of which depends on the conditions imposed on the system ($0 \leqslant q \leqslant q_{max}$).

** According to BUTLER AND KAYE, the ligand is a weak acid and its active form as complexing agent is only the ionized form, X.

*** According to BUCK, eqn. (6) is a general one, valid for any ligand concentration; in fact, it is a limiting case as will be shown.

The constant, ε, is related to the normal amalgam potential of the metal considered, E^0_{am}, by the equation:

$$\varepsilon = E^0_{am} + (RT/nF) \ln a_{Hg} \tag{7}$$

The following symbols are used in the text (for the sake of simplicity, the charges are not included):

C^0_M — concentration of metal ions at the electrode surface,
C^0_X — concentration of complex-forming ion at the electrode surface,
$C^0_{MX_q}$ — concentration of the metal complex at the electrode surface,
C^0_{am} — concentration of amalgam at the drop surface,
C_M — concentration of metal ions in solution,
C_X — concentration of the ligand in solution,
C_{MX_q} — concentration of the metal complex in solution,
C^{tot}_X — total concentration (analytical) of the ligand in solution,
C^{tot}_M — total concentration of metal in solution,
$f_M, f_X, f_{MX_q}, f_{am}$ — the corresponding activity coefficients,
$k_M, k_X, k_{MX_q}, k_{am}$ — the corresponding Ilkovič constants.

The dissociation constant of the complex, obviously the same in solution as at the electrode surface, is:

$$\beta_q = (C_X f_X)^q C_M f_M / C_{MX_q} f_{MX_q} = (C^0_X f_X)^q C^0_M f_M / C^0_{MX_q} f_{MX_q} \tag{8}$$

I. EQUATION OF THE POLAROGRAPHIC WAVE

1. Derivation of equation

The potential at the dropping electrode is given by the thermodynamic relation:

$$E = \varepsilon - (RT/nF) \ln (C^0_{am} f_{am} / C^0_M f_M) \tag{9}$$

To obtain the equation of the polarographic wave, that is $E = E(i)$, the concentrations must be expressed in terms of current.

The relationship between cathodic current and internal amalgam surface is:

$$i = k_{am} C^0_{am} \tag{10}$$

or

$$C^0_{am} = i/k_{am} \tag{11}$$

Combining eqn. (11) with eqn. (9), gives:

$$E = \varepsilon - (RT/nF) \ln (i f_{am} / k_{am} f_M C^0_M) \tag{12}$$

The current is carried, on the solution side of the interface, by both the free and complexed metal ions; furthermore, the total current, i, is the sum of two partial currents: i_M due to the metal ions and i_{MX_q} due to the complexed metal ions:

$$i = i_M + i_{MX_q} \tag{13}$$

If migration does not exist and if the diffusion layer is sufficiently thin so that the concentration gradient is constant, then:

$$i_M = k_M(C_M - C_M^0) \tag{14}$$

$$i_{MX_q} = k_{MX_q}(C_{MX_q} - C_{MX_q}^0) \tag{15}$$

At the diffusion limit, eqns. (14) and (15) become:

$$i_M^d = k_M C_M \tag{16}$$

$$i_{MX_q}^d = k_{MX_q} C_{MX_q} \tag{17}$$

resulting in:

$$i_d - i = k_M C_M^0 + k_{MX_q} C_{MX_q}^0 \tag{18}$$

If $C_{MX_q}^0$ is expressed in terms of C_M^0 and β_q:

$$i_d - i = k_M C_M^0 + k_{MX_q} C_M^0 (C_X^0 f_X)^q f_M / \beta_q f_{MX_q} \tag{19}$$

The concentration, C_X^0, of the ligand at the electrode surface is equal to the concentration of the ligand in the bulk solution plus the variation of the concentration due to the release of the ligand out of the complex at the moment of metal ion reduction:

$$C_X^0 = C_X + \Delta C_X \tag{20}$$

Since the complex has the formula MX_q, it is obvious that (see Fig. 1):

$$\Delta C_X = q(i_{MX_q}/k_X) \tag{21}$$

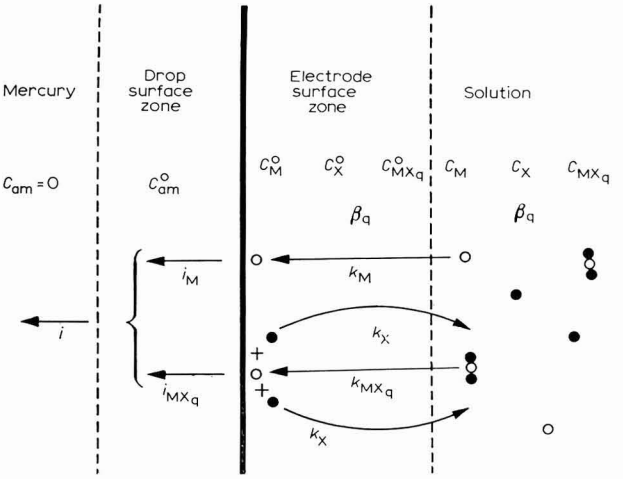

Fig. 1. Distribution of concns. and diffusion of ions in the neighbourhood of the dropping electrode. (○), metal ion M; (●), ligand X; (●○●), complex MX_q.

From eqns. (20), (21), (13) and (14):

$$C_X^0 = C_X + q\{i - k_M(C_M - C_M^0)\}/k_X \tag{22}$$

The value of $C_X{}^0$ may be introduced into eqn. (19), and suitable rearrangement gives:

$$\begin{aligned} i_d - i = k_M C_M^0 + \frac{k_{MX_q} f_M}{\beta_q f_{MX_q} k_M} \left(\frac{q f_X}{k_X}\right)^q \\ \times \left[\frac{k_X}{q} C_X - k_M(C_M - C_M^0) + i\right]^q k_M C_M^0 \end{aligned} \tag{23}$$

an equation which relates $C_M{}^0$ to the current. The concentration of metal ions and of complexing agent can be obtained from the total concentration by the following method:

$$\begin{cases} C_M = C_M^{tot} - C_{MX_q} \\ C_X = C_X^{tot} - qC_{MX_q} \\ C_M C_X^q = \beta_q C_{MX_q} f_{MXq} / f_M f_X^q \end{cases} \tag{24}$$

If we note that:

$$y = k_M C_M^0 \tag{25}$$

and

$$Q = (k_{MX_q} f_M / f_{MX_q} k_M)\,(q f_X / k_X)^q \tag{26}$$

then relation (23) can be written in terms of y:

$$\Phi_{(y)} = y \frac{Q}{\beta_q} \left(\frac{k_X}{q} C_X - k_M C_M + i + y\right)^q + y + i - i_d = 0 \tag{27}$$

and C_M^0 will be given by:

$$C_M^0 = \varphi(i_d, i, \beta_q, q, C_M^{tot}, C_X^{tot}, f_M, f_X, f_{MX_q}, k_M, k_X, k_{MX_q})/k_M \tag{28}$$

where φ is the solution to equation $\Phi_{(y)} = 0$.

The value of $C_M{}^0$ obtained in this way may now be introduced into eqn. (12), and taking into account the half-wave potential relation of the simple metal ion:

$$E_{\frac{1}{2}}^M = \varepsilon - (RT/nF) \ln (f_{am} k_M / f_M k_{am}), \tag{29}$$

the required equation of the polarographic reversible waves for simple and complexed metal ions is obtained:

$$E = E_{\frac{1}{2}}^M - (RT/nF) \ln (i/\varphi) \tag{30}$$

2. Function $\Phi_{(y)}$ has a single real solution

To obtain results with physico-chemical meaning, the function $\Phi_{(y)}$ must have only a single real solution.

Demonstration

(a) $\Phi_{(y)}$ has at the most only a single real solution. Function $\Phi_{(y)}$ is defined in the domain $y=0$, $y=k_M C_M$. $\Phi_{(y)}$'s derivative is:

$$\frac{d\Phi_{(y)}}{dy} = \frac{Q}{\beta_q}\left(\frac{k_X}{q} C_X - k_M C_M + i + y\right)^{q+1} \cdot \left[\frac{k_X}{q} C_X - k_M C_M + i + (q+1)y\right] + 1 \tag{31}$$

Since $i+y \geqslant k_M C_M$ ($i \geqslant i_M$) and C_X, β_q and Q cannot be negative, the derivative does not have real solutions, *i.e.*, the function may have at most only one real solution.

(b) The real solution, φ, does exist. The values of the function $\Phi_{(y)}$ at the end of the interval are:

$$\Phi_{(0)} = i - i_d \leqslant 0 \tag{32}$$

$$\Phi_{(k_M C_M)} = k_M C_M \frac{Q}{\beta_q}\left(\frac{k_X}{q} C_X + i\right)^q + k_M C_M + i - i_d \tag{33}$$

Introducing into eqn. (33) the expressions of β_q and Q from eqns. (8) and (26), and writing the parenthesis in the form $\{(k_X/q)C_X\}^q + iP_{q-1}$ results in:

$$\Phi_{(k_M C_M)} = k_{MX_q} C_{MX_q} + k_M C_M \frac{Q}{\beta_q} iP_{q-1} + k_M C_M + i - i_d = k_M C_M \frac{Q}{\beta_q} iP_{q-1} + i \geqslant 0 \tag{34}$$

The sign of the function $\Phi_{(y)}$ at the ends of the interval varies with the parameter, i:

$$\begin{cases} i=0 & \Phi_{(0)}<0 & \Phi_{(k_M C_M)}=0 \\ 0<i<i_d & \Phi_{(0)}<0 & \Phi_{(k_M C_M)}>0 \\ i=i_d & \Phi_{(0)}=0 & \Phi_{(k_M C_M)}>0 \end{cases} \tag{35}$$

It is obvious that within the definition domain, $\Phi_{(y)}$ changes its sign, therefore the real solution φ exists.

3. A possibility of simplification in solving equation $\Phi_{(y)}=0$ with numerical coefficients

If we use the notation:

$$\delta = (k_X/q)\, C_X - k_M C_M \tag{36}$$

$\Phi_{(y)}$ can be written:

$$\Phi_{(y)} = y\,(Q/\beta_q)\,(\delta + i + y)^q + y + i - i_d = 0 \tag{37}$$

The change of variable:

$$z = \delta + i + y \tag{38}$$

and rearrangement of terms gives:

$$\Psi_{(z)}=z^{q+1}-(\delta+i)z^{q}+\frac{\beta_q}{Q}z-\frac{\beta_q(\delta+i_d)}{Q}=0 \tag{39}$$

For $q>2$, the function $\Psi_{(z)}$ is simplified; it has only four terms instead of $q+2$ for function $\Phi_{(y)}$.

C_M^0 is related to the solution ψ of function $\Psi_{(z)}$ by the expression:

$$C_M^0=(\psi-\delta-i)/k_M \tag{40}$$

Introducing C_M^0 from eqn. (40) into eqn. (12) and writing:

$$i_d^*=\psi-\delta \tag{41}$$

we obtain:

$$E=E_{\frac{1}{2}}^M-(RT/nF)\ln\{i/(i_d^*-i)\} \tag{42}$$

Thus, the variation of the potential of the dropping electrode in terms of current has the same form as the case of the simple metal ion, with the difference that instead of i_d there appears i_d*. This can formally be considered as a corrected diffusion current.

II. SPECIAL FORMS OBTAINED FROM THE GENERAL EQUATION WITH DIFFERENT LIMITING CONDITIONS

For simplification, in the following section, the notation:

$$\theta=\frac{k_X}{q}C_X-k_M(C_M-C_M^0)+i \tag{43}$$

will be used.

1. The case of the simple metal ion

The limiting conditions: there is no ligand in solution and thus no complex is formed, *i.e.*,

$$C_X^{tot}=0 \tag{44}$$

Taking into account eqns. (24), (25), (13–15), gives:

$$(k_X/q)C_X-k_M C_M+i+k_M C_M^0=0 \tag{45}$$

$$\varphi=i_d-i \tag{46}$$

and subsequently:

$$E=E_{\frac{1}{2}}^M-(RT/nF)\ln\{i/(i_d-i)\} \tag{47}$$

which is the equation of the polarographic wave for simple metal ions (eqn (3)).

2. Lingane case

The limiting conditions are: the ligand is in large excess ($C_X = C_X^{tot}$) and the current transport to the dropping electrode is due to the metal ions from the complex (β_q-low*), *i.e.*,

$$\begin{cases} \theta = (k_X/q) C_X^{tot} \\ y \ll (Q/\beta_q)\theta^q y \end{cases} \tag{48}$$

φ will be

$$\varphi = \frac{(i_d - i)\beta_q f_{MX_q} k_M}{k_{MX_q} f_M (f_X C_X^{tot})^q} \tag{49}$$

and

$$E = E_{\frac{1}{2}}^M + \frac{RT}{nF} \ln \frac{\beta_q f_{MX_q} k_M}{f_M k_{MX_q}} - q \frac{RT}{nF} \ln C_X^{tot} f_X - \frac{RT}{nF} \ln \frac{i}{i_d - i} \tag{50}$$

and taking in account the expression for $E_{\frac{1}{2}}^M$ (eqn. (29))

$$E = \varepsilon + \frac{RT}{nF} \ln \frac{\beta_q f_{MX_q} k_{am}}{f_{am} k_{MX_q}} - q \frac{RT}{nF} \ln C_X^{tot} f_X - \frac{RT}{nF} \ln \frac{i}{i_d - i} \tag{51}$$

which is the Lingane equation (eqn. (4)).

3. Butler and Kaye's case

The limiting conditions are: there is no ligand excess in solution ($C_X = 0$) and the current transport to the dropping electrode is accomplished by the metal ions from the complex (to obtain these conditions it is also necessary that $C_M = 0$ and β_q should be low), *i.e.*,

$$\begin{cases} \theta = i \\ y \ll (Q/\beta_q)\theta^q y \end{cases} \tag{52}$$

The resulting value for φ is given by:

$$\varphi = \frac{(i_d - i)\beta_q f_{MX_q} k_M k_X^q}{i^q q^q k_{MX_q} f_M f_X^q} \tag{53}$$

and for E:

$$E = E_{\frac{1}{2}}^M + \frac{RT}{nF} \ln \frac{\beta_q f_{MX_q} k_M}{k_{MX_q} f_M} - q \frac{RT}{nF} \ln \frac{f_X q}{k_X} - \frac{RT}{nF} \ln \frac{i^{q+1}}{i_d - i} \tag{54}$$

or:

$$\begin{aligned} E = \varepsilon &+ \frac{RT}{nF} \ln \frac{\beta_q f_{MX_q} k_{am}}{f_{am} k_{MX_q}} - q \frac{RT}{nF} \ln f_X \\ &- q \frac{RT}{nF} \ln \frac{q}{k_X} - \frac{RT}{nF} \ln \frac{i^{q+1}}{i_d - i} \end{aligned} \tag{55}$$

* β_q is considered low if y can be ignored in comparison with $(Q/\beta_q)\theta^q y$; otherwise β_q is considered high. It must be emphasized that a general numerical value which would separate β_q-low from β_q-high cannot be given, because $Q\theta^q$ is not a constant.

The difference between eqns. (55) and (5), is that the term $q(RT/nF)\ln f_X$ appears in eqn. (55) instead of the term

$$q\frac{RT}{nF}\ln f_X\frac{\alpha f_{HX}}{C_H f_H f_X+\alpha f_{HX}}$$

in eqn. (5), owing to the fact that BUTLER AND KAYE considered the ligand a weak acid dissociated according to the equilibrium:

$$HX \rightleftharpoons H+X \tag{56}$$

with the constant α, and only the ionized form X active as complexing agent. The present work does not consider such an equilibrium.

4. Buck's case

The limiting conditions are: the ligand is present in large excess ($C_X=C_X^{tot}$) and the complex has low stability (β_q is large), *i.e.*,

$$\begin{cases}\theta=(k_X/q)C_X^{tot}\\ y \text{ cannot be neglected in comparison with } (Q/\beta_q)\theta^q y\end{cases} \tag{57}$$

The value for φ will be:

$$\varphi=\frac{(i_d-i)\beta_q f_{MX_q}k_M}{\beta_q f_{MX_q}k_M+f_M k_{MX_q}f_X^q(C_X^{tot})^q} \tag{58}$$

and for E:

$$E=E_{\frac{1}{2}}^M-\frac{RT}{nF}\ln\left[\frac{k_{MX_q}f_M f_X^q}{f_{MX_q}k_M}\cdot\frac{(C_X^{tot})^q}{\beta_q}+1\right]-\frac{RT}{nF}\ln\frac{i}{i_d-i} \tag{59}$$

Equation (6) given by BUCK is valid when all the diffusion coefficients are equal. For various diffusion coefficients, BUCK obtained the relation:

$$E_{\frac{1}{2}}^{MX_q}=\varepsilon+\frac{RT}{nF}\ln\frac{f_{MX_q}\beta_q}{f_{am}f_X^q}-q\frac{RT}{nF}\ln C_X-\frac{RT}{nF}\ln\frac{k_{MX_q}}{f_{am}}\left(1+\frac{k_M f_{MX_q}\beta_q}{k_{MX_q}f_M C_X^q f_X^q}\right) \tag{60}$$

which by taking into account eqn. (29), can be rearranged and rewritten

$$E_{\frac{1}{2}}^{MX_q}=E_{\frac{1}{2}}^M-\frac{RT}{nF}\ln\left(\frac{k_{MX_q}f_M f_X^q}{k_M f_{MX_q}}-\frac{C_X^q}{\beta_q}+1\right) \tag{61}$$

i.e., relation (59) in which $i=\frac{1}{2}i_d$.

When C_X is very large or β_q decreases, term 1 from the parenthesis may be neglected and eqn. (59) becomes Lingane's equation.

Equation (59) can be transformed into the polarographic equation of the

simple metal ion by neglecting the term $k_{MX_q} f_M f_X^q C_X^q / k_M f_{MX_q} \beta_q$ in the presence of term 1. As there are two parameters, C_X and β_q, two possibilities will occur:

(a) $\beta_q \to \infty$. The supplementary condition $\beta_q \to \infty$ is not in contradiction with the fundamental condition, β_q-high, for which eqn. (59) was inferred. Therefore, this method of obtaining the simple metal ion equation has a real physico-chemical significance.

(b) C_X *decreases to 0.* For C_X decreasing, $i - k_M(C_M - C_M^0)$ from eqn. (43) cannot be neglected in comparison with $(k_X/q)C_X$, and thus eqn. (59) inferred for the case when $(k_X/q)C_X \gg i - k_M(C_M - C_M^0)$ no longer has a real meaning. Consequently, BUCK's affirmation that eqn. (59) is a general equation is not valid; as it has been shown, eqn. (59) is a limiting case.

5. The case of a slight ligand excess, the complex being stable (not yet described in the literature)

The limiting conditions are: the excess of the ligand is small (C_X is low) and the transport of the current to the dropping electrode is due to the metal ions from the complex (β_q-low), *i.e.*,

$$\begin{cases} \theta = (k_X/q)C_X + i \\ y \ll (Q/\beta_q)\theta^q y \end{cases} \tag{62}$$

This leads to:

$$\varphi = \frac{(i_d - i)\beta_q f_{MX_q} k_M}{k_{MX_q} f_M \left(\frac{q f_X}{k_X}\right)^q \left(\frac{k_X}{q} C_X + i\right)^q} \tag{63}$$

and

$$E = E_{\frac{1}{2}}^M + \frac{RT}{nF} \ln \frac{\beta_q f_{MX_q} k_M}{k_{MX_q} f_M} - q \frac{RT}{nF} \ln \frac{f_X q}{k_X} - \frac{RT}{nF} \ln \frac{i\left(\frac{k_X}{q} C_X + i\right)^q}{i_d - i} \tag{64}$$

or:

$$\begin{aligned} E = E_{\frac{1}{2}}^M &+ \frac{RT}{nF} \ln \frac{\beta_q f_{MX_q} k_M}{k_{MX_q} f_M} - q \frac{RT}{nF} \ln \frac{q f_X}{k_X} \\ &- \frac{RT}{nF} \ln \left[\left(\frac{k_X}{q} C_X\right)^q \frac{i}{i_d - i} + \frac{q!}{1!(q-1)!} \left(\frac{k_X}{q} C_X\right)^{q-1} \frac{i^2}{i_d - i} \right. \\ &\left. + \frac{q!}{2!(q-2)!} \left(\frac{k_X}{q} C_X\right)^{q-2} \frac{i^3}{i_d - i} + \ldots + \frac{i^{q+1}}{i_d - i} \right] \end{aligned} \tag{65}$$

According to whether the values of C_X are very high or equal to zero, the parenthesis will reduce to the first or the last term, and the cases of LINGANE, and BUTLER AND KAYE, respectively, will result. For C_X-low, the terms have values comparable with each other and must all be taken into account.

6. There is no other limiting case

If the following notation is used:

$$\begin{cases} A=(k_X/q)C_X \\ B=-k_M(C_M-C_M^0) \\ C=i \end{cases} \tag{66}$$

then:

$$\theta=A+B+C \tag{67}$$

The special forms of the derived equations depend on the β_q-value and the form of the expression for θ, by neglecting different terms. All the forms that θ can take and their meaning when β_q is high or low are as follows:

1. $\theta=A$. β_q-low—LINGANE's case—II.2. β_q-high—BUCK's case—II.4.

2. $\theta=B$. Impossible, independent of β_q-value: C cannot be neglected in the presence of B because always $C\geqslant|B|$ $(i\geqslant i_M)$.

3. $\theta=C$. β_q-low—BUTLER AND KAYE's case—II.3. β_q-high—impossible: $\theta=C$ would mean that in the solution there exists only a non-dissociated complex; but as β_q is high, this situation is impossible.

4. $\theta=A+B$. Impossible, independent of β_q-value: see point 2.

5. $\theta=A+C$. β_q-low—case II.5. β_q-high—impossible: $\theta=A+C$ means $i\geqslant i_M$, *i.e.*, the whole of the metal ion is complexed but in the given conditions (β_q-high and C_X-low so that C cannot be neglected in comparison with A) this situation is impossible.

6. $\theta=B+C$.—$C_X^{tot}=0$—the case of simple metal ion—II.1.—$C_X^{tot}<qC_M^{tot}$—β_q-low—the general case: although $C_X\approx 0$, still $\theta=0$ and then equation in y is of $q+1$ grade.—β_q-high—impossible: if β_q is high and $C_X^{tot}\neq 0$, then A cannot be neglected the presence of $B+C$.

7. $\theta=A+B+C$.—the general case.

Therefore, the five limiting cases presented (four from the literature and one inferred in this paper) are the only limiting equations that exist. Figure 2 shows schematically, the limiting equations field of applicability.

III. DISCUSSION

The inferred equation (of the polarographic waves for simple and complexed metal ions when the metal ion is reduced with amalgam formation and the ligand is a non-hydrolysable substance) involves all the limiting equations reported in the literature. They are: the classical equation for the simple metal ion; the equation deduced by LINGANE; BUTLER AND KAYE's equation and that deduced by BUCK. Another limiting equation not so far presented in the literature has been inferred from the same general equation. It refers to the case of a slight ligand excess. This last limiting equation is of special interest because it is available from the domain of low ligand concentrations.

The inferred equation includes all ligand concentrations and allows the dis-

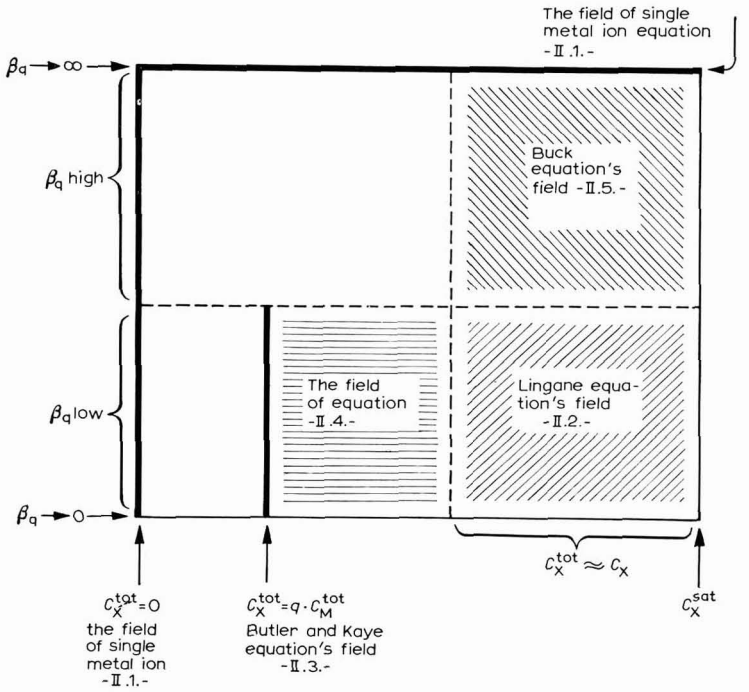

Fig. 2. Schematic representation of the field of applicability of the limiting equations. C_X^{sat}, satd. ligand concn. For the non-hatched area, only the general equation may be applied, *i.e.*, the general equation has no limiting form and must be applied as such.

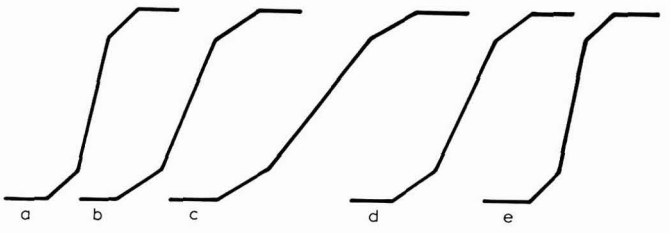

Fig. 3. The theoretical shape of the polarographic wave, *vs.* the ligand concn. in soln. (a), $C_X^{tot}=0$; (b), $0<C_X^{tot}<qC_M^{tot}$; (c), $C_X^{tot}=qC_M^{tot}$; (d), $qC_M^{tot}<C_X^{tot}<(C_X^{tot}\approx C_X)$; (e), $C_X^{tot}\approx C_X$.

cussion of the shape of the polarographic waves for C_X^{tot} varying from zero to C_X^{sat} (Fig. 3). When $C_X^{tot}=0$, the potential at the dropping electrode is dependent upon $i/(i_d-i)$ and the polarographic wave is classical in shape; the slope of the wave depends on the metal ion charge. For $C_X^{tot}=qC_M^{tot}$ (BUTLER AND KAYE) the potential at the dropping electrode depends on $i^{q+1}/(i_d-i)$ and the slope of the polarographic wave decreases with the increasing value of q. For a large ligand excess, *i.e.*, $C_X^{tot}\approx C_X$, the initial relation $E=E\{i/(i_d-i)\}$ is found (LINGANE). Consequently, in the concentration range $0<C_X^{tot}<qC_M^{tot}$ and $qC_M^{tot}<C_X^{tot}<(C_X^{tot}\approx C_X)$, the potential at the dropping

electrode will be a function of a sum of terms with i-powers from 1 to $q+1$, *i.e.*,

$$E=E \sum_{j=0}^{q} A_j \frac{i^{j+1}}{i_d-i}$$

Therefore, with increasing C_X^{tot}, the polarographic waves slope continuously, reach a maximum slope for $C_X^{tot}=qC_M^{tot}$ and then flatten out. The relation

$$E=E \sum_{j=0}^{q} A_j \frac{i^{j+1}}{i_d-i}$$

for the domain of concentration $qC_M^{tot} < C_X^{tot} < (C_X^{tot} \approx C_X)$ is clearly shown by eqn. (65). For the domain $0 < C_X^{tot} < qC_M^{tot}$ this relation is expressed implicitly in eqns. (27) and (30).

It is evident from the above discussion that small quantities of substances present as impurities and able to complex metal ions can strongly interfere with the shape of the polarographic wave, especially at small metal ion concentrations*. Therefore, the estimation of the number of electrons changed at the electrode or the test of reversibility can lead to erroneous results if the reagents used as supporting electrolyte are not of the highest purity.

SUMMARY

In the polarographic determination of a solution containing the complex, MX_q, with dissociation constant β_q, the total current, i, is a sum of two currents: i_M due to the simple metal ions and i_{MX_q} due to the complexed metal ions. Since, on reducing the metal ion the complex is broken down, the free ligand concentration at the dropping electrode is: $C_X^0=C_X+qi_{MX_q}/k_X$, C_X being the concentration of free ligand in the bulk solution. These considerations lead to the following equation of the polarographic waves:

$$E=E_{\frac{1}{2}}^{M}-(RT/NF) \ln (i/\varphi)$$

being the solution of the equation:

$$\Phi_{(y)}=y \frac{1}{\beta_q} \frac{k_{MX_q} f_M}{f_{MX_q} k_M} \left(\frac{q f_X}{k_X}\right)^q \left(\frac{k_X}{q} C_X - k_M C_M + i + y\right)^q + y + i - i_d = 0$$

where C_M is the concentration of the metallic ion in the bulk solution, f the activity coefficients and k the respective Ilkovič constants. It has been demonstrated that the equation has only one real solution.

* The method of DETRICK AND FREDERICK[9] gives polarographic waves for metal ion concentrations of 10^{-7}–10^{-9} M.

All the known special equations appear as limiting conditions; *i.e.*, the equation of (i) the simple metal ion; (ii) LINGANE; (iii) BUCK; and (iv) BUTLER AND KAYE, as well as another equation for the case of slight ligand excess, not dealt with in the literature. It has been demonstrated also that no other limiting equation of any physico-chemical meaning can be deduced.

The relation between the polarographic wave shape and the ligand concentration is also discussed.

REFERENCES

1 J. J. LINGANE, *Chem. Rev.*, 29 (1941) 1.
2 D. D. DEFORD AND N. D. HUME, *J. Am. Chem. Soc.*, 73 (1951) 5321.
3 W. B. SCHAAP AND D. L. MCMASTERS, *J. Am. Chem. Soc.*, 83 (1961) 4699.
4 H. A. LAITINEN, E. I. ONSTOTT, J. C. BAILAR, JR. AND S. SWANN JR., *J. Am. Chem. Soc.*, 71 (1949) 1550.
5 P. KIVALO AND J. RASTAS, *Suomen Kemistilehti*, B 30 (1957) 128.
6 C. G. BUTLER AND R. C. KAYE, *J. Electroanal. Chem.*, 8 (1964) 463.
7 J. HEYROVSKÝ AND J. KŮTA, *Tratat de Polarografie*, Academy R.P.R., 1959, p. 118.
8 R. P. BUCK, *J. Electroanal. Chem.*, 5 (1963) 295.
9 F. DETRICK AND M. FREDERICK, *Anal. Chem.*, 36 (1964) 1143.

ELECTROANALYTICAL CHEMISTRY AND INTERFACIAL ELECTROCHEMISTRY
Elsevier Sequoia S.A., Lausanne – Printed in The Netherlands

ELECTROCHEMICAL-SPECTROSCOPY USING TIN OXIDE-COATED OPTICALLY TRANSPARENT ELECTRODES

JERZY W. STROJEK AND THEODORE KUWANA
Department of Chemistry, Case Western Reserve University, Cleveland, Ohio 44106 (U.S.A.)
(Received August 24th, 1967)

The electrochemical properties of optically transparent electrodes (OTE) and the application of these electrodes to the spectral determination of electrochemical parameters will be discussed.

In recent years, there has been much interest in the development of physical methods by which an electrochemical process may be concurrently examined. These methods are intended to provide additional information on the course of an electrode reaction. Examples of such methods are: electron spin resonance[1], which is used to detect and characterize free radical intermediates or products; and ellipsometry[2], which monitors changes occurring on the surface of an electrode. These methods provide useful information but have their limitations and the development of additional techniques applicable to electrochemical studies is desirable.

Since our interest has been in organic electrode processes where many light-absorbing species are encountered, the application of spectroscopic techniques was explored. An optically transparent electrode would have many advantages but this idea is not new, since thin films of certain metals such as gold are transparent in the visible region of the spectrum, and electrodes made from thin metal layers on glasses have been used in connection with photovoltaic studies[3]. The optical properties of most metal coatings are, however, limited at the shorter wavelengths, particularly at coating thicknesses where the resistance is low.

In the search for other materials as possible OTE, glasses coated with tin oxide were investigated. The semiconductor properties of tin oxide are well known, and glasses coated with "doped" tin oxide have been available commercially for many years with the trade names of Nesa and Electropane glasses. Antimony is the most commonly used doping material and the resulting tin oxide coating is a *n*-type semiconductor. The surface is quite inert to chemical attack and coupled with a conducting surface, serves well as an electrode that is transparent in the visible region of the spectrum. The applicability of these glasses to optical studies during electrochemical processes has already been demonstrated[4]. When conventional transmission spectroscopy with the incident light perpendicular to the surface of the OTE is used, a solution layer of minimum thickness of the order of 10^4 Å may be spectrally monitored (depending of course, on the concentration and molar absorptivity of the light-absorbing species). Internal reflection spectroscopy (IRS) lowers this thickness by one or two orders of magnitude; therefore electrochemical processes well within the thickness of the diffusion layer may be followed spectrally[5,6]. Thus, the advantages of OTE in mechanism studies are quite obvious. In

this paper, a more detailed examination of the electrochemical properties (and their general applications in connection with transmission spectroscopy) of these tin oxide-coated electrodes will be presented.

EXPERIMENTAL

Cyclic voltammetry and chronopotentiometry were carried out using solid state operational amplifier equipment of standard circuitry[7]. A Wenking model TRS61 potentiostat was used for controlled-potential coulometry experiments. A Moseley model 7035A X-Y recorder, a Sanborn model 320 dual-channel recorder, a Tektronix model 564 storage oscilloscope, and a Midwestern Instruments model 800R oscillographic recorder were employed for signal monitoring. The latter recorder can accept 25 channels and has a maximum chart speed of 6000 in./min.

For purely electrochemical studies, the ratio of surface area to surface-resistance should be a maximum and a cell with a thin circular ring of conducting surface is therefore used as shown in Fig. 1. The ratio increases as the width of the conducting ring decreases, assuming resistance is linearly proportional to width. For spectral studies, a sandwich-type cell is convenient and the one shown in Fig. 2 has provisions for nitrogen purging. A conducting glass plate (W.E.) serves as one window of the cell and the second window is a glass plate or a thin sheet of irradiated Kel-F (Fluorocarbon Corp., Santa Ana, California). Kel-F does not fracture easily, is chemically inert, and has excellent optical properties even in the ultraviolet region of the spectrum.

Electrical contact to the conducting tin oxide surface can be obtained by making a mechanical contact with a thin metal plate or by coating the outer surface with liquid silver paint. The contact is isolated from the solution by Teflon or Neoprene O-ring seals (*e.g.*, see Fig. 1). A metal contact is preferable if it can be held tightly against the conducting tin oxide surface. Care must always be taken to ensure that the contact does not act as a junction diode or have excessive ohmic resistance. Silver paint did not give reproducible results.

The tin oxide-coated glasses were obtained from two commercial sources. The glasses from both were apparently doped with antimony but exact details about the coating procedures are not known. Resistances varied considerably depending on the level of doping and thickness of the coating. Surfaces with resistances as low as 5–10 Ω square^{-1} have been prepared. The substrate from one source was always borosilicate glass with the tin oxide surface having a reported carrier level of between 10^{20} and 10^{21} carrier cm^{-3}.

A shielded auxiliary electrode and a saturated calomel reference electrode were used. All potentials are reported with respect to this reference electrode.

Spectral scans were made on a Cary model 15 spectrometer. For set wavelength studies, either a narrow band-pass interference filter or a Bausch and Lomb grating monochromator (1350 grooves mm^{-1}) were used for isolating the required wavelength of light. An EMI low-noise No. 6256S photomultiplier tube in a Pacific Photomultiplier housing with divider circuit was used for monitoring light intensity. The collector (anode) current was amplified using a Philbrick P-12Q operational amplifier in the current-follower mode. High voltage to the photomultiplier tube was supplied by Atomic Instrument Co., Super Stable HV model 312.

Organic reagents were purified by standard procedures of recrystallization or vacuum sublimation. Water was twice distilled, the second distillation being from alkaline permanganate with a 1-m long vacuum-jacketed, glass-packed column.

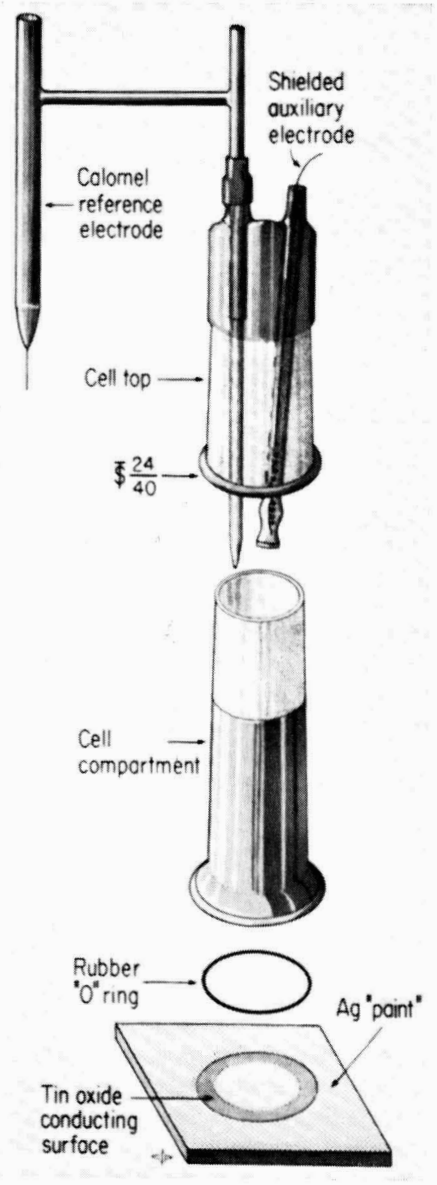

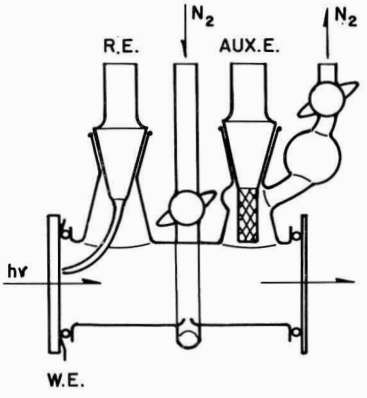

Fig. 1. Electrochemical cell with ring-conducting electrodes.

Fig. 2. Sandwich-type cell: (W. E.), transparent conducting glass electrode; (R. E.), connection to a ref. satd. calomel electrode; (AUX. E.), connection to an auxiliary electrode.

RESULTS AND DISCUSSION

Properties of doped tin oxide glasses and quartz

The thickness of commercial coatings of typical coated glasses showing optical absorbance of less than 0.2 from 6000–3600 Å (Fig. 3A) is about one micron. Below this wavelength, the absorbance increases sharply owing to absorption by the glass.

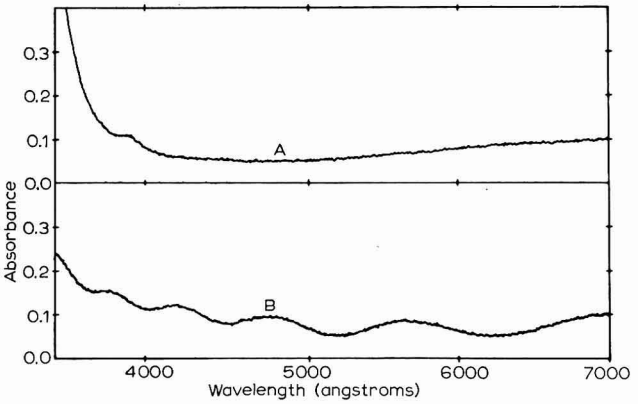

Fig. 3. Absorption spectra of tin oxide-coated glass; (A), thin coating; (B), thick coating.

For thicker coatings, an interference pattern is present on the spectrum (Fig. 3B). For transmission to shorter wavelengths, coatings on quartz plates can be used. These plates were usually higher in resistance, 50–500 Ω square^{-1}.

Tin oxide surfaces were very stable to chemical attack with no visible changes when immersed in solutions of pH 1–10 or in mild oxidizing or reducing solutions over a period of 1 day. When they had been used as electrodes for three years, visible surface deformation with "cracking" along crystalline grain boundaries was encountered only once. The reason for this is unknown since it could not be reproduced. Surface properties of tin oxide coatings are being investigated by LAITINEN and co-workers[8].

Electrochemical characteristics

The useful potential ranges of these electrodes are slightly greater than those of platinum and gold for similar background solutions. Typical background i–E curves are shown in Fig. 4 for various electrolytes. If these OTE are polarized considerably beyond the cathodic and anodic background limits, irreversible alterations, which affect the electrochemical characteristics, occur.

Previously, voltammetric and chronopotentiometric experiments[4] indicated that these OTE behave quite similarly, in many respects, to metal electrodes except that the current–potential (i–E) or potential–time (E–t) curves deviated from the ideal curves, partly owing to the internal resistance of the conducting surface. The i–E curves for linear sweep voltammetry are not easily corrected as in the case of the usual uncompensated resistance, which can be corrected, for example, electronically by a positive feedback arrangement to the control amplifier of the potentiostat[9]. With OTE, the surface resistance creates a non-equipotential surface and the devi-

ations are no longer a linear function of current. Thus, such plots as the peak current, i_p, *vs.* concentration, C, at a constant scan rate, v, are non-linear and manual corrections, as applied by DELAHAY AND STIEHL[10] for peak currents in connection with oscillographic polarography, also give only approximate results.

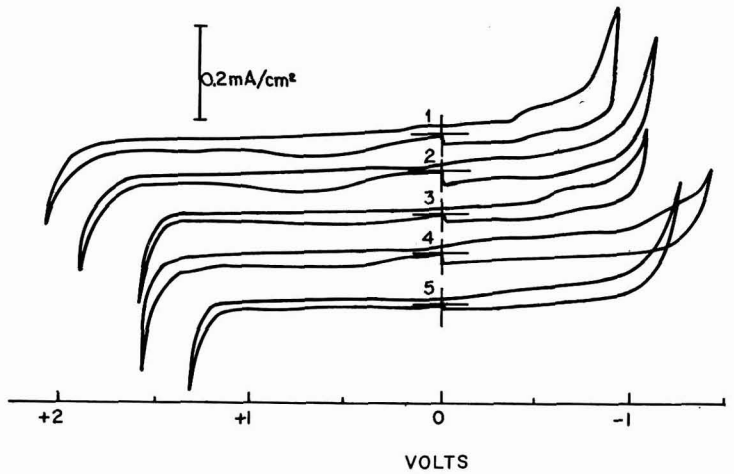

Fig. 4. Background i–E curves for OTE (6 Ω square^{-1}, area 5.11 cm^2): (1), phosphate buffer pH 2; (2), phosphate buffer pH 4; (3), acetate buffer pH 4.5; (4), 0.2 M KCl; (5), 0.2 M ammonium acetate.

TABLE 1

CYCLIC CHRONOPOTENTIOMETRY AT OTE

n	a_n (exptl.)	a_n (calcd.)	n	a_n (exptl.)	a_n (calcd.)
1	1.000	1.000	11	0.502	0.504
2	0.321	0.333	12	0.362	0.382
3	0.593	0.588	13	0.502	0.498
4	0.344	0.355	14	0.362	0.385
5	0.534	0.546	15	0.502	0.493
6	0.357	0.366	16	0.371	0.388
7	0.511	0.525	17	0.507	0.489
8	0.353	0.373	18	0.363	0.390
9	0.516	0.513	19	0.500	0.486
10	0.348	0.378	20	0.377	0.392

For chronopotentiometry, if the electrode area is large, transition times are poorly defined owing to the unequal distribution of current on the surface. Improvement is made by use of a cell with a thin ring of conducting surface (see Fig. 1) and transition times in close agreement with those calculated can be obtained.

The behaviour of this thin ring cell was also tested using cyclic chronopotentiometry. For a solution of 1.124×10^{-3} M potassium ferrocyanide in 0.1 M sulfuric acid, the conditions given by HERMAN AND BARD[11], $i_{anodic} = i_{cathodic}$, $C_R{}^0 = 0$, were satisfied. The experimental values of transition times were in excellent agreement with those calculated, particularly for odd values of n as may be seen in the data of Table 1.

The high density of carriers and the ability of the electrode to function both as a cathode and anode (within normal potential ranges) suggest that these doped tin oxide surfaces behave similarly to "poor" metallic conductors. The resistances vary from sample to sample and actual values depend on the method of measurement. More important is the question of whether resistance measurements are significant, since in these electrodes the resistance alone cannot account for the observed deviations of i–E or E–t curves. Recognizing this limitation, one finds in practice that when the currents in the electrolyses are small compared to the semiconductor saturation current, reproducible results can be obtained for a given set of experimental conditions.

The semiconductor properties of the surface do, however, manifest themselves markedly on the character of i–E or E–t curves when the type and/or concentration of supporting electrolyte, and pH are varied. For example, it is well known that the potential corresponding to the polarographic half-wave potential for ferricyanide becomes more positive in value as the pH decreases, owing to the protonation of ferrocyanide. The expected half-wave potentials *vs.* pH, corrected for ionic strength using the Davies equation[12], are plotted in Fig. 5. The i–E curves (cyclic scan) at a *platinum* electrode for pH-values of 1.5, 2.5, 3.5, and 4.5 are shown in Fig. 6A. The

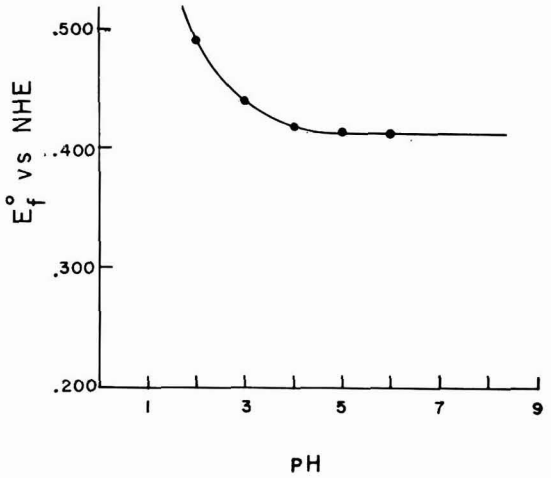

Fig. 5. Formal potential of ferricyanide/ferrocyanide *versus* pH

potential shifts are as predicted, and there are no observable changes in the i_p-values or in the slopes of the i–E curves. At OTE however, the i–E curves are very dependent on pH. As the pH increases, the i_p-values decrease and the i–E profiles appear less reversible. The effect of pH is more pronounced with the higher resistant electrodes, but is independent of whether the solution initially contains ferrocyanide with the scan direction anodic and then reversed, or only ferricyanide with the scan direction cathodic and then reversed. Examples of these i–E curves for OTE with resistances of 6 and 35 Ω square^{-1} are given in Fig. 6 (B and C). Between pH 1.5 and 2.5, there is an inversion in the direction of change of i_p with pH indicating two competing effects: first, the already discussed shift of potential with protonation of ferrocyanide

and secondly, the increased overpotential to the electrode reaction with increased pH. Studies are in progress to elucidate this latter effect further, particularly with regard to the effect of pH and ions on the tin oxide–solution interface structure.

Measurement of differential capacitance

Differential capacitances were determined for various electrolytes and pH-values by using a method similar to that of KEMULA AND STROJEK[13]; i–E profiles when a small triangular wave of *ca.* 5 mV at a frequency of *ca.* 5 Hz was superimposed

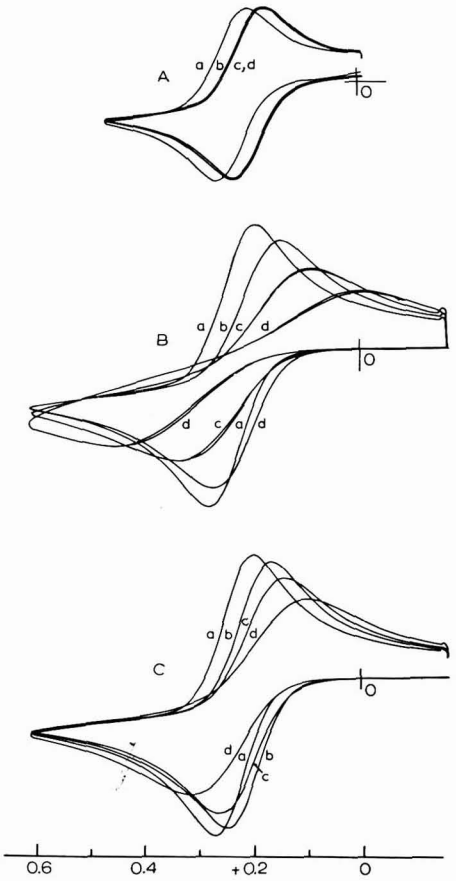

Fig. 6. Voltammetric curves of 10^{-3} M ferrocyanide at different pH-values and electrodes: (A), platinum, area 4.1 cm^2; (B), OTE 35 Ω square^{-1}, area 5.11 cm^2; (C), OTE 6 Ω square^{-1}, area 5.11 cm^2; (a–d), pH 1.5, 2.5, 3.5, and 4.5, respectively.

on a slowly changing d.c. bias voltage, were evaluated. The total capacitance has contributions from both double-layer and semiconductor capacitance. The latter capacitance is complex and depends on the type of semiconductor[14].

There is a potential region in which the differential capacitance remains fairly independent of electrolytes such as KCl, Na_2SO_4, $KClO_4$, their concentration and pH, and depends mainly on the particular semiconductor. For example, an OTE with a

resistance of 6 Ω cm^{-2} gave a differential capacitance of 2.4 μF cm^{-2} in 0.03–1.0 *M* KCl solutions (pH 6.5) over the potential range −0.3 to +0.4 V. Another OTE of 100 Ω cm^{-2} resistance gave a capacitance of 10–15 μF cm^{-2} in the potential range +0.3 to −0.1 V, but at more negative potentials the reciprocal of the square root of the capacitance varied linearly with electrode potential (Fig. 7), as is usually found when electrons in the space charge layer are depleted[14]. The capacitance values

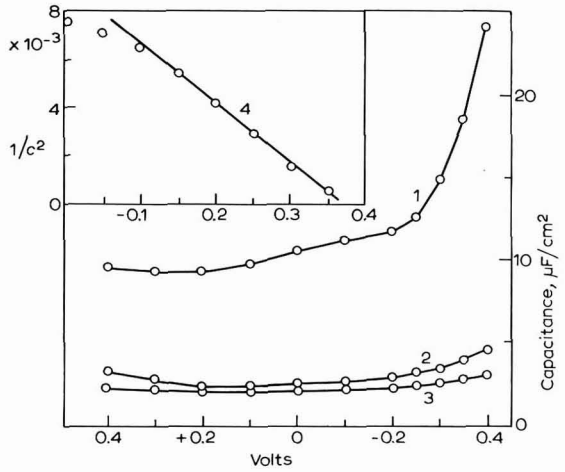

Fig. 7. Differential capacitance of OTE in 0.2 *M* KCl soln.; (1), 100 Ω square^{-1}; (2), 35 Ω square^{-1}; (3), 6 Ω square^{-1}; (4), plot of C^{-2} *vs.* potential for OTE, 100 Ω square^{-1}.

are fairly large and undoubtedly, the double layer is contributing to the measurements. In the region where the differential capacitance is low and fairly independent of potential and the type of electrolyte, the capacitance is primarily determined by the semiconductor. Capacitances under a wide variety of conditions with different OTE are being extensively examined.

Transmission spectroscopy at OTE

For an electrode reaction:

$$R \rightleftharpoons Ox + ne^- \tag{1}$$

it can be easily shown that the absorbance, A, for the light-absorbing species, Ox, is given by:

$$A = a\delta(it/nFV) = a\delta C_{Ox} \tag{2}$$

where a is the molar absorptivity of Ox, δ is the path length in cm, and the other terms have their usual significance. This assumes that Beer–Lambert Law of light absorption is obeyed. Thus, it is a simple matter to follow the concentration of a light-absorbing species formed during the course of an electrode reaction, particularly for a constant-current electrolysis where A is proportional to time, t.

For chronopotentiometry, the transition time, τ, defined by Sand's equation[15], is determined from the potential–time curve. This time, τ_A, corresponds to the linear portion of the absorbancy–time pattern which follows eqn. (2). At $t > \tau_A$, A varies as

the square root of time. Values of the chronopotentiometric constant, $i\tau^{\frac{1}{2}}/C^0$, are compared to $i\tau_A^{\frac{1}{2}}/C^0$ which is evaluated spectrally, in Table 2. The relative ease and precision of evaluating τ_A at reasonable times certainly depends on the value of a. These spectral measurements will be valuable when the transition time is poorly defined or when there are complications to the electrode reactions.

TABLE 2

SPECTRAL DETERMINATION OF TRANSITION TIMES

o-Tolidine oxidation[a]			*Ferrocyanide oxidation*[b,c]		
i (μA)	$i\tau^{\frac{1}{2}}$ ($\mu A\ sec^{\frac{1}{2}}$)	$i\tau_A^{\frac{1}{2}}$ ($\mu A\ sec^{\frac{1}{2}}$)	i (μA)	$i\tau^{\frac{1}{2}}$ ($\mu A\ sec^{\frac{1}{2}}$)	$i\tau_A^{\frac{1}{2}}$ ($\mu A\ sec^{\frac{1}{2}}$)
147	713	718	186	1478	1324
186	694	—	285	1369	1535
222	663	666	317	1368	1505
222	692	702	395	1401	1403
222	639	692			
285	622	655			
Av.	670±29	687±21		1404±30	1442±75

[a] 1.13 mM o-tolidine; pH 1.6 phosphate buffer; λ_{max} 4370 Å.
[b] 1.52 mM ferrocyanide; 0.1 M KCl; λ_{max} 4200 Å.
[c] Area of electrode different between (a) and (b).

For a semi-infinite diffusion-controlled chronoamperometric experiment at a planar electrode, the current, i_t, as a function of time obeys the Cottrell equation[15]:

$$i_t = nFD_R^{\frac{1}{2}}C_R^0 A/\pi^{\frac{1}{2}}t^{\frac{1}{2}} \tag{3}$$

The concentration of Ox monitored spectrally, if integrated through a thickness, δ, is given by:

$$\int_0^{\delta} C_{Ox}\,d\delta = \frac{1}{A}\int_0^t \frac{i}{nF}\,dt \tag{4}$$

Substituting for i from the Cottrell equation and integrating gives:

$$C_{Ox} = C_R^0 D_R^{\frac{1}{2}} 2t^{\frac{1}{2}}/\pi^{\frac{1}{2}}\delta \tag{5}$$

and since $C_{Ox} = A/a\delta$, with substitution and rearrangement of terms, the resulting equation is:

$$A/aC_R^0(D_R t)^{\frac{1}{2}} = 2/\pi^{\frac{1}{2}} = 1.128 \tag{6}$$

It is convenient to evaluate D_R experimentally if a is known, or conversely, a if D_R is known. More important, any deviation from this constant of 1.128 during a chronoamperometric experiment can be used as an indication that the electrode reaction is proceeding non-ideally. It is particularly useful in evaluating the mechanism and kinetics of homogeneous chemical reactions that follow the charge-transfer step.

The oxidation of ferrocyanide to ferricyanide is a well behaved 1-electron step electrode reaction. Since ferricyanide absorbs at 4200 Å with a molar absorptivity of 1.02×10^3 l mole^{-1} cm^{-1}, it can be followed spectrally during a chronoamperometric experiment. The diffusion coefficient of ferrocyanide was calculated from the current

decay profile during the experiment, using the Cottrell equation. The geometrically-measured area was used and may account for the diffusion coefficient being higher than the literature value[16]. The plots of i *vs.* $t^{-\frac{1}{2}}$ and A *vs.* $t^{\frac{1}{2}}$, shown in Fig. 8(A and B), are linear and the average value of the constant calculated from duplicate runs was 1.13 ± 0.01 in agreement with the theoretical value of 1.128.

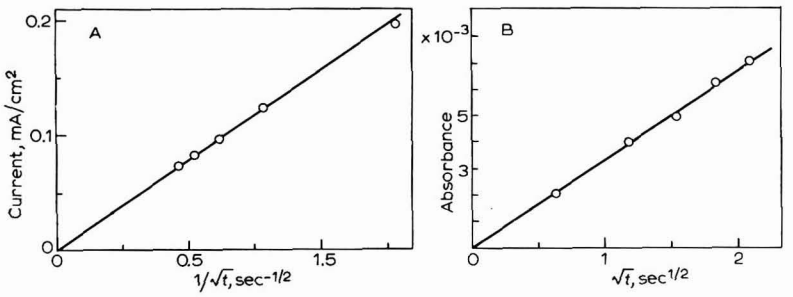

Fig. 8. Chronoamperometric oxidation of ferrocyanide at OTE.

o-Tolidine undergoes a diffusion-controlled, 2-electron transfer electrode reaction at pH 2 and obeys the Cottrell equation. The product of the 2-electron reaction absorbs at 4370 Å with a molar absorptivity of 61,000 l mole^{-1} cm^{-1}. A diffusion coefficient value of 0.65×10^{-5} cm sec^{-1} was calculated using the geometrically-measured area for the electrode. The calculated value of the constant for triplicate runs was 1.14 ± 0.01. The n-value and molar absorptivity, a, were evaluated from coulometric experiments.

The electrode reaction of *o*-tolidine is pH-dependent and as the pH is increased, a split wave develops. This pH-dependence is expected in view of previous potentiometric data[17] and suggests two successive, 1-electron steps. The product of the first wave at pH 4 shows two absorption bands at 3650 and 6300 Å. The formation and removal of the products of the oxidation and subsequent reduction waves at pH 4, can be clearly followed by monitoring spectrally at 4370 and 6300 Å during a cyclic voltammetric scan. Assuming a general scheme for the electrode reaction to be:

$$A \rightarrow B + e^- \tag{8}$$

$$B \rightarrow C + e^- \tag{9}$$

with an equilibrium reaction:

$$A + C \underset{k_b}{\overset{k_f}{\rightleftharpoons}} 2B \tag{10}$$

where k_f and k_b are the rate constants for the forward and reverse reactions in the equilibrium, a $K_{equil.}$ may be calculated using the relationship:

$$E_2 - E_1 = (RT/nF) \ln K_{equil.} \tag{11}$$

where E_1 and E_2 are the half-wave potentials for the first and second waves, respectively. A theoretical analysis of the effect of such a disproportionation equilibrium on the characteristics of the i–E curves has been discussed by HALE[18]. For our present purpose, the spectral characteristics at wavelengths of 4370 and 6300 Å

during application of a step potential followed by disconnection of the electrode (relaxation), will be discussed. Values of k_f will be evaluated from the initial portions of the relaxation. Details of the electrochemistry and spectroscopy of *o*-tolidine will be presented in a subsequent paper.

In Fig. 9, the current, potential, and absorbances as a function of time are recorded for a step potential followed by relaxation for *o*-tolidine oxidation in phosphate buffer at pH 4.0. The potential is stepped from 0.25 to 0.75 V which is

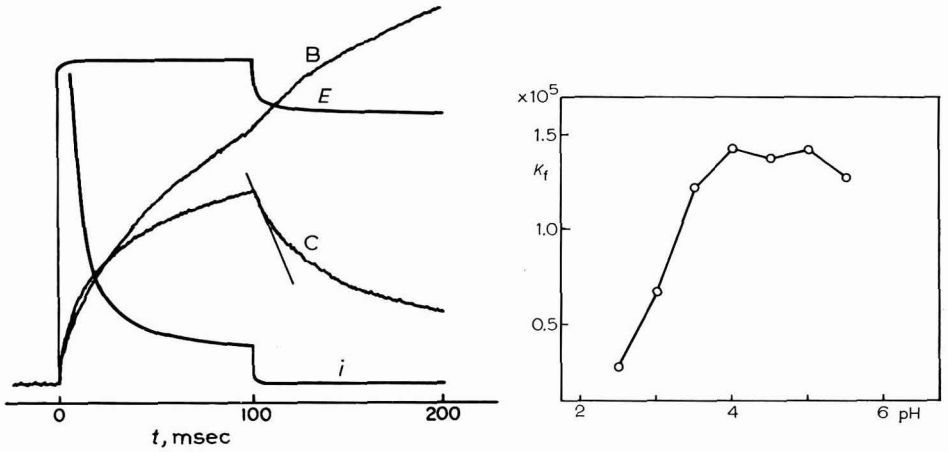

Fig. 9. Chronoamperometric oxidation of *o*-tolidine followed by relaxation: (*i*), current; (*E*), potential; (B, C), absorbance at wavelengths of 6300 and 4370 Å.

Fig. 10. Rate constant *vs.* pH.

sufficiently positive for oxidation of *o*-tolidine (A) to product (C). As C diffuses from the electrode into the bulk solution, it encounters A diffusing toward the electrode and B is formed through the disproportionation reaction. The relative concentrations of these three species in the reaction layer are governed, of course, by the values of k_f, k_b and $k_{equil.}$and favor the formation of B at the expense of C during the relaxation. It should be remembered that the light at these monitoring wavelengths is passing through the entire solution and, consequently, the absorbance values reflect the integrated concentrations. The change in concentration of C during relaxation is given by:

$$\frac{\Delta[C]}{\Delta t} = k_f[A][C] - k_b[B]^2 \tag{12}$$

and for small Δt during initial part of the relaxation, $k_b[B]^2 < k_f[A][C]$, therefore:

$$\frac{\Delta[C]}{[C]\Delta t} \cong k_f[A] \tag{13}$$

where $\Delta[C]/\Delta t$ is determined by drawing a tangent to the initial part of the absorbance for C during relaxation. The average concentrations of A and C during the time interval, Δt, were used. Values of k_f evaluated as a function of pH by the above method are plotted in Fig. 10. These values initially increase with pH and then become

fairly constant at about pH 3.8. This pH is near the pK_a of *o*-tolidine, and this suggests that the mono-protonated form is involved in the rate-determining step. It is clear that more precise calculations of rate constants in the disproportionation equilibrium require knowledge of the concentration profiles for each of the species and of the equilibrium constant. Computer calculations are in progress[19].

For studies in the ultraviolet region, quartz plates were coated with antimony-doped tin oxide. Preliminary results on the oxidation of *p*-aminophenol, which has been extensively studied electrochemically[20], have indicated that not only could the rate of hydrolysis of quinoneimine to quinone be determined, but more significantly, an additional spectral band not attributable to these two products was observed. The spectral changes that occur during and after controlled-potential coulometric oxidation of *p*-aminophenol in phosphate buffer at pH 3.5 may be seen by examination of the spectra in Fig. 11. Spectrum 1 is for *p*-aminophenol and the

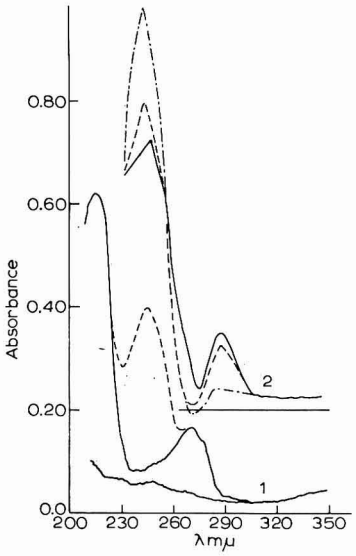

Fig. 11. Spectra of *p*-aminophenol and its electrochemical oxidation products: tin oxide-coated quartz OTE, 50 Ω square^{-1}. (1), $5 \cdot 10^{-5}$ *M* *p*-aminophenol; (2), 10^{-3} *M* *p*-aminophenol at various times after oxidation (soln. in ref. and sample beam of spectrometer identical initially, only latter oxidized).

dotted curve is for *p*-benzoquinone with maximum absorption at a wavelength of 245 mμ. Spectra were taken by placing identical solutions in the sample and reference compartments of the spectrometer and then electrolyzing the solution in the sample compartment (spectra labelled in Fig. 11 as series 2). The band at 245 mμ increases with electrolysis. The shoulder on this band at *ca.* 260 mμ is probably the quinoneimine, and decreases when the electrolysis is stopped. When the solution is allowed to stand, a new band-wavelength of 287 mμ appears while the band at 245 mμ decreases.The new band is believed to be due to a product formed from the addition reaction of either quinone or quinoneimine and *p*-aminophenol. The rate constant for this reaction, based on quinone decrease, is estimated as $2 \cdot 10^{-3}$ sec^{-1} (as a first-order

reaction). Whether or not quinoneimine is participating, is not known and further examination is warranted.

The use of OTE for the investigation of electrochemical processes offers many advantages for mechanism studies. It can be particularly valuable in cases where a chemical reaction follows the initial charge-transfer step. There are also instances in which it can help in the evaluation of electrochemical parameters.

ACKNOWLEDGEMENT

The contributions of DONALD LEEDY and FRANK A. SCHULTZ to this investigation are gratefully acknowledged. Financial support was provided by Grant No. GM 14036 from the Research Grant Branch of National Institutes of Medical Sciences, National Institutes of Health and by National Science Foundation, Grant No. GP 6479.

REFERENCES

1 R. N. ADAMS, *J. Electroanal. Chem.*, 8 (1964) 151.
2 A. K. N. REDDY AND J. O'M. BOCKRIS, *Proceedings of the Symposium on the Ellipsometer and its Use in the Measurement of Surfaces and Thin Films, J. Res. Natl. Bur. Std.*, (1963) 229.
3 A. W. COPELAND, O. D. BLACK AND A. B. GARRETT, *Chem. Rev.*, 31 (1942) 177.
4 T. KUWANA, R. K. DARLINGTON AND D. W. LEEDY, *Anal. Chem.*, 36 (1964) 2023.
5 W. N. HANSEN, T. KUWANA AND R. A. OSTERYOUNG, *ibid.*, 38 (1966) 1810.
6 V. S. SRINIVASAN AND T. KUWANA, to be published.
7 *Operational Amplifier Symposium, Anal. Chem.*, 35 (1963) 1770–1833.
8 H. LAITINEN, University of Illinois, U.S.A., private communication.
9 E. R. BROWN, T. G. MCCORD, D. E. SMITH AND D. D. DEFORD, *Anal. Chem.*, 38 (1966) 1119, and references therein.
10 P. DELAHAY AND G. L. STIEHL, *J. Phys. Chem.*, 55 (1951) 570.
11 H. HERMAN AND A. BARD, *ibid.*, 35 (1963) 1121.
12 J. N. BUTLER, *Ionic Equilibrium*, Addison-Wesley Publishing Co., Inc., Reading, Mass., 1964, p. 447.
13 W. KEMULA AND J. W. STROJEK, *Chem. Anal. Warsaw*, (in Polish), 10 (1965) 1327.
14 H. GERISCHER, *Adv. Electrochem. Electrochem. Eng.*, edited by P. DELAHAY AND C. W. TOBIAS, 1 (1961) 139.
15 P. DELAHAY, *New Instrumental Methods in Electrochemistry*, Interscience, New York, 1954.
16 M. VON STACKELBERG, M. PILGRAM AND V. TOOME, *Z. Elektrochem.*, 57 (1953) 342.
17 W. MANSFIELD CLARK, *Oxidation and Reduction Potentials of Organic Systems*, Williams and Wilkins Co., Baltimore, 1960, p. 397.
18 J. M. HAŁE, *J. Electroanal. Chem.*, 8 (1964) 181.
19 J. W. STROJEK, S. FELDBERG AND T. KUWANA, to be published.
20 D. HAWLEY AND R. N. ADAMS, *J. Electroanal. Chem.*, 10 (1965) 376, and references therein.

ELECTROANALYTICAL CHEMISTRY AND INTERFACIAL ELECTROCHEMISTRY
Elsevier Sequoia S.A., Lausanne – Printed in The Netherlands

SURFACE DIFFUSION AND GALVANOSTATIC TRANSIENTS. I

S. K. RANGARAJAN
Central Electrochemical Research Institute, Karaikudi 3 (India)
(Received April 3rd, 1967)

1. Two observations which have led to the postulation of surface-diffusion as a possible slow step in galvanostatic metal deposition (and dissolution) experiments are that (i) the rise-times of η–t curves and (ii) the "steady-state" η-values are appreciably greater than those predicted by the charge-transfer step alone. Various authors[1–10] have shown that a "surface-diffusion" model is adequate, in many cases, for the interpretation of galvanostatic transients. Attempts have also been made to evaluate the relevant parameters characterising the model. Under conditions not involving diffusion in the solution phase, the basic steps constituting the overall transfer

$$M^{z+}\,(\text{solution}) \rightleftharpoons M\,(\text{lattice})$$

are: (A) charge transfer at the planar site and (B) adatom transport to the lattice-building sites. Assuming edges to be "ideal sinks" (or sources) and an average "inter-growth-line distance", l, we can evaluate the following constants:

(i) i_0, exchange current density and $c_{ad}{}^0$, adatom concentration defined in (A) above;

(ii) D_a/l^2 (time^{-1}) where D_a is the surface-diffusion coefficient introduced by (B).

2. We give below the conclusions drawn by BOCKRIS *et al.* and the procedure adopted by them to evaluate i_0, $c_{ad}{}^0$ and D_a/l^2.

$$\text{(a)}\ \eta_{t\to 0} = a + bt \text{ where } a = RTi/zFi_0 \text{ and } b = [RT/z^2(F^2)](i/c_{ad}{}^0) \tag{1}$$

$$d\ln(\eta_t - \eta_\infty)/dt = -v_0/c_{ad}{}^0 \tag{2}$$

$$\eta_{t\to\infty} = RT/zF(i/i_0 + i/zFv_0) \tag{3}$$

and a study of $\eta_{t\to\infty}$–log i curves can be used to find i_0, α_c and α_a.

(b) v_0, defined in eqns. (2) and (3), is termed the "surface-diffusion velocity" and is identified[2–10] with $D_a c_{ad}{}^0/l^2$ and hence is supposedly independent of i_0.

$$v_0 = D_a c_{ad}{}^0/l^2 \tag{4}$$

(c) The rise-times for the galvanostatic and the potentiostatic transients, τ_g and τ_p, respectively, are given[9] as

$$\tau_g = 2c_{ad}{}^0/v_0 \tag{5}$$

and

$$\tau_p = 2c_{ad}{}^0/(2v_0 + pc_{ad}{}^0) \tag{6}$$

so that

$$(\tau_g/\tau_p) = 2 + i_0/zFv_0, \quad \eta \to 0 \tag{7}$$

It has been suggested[9] that (i_0/v_0) can also be deduced from eqn. (7).

(d) A sort of "coverage effect" for the cathodic rate is introduced[4,6,8] in the following way allowing for a "finiteness" of metal atoms on the surface.

$$i = i_0[(c_{ad}/c_{ad}^0) \exp(\alpha_a F\eta/RT) - (G-c_{ad})/(G-c_{ad}^0) \exp(-\alpha_c F\eta/RT)] \tag{8}$$

In eqn. (8), G is the total number of metal atoms on the surface. With

$$r = i_0/zFv_0 \tag{9}$$

and

$$\theta' = c_{ad}^0/(G-c_{ad}^0)\,, \tag{10}$$

the i–η relationship was proved to be:

$$i/i_0 = [\exp(\alpha_a F\eta/RT) - \exp(-\alpha_c F\eta/RT)] \cdot [1 + r\exp(\alpha_a F\eta/RT) + \theta' r \exp(-\alpha_c F\eta/RT)]^{-1} \tag{11}$$

Equation (11) predicts, in particular, surface-diffusion controlled limiting currents and experimental evidence is adduced[6,8] to support this claim.

(e) The theory of galvanostatic transients that results in eqns. (1)–(11) is worked out[2,8] assuming that the instantaneous adion concentration is governed by the equation

$$\partial c_{ad}/\partial t = i/zF - [(D_a/l^2)(c_{ad}/c_{ad}^0) - 1] \tag{12}$$

with $c_{ad} = c_{ad}^0$ at $t = 0$.

3. We now show that many of the equations cited need modifications to avoid erroneous conclusions.

A. Steady-state potential

Whereas the complications inherent in deriving an *exact* potential–time profile under galvanostatic conditions are obvious[11,12], the problem of obtaining the i–η $(t \to \infty)$ relationship is extremely simple. As long as the mass transfer problems in the solution phase are ignored and $t \gg \tau_g$, one need only solve

$$D_a \partial^2 c_{ad}/\partial x^2 + (i_0/zF)[\exp(\alpha_c F\eta_\infty/RT) - (c_{ad}(x)/c_{ad}^0) \exp(-\alpha_a F\eta_\infty/RT)] = 0 \tag{13}$$

The boundary conditions are

$$(\partial c_{ad}/\partial x)_{x=l} = 0 \tag{14}$$

and

$$c_{ad} = c_{ad}^0 \quad \text{at} \quad x = 0; \tag{15}$$

and

$$i/i_0 = [\exp(\alpha_c F\eta_\infty/RT) - (c_{av}/c_{ad}^0) \exp(-\alpha_a F\eta_\infty/RT)] \tag{16}$$

where

$$c_{av} = (1/l) \int_0^l c_{ad}(x)\,dx$$

and

$$\eta_\infty = \eta(t \gg \tau_g). \tag{17}$$

In eqns. (13)–(17), no restrictions are placed on the magnitude of i and the model is the same as assumed by BOCKRIS *et al.*

The solution of (13) with (14)–(17) gives

$$i = i_0[\exp(\alpha_c F\eta_\infty/RT) - \exp(-\alpha_a F\eta_\infty/RT)] \cdot \tanh[\Omega \exp(-\alpha_a F\eta_\infty/2RT)] \cdot [1/\Omega] \cdot \exp(\alpha_a F\eta_\infty/2RT)\ . \tag{18}$$

$$\Omega = \sqrt{i_0/zFc_{ad}{}^0 D_a} \cdot l \tag{19}$$

(In eqn. (18) and in the following equations, we use η and η_∞ in an interchangeable sense.) Equation (18) shows that the i–η relationships under potentiostatic and galvanostatic (steady) conditions are identical.

Let $i\Omega/i_0 \ll 1$.

Then

$$(\alpha_c + \alpha_a) F\eta/RT = (i/i_0)\Omega \coth \Omega \tag{20}$$

Equation (3) differs radically from eqn. (20) if $v_0 = D_a c_{ad}{}^0/l^2$, as assumed by MEHL AND BOCKRIS (eqn. (14)). That it is wrong to identify v_0 with $(D_a c_{ad}{}^0/l^2)$ is shown in Appendix I.

B. Galvanostatic rise-times

Although the i *vs.* η behaviour (eqn. (18)) is derived easily—without any restriction on the magnitude of i (or η)—the same cannot be said of galvanostatic rise-times. Two limiting cases[14], however, offer themselves for easy analysis.

$$(i)\ \alpha_a = 0 \tag{21}$$

Writing

$$(i_0/zF)(\exp(\alpha_c F\eta/RT) - 1) = \phi(t) \tag{22}$$

and

$$\Phi(p) = p\int_0^\infty \exp(-pt)\,\phi(t)\,dt \tag{23}$$

it can be proved that

$$\Phi(p) = (i/zF)[p/(p+k_2) + k_2/(p+k_2) \cdot \tanh(\sqrt{(p+k_2)/D_a} \cdot l) \cdot (1/(\sqrt{(p+k_2)/D_a} \cdot l))]^{-1} \tag{24}$$

$(ii)\ zF\eta/RT \ll 1$

Let

$$\bar{\eta}(p) = p\int_0^\infty \exp(-pt) \cdot \eta(t)\,dt \tag{25}$$

Then

$$(\alpha_c + \alpha_a) F\bar{\eta}(p)/RT = (i/i_0)[p/(p+k_2) + k_2/(p+k_2) \cdot \tanh(\sqrt{(p+k_2)/D_a} \cdot l)/(\sqrt{(p+k_2)/D_a} \cdot l)]^{-1} \tag{26}$$

In eqns. (24) and (25),

$$k_2 = i_0/(zFc_{ad}{}^0) \tag{27}$$

Whereas eqn. (24) is derived without assuming that η is small, (25) is true for small $zF\eta/RT$. The nature of the poles of functions in the right-hand side of eqns. (24) or (25) must be studied to evaluate the rise-time. Such a study suggests that, when surface diffusion is indeed important,

$$\tau_g \simeq (2X_0/k_2) \coth X_0 , \tag{28}$$

where X_0 is a non-zero real root of

$$\tanh X + X(X^2/\Omega^2 - 1) = 0 \tag{29}$$

(*Note*: There is no ambiguity in eqn. (28) because eqn. (29) has only three real roots: $-X_0$, 0 and X_0).

$|X_0| < \Omega$ and for large Ω,

$$\tau_g \underset{\sim}{>} 2(\Omega - \tfrac{1}{2})/k_2 \tag{30}$$

Illustration	Ω^2	10	50	100
	X_0	2.44	6.5	9.5

A comparison of eqn. (30) and eqns. (2) or (5) shows that $\tau_g \neq 2c_{ad}{}^0/v_0 = 2l^2/D_a$. Under conditions favourable to surface diffusion, $\tau_g \simeq 2l\sqrt{zFc_{ad}{}^0/i_0 D_a}$ and

$$\tau_g/\tau_p \simeq (\Omega - \tfrac{1}{2}) \tag{31}$$

It is interesting that such a change in the order of rise-times in the potentiostatic and galvanostatic cases is possible. *Both* τ_g and τ_p depend upon i_0 and $c_{ad}{}^0$ (*cf.* ref. 9).

We have shown above that the steady-state overpotential and the galvanostatic rise-times as given by eqns. (3)–(5) are incorrect. An alternative expression for τ_g/τ_p (*cf.* eqns. (7) and (31)) was also presented, but, under limiting conditions ($\Omega \gg 1$), it is possible to retain eqns. (3) and (5) by abandoning (4) and writing instead,

$$v_0/c_{ad}{}^0 \simeq k_2/\Omega \tag{32}$$

The significance of eqn. (32) is explained in Appendix I.

C. Illustration

(i) Surface-diffusion process in the electrodeposition of silver from molten halides[10]:

$T = 450°$, $i_0 = 190$ A cm^{-2}, $c_{ad}{}^0 = 9 \cdot 10^{-10}$ mol cm^{-2}, $Fv_0 \sim 3.3$ A cm^{-2}, $k_2 \sim 2 \cdot 10^6$ sec^{-1}. The *correct* values for Ω and D_a/l^2 are $\Omega = 54$, $D_a/l^2 \sim 6.0 \times 10^2$ sec^{-1} from eqns. (20) and (30), whereas eqn. (4) would give $\Omega \sim 7.4$ and $D_a/l^2 \sim 3.66 \times 10^4$.

(ii) Deposition of gallium[6]

$T = \pm 0.5°$, $i_0 = 1.4 \times 10^{-4}$ A cm^{-2}, $c_{ad}{}^0 = 5 \cdot 10^{-11}$ m cm^{-2}, $zFV_0 = 5.5 \times 10^{-5}$ A cm^{-2}, $k_2 \sim 10$ sec^{-1}, $\Omega \sim 3$, $D_a/l^2 \sim 1$ sec^{-1}. Equation (4) gives $\Omega < 1.6$ and $D_a/l^2 \sim 4$ sec^{-1}.

D. i–η Curves under "coverage-effects"

If we assume, with BOCKRIS, the expression for i as given by eqn. (8), it is easy to set up and solve steady-state diffusion equations appropriate to the model used. The result is

$$i/i_0 = [\exp(\alpha_c F\eta/RT) - \exp(-\alpha_a F\eta/RT)] \cdot \tanh [\Omega \times$$
$$\sqrt{\exp(-\alpha_a F\eta/RT + \theta' \exp(\alpha_c F\eta/RT)}] \cdot [\Omega \sqrt{\exp(-\alpha_a F\eta/RT) + \theta' \exp(\alpha_c F\eta/RT)}]^{-1} \tag{33}$$

(Ω, θ' are given by eqns. (19) and (10), respectively). That eqn. (33) is essentially different from (11) is obvious. The error committed by using (11) (in evaluating various parameters) can be serious indeed.

Equation (33) reduces to (18) as $\theta' \to 0$, as it should be—whereas (11) reduces to an erroneous i–η relationship. Again, eqn. (11) predicts *limiting* currents[4,6,8] while (33) *does not*. On the other hand, (33) implies that, if $\theta' \ll 1$, a change in cathodic Tafel slope from its true value of $2.303\ RT/\alpha_c F$ to one that is twice this, is possible.

On the (cathodic) η–log i plot, eqn. (33) marks three types of behaviour:

(i) $1 \gg (\alpha_c + \alpha_a) F\eta/RT$

linear η–i as given by eqn. (20); $d\eta/di \simeq \Omega/i_0$

(ii) $\theta' \exp(\alpha_c + \alpha_a) F\eta/RT \ll 1$, $\exp(\alpha_a F\eta/2RT) \gg \Omega$;

linear η–log i

slope $2.303\ RT/\alpha_c F$
intercept $\ln i_0$.

(iii) $\theta' \exp(\alpha_c + \alpha_a) F\eta/RT \gg 1$, $\Omega/\theta' \exp(\alpha_c F\eta/RT) > 5$

linear	η–log i
slope	$2(2.303\ RT/\alpha_c F)$
intercept	$\ln(i_0/\Omega/\theta')$

A change-over in the cathodic Tafel slopes as indicated above by (ii) and (iii) is a direct consequence of "the coverage-effect" introduced in the model (eqn. (18) predicts only a transfer* to (ii) from (i) and no transition to (iii) is suggested).

E. To sum up, the theory of the surface-diffusion model predicts that:

(a) The steady-state overpotential, η, is related to i through $(\alpha_c + \alpha_a) F\eta/RT = i\Omega \coth \Omega/i_0$ if $|zF\eta/RT| \ll 1$.

(b) The galvanostatic rise-time, τ_g, for small current densities is given approximately by:

$$\tau_g = 2(\tanh X_0/X_0)(1/k_2)$$

where X_0 is the real root of

$$\tanh X + X(X^2/\Omega^2 - 1) = 0$$

(c) The "velocity of surface-diffusion", v_0 of BOCKRIS, wrongly identified with $(D_a c_{ad}{}^0/l^2)$, can at best be formally equated with $k_2{}^0/\Omega$ to obtain better results under limiting conditions (Ω: large).

(d) The i–η curves deduced from eqn. (33) under "*coverage-effects*" are erroneous and a corrected equation for the same model gets rid of the prediction of "limiting-currents". On the other hand, a doubling of the slopes is predicted.

(e) The theoretical analysis (eqns. (18) and (33)) shows that *if* surface-diffusion ever controls at near-equilibrium conditions, it subsequently continues to dominate in the anodic side, until, of course, the theoretical model itself fails to represent the phenomenon. And, for large anodic overpotentials (or currents), even though a Tafel

* If Ω is large enough, an anomalous intermediate behaviour is *possible*, *viz.*, a Tafel behaviour with the slope $(RT/(\alpha_c + \alpha_a/2)F)$ over the region: $1 \ll \exp(\alpha_a F\eta/RT) < (\Omega/5)^2$. Such an effect, if observed, can be important evidence in favour of the surface-diffusion model.

behaviour may be observed, the slope is equal to $2(2.303\ RT/\alpha_a F)$ (twice its "true" slope) and "i_0" calculated in the usual way from this Tafel-intercept $= i_0^{app} = i_0/\Omega$. No experimental confirmation, however, is reported*†.

Lastly, a comment on the model. In the foregoing discussions, a criticism of the theory of BOCKRIS *et al.* (assuming the same model as theirs) was presented. We point out that "a slow rise-time" and "a large overpotential" are not unique to a "slow surface-diffusion" model. A model that assumes a fast diffusion on the surface followed by a slow incorporation at the lattice-building sites exhibits similar characteristics[13–15]. If the condition $D_a(\partial c_{ad}/\partial x) = k_3(c_{ad} - c_{ad}^0)$ at the edge ($x = 0$) is used instead of (15), it is easy to show that a rise-time, $\tau_g \simeq 1/k_3$, results for the latter model. More exactly, $\tau_g \simeq k_2/[\Omega + k_2 l/k_3]$ and $\tau_p \simeq k_2$ (see Appendix I) for large Ω. This amounts to identifying v_0 with $(k_3 c_{ad}^0/l)$. Although a similar discussion of i–η curves for this model could be useful, we omit this, for the sake of brevity.

Results concerning the η–t profiles for the generalised galvanostatic case will be communicated later.

ACKNOWLEDGEMENT

The author thanks Professor K. S. G. Doss, Director, Central Electrochemical Research Institute, Karaikudi, India, for very useful discussions.

SUMMARY

The theoretical results concerning the galvanostatic transients in the problem of electrodeposition, with surface-diffusion as a slow-step, are derived. The explanations offered and the theory presented by BOCKRIS *et al.* are critically discussed, and modifications are proposed.

APPENDIX I

The error involved in using eqn. (12) instead of the more accurate eqn. (13) is reflected through the approximation implicit** in

$$D_a \partial^2 c_{ad}/\partial x^2 \simeq D_a/l^2 (c_{ad} - c_{ad}^0) \qquad (A.1)$$

(A.1) helps to get rid of the dependence of c_{ad} on x and therefore $c_{ad} = c_{ad}^{av}$ where

$$c_{ad}^{av} = 1/l \int_0^l c_{ad} \cdot dx \, . \qquad (A.2)$$

The solution of eqn. (12) is a function of t only and with

* It has been noted during gallium deposition and dissolution, that $d\eta/d \log i_a = 45$–55 mV and thus, if surface-diffusion control as discussed above, exists, $d\eta/d(\log i_a) \simeq (2.303)\, 2RT/\alpha_a F$, making a value of 2.5 for α_a plausible. Also $d\eta/di = RT/F(\alpha_c + \alpha_a)(1/i_0 + 1/zFv_0)$ (eqn. (23) of ref. 6), shows a reasonable agreement with experiments if $\alpha_c + \alpha_a = 3$. Again, the relationship, $d \ln i_0/d \ln (H_2GaO_3^-) = 1 - \beta/3$, is true for mechanism (A) (ref. 6) as well as (D). The above reasoning shows that mechanism (A) need not be ruled out as improbable.

† Also see ref. (7) where $i_{0,a}$ (Tafel) $< i_{0,c}$ (Tafel).

** (A.1) does not imply a linear concentration gradient (*cf.* refs. 2–8).

$$i = i_0[\exp(\alpha_c F\eta/RT) - (c_{ad}{}^{av}/c_{ad}{}^0)\exp(-\alpha_a F\eta/RT)] \tag{A.3}$$

or eqn. (8), the derivation of the η–t profile as given by (1)–(3) is immediate.

But even for $|zF\eta/RT| \ll 1$, (A.1) is very approximate, if not arbitrary. A more realistic, though *heuristic*, procedure is given below:

Integrate (13) from $x=0$ to $x=l$ with respect to x. Then using (14) and (A.2)–(A.3),

$$\partial c_{ad}{}^{av}/\partial t = -(D_a/l)(\partial c_{ad}/\partial x)_{x=0} + i/zF\,. \tag{A.4}$$

At this stage, we resort to an approximation

$$(\partial c_{ad}/\partial x)_{x=0} = (c_{ad}{}^{av} - c_{ad}\ (x=0))/\delta \tag{A.5}$$

$$= (c_{ad}{}^{av} - c_{ad}{}^0)/\delta \text{ if } c_{ad}\ (x=0) = c_{ad}{}^0 \tag{A.6}$$

(A.5) assumes a linear concentration gradient in the interval $(0, \delta)$, and for $x > \delta$, $c_{ad} = c_{ad}{}^{av}(t)$. Such "cut-off" models can give interesting results under *limiting* conditions. Thus, an "estimate" for δ, *viz.*, $\sqrt{D\tau}$, where τ is the "life-time" for an adatom, suggests itself. $\tau \simeq 1/k_2$ and thus $\delta \sim \sqrt{D/k_2}$ $(\ll l)$.

An essential condition for this linearisation to hold is $(\delta/l) \ll 1$ (note that $\partial c_{ad}/\partial x)_{x=l} = 0 \neq \partial c_{ad}/x)_{x=0}$) *i.e.*, $\Omega \gg 1$

(A.4) and (A.5) then give

$$\partial c_{ad}{}^{av}/\partial t = -(D_a/\delta l)(c_{ad}{}^{av} - c_{ad}{}^0) + i/zF \tag{A.7}$$

Hence, under *limiting* conditions, one could possibly identify $v_0/c_{ad}{}^0$ with $D_a/\delta l = k_2/\Omega$. This explains how an agreement can be found at all, under the condition $\Omega \gg 1$, if we take $v_0/c_{ad}{}^0 = k_2/\Omega$ instead of equating v_0 with $D_a c_{ad}{}^0/l^2$.

This heuristic reasoning may be extended to the case when the lattice incorporation is slow. We abandon, then, the assumption of an equilibrium at the growth-edges, *i.e.*, $c_{ad}(0) \neq c_{ad}{}^0$. Instead, we have

$$D_a \partial c_{ad}/\partial x = k_3(c_{ad} - c_{ad}{}^0) \quad \text{at } x=0. \tag{A.8}$$

(A.5) is still true but (A.6) is not.

$$(D_a \partial c_{ad}/\partial x)_{x=0} = D_a(c_{ad} - c_{ad}(x=0))/\delta \tag{A.9}$$

$$= k_3(c_{ad}\ (x=0) - c_{ad}{}^0)$$

Eliminating $c_{ad}\ (x=0)$, (A.4) can be rewritten as

$$\partial c_{ad}{}^{av}/t = -\{D_a/[l\delta(1 + D_a/k_3\delta)]\} \cdot (c_{ad}{}^{av} - c_{ad}{}^0) + i/zF \tag{A.10}$$

(A.10) reduces to (A.7) as $(k_3\delta/D_a) \to \infty$. Thus

$$v_0/c_{ad}{}^0 \sim k_2/[\Omega + k_2 l/k_3] \ (\Omega\text{: large})$$

$$\to k_3/l, \text{ if } k_2 l/k_3 \gg \Omega \gg 1.$$

REFERENCES

1 H. GERISCHER, *Z. Elektrochem.*, 62 (1958) 256.
2 W. MEHL AND J. O'M. BOCKRIS, *Can. J. Chem.*, 37 (1958) 190; *J. Chem. Phys.*, 27 (1957) 817.
3 A. R. DESPIC AND J. O'M. BOCKRIS, *J. Chem. Phys.*, 32 (1960) 389.
4 J. O'M. BOCKRIS AND M. ENYO, *Trans. Faraday Soc.*, 58 (1962) 1187.

5 H. KITA, M. ENYO AND J. O'M. BOCKRIS, *Can. J. Chem.*, 39 (1961) 1670.
6 J. O'M. BOCKRIS AND M. ENYO, *J. Electrochem. Soc.*, 109 (1962) 48.
7 J. O'M. BOCKRIS AND H. KITA, *J. Electrochem. Soc.*, 109 (1962) 928.
8 J. O'M. BOCKRIS AND A. DANJANOVIC, *Modern Aspects of Electrochemistry*, No. 3, edited by J. O'M. BOCKRIS AND B. E. CONWAY, Butterworths, London, ch. IV.
9 A. DAMJANOVIC AND J. O'M. BOCKRIS, *J. Electrochem. Soc.*, 110 (1963) 1035.
10 T. B. REDDY, *J. Electrochem. Soc.*, 113 (1966) 117.
11 M. FLEISCHMANN AND H. R. THIRSK, *Advan. Electrochem. Electrochem. Eng.*, edited by P. DELAHAY, Interscience, New York, 1963, ch. III.
12 S. K. RANGARAJAN, *Can. J. Chem.*, 43 (1965) 1052.
13 M. FLEISCHMANN AND J. A. HARRISON, *J. Electroanal. Chem.*, in press.
14 M. FLEISCHMANN, S. K. RANGARAJAN AND H. R. THIRSK, *Trans. Faraday Soc.*, 63 (1967) 1240.
15 J. A. HARRISON, S. K. RANGARAJAN AND H. R. THIRSK, *J. Electrochem. Soc.*, 113 (1966) 1120.

ANNOUNCING .....

advances in
MOLECULAR RELAXATION PROCESSES
an international journal

Editors:

W.J. ORVILLE-THOMAS (Salford, Great Britain)
J. MEIXNER (Aachen, Germany)

Consultant Editor:

C.J.F. BÖTTCHER (Leyden, The Netherlands)

ELSEVIER PUBLISHING COMPANY AMSTERDAM

advances in MOLECULAR RELAXATION PROCESSES

An International Journal Devoted to the Study of the Phenomena of Viscoelasticity and Acoustic, Dielectric and Magnetic Relaxation

The field of relaxation processes is very diversified. It comprises phenomena in viscoelasticity, acoustics, in the electrical and magnetic behaviour of materials. There are physical, chemical and engineering aspects. Nevertheless relaxation processes belong, at least from a theoretical point of view, to a well defined and consistent field of natural science.

The exploration and cultivation of relaxation processes has led to considerable insight into molecular mechanisms which are responsible for the observed relaxation behaviour of materials under various external influences. It has also led to such powerful research tools as magnetic resonance and relaxation.

Recently molecular relaxation studies have emerged as one of the fastest growing and most exciting new fields in chemical physics. In these studies equilibrium systems are perturbed by a sudden change in an external parameter (e.g. temperature or electric field strength) so that a time-lag occurs between the external change and the new equilibrium position: i.e. there is a definite delay between 'cause' and 'effect' and the system is said to 'relax'. The way in which relaxation occurs is related to the rate constants for the reactions involved in the equilibrium. Since the range of half-times accessible using the various relaxation techniques extends from 10^{-9} to over 1 sec. a large part of the fast-reaction kinetic field can be covered. Particularly interesting developments concern chemical reactions in biological systems.

It is intended to publish authoritative review articles covering all aspects of molecular relaxation processes based on the increasing variety of methods which have become available in recent years and which will undoubtedly increase in the future. In addition significant original work in paper or review form is acceptable. Authors are encouraged to be speculative as well as informative.

EDITORS of the journal are
Professor W.J. Orville-Thomas, University of Salford,
SALFORD 5, Great Britain

and

Professor J. Meixner, Institut für Theoretische Physik, Technische Hochschule
Templergraben 55, 51 AACHEN, Germany

CONSULTANT EDITOR is C.J.F. Böttcher, LEYDEN, The Netherlands

PUBLICATION will be in approximately one volume of four issues per year.

SUBSCRIPTION PRICES are £10.9.6, US$25.00, Dfl. 90.00 per volume plus postage. Subscription orders may be sent to your regular supplier or to:

ELSEVIER PUBLISHING COMPANY, P.O. Box 211, AMSTERDAM, The Netherlands

SPECIMEN COPIES will be sent by the publishers on request.

LANGUAGES will be English, French and German, but manuscripts should preferably be submitted in English.

MANUSCRIPTS may be submitted to one of the Editors. It is requested that unsolicited reviews are cleared with the Editors before the manuscript is submitted so that duplication of effort may be avoided. Manuscripts should be in double-spaced typing. References should be given at the end of the paper; they should be numbered consecutively and the numbers should appear in the text at the appropriate places.

ILLUSTRATIONS should follow these rules: line drawings to be preferably in a form suitable for reproduction, drawn in Indian ink on drawing paper or tracing paper, with lettering etc. in pencil; photographs to be submitted as clear black-and-white prints on glossy paper. Legends to the illustrations should be typed on a separate page of the manuscript, and not underneath the drawings or on the reverse of photographs. All illustrations should be numbered consecutively throughout the paper.

PROOFS will be sent to the author who should check them against his own carbon copy of the manuscript.

CONTENTS:

VOLUME 1, No. 1

VOLUME 1, No. 2

FORTHCOMING PAPERS

journal of MOLECULAR STRUCTURE

Editors: W.J. Orville-Thomas (Salford, Great Britain)
J. Lecomte (Paris, France)
E. Lippert (Berlin, Germany)

The main object of this journal is to overcome the fragmentation of structural work between numerous publications and to speed up publication. The journal appears bi-monthly and one volume is published per year. Subscription price: £10.9.6, US$25.00, Dfl. 90.00 per volume (plus postage).

A selection of published papers:

Time-dependent interactions in di-tert-butyl-nitroxide (DBNO) as studied by ESR and proton relaxation
D. Stehlik, H. Brunner and K.H. Hausser (Heidelberg, Germany)

Group vibrations and the vibrational analysis of molecules containing methyl groups. III. Dimethyl ether, dimethyl sulphide, dimethyl selenide and dimethyl telluride
J.M. Freeman and T. Henshall (Salford, Great Britain)

Zur Konfigurationsanalyse der Tercyclohexyle
W. Brügel, E. Kuss, P. Pollmann und H. Stegemeyer (Ludwigshafen/Rh. und Hanover, Germany)

Propriétés statistiques des interactions moléculaires dans les solutions liquides. I. Formulation générale. II. Application au calcul des hauteurs de barrières de potentiel s'opposant à la libre rotation de HCl dissout dans CCl_4
L. Bonamy, D. Robert et L. Galatry (Besançon, France)

Electron diffraction by gases. The molecular structure of 1,4-cyclohexadiene
G. Dallinga and L.H. Toneman (Amsterdam, The Netherlands)

Experimental and semi-theoretical investigations of O, S, and Se-amides and ureas. I. The electronic configurations
A. Ažman, M. Drofenik, D. Hadži and B. Lukman (Ljubljana, Yugoslavia)

Vibrational spectrum and structure of solid $TlAu(CN)_2$
H. Stammreich. B.M. Chadwick and S.G. Frankiss (Sao Paulo, Brazil and London, Great Britain)

The vibrational spectra and structure of methyl acrylate and vinyl acetate
W.R. Feairheller Jr. and J.E. Katon (Dayton, Ohio, U.S.A.)

Further details are available on request from the publishers:

ELSEVIER PUBLISHING COMPANY - P.O. Box 211 - Amsterdam, The Netherlands

PRINTED IN THE NETHERLANDS

ELECTROANALYTICAL CHEMISTRY AND INTERFACIAL ELECTROCHEMISTRY
Elsevier Sequoia S.A., Lausanne – Printed in The Netherlands

THE CONGRUENCE OF THE ADSORPTION ISOTHERM WITH RESPECT TO THE ELECTRODE POTENTIAL OR CHARGE AND THE CHOICE OF AN INDEPENDENT ELECTRIC VARIABLE

A. N. FRUMKIN, B. B. DAMASKIN AND A. A. SURVILA
Moscow State University, Institute of Electrochemistry, Academy of Sciences of the USSR, Moscow (USSR)
(Received July 10th, 1967)

It is known that the adsorption isotherm of a solution component at constant electrode potential (E) can be obtained by a strictly thermodynamic method from the basic equation of electrocapillarity[1], which to the first approximation (that is with the concentration (c) substituted for the activity and at constant concentration of the other solution components) can be written as:

$$\mathrm{d}\sigma = -q\,\mathrm{d}E - RT\Gamma\,\mathrm{d}\ln c \tag{1}$$

where σ is the interfacial tension, q the electrode charge density, Γ the Gibbs adsorption, R the gas constant and T the absolute temperature.

In order to find the adsorption isotherm at q=const. by a thermodynamic method, it is necessary to introduce a new function[2]:

$$\xi = \sigma + qE \tag{2}$$

which enables the basic equation of electrocapillarity to be written in the form:

$$\mathrm{d}\xi = E\,\mathrm{d}q - RT\Gamma\,\mathrm{d}\ln c \tag{3}$$

The adsorption isotherms obtained from the experimental data by means of eqns. (1) and (3) are self-consistent in the sense that by calculating (by means of eqn. (1)) the Γ–c curve at E=const. and knowing the dependence of q on E at different concentrations of the adsorbed substance, it is possible to plot the Γ–c curve at q=const., which exactly coincides with the adsorption isotherm calculated by means of eqn. (3). Thus, with a strictly thermodynamic approach to the investigation of the adsorption isotherms, the choice of an electric variable is of no fundamental importance and is determined by considerations of expediency or convenience. For instance, in studying the adsorption of inorganic ions, it is more convenient to consider the isotherms at q=const., since according to the Gouy–Chapman theory, the diffuse layer structure is determined by the value of the charge.

This is not the case, however, when the thermodynamic approach to the investigation of adsorption on electrodes is supplemented by some model assumptions, in particular by the assumption of the congruence of the adsorption isotherm with respect to one of the electric variables. The condition of the congruence of the isotherm with respect to the potential can be written in the form of an equation:

$$Bc = f(\Gamma) \tag{4}$$

and a similar condition of congruence with respect to the electrode charge as the equation:

$$Gc = f(\Gamma) \tag{5}$$

where $B = B(E)$ and $G = G(q)$ represent adsorption equilibrium constants, which are functions of E and q, respectively, and $f(\Gamma)$ is a function of Γ*. The discussion in connection with the choice of an electric variable[3-5] is essentially bound up with the question as to whether eqns. (4) and (5) are compatible, and if not, which of them agrees better with the experimental data. Let us consider this question in more detail.

It was shown by PARSONS[5] for the case of adsorption on mercury of *n*-butanol from its solutions in 0.1 *N* NaF used as a supporting electrolyte, that the curves of the dependence of the two-dimensional pressure at constant potential, $\Delta\sigma = \sigma_0 - \sigma$, or at constant charge, $\Delta\xi = \xi_0 - \xi$, upon log c, measured at different E or q, respectively, will coincide with the accuracy of the order of 3–4 dyn cm^{-1} if these curves are shifted along the abscissa (the values of σ_0 and ξ_0 are for a pure supporting electrolyte solution). Since the shape of the adsorption isotherm is determined by those of the $\Delta\sigma$–log c curves at E = const., or of the $\Delta\xi$–log c curves at q = const. (see eqns. (1) and (3)), it can be concluded from PARSONS' data that eqns. (4) and (5) are compatible and thus it is possible to choose the one that is more convenient for use. A similar conclusion was drawn also from PAYNE's studies[6] on the adsorption on mercury of NO_3^- and ClO_4^- anions.

The analysis of eqns. (4) and (5) shows, however, that their compatibility depends on the fulfilment of definite conditions since they correspond to different models of the adsorption layer. In fact, it follows from eqns. (1) and (4) that:

$$\frac{\partial \ln B}{\partial E} = -\left(\frac{\partial \ln c}{\partial E}\right)_\Gamma = \frac{1}{RT}\left(\frac{\partial q}{\partial \Gamma}\right)_E \tag{6}$$

which gives after integration,

$$q = RT\left(\frac{\partial \ln B}{\partial E}\right)\Gamma + q_0 = A\left(\frac{\partial \ln B}{\partial E}\right)\theta + q_0 \tag{7}$$

where $\theta = \Gamma/\Gamma_m$; Γ_m is the limiting value of Γ, q_0 the value of q at $\theta = 0$ and $A = RT\Gamma_m$. Let the charge at $\theta = 1$ and the given potential be q', then

$$q' = A\left(\frac{\partial \ln B}{\partial E}\right) + q_0 \tag{8}$$

It follows from (7) and (8) that:

$$q = q_0(1-\theta) + q'\theta \tag{9}$$

from which the true differential capacity, C_{true}, is

$$C_{true} = \left(\frac{\partial q}{\partial E}\right)_\theta = C_0(1-\theta) + C'\theta \tag{10}$$

where $C_0 = \mathrm{d}q_0/\mathrm{d}E$ and $C' = \mathrm{d}q'/\mathrm{d}E$.

* In our treatment we neglect the difference between the total potential drop and the potential drop in the adsorbed layer; this does not lead to serious errors in the concentration range considered.

Thus, the assumption that the adsorption isotherm is congruent with respect to the potential corresponds to the model of the surface layer in the form of two parallel capacitors[7]. There are water molecules between the plates of one, and particles of adsorbed substance between the plates of the other.

On the other hand, it follows from eqns. (3) and (5) that:

$$\frac{\partial \ln G}{\partial q} = -\left(\frac{\partial \ln c}{\partial q}\right)_{\Gamma} = -\frac{1}{RT}\left(\frac{\partial E}{\partial \Gamma}\right)_{q} \tag{11}$$

which gives on integration:

$$E = -RT\left(\frac{\partial \ln G}{\partial q}\right)\Gamma + E_0 = -A\left(\frac{\partial \ln G}{\partial q}\right)\theta + E_0 \tag{12}$$

where E_0 is the value of E at $\theta = 0$, corresponding to a given charge, q. If the potential at a given charge, q, and at $\theta = 1$ is E',

$$E' = -A\left(\frac{\partial \ln G}{\partial q}\right) + E_0 \tag{13}$$

From eqns. (12) and (13) we find:

$$E = E_0(1-\theta) + E'\theta \tag{14}$$

and further

$$\frac{1}{C_{\text{true}}} = \left(\frac{\partial E}{\partial q}\right)_{\theta} = \frac{1-\theta}{C_0} + \frac{\theta}{C'} \tag{15}$$

Thus, the assumption that the adsorption isotherm is congruent with respect to the charge corresponds to the model of two capacitors connected in series.

It can be readily seen that the difference between these two models disappears at $C_0 = C'$, when eqns. (10) and (15) give the same result: $C_{\text{true}} = C_0$. In other words, at $C_0 = C'$, the model of two parallel capacitors does not contradict the summation of the potential differences in the solvent layer and in the adsorbed substance layer. Thus, the compatibility of eqns. (4) and (5) is determined by the fulfilment of the condition, $C_0 = C'$. This condition is approximately fulfilled in the case of adsorption of NO_3^- and ClO_4^- anions on mercury, which accounts for PAYNE's experimental data[6].

If the condition $C_0 = C'$ is fulfilled, the choice of an independent variable is not of fundamental importance and is determined, as has been pointed out above, by considerations of expediency. Such is not the case with the adsorption on mercury of neutral molecules of aliphatic compounds. Here C_0 is much larger than C', eqns. (4) and (5) become incompatible and the choice depends on how well the models corresponding to one of them agree with experimental data.

Before the different methods of comparing eqns. (4) and (5) with experimental data are considered, it should be noted that in the case of adsorption of neutral organic molecules, it is hardly possible to explain the physical meaning of the model of two capacitors connected in series. Other conditions being equal, this fact gives preference to the isotherms that are congruent with respect to the electrode potential.

As has been pointed out above, the method of two-dimensional pressure used by PARSONS[5] for the analysis of the system, 0.1 N NaF + n-C_4H_9OH, where $C_0/C' \approx$

4–5, did not bring out the difference between eqns. (4) and (5), although judging by the results of the analysis of these equations, this difference must exist. Let us demonstrate this result to be due to an insufficient sensitivity of the method of two-dimensional pressure. To this end, let us assume that the adsorption of the organic substance rigorously obeys eqn. (4), the quantities C_0 and C' being independent of the potential. In this case,

$$q_0 = q_m + C_0(E - E_m) \quad \text{and} \quad q' = q_m + C'(E - E_m) \tag{16}$$

where E_m and q_m are the abscissa and the ordinate of the intersection point of the straight lines of the q_0–E and q'–E dependencies (see Fig. 1), which corresponds to

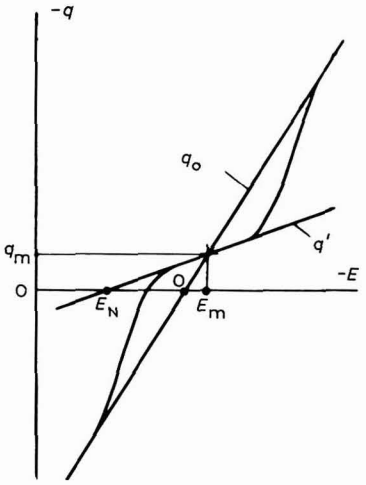

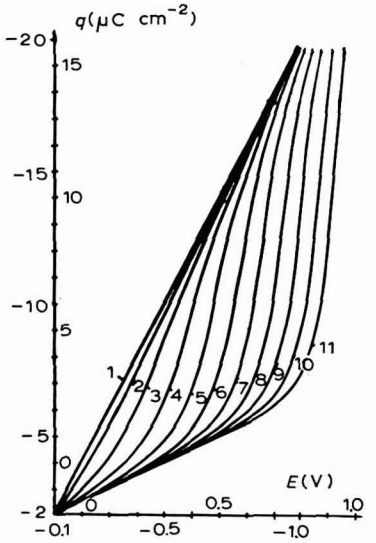

Fig. 1. Schematic representation of dependence of electrode charge on potential in the presence of aliphatic compounds at C_0 = const. and C' = const.

Fig. 2. Dependence of electrode charge on potential at different concns. of organic substance theoretically calcd. using the model of two parallel capacitors. Organic substance concn.: (1), 0; (2), 2.51×10^{-2}; (3), 6.3×10^{-2}; (4), 0.159; (5), 0.398; (6), 1.0; (7), 2.51; (8), 6.3; (9), 15.9; (10), 39.8; (11), 100 M.

the maximum adsorption of the organic substance and to the minimum on the differential capacity curves. Introducing (16) into eqn. (8), we obtain:

$$\frac{\partial \ln B}{\partial E} = -\frac{C_0 - C'}{A}(E - E_m) \tag{17}$$

which on integration gives:

$$B = B_m \exp[-\alpha(E - E_m)^2] \tag{18}$$

where $\alpha = (C_0 - C')/2A$ and B_m is the value of B at $E = E_m$.

Equation (18) in combination with the equation of Frumkin's isotherm[8] leads to:

$$Bc = \{\theta/(1-\theta)\} \exp(-2a\theta) \tag{19}$$

where a—the parameter of intermolecular interaction—enables the θ–E dependence to be calculated for different concentrations of the organic substance, provided all the parameters contained in these equations are given. Then, by means of the equation

$$q = q_m + [C_0(1-\theta) + C'\theta](E - E_m) \quad (20)$$

which is obtained by substituting (16) into (9), it is possible to calculate a set of q–E curves, and by means of the equation[8]:

$$\sigma = \tfrac{1}{2}C_0E^2 + A[\ln(1-\theta) + a\theta^2] \quad (21)$$

—a set of electrocapillary curves in the presence of different concentrations of organic substance. These data are sufficient for plotting the $\Delta\sigma$–log c curves at different E, which, as specified by the conditions of the calculations, should coincide when shifted along the abscissa, and the $\Delta\xi$–log c curves at different q, which should not coincide when shifted in a similar manner.

We have performed this calculation choosing parameters similar to those corresponding to the 0.1 N NaF + n-C_4H_9OH system[9]: $C_0 = 20$ μF cm^{-2}, $C' = 5$ μF cm^{-2}, $A = 1$ μJ cm^{-2}, $a = 1$, $B_m = 10$ l mol^{-1}, $\alpha = (C_0 - C')/2A = 7.5$ V^{-2}, $E_m = -0.1$ V

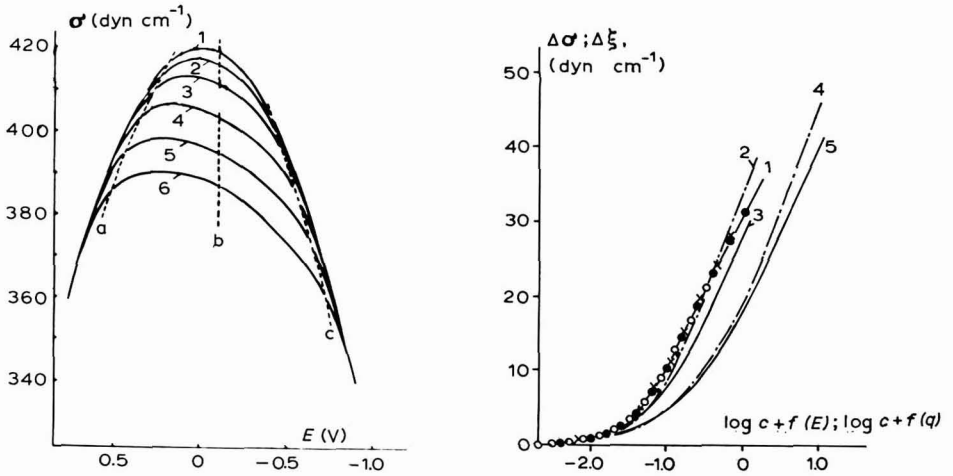

Fig. 3. Electrocapillary curves at different organic substance concns. theoretically calcd. using the model of two parallel capacitors. Organic substance concn.: (1), 0; (2), 2.5×10^{-2}; (3), 6.3×10^{-2}; (4), 0.159; (5), 0.398; (6), 1.0 M. Dashed lines connect the points with a constant surface charge: (a), $q = +4$; (b), $q = -2$; (c), $q = -8$ μC cm^{-2}.

Fig. 4. Dependence of two-dimensional pressure at E = const. ($\Delta\sigma$) and at q = const. ($\Delta\xi$) on the log of organic substance concn. calcd. using the model of two parallel capacitors: (1), $q = -2$ μC cm^{-2}; (○ ○), $E = +0.3$ V; (● ●), $E = 0$; (× ×), $E = -0.3$ V; (2), $q = -8$; (3), $q = +4$; (4), $q = -16$; (5), $q = +12$ μC cm^{-2}. The functions $f(E)$ and $f(q)$ are chosen so that all curves should coincide in the range of $\Delta\sigma$ and $\Delta\xi$ values of the order of 0.3–0.5 dyn cm^{-1}.

and $q_m = C_0E_m = -2$ μC cm^{-2}. The calculated $\Delta\sigma$–log c and $\Delta\xi$–log c curves were shifted along the abscissa until they coincided at the smallest values of $\Delta\sigma$ or $\Delta\xi$ (of the order of 0.3–0.5 dyn cm^{-1}).

Some of the results obtained are presented in Figs. 2–4. As expected, the $\Delta\sigma$–log c curves measured at different E coincide completely (Fig. 4). As to the $\Delta\xi$–log c curves, in the range of charges where the adsorption of ordinary organic compounds

leads to an appreciable decrease in interfacial tension, the discrepancy in the calculated values of $\Delta\xi$ does not exceed 3–4 dyn cm^{-1}, *i.e.*, lies approximately within the scatter of the experimental data (see ref. 5). In order to find the discrepancy in the $\Delta\xi$–log c curves, which lies definitely outside the experimental error limits, it would be necessary to investigate the dependence of $\Delta\xi$ on log c at charges that are much more removed from q_m, *e.g.*, at $q=12$ and $q=-16$ μC cm^{-2} (see curves 4 and 5 in Fig. 4). Under such conditions, however, the product $B_m \cdot c$ should reach 50 to 1000, which cannot be realized in practice owing to the limited solubility of organic substances with high surface activity. The two-dimensional pressure method cannot be used, therefore, as a criterion in choosing one of the two equations, (4) and (5). It is of interest to seek for other more sensitive methods.

One such method suggested[10] consists in the analysis of the experimental dependence of the shift of the point of zero charge, $E_{q=0}$, on the adsorption value of the organic substance, Γ. Provided that $C_0=$const. and $C'=$const., it follows from Fig. 1 that the equations of the straight lines, q_0, E, and q', E can be written as:

$$q_0 = C_0 E \quad \text{and} \quad q' = C'(E - E_N) \tag{22}$$

where E_N is the limiting value of E, corresponding to $\theta=1$. Thus, when the adsorption isotherm is congruent with respect to the potential, we obtain from eqns. (9) and (22):

$$E_{q=0} = E_N \theta / [(C_0/C')(1-\theta)+\theta] \tag{23}$$

On the other hand, when the adsorption isotherm is congruent with respect to the charge, we obtain from eqn. (14), taking into consideration that at $q=0$, $E_0=0$ and $E'=E_N$ (see Fig. 1):

$$E_{q=0} = E_N \theta \tag{24}$$

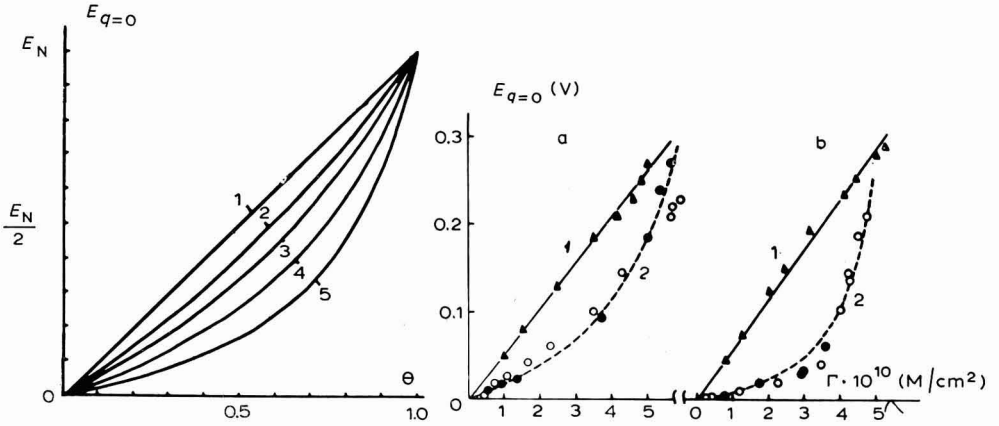

Fig. 5. Dependence of adsorption potential on surface coverage calcd. by means of eqn. (23) for the following values of the ratio C_0/C': (1), 1; (2), 1.5; (3), 2; (4), 3; (5), 5.

Fig. 6. Dependence of adsorption potential on adsorption of *n*-propanol (a) and caproic acid (b) at the soln./air (1) and soln./mercury (2) interfaces. The data have been obtained: (○ ○), from the maximum on the electrocapillary curves; (● ●), from the minimum on the differential capacity curves in dilute solns.; (---), calcd. by means of eqn. (23) at: (a), $E_N = 0.31$ V, $C_0/C' = 3.5$; $\Gamma_m = 6 \cdot 10^{-10}$ mole cm^{-2}; (b), $E_N = 0.29$ V, $C_0/C' = 7$, $\Gamma_m = 5 \cdot 10^{-10}$ mole cm^{-2}.

It follows from a comparison of eqns. (23) and (24), that a characteristic feature of the systems obeying eqn. (4) is the non-linearity of the dependence of $E_{q=0}$ on θ (or on Γ), which increases with increasing C_0/C' (see Fig. 5). As expected, at $C_0=C'$ both models give the same result.

Figure 6 shows the experimental dependencies of $E_{q=0}$ on Γ for the case of adsorption on mercury of *n*-propanol (a) and *n*-caproic acid (b) obtained by two methods. It is clear from the figure that these dependencies deviate appreciably from the straight line and agree well with eqn. (23). The same result was obtained for the case of adsorption on mercury of *n*-valeric acid and *n*-amylamine[10]. It should be noted that curves of the dependence of $E_{q=0}$ on Γ of a similar shape were obtained for camphor[11], *n*-butylamine[12] and some other aliphatic compounds[13], although they were explained differently, *viz.*, by the change in the orientation of adsorbed dipoles. Since in the same systems at the solution/air interface an approximately linear dependence of the adsorption potential drop on Γ is observed (see Fig. 6), this explanation cannot be considered as correct. Recently, a non-linear dependence of $E_{q=0}$ on Γ at the solution/mercury interface has been obtained also in the presence of tetrapropyl- and tetrabutyl-ammonium cations[14]. The results obtained show that in all the systems investigated, the assumption of the adsorption isotherm being congruent with respect to the electrode potential is in better agreement with experiment than the same assumption with respect to the electrode charge. It should be emphasized, however, that at $C_0/C' \leqslant 2$ (*e.g.*, in the case of adsorption on mercury of acetanilide molecules[15]) the curvature of the dependence of $E_{q=0}$ on θ (or on Γ) becomes insignificant, as is evident from Fig. 5, and owing to the scatter of the experimental points, this method cannot be used for the choice between eqns. (4) and (5).

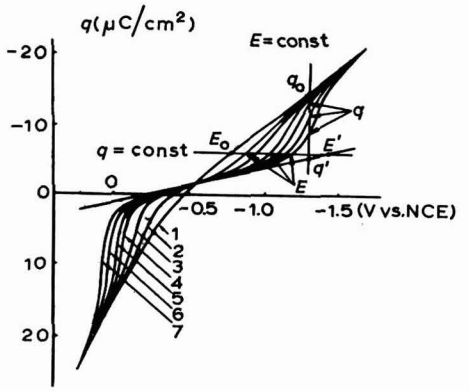

Fig. 7. Dependence of mercury electrode charge on potential in 0.1 *N* Na_2SO_4 solns. with different additions of *n*-butanol: (1), 0; (2), 0.05; (3), 0.1; (4), 0.2; (5), 0.4; (6), 0.6; (7), 0.8 *M*.

Another method for choosing between eqns. (4) and (5) is based on the analysis of the experimental E–q curves, measured at different concentrations of organic substance, by means of eqns. (9) and (14). This method can be explained by taking as an example the case of the system, 0.1 *N* Na_2SO_4 + *n*-C_4H_9OH, for which we have measured the differential capacity curves and obtained the q–E curves by a numerical

"backward" integration of the former*. The data obtained are given in Fig. 7, where an explanation of the graphical determination of the values of q_0, q and q' at a given E and of the values of E_0, E and E' at a given q is also presented. As the quantity C' is usually assumed constant in this method, the dependence of q' on E (or E' on q, which is the same thing) is a straight line with slope C', passing through a common intersection point of all q–E curves.

Thus, eqns. (9) and (14) can be used for calculating the adsorption isotherm in the θ–c coordinates both at E=const. and at q=const. When these isotherms are calculated at the point with coordinates (E_m, q_m), eqns. (10) and (15) are used, respectively, since at the minimum on the C–E curves at $E=E_m$, $C=C_{true}$. Then, the isotherms obtained can be given in relative coordinates, *e.g.*, θ *vs.* $y=c/c_{\theta=0.3}$. This enables the shape of the isotherms obtained at different E or q to be compared. The results of such a comparison for the system, 0.1 N Na_2SO_4+n-C_4H_9OH, is shown in Fig. 8. It is clear from the figure that the isotherms obtained are congruent with respect to the potential and incongruent with respect to the charge.

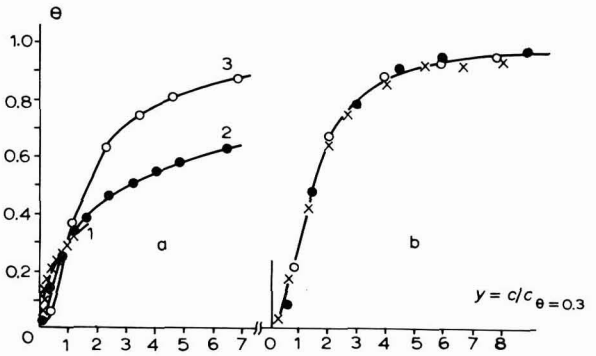

Fig. 8. Adsorption isotherms of n-butanol in the coordinates θ *vs.* $y = c/c_{\theta=0.3}$. (a), at q = const.: (1), $q = -9$; (2), $q = -6$; (3), $q = -1.55$ μC cm^{-2}. (b), at E = const.: (○ ○), $E = -0.55$; (● ●), $E = -0.8$; (× ×), $E = -1.0$ V (NCE).

In order to compare the sensitivity of this method with that of the two-dimensional pressure, we obtained by means of the "backward" integration of the q–E curves shown in Fig. 7, the corresponding electrocapillary curves and plotted the $\Delta\sigma$–log c curves for the potentials: -0.2, -0.55, -1.0 V (NCE) and $\Delta\xi$–log c curves for the charges $+7.0$, -1.55, -9.0 μC cm^{-2}. The data obtained are shown in Fig. 9. Owing to the low sensitivity of the two-dimensional pressure method, it is impossible to choose between eqns. (4) and (5) which is in agreement with PARSONS' results[5] and the model calculation given above.

Let us consider one more method, which enables a choice to be made between the models of two parallel- and two series-connected capacitors. This method consists in a theoretical calculation of the q–E curve and a comparison of its shape with that of the experimental charge–potential curve. Such a calculation for the model of

* The "backward" integration method proposed by GRAHAME *et al.*[16] consists in carrying out the integration from a sufficiently negative potential, E, at which the substance being investigated has been completely desorbed from the surface, so that a corresponding quantity (q or σ) in a pure supporting electrolyte solution can be used as a constant of integration.

two parallel capacitors has already been considered by us above, a comparison of Figs. (2) and (7) shows the shapes of the theoretically-calculated and experimental q–E curves to be in good agreement.

It follows from Fig. 1 that in the case of the model of two series-connected capacitors at C_0=const. and C'=const. we have

$$E_0 = E_m + (q - q_m)/C_0 \quad \text{and} \quad E' = E_m + (q - q_m)/C' \tag{25}$$

Substituting (25) into (13), we obtain:

$$\frac{\partial \ln G}{\partial q} = -\frac{C_0 - C'}{AC_0C'}(q - q_m) \tag{26}$$

which on integration gives:

$$G = G_m \exp[-\beta(q - q_m)^2] \tag{27}$$

where G_m is the value of G at $q = q_m$ and $\beta = (C_0 - C')/2AC_0C' = \alpha/C_0C'$.

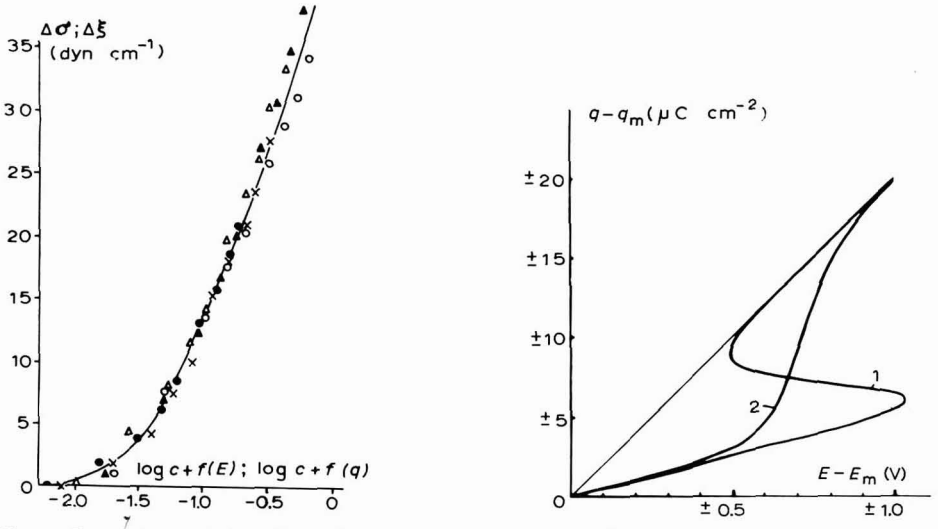

Fig. 9. Dependence of two-dimensional pressure on the log of concn. of n-butanol: (○), E = −0.55 V, q = −1.55 μC cm^{-2}; (●), E = −1.0 V; (×), E = −0.2 V (NCE); (△), q = +7 μC cm^{-2}; (▲), q = −9 μC cm^{-2}.

Fig. 10. Dependence of charge on potential theoretically calcd. using the model of (1), two series-connected capacitors; (2), two parallel capacitors.

The condition q=const. becomes identical with the condition E=const. in the point q_m, E_m, as all q–E curves cross in this point. The value of G_m should, therefore, be numerically equal to that of B_m in eqn. (18) and the parameter of intermolecular interaction, a, contained in the isotherm

$$G_m c \exp[-\beta(q - q_m)^2] = \{\theta/(1 - \theta)\} \exp(-2a\theta) \tag{28}$$

should not differ from the value of a in eqn. (19). Thus, in eqn. (28) it was assumed that G_m=10 l mole^{-1}, β=0.075 (cm^2/μC)^2 and a=1. When the dependence of θ on

$(q-q_m)$ had been calculated by means of this equation, it was possible using the equation

$$E-E_m=\{(1-\theta)/C_0+\theta/C'\}(q-q_m) \tag{29}$$

(which is obtained by substituting (25) into (14)) to calculate the q–E curve in the coordinates $(q-q_m)$ *vs.* $(E-E_m)$. The q–E curve thus calculated for the concentration, $c=1.32$ M, is shown in Fig. 10, where it is compared with the charge–potential curve calculated under the same conditions, but using the model of two parallel capacitors.

It is evident from the figure that the q–E curve calculated using the model of two series-connected capacitors has an anomalous form and in a certain charge range corresponds to negative differential capacity values. For the shape of the above curve to be in agreement with that of the experimental q–E curves, it is necessary to assume that the parameter of intermolecular interaction, a, contained in Frumkin's isotherm (28) decreases sharply and even becomes negative with the charge moving away from q_m. This fact testifies that the experimental isotherms are incongruent with respect to the electrode charge, and has already been noted[4], although proved incorrectly as pointed out by PARSONS[5].

Thus, in the case of adsorption on mercury of aliphatic compounds, when the capacity in the supporting electrolyte solution, C_0, is much larger than the capacity in the presence of the adsorbed substance, C', and hence eqns. (4) and (5) are incompatible, the experimental data are better described by the isotherms that are congruent with respect to the potential than by those that are congruent with respect to the charge. This result is to be expected, since the surface layer model corresponding to the isotherm that is congruent with respect to the electrode potential has a more real physical significance.

The congruence of the adsorption isotherm with respect to the potential is an approximation that corresponds to the exact realization of the model of two parallel capacitors, *i.e.*, to the strict equipotentiality of both sides of the electric double layer[17]. This approximation is best realized in the case of adsorption on mercury of aliphatic compounds, although even in this case, owing to the discrete nature of the adsorbed dipoles of organic substance, the condition of equipotentiality of the ionic side of the double layer is somewhat impaired. For this reason, in describing C–E curves in the presence of aliphatic compounds quantitatively, it is necessary to introduce an additional correction for some small changes in α with the potential[18], *i.e.*, for the deviations of the real system from an ideal one described by an isotherm that is strictly congruent with respect to the electrode potential.

SUMMARY

In a strictly thermodynamic approach to the investigation of the adsorption isotherm, the choice of an electric variable is of no fundamental importance and is determined by considerations of expediency or convenience. This is not the case, however, when the thermodynamic approach to the investigation of adsorption is supplemented by the assumption of the congruence of the adsorption isotherm with respect to the electrode potential or charge. These assumptions are only compatible provided the double-layer capacity in the supporting electrolyte solution, C_0, does

not differ from the capacity, C', at complete surface coverage with adsorbed substance. If C_0 markedly exceeds C' as, for example, in the case of adsorption of aliphatic compounds on mercury, the assumption of the congruence of the adsorption isotherm with respect to the electrode potential is in better agreement with the experimental data. Moreover, this assumption corresponds to a clear and consistent physical picture of the surface layer in the presence of adsorbed molecules of organic substance (the model of two parallel capacitors).

ADDENDUM

The conclusions of this paper are not inconsistent with the latest experimental results of DUTKIEWICZ, GARNISH AND PARSONS[19], which were kindly communicated to us by Dr. PARSONS before publication. In fact, adsorption of glycols reduces only slightly the capacity of a mercury electrode. Therefore, the adsorption behaviour of butane-1,4-diol and 2-butyne-1,4-diol can be described within experimental error by means of eqn. (4) as well as eqn. (5). In the case of adsorption of *n*-butanol and ether however, it follows from Figs. 6–9 in ref. 19 that the experimental data deviate from both the models investigated, these deviations being rather less significant for the model of two parallel capacitors. Thus, the deviation of the experimental points on the q–I' curves (see Figs. 6 and 8 in ref. 19) from a mean linear dependence amounts to no more than 0.5 μC cm^{-2}, which only slightly exceeds the accuracy in the charge determination. On the other hand, the deviation of the experimental points in Figs. 7 and 9 from the mean linear dependence, in some cases is as large as 0.10–0.15 V. Finally, in connection with the paper under discussion, it should be stressed once more that the choice of the independent electrical variable based on considerations of convenience (*e.g.*, the possibility of obtaining symmetrical curves for cathodic and anodic adsorption regions of an organic substance) cannot serve as a criterion for the choice of the independent variable. This can be decided only on the basis of an analysis of the physical significance of the underlying model.

REFERENCES

1 A. N. FRUMKIN, *Z. Physik. Chem.*, 103 (1923) 55.
2 R. PARSONS, *Trans. Faraday Soc.*, 51 (1955) 1518; 55 (1959) 999.
3 R. PARSONS, *J. Electroanal. Chem.*, 7 (1964) 136.
4 B. B. DAMASKIN, *J. Electroanal. Chem.*, 7 (1964) 155.
5 R. PARSONS, *J. Electroanal. Chem.*, 8 (1964) 93.
6 R. PAYNE, *J. Phys. Chem.*, 69 (1965) 4113; 70 (1966) 204.
7 A. N. FRUMKIN, *Z. Physik*, 35 (1926) 792.
8 A. N. FRUMKIN, *Z. Physik. Chem.*, 116 (1925) 466.
9 B. B. DAMASKIN, A. A. SURVILA AND L. E. RYBALKA, *Elektrokhimiya*, 3 (1967) 146.
10 A. N. FRUMKIN, B. B. DAMASKIN, V. M. GEROVICH AND R. I. KAGANOVICH, *Dokl. Akad. Nauk SSSR*, 158 (1964) 706.
11 A. G. STROMBERG AND L. S. ZAGAINOVA, *Zh. Fiz. Khim.*, 31 (1957) 1042.
12 I. ZWIERZYKOWSKA, *Roczniki Chem.*, 39 (1965) 101.
13 R. G. BARRADAS, P. G. HAMILTON AND B. E. CONWAY, *J. Phys. Chem.*, 69 (1965) 3411.
14 B. B. DAMASKIN, R. I. KAGANOVICH, V. M. GEROVICH AND S. L. DIATKINA, *Elektrokhimiya*, in press.
15 R. PARSONS AND F. G. R. ZOBEL, *Trans. Faraday Soc.*, 62 (1966) 3511.
16 D. C. GRAHAME, E. M. COFFIN, J. I. CUMMINGS AND M. A. POTH, *J. Am. Chem. Soc.*, 74 (1952) 1207.
17 A. N. FRUMKIN, B. B. DAMASKIN AND A. A. SURVILA, *Elektrokhimiya*, 1 (1965) 738.
18 B. B. DAMASKIN, *Usp. Khim.*, 34 (1965) 1764.
19 E. DUTKIEWICZ, J. D. GARNISH AND R. PARSONS, *J. Electroanal. Chem.*, 16 (1968) 505.

ELECTROANALYTICAL CHEMISTRY AND INTERFACIAL ELECTROCHEMISTRY
Elsevier Sequoia S.A., Lausanne – Printed in The Netherlands

THE ADSORPTION OF SOME C_4-COMPOUNDS ON MERCURY ELECTRODES IN THE ABSENCE OF SPECIFIC IONIC ADSORPTION

E. DUTKIEWICZ*, J. D. GARNISH† AND ROGER PARSONS**
Department of Physical Chemistry, The University, Bristol 8 (England)
(Received August 15th, 1967)

INTRODUCTION

The adsorption of organic molecules on mercury electrodes has been studied many times since the pioneering work of GOUY[1,2]. Much of this work is summarised in the review by FRUMKIN AND DAMASKIN[3]. These authors have shown that the experimental capacity curves in the presence of aliphatic compounds can be fitted by equations based on the following assumptions[4]:

(1) The charge on the electrode at a given electrode potential is given by:

$$q = q^{b}(1-\theta) + q^{s}\theta \tag{1}$$

where θ is the fraction of the surface occupied by the organic compound, q^{b} is the charge of this potential when $\theta = 0$ and q^{s} that when $\theta = 1$.

(2) The adsorption at a given potential may be expressed by an adsorption isotherm of the form:

$$\theta e^{A\theta}/(1-\theta) = \beta c \tag{2}$$

where β is the adsorption coefficient and $\log \beta$ is an approximately quadratic function of potential as follows from (1).

(3) The saturation surface coverage used in calculating θ is not constant, but depends linearly on the amount adsorbed. Alternatively, A is considered to be potential-dependent.

The fit to the experimental results is very good and capacity curves are undoubtedly a sensitive indication of the character of the adsorption. On the other hand, the various assumptions enter into the capacity in a relatively complicated way so that it is not clear whether the fit is due to fulfilment of each assumption, or to cancellation of error in one by an opposite error in another. Hence it seems desirable to examine some simple systems in a manner which should show how each assumption is separately obeyed.

Simple aliphatic compounds with four carbon atoms were chosen for this study, and fluoride solutions were used as the base electrolyte to avoid the complication of specific ionic adsorption. Different types of adsorption behaviour were obtained by using *n*-butanol, butan-1,4-diol, 2-butyne-1,4-diol and diethyl ether.

* Present address: Department of Physical Chemistry, University of Poznan, Poland.
† Present address: Wantage Research Laboratory (A.E.R.E.), Wantage, Berkshire, England.
** To whom correspondence and reprint requests should be addressed.

EXPERIMENTAL

All measurements were made using the capillary electrometer previously described[5,6], although for the measurements with the diols the cell was modified so that it could be immersed in a water thermostat. The water was maintained at 25° by a Techne "Tempunit" which also circulated water through the jacket of the mercury manometer used in measuring the pressure. The potential of the mercury electrode in the capillary was measured with respect to a calomel electrode (saturated, when the diols were used, and normal for the butanol and ether experiments) using a Croydon type P3 potentiometer and a Pye "Scalamp" 1400-Ω galvanometer. The height of the column of mercury required to bring the mercury–solution meniscus to a reference point on the capillary was measured using a P.T.I. 1-m cathetometer. A total height of about 75 cm could be measured with an accuracy of 0.01 cm, leading to a reproducibility of the interfacial tension measurements, in general, to ± 0.1 dyn cm^{-1}, although on the extreme positive branch of the curve, errors of up to 0.5 dyn cm^{-1} were noted in reproducing the measurements. Interfacial tensions were calculated from the measured height of mercury (corrected for the head of the solution) by assuming that the interfacial tension between mercury and 0.1 *M* fluoride solutions is the same as that for mercury–pure water. The latter is obtained from GOUY's data[7] as 425.6 dyn cm^{-1} at 25°.

NH_4F (B.D.H.) was dissolved in twice-distilled water and the composition determined by analysing the ammonium content[8]; electrocapillary curves for these solutions were in good agreement[9] with those for KF solutions of the same concentration, the KF being prepared as described previously[10].

A few grams of alumina were added to 500 ml of B.D.H. AnalaR butanediol and the mixture distilled *in vacuo* in a stream of dry nitrogen. The middle 60% fraction was collected. This procedure was repeated once. Butynediol is available only in a technical grade as a brown, sticky solid which melts at 53°. It was distilled *in vacuo* in a slow stream of dry nitrogen at approximately 128° and 5 mm Hg. The condenser and receiver were thermostatted at 58° to avoid solidification which rapidly blocked the system. The purified substance melted at 56.5–56.8°. The distillation was repeated once more and the purified diol used as quickly as possible. It began to revert to its former yellow brown colour if left exposed to the atmosphere for a day, although it remained white for up to three days if cooled in solid CO_2 in an atmosphere of nitrogen. Any sample that showed visible discolouration was rejected and repurified before use.

B.D.H. AnalaR butanol was distilled twice from alumina before use. B.D.H. AnalaR diethyl ether was shaken with 5% aqueous ferrous ammonium sulphate, dried over calcium chloride and sodium wire, then distilled using an 80-cm fractionating column.

Mercury was passed through 3% nitric acid in a fine stream, agitated with air in 15% sulphuric acid, dried, and distilled three times in a stream of air at low pressure.

RESULTS AND ANALYSIS

(*a*) *General*

Values of $\xi (= \gamma + qE$, where γ is the interfacial tension and q the charge on

the metal at potential, E) were calculated using the computer programme described previously[9]. The programme also provides values of ϕ ($=\xi^b-\xi$, where ξ^b is the value of ξ in the absence of the organic addition), the surface pressure. As pointed out previously[9], these quantities are obtained with an accuracy comparable to that of the original interfacial tension measurements. The largest inaccuracy here is probably in the base fluoride solutions at the more positive potentials; however, it is unlikely[9] that this exceeds 1.6 dyn cm^{-1} at the largest charge ($+10\mu$C cm^{-2}) used in the analysis; over most of the range it will be much less than this. Values of q obtained from the programme agree well with those obtained by graphical differentiation, and for the base solution, agree also with integrated capacity curves, although small deviations occur at positive charges[9].

The surface excess of the organic compound was obtained by graphical differentiation in order to avoid introducing any bias by fitting the data to a theoretical curve at an early stage in the analysis. In each case, the activity was taken as equal to the concentration. This seems to be justified by the data of BUTLER *et al.*[11] for *n*-butanol, from which it can be calculated that the change in $\log_{10}$(activity coefficient) for butanol in water between the infinitely dilute solution and 0.5 M is 0.03. Neglect of this correction causes a negligible error. Similar conclusions may be drawn for ether from the freezing-point measurements of BOURION AND ROUYER[12]

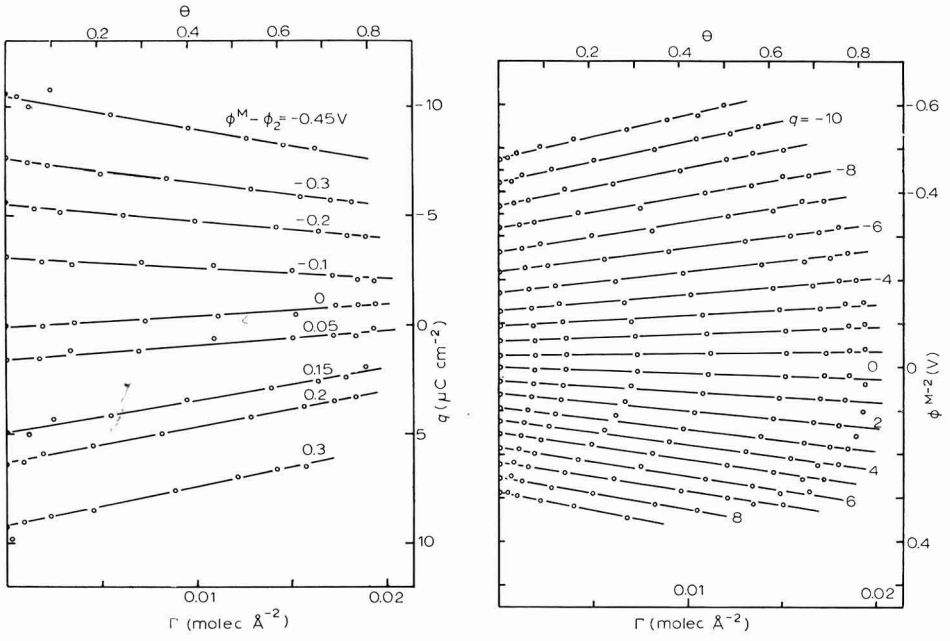

Fig. 1. Plot of charge on the mercury electrode as a function of amount of 2-butyne-1,4-diol adsorbed from aq. 0.095 M NH_4F. Each line corresponds to the constant value of the rational potential drop across the inner layer given near the line in volts.

Fig. 2. Plot of rational potential drop across the inner layer as a function of amount of 2-butyne-1, 4-diol adsorbed from aq. 0.095 M NH_4F. Each line corresponds to the constant value of the charge on the mercury electrode given near the line in μC cm^{-2}.

although these are not very accurate. It seems reasonable to assume that the much more soluble diols also deviate very little from ideality in the region below 1 M.

The rational potential drop across the inner layer (ϕ^{M-2}) was calculated by subtracting from the measured potential of the mercury with respect to the calomel electrode, the value of this potential at the point of zero charge in the base solution and the potential drop across the diffuse layer (ϕ_2). ϕ_2 was calculated from the charge on the metal using the Gouy–Chapman theory (eqn. (44) of ref. 13).

(b) Diols

Equation (1) was tested by plotting q against Γ, the surface excess of the diol at constant ϕ^{M-2}. A plot of this type for butynediol is shown in Fig. 1, where it is seen that linear relations are obtained within experimental error, thus showing that eqn. (1) can represent these results. A similar plot is obtained for butanediol. However, it must be noted that for both these systems the alternative plot[14] of ϕ^{M-2} against Γ at constant charge is an equally good representation of the results; the plot for butynediol is shown in Fig. 2. Thus a straightforward test involving the single non-thermodynamic assumption verified for this system leads to no clear decision as to whether eqn. (1) or its constant charge analogue is preferable.

Equation (2) was examined in the integrated form of the surface pressure–concentration relation using the methods described previously[15]. Both the ϕ–log c plots at constant q and the π–log c plots at constant ϕ^{M-2} are congruent (the isotherm shape is independent of the electrical variable) and may be fitted by eqn. (2) with $A = 0$, *i.e.*, by the Langmuir isotherm. This appears to give a better fit than the Zhukovitskii–

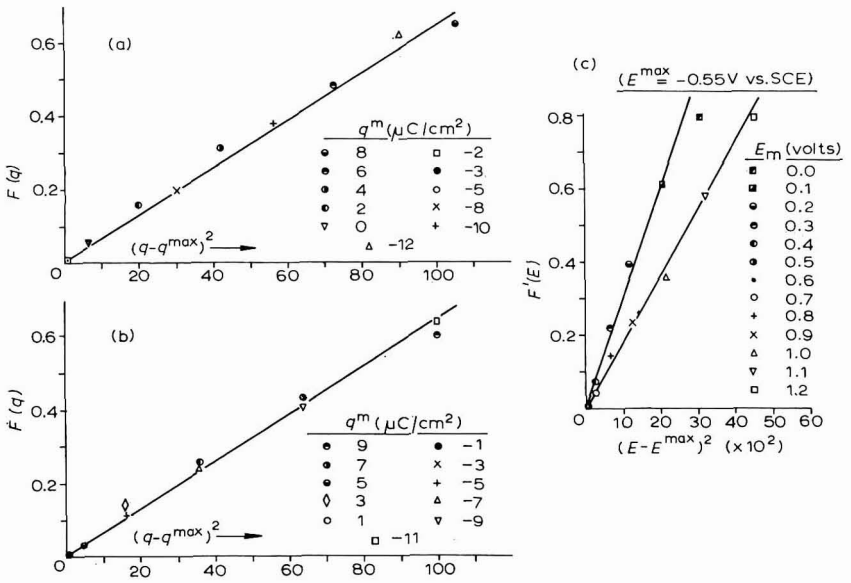

Fig. 3. (a), Plot of shift along the log concn. axis required to superimpose the surface pressure curves at constant charge of 1,4-butanediol on that at $q^{max} = -2.5$ μC cm^{-2} plotted as a function of square of the deviation of the charge from this value; (b), similar plot for 2-butyne-1,4-diol, $q^{max} = -1.0$ μC cm^{-2}; (c), similar plot for butanediol, but using constant potential isotherms and plotting against square of the deviation of the potential from −0.55 V (*vs.* SCE).

Flory–Huggins isotherm[16–18]. The reduced standard free energy of adsorption ($\log \beta$) is closely a quadratic function of q for the constant charge isotherms. This is shown in Fig. 3(a and b) where $\log \beta$ is plotted against $(q-q^{max})^2$, where q^{max} is the charge at which adsorption from a given solution reaches a maximum. It is particularly notable that the points for the positive and negative branches of the curve coincide satisfactorily on the same straight line. In contrast, the plot of $\log \beta$ against $(E-E^{max})^2$ shows different straight lines for the positive and negative branches (Fig. 3(a)). This seems to be the best reason for preferring to use the charge as the electrical variable for this system.

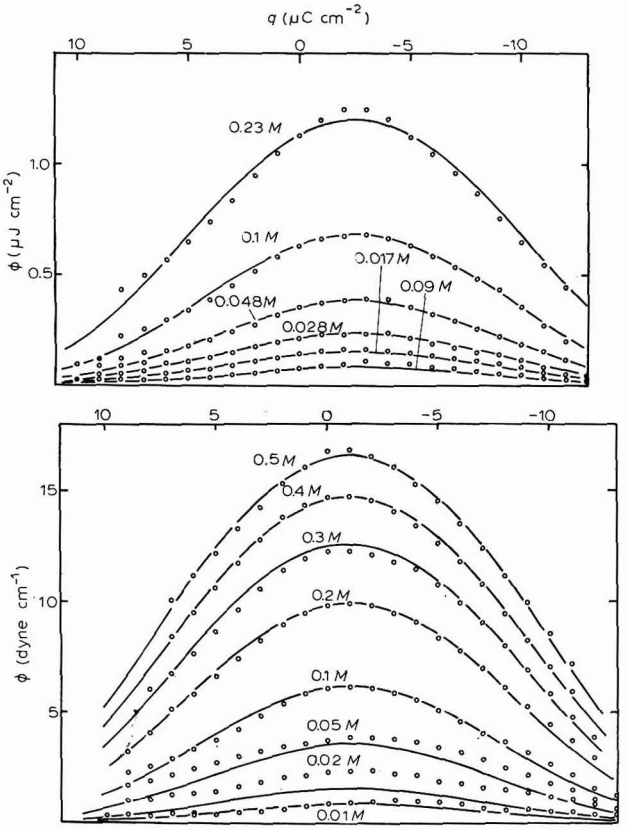

Figs. 4-5. Plots of surface pressure due to: (4) butane-1,4-diol, (5) 2-butyne-1,4-diol, adsorbed on a mercury electrode from aq. 0.095 M NH_4F as a function of charge on the electrode. Bulk concns. of the diols are indicated, in the figures. Points are experimental results; lines are calcd. from eqn. (3) with constants given in Table 1.

The accuracy of the fit with the experimentally-measured curves may be judged from Figs. 4 and 5 where the experimental values (ϕ) (points) of the surface pressure are compared with lines calculated from the expression,

$$\phi = kT\Gamma_s \ln[1 + c\beta_0 \exp\{-b(q-q^{max})^2\}] \quad (3)$$

with the constants given in Table 1. The saturation coverage, Γ_s, was calculated by

measuring the shadow areas of Courtauld atomic models on a plane, the long axis of the molecule being parallel to the plane. The other constants were obtained empirically from the data being discussed. The fit is well within the experimental error, although apparently systematic deviations are found for one concentration (0.02 M) of butynediol.

(c) *n-Butanol*

The corresponding test of eqn. (1) for n-butanol is shown in Fig. 6, from which it is evident that this system departs from the linear dependence of q on Γ, expected

TABLE I

ADSORPTION CHARACTERISTICS OF SOME NEUTRAL MOLECULES ON MERCURY ELECTRODES

	Butane-1,4-diol	*2-Butyne-1,4-diol*	*n-Butanol*	*Diethyl* ether*	*Acet-** anilide*
Γ_s (molec Å^{-2})	0.0263	0.0238	0.0475	0.035	0.0215
β_0 (l mole^{-1})	9.78	9.78	11.5	8.5	6.17×10^3
b (cm^4 μC^{-2})	0.015	0.015	0.028	0.0088	0.029
q^{max} (μC cm^{-2})	−2.5	−1.0	−2.0	−4.5	0.0

* Fits eqn. (2) with $A = -2$.
** Fits eqn. (2) with $A = +3$ and $1-\theta$ put equal to 1 (ref. 21).

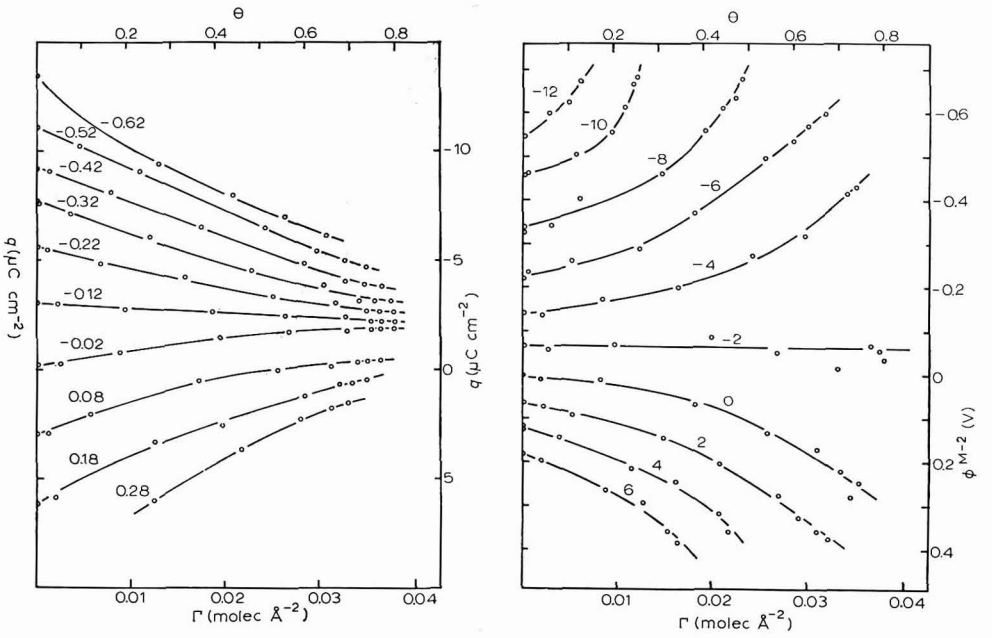

Fig. 6. Plot of charge on the mercury electrode as a function of amount of n-butanol adsorbed from aq. 0.1 M KF. Each line corresponds to the constant value of the rational potential drop across the inner layer given near the line in volts.

Fig. 7. Plot of rational potential drop across the inner layer as a function of amount of n-butanol adsorbed from aq. 0.1 M KF. Each line corresponds to the constant value of the charge on the mercury electrode given near the line in μC cm^{-2}.

from eqn. (1). The alternative plot of Fig. 7 shows that neither is there a linear dependence of ϕ^{M-2} upon Γ. Essentially the same conclusion is found from the data of KRYUKOVA AND FRUMKIN[19]. These results suggest that the assumption made in deriving eqn. (1), or its constant charge analogue, is invalid. The only non-thermodynamic assumption necessary in this derivation (see ref. 14) is that the adsorption isotherm is of the form $F(\Gamma)=\beta c$ where the function F is independent of the electrical variable chosen. The incorrectness of this assumption for this system is confirmed by a close inspection of the surface pressure–log concentration plots from which it is evident that the scatter obtained when they are superimposed[17] is due to a systematic change in shape with change in electrical variable. This deviation from congruence also becomes clear if an attempt is made to fit the experimental data in the manner described in Figs. 6 and 7. Unfortunately, once this assumption is dropped, there is no unambiguous way to decide which electrical variable is preferable. The introduction of a variable function F, and, as also seems necessary for this system, a deviation from the quadratic dependence of log β, means that enough adjustable parameters are available to fit the data within experimental accuracy on either choice of variable.

At q^{max}, the adsorption fits a Langmuir isotherm with the constants shown in Table 1. As $|q-q^{max}|$ increases, the isotherm becomes flatter in a way that would correspond to increasing repulsion between the adsorbed molecules. If the surface pressure curves are superimposed as shown previously[17], the value of the coefficient b shown in the table is obtained from the points in the region of maximum adsorption. There seems to be a tendency for b to decrease as $|q-q^{max}|$ becomes large.

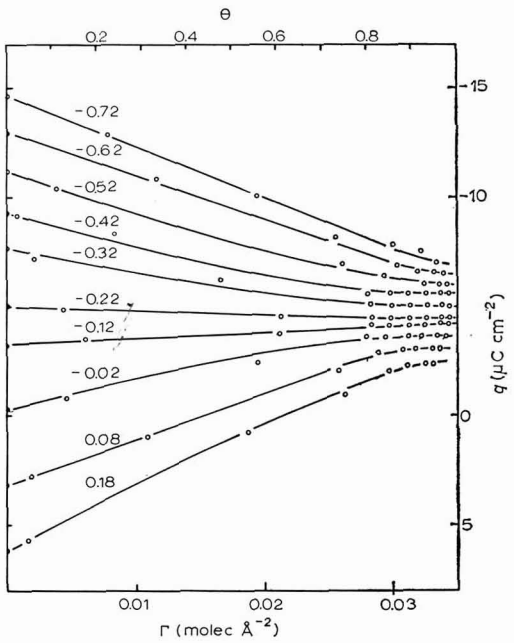

Fig. 8. Plot of charge on the mercury electrode as a function of amount of diethyl ether adsorbed from aq. 0.1 M NH_4F. Each line corresponds to the constant value of the rational potential drop across the inner layer given near the line in volts.

As in the case of the diols, when q is used as the electrical variable, the charge-dependence is symmetrical about q^{max}. On the other hand, if E is used as the electrical variable, the dependence of log β on $(E-E^{max})^2$ is more accurately linear over the accessible range but the slope for the negative charges is less than that for the positive charges, as shown for butanediol in Fig. 3(c).

(d) Ether

The plots given in Figs. 8 and 9 show that the behaviour of ether is in the same class as that of *n*-butanol although it seems likely that both plots are linear like those of the diols at low coverages. The data at low coverage are not sufficient

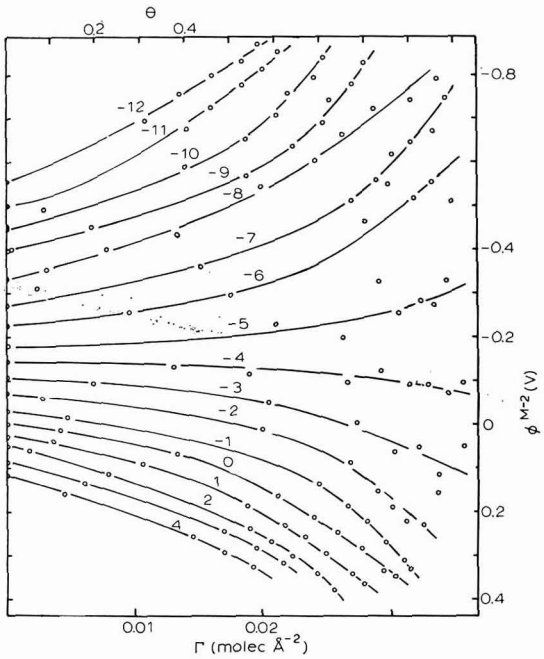

Fig. 9. Plot of rational potential drop across the inner layer as a function of amount of diethyl ether adsorbed from aq. 0.1 *M* NH_4F. Each line corresponds to the constant value of the charge on the mercury electrode given near the line in $\mu C\ cm^{-2}$.

to be completely certain of this, but the curvature does become much more pronounced at high coverages. Again, the surface pressure–log concentration plots show that the isotherm changes shape with variation of the electrical variable. At q^{max}, the data fit eqn. (2) approximately with $A=-2$ indicating strong attraction between the adsorbed species. As $|q-q^{max}|$ increases, the isotherm flattens corresponding to an increase in A. Superimposition of the surface pressure curves is possible if a rather large scatter is accepted and yields values of log β which are approximately linearly dependent on $(q-q^{max})^2$ with the same slope on either side of q^{max}. A similar type of analysis for the isotherm at constant E yields the same type of difference between the positive and negative branches in the dependence of log β on $(E-E^{max})^2$ as found for the other compounds. However, it should be remarked that the analysis

is less reliable for ether than for the other compounds because the existence of strong attraction between the adsorbed molecules leads to an isotherm in which the surface reaches high coverages at very low surface pressures. Hence, the information required about the nature of the isotherm is contained in the results at these low surface pressures which are the least accurate data.

DISCUSSION

The data reported here suggest that eqn. (1) is valid for some systems and not others; in none of these cases does major reorientation of adsorbed molecules seem to be important. They also suggest that when eqn. (1) is valid, the alternative assumption based on charge as the electrical variable is equally valid. Similarly, when eqn. (1) is invalid, the alternative is equally invalid. Consequently, this method of test does not lead to a definite conclusion about the nature of the electrical variable.

Assumption (2) is verified for the systems studied here in that they can all be fitted by eqn. (2) although the data indicate that for *n*-butanol and ether, the interaction coefficient, A, is dependent on the electrical state of the interphase. The dependence of log β on the electrical variable is approximately quadratic, but the dependence is more accurately quadratic if charge rather than potential is used as the variable.

Assumption (3) is verified in the sense that A is found to be potential-dependent. It is difficult to test it in the form of a dependence of Γ_s on Γ since this amounts to adding another adjustable parameter to eqn. (2). With the present accuracy of the results, such a fit would not be significant.

An alternative approach to neutral molecule adsorption from aqueous solutions has been discussed by BOCKRIS, DEVANATHAN AND MÜLLER[20]. They regard the displacement of water as the most important feature of the adsorption process and calculate the adsorption energy on this basis. They show that an adsorption curve qualitatively similar to that obtained experimentally for 0.1 M butanol in 0.1 N HCl, can be calculated assuming a two-position model for the water with allowance for lateral interaction. Butanol is assumed to replace two water molecules when it adsorbs, which is approximately consistent with the assumed molecular area of 21 Å^2 although it is inconsistent with the use of a Langmuir isotherm as the basic form unless the water is assumed to exist on the surface as dimers.

However, apart from detailed defects in the B.D.M. theory, it seems that the general form of the theory predicts a stronger charge-dependence of the free energy of adsorption with larger molecular area of the adsorbing organic molecule; in the present terminology, b should increase with $A_s = 1/\Gamma_s$. The present results do not conform with this trend as can be seen from Table 1. The largest value of b is found for *n*-butanol which has the smallest molecular area. A similar value of b is also found for acetanilide[21] which occupies an area over twice that of *n*-butanol; since this is an aromatic compound, the B.D.M. theory might not be expected to apply to it without modification. The smallest value of b is found for ether which has a molecular area intermediate between that of butanol and those of the diols. It should be emphasized that the method used for deriving b does not depend on any assumptions about the equation of the isotherm. It seems reasonable to conclude from these facts that an essential feature of organic adsorption is omitted from the

B.D.M. theory. The fact that q^{max} is different for these compounds and that ether and acetanilide have A-values different from zero, suggests that variations in the polarity of the adsorbed species is leading to this disagreement with the B.D.M. theory and that the missing feature is the allowance for the interaction between the water and the adsorbed species on the electrode surface.

Finally, it seems worth commenting upon the similarity of the behaviour of butanediol and butynediol. The adsorption behaviour of an aliphatic compound containing a triple bond has been studied recently by BARRADAS AND HAMILTON[22] in the series propargyl, allyl and n-propyl alcohols, adsorbed from aqueous 1 M KCl. Although complicated by the specific adsorption of the anion, their results show that increasing unsaturation appears to cause increasing orientation of the molecule parallel to the electrode surface. The present results are free from these complications since both diols adsorb with their long axis parallel to the electrode surface. They thus enable a clear separation of the effect of the triple bond. It is evident that this has no effect on the shape of the adsorption isotherm, so that the interaction between molecules on the surface is unaffected by the presence of the triple bond. It has no effect on the charge-dependence of the standard free energy of adsorption, but does affect the charge at which adsorption reaches a maximum. This difference could be described as a chemical (charge-independent) contribution to the adsorption energy due to the ability of the electrons in the triple bond to interact with the electrode. Besides this interaction there is also likely to be an effect due to the different dipole moments of the two diols. The presence of a triple bond causes butynediol to be a rigid molecule with all its atoms co-linear. Consequently, when it adsorbs flat on the surface, the component of its dipole moment perpendicular to the surface is zero. Butanediol, on the other hand, is flexible and is likely to be oriented with the hydroxyl groups towards the bulk electrolyte, the perpendicular component of the dipole thus being with the negative end towards the metal. This effect alone would lead to a position of maximum adsorption for butanediol at a more positive charge than that for butynediol. Thus the observed shift in the opposite direction confirms that the interaction of the electrons of the triple bond with the metal surface is significant. However it is surprising that there is no significant dependence of this effect on the charge on the metal surface.

Addendum

We agree with the comment of FRUMKIN, DAMASKIN AND SURVILA that considerations of convenience cannot serve as a criterion for the choice of independent variable (see ref. 17).

On the other hand we doubt whether a clear distinction can be drawn between the deviations from linearity in Figs. 6 and 8 and those in Figs. 7 and 9 of our paper. In both these systems, the capacity of a saturated layer of the organic compound is about 5 μF cm^{-2}; thus a deviation of 0.5 μC cm^{-2} is equivalent to a deviation of 0.1 V.

ACKNOWLEDGEMENTS

We are grateful to the British Council for awarding a fellowship to E.D. and to the Science Research Council for awarding a Research Studentship to J.D.G. The paper was written while R.P. was a visiting Professor at California Institute of

Technology; he is grateful to this Institute for hospitality as well as to the National Science Foundation for a Senior Foreign Scientist Fellowship.

SUMMARY

The adsorption of butane-1,4-diol, 2-butyne-1,4-diol, *n*-butanol and diethyl ether on a mercury electrode from 0.1 *M* aqueous fluoride solutions at 25° has been studied using a capillary electrometer. The results have been used to examine the basic assumptions of the theory of adsorption of neutral molecules at mercury electrodes. Although distinction is difficult, there is some evidence that charge is the electrical variable to be preferred. It is suggested that the version of the water competition theory due to BOCKRIS *et al.* neglects the interaction between water and the adsorbed species, which plays a significant role in the adsorption behaviour. The effect of the triple bond is probably largely due to the increased rigidity of the molecule and not to a direct interaction with the electrode.

REFERENCES

1 G. GOUY, *Ann. Phys. Chim.*, 8 (1906) (8) 291.
2 G. GOUY, *ibid.*, 9 (1906) (8) 75.
3 A. N. FRUMKIN AND B. B. DAMASKIN, *Modern Aspects of Electrochemistry III*, edited by J. O'M. BOCKRIS AND B. E. CONWAY, Butterworths, London, 1964, chap. 3.
4 A. N. FRUMKIN, *Z. Physik.*, 35 (1926) 792.
5 K. M. JOSHI AND R. PARSONS, *Electrochim. Acta*, 4 (1961) 129.
6 R. PARSONS AND F. G. R. ZOBEL, *J. Electroanal. Chem.*, 9 (1965) 333.
7 G. GOUY, *Ann. de Phys.*, 6 (1916) 5.
8 A. I. VOGEL, *Quantitative Inorganic Analysis*, Longmans, Green, London, 2nd ed. 1959, p. 247.
9 J. LAWRENCE, R. PARSONS AND R. PAYNE, *J. Electroanal. Chem.*, 16 (1968) 193.
10 E. DUTKIEWICZ AND R. PARSONS, *J. Electroanal. Chem.*, 11 (1966) 100.
11 J. A. V. BUTLER, D. W. THOMSON AND W. H. MACLENNAN, *J. Chem. Soc.*, (1933) 674.
12 F. BOURION AND E. ROUYER, *Compt. Rend.*, 194 (1932) 1240.
13 D. C. GRAHAME, *Chem. Rev.*, 41 (1947) 441.
14 R. PARSONS, *Trans. Faraday Soc.*, 55 (1959) 999.
15 R. PARSONS, *Proc. Roy. Soc. London*, A261 (1961) 79.
16 S. LEVINE, G. M. BELL AND D. CALVERT, *Can. J. Chem.*, 40 (1962) 518.
17 R. PARSONS, *J. Electroanal. Chem.*, 8 (1964) 93.
18 B. B. DAMASKIN, *Elektrokhimiya*, 1 (1965) 63.
19 T. A. KRYUKOVA AND A. N. FRUMKIN, *Zh. Fiz. Khim.*, 23 (1949) 819.
20 J. O'M. BOCKRIS, M. A. V. DEVANATHAN AND K. MÜLLER, *Proc. Roy. Soc. London*, A274 (1963) 55.
21 R. PARSONS AND F. G. R. ZOBEL, *Trans. Faraday Soc.*, 62 (1966) 3511.
22 R. G. BARRADAS AND P. G. HAMILTON, *Can. J. Chem.*, 43 (1965) 2468.

ELECTROANALYTICAL CHEMISTRY AND INTERFACIAL ELECTROCHEMISTRY
Elsevier Sequoia S.A., Lausanne – Printed in The Netherlands

THE KINETICS OF ADSORPTION OF NEUTRAL ORGANIC COMPOUNDS AT A MERCURY ELECTRODE

R. D. ARMSTRONG, W. P. RACE AND H. R. THIRSK
Department of Physical Chemistry, University of Newcastle upon Tyne, Newcastle upon Tyne, (England)
(Received July 27th, 1967)

INTRODUCTION

FRUMKIN AND MELIK-GAIKAZYAN[1] first considered the frequency-dependence of the impedance of an electrode at which there was adsorption of neutral molecules. For the case where the adsorption kinetics were entirely controlled by the rate of the heterogeneous process, they deduced the following equations for the electrode impedance.

$$C_p = C_\infty + \Delta C\left(\frac{\partial v}{\partial \Gamma}\right)^2_{\phi,c} \Big/ \left\{\omega^2 + \left(\frac{\partial v}{\partial \Gamma}\right)^2_{\phi,c}\right\} \tag{1}$$

$$1/\omega R_p = \Delta C\left(\frac{\partial v}{\partial \Gamma}\right)_{\phi,c} \omega \Big/ \left\{\omega^2 + \left(\frac{\partial v}{\partial \Gamma}\right)^2_{\phi,c}\right\} \tag{2}$$

where the symbols are defined in the notation section.

If

$$\tau_H = \left(\frac{\partial \Gamma}{\partial v}\right)_{\phi,c}$$

is defined as the relaxation time of the heterogeneous adsorption process, then (1) and (2) become

$$C_p = C_\infty + \Delta C/(1+\omega^2\tau_H^2) \tag{3}$$

$$1/\omega R_p = \Delta C\omega\tau_H/(1+\omega^2\tau_H^2) \tag{4}$$

These equations have the same form as the Debye–Pellat equations for the relaxation of polarisation in a dielectric where there is a single relaxation time. Thus a plot of $1/\omega R_p$ *vs.* C_p should take the form of a semi-circle in this case with centre $C_p = \Delta C/2 + C_\infty$, $1/\omega R_p = 0$.

In the situation where the kinetics of adsorption are diffusion-controlled, the expressions for the electrode impedance are:

$$C_p = C_\infty + \frac{\Delta C\left[\left(\frac{\partial \Gamma}{\partial c}\right)_\phi \left(\frac{\omega}{2D}\right)^{\frac{1}{2}} + 1\right]}{\left[\left(\frac{\partial \Gamma}{\partial c}\right)_\phi \left(\frac{\omega}{2D}\right)^{\frac{1}{2}} + 1\right]^2 + 1} \tag{5}$$

$$\frac{1}{\omega R_p} = \frac{\Delta C\left(\frac{\partial \Gamma}{\partial c}\right)_\phi \left(\frac{\omega}{2D}\right)^{\frac{1}{2}}}{\left[\left(\frac{\partial \Gamma}{\partial c}\right)_\phi \left(\frac{\omega}{2D}\right)^{\frac{1}{2}} + 1\right]^2 + 1} \tag{6}$$

Let a mean diffusion-controlled relaxation time be defined by the relation

$$\tau_D = \left(\frac{\partial \Gamma}{\partial c}\right)_\phi^2 / D$$

and a Cole–Cole[2] distribution of relaxation times about τ_D be assumed, with the particular value $\alpha = \frac{1}{2}$ in their eqn. (13), which for the case of the relaxation of dielectric polarisation leads to the frequency-dependence of the real (ε') and imaginary (ε'') parts of the complex dielectric constant (ε^*) given below:

$$\varepsilon' = \varepsilon_\infty + \frac{(\varepsilon_0 - \varepsilon_\infty)\left[1 + (\omega\tau_D)^{1-\alpha}\sin\left(\frac{1}{2}\alpha\pi\right)\right]}{1 + 2(\omega\tau_D)^{1-\alpha}\sin\left(\frac{1}{2}\alpha\pi\right) + (\omega\tau_D)^{2(1-\alpha)}} \tag{7}$$

$$\varepsilon'' = \frac{(\varepsilon_0 - \varepsilon_\infty)(\omega\tau_D)^{1-\alpha}\cos\left(\frac{1}{2}\alpha\pi\right)}{1 + 2(\omega\tau_D)^{1-\alpha}\sin\left(\frac{1}{2}\alpha\pi\right) + (\omega\tau_D)^{2(1-\alpha)}} \tag{8}$$

Equations (5) and (6) can then be written

$$C_p = C_\infty + \frac{\Delta C\left[1 + \left(\frac{1}{2}\omega\tau_D\right)^{\frac{1}{2}}\right]}{1 + (2\omega\tau_D)^{\frac{1}{2}} + \omega\tau_D} \tag{9}$$

$$1/\omega R_p = \Delta C\left(\tfrac{1}{2}\omega\tau_D\right)^{\frac{1}{2}} / \{1 + (2\omega\tau_D)^{\frac{1}{2}} + \omega\tau_D\} \tag{10}$$

Equations (9) and (10) require that $1/\omega R_p$ *vs.* C_p should take the form of a quarter-circle, intersecting the C_p-axis at values of C_∞, and $(C_\infty + \Delta C)$. This is analogous to the behaviour of ε'' *vs.* ε' when $\alpha = \frac{1}{2}$ in eqns. (7) and (8).

The consistency of the concept of a mean relaxation time for diffusion-controlled adsorption can be shown by considering a potentiostatic perturbation involving a substance obeying a linear adsorption isotherm, $\Gamma = Kc$. DELAHAY AND TRACHTENBERG[3] have shown that the surface concentration of adsorbed substance, Γ_t, after time t (where $\Gamma = 0$ at $t = 0$) is given by

$$\Gamma_t/\Gamma_e = 1 - \exp(Dt/K^2)\,\mathrm{erfc}\,(D^{\frac{1}{2}}t^{\frac{1}{2}}/K) \tag{11}$$

where $\Gamma_e = \Gamma_t$ as $t \to \infty$.

This result can also be derived as follows. For a single relaxation time

$$\Gamma_t/\Gamma_e = 1 - \exp(-t/\tau_D) \tag{12}$$

whereas for a distribution of relaxation times about τ_D described by the function $f(\tau)\,d\tau$,

$$\Gamma_t/\Gamma_e = \int_0^\infty f(\tau)\,d\tau - \int_0^\infty \exp(-t/\tau_D) f(\tau)\,d\tau \tag{13}$$

For the Cole–Cole distribution, with $\alpha = \frac{1}{2}$ in their eqn. (13):

$$f(\tau) = \tau_D^{\frac{1}{2}} / \{\pi\tau^{\frac{1}{2}}(\tau_D + \tau)\} \tag{14}$$

Inserting this in (13) and integrating gives:

$$\Gamma_t/\Gamma_e = 1 - \exp(t/\tau_D)\ \mathrm{erfc}\,(t/\tau_D)^{\frac{1}{2}} \tag{15}$$

This is identical with (11) since in this case $\tau_D = K^2/D$.

The situation with mixed diffusion and heterogeneous control was treated in its most general form by LORENZ[4]. The electrode impedance may be expressed by the relations:

$$C_p = C_\infty + \frac{\Delta C[(\frac{1}{2}\omega\tau_D)^{\frac{1}{2}} + 1]}{[(\frac{1}{2}\omega\tau_D)^{\frac{1}{2}} + \omega\tau_H]^2 + [(\frac{1}{2}\omega\tau_D)^{\frac{1}{2}} + 1]^2} \tag{16}$$

$$\frac{1}{\omega R_p} = \frac{\Delta C[(\frac{1}{2}\omega\tau_D)^{\frac{1}{2}} + \omega\tau_H]}{[(\frac{1}{2}\omega\tau_D)^{\frac{1}{2}} + \omega\tau_H]^2 + [(\frac{1}{2}\omega\tau_D)^{\frac{1}{2}} + 1]^2} \tag{17}$$

In this case, if τ_H and τ_D are of the same order, a plot of $1/\omega R_p$ *vs.* C_p gives a gradual transition from a quarter-circle (at low frequencies when there is effectively complete diffusion control) to a semi-circle (at high frequencies when the control is effectively heterogeneous). LORENZ AND MOCKEL[5] have analysed the behaviour of the quantity $\omega(C_p - C_\infty)R_p$, or $\omega C_p{}^* R_p$ as a function of $\omega^{-\frac{1}{2}}$ for various ratios of $\tau_H : \tau_D$. From eqns. (16) and (17), it follows that

$$\omega C_p{}^* R_p = \{1 + (2/\omega\tau_D)^{\frac{1}{2}}\}/\{1 + (2\omega/\tau_D)^{\frac{1}{2}}\tau_H\} \tag{18}$$

Taking ΔC to be 100 μF cm^{-2} and $C_\infty = 0$, we have analysed the three specific cases where:

(a) $\tau_D = 10^{-7}$ sec; $\tau_H = 0$;

(b) $\tau_D = 10^{-7}$ sec; $\tau_H = 10^{-7}$ sec;

(c) $\tau_D = 0$; $\tau_H = 10^{-7}$ sec;

corresponding to pure diffusion, mixed, and pure reaction control, respectively. In Figs. 1 and 2 we show the behaviour of C_p and $1/\omega R_p$ as functions of log ω, and in Fig. 3 the respective Cole–Cole plots. Figure 4 shows the same hypothetical situations plotted after the manner of LORENZ. From inspection of the forms of Figs. 1–4, the following points may be appreciated.

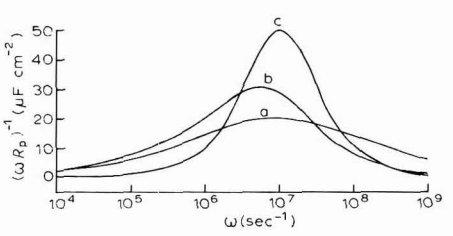

Fig. 1. Variation of $1/\omega R_p$ with log ω for hypothetical values of τ_H and τ_D: (a) $\tau_D = 10^{-7}$ sec, $\tau_H = 0$; (b) $\tau_D = \tau_H = 10^{-7}$ sec; (c) $\tau_D = 0$, $\tau_H = 10^{-7}$ sec.

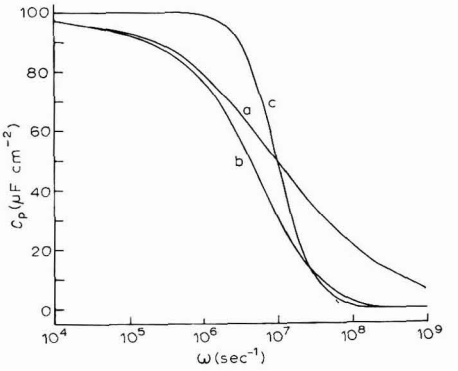

Fig. 2. The dependence of C_p on log ω. (a), (b) and (c) as in Fig. 1.

(1) At any given frequency, the value of $\omega C_p{}^* R_p$ for pure diffusion control exceeds that for partial reaction control. Also, from eqn. (18), in the case of mixed diffusion and reaction control, low-frequency values of $\omega C_p{}^* R_p$ will lie on a line parallel to the line for pure diffusion control, but lying beneath it by an amount $2\tau_H/\tau_D$, thus extrapolating to an intercept of $1-2\tau_H/\tau_D$ on the $\omega C_p{}^* R_p$-axis. Thus for the case where $\tau_H = \tau_D$, as in the mixed case analysed in Figs. 1–4, the extrapolation of low-frequency data gives an intercept of -1, as shown by the broken line in Fig. 4.

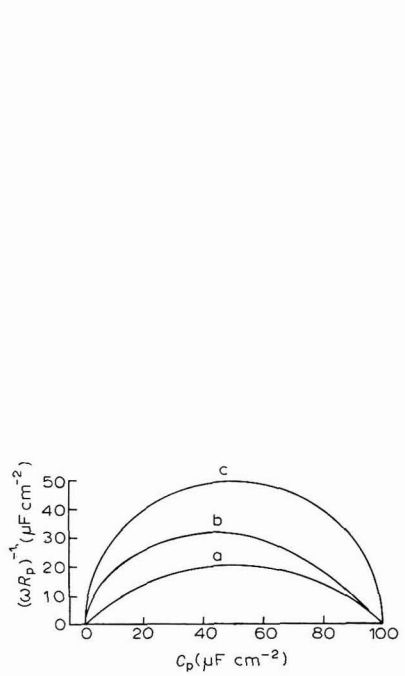

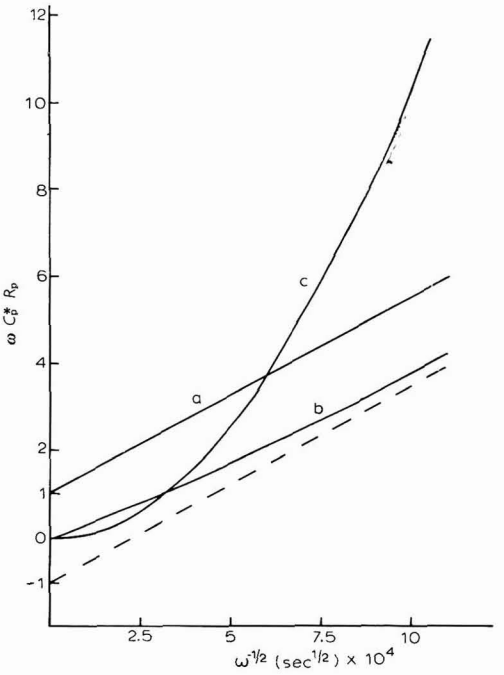

Fig. 3. The hypothetical dependence of C_p on $1/\omega R_p$. (a), (b) and (c) as in Fig. 1.

Fig. 4. The hypothetical dependence of $\omega C_p R_p$ on $\omega^{-\frac{1}{2}}$. Broken line drawn with same slope as line (a), would represent the extrapolation of line (b) from low-frequency data.

(2) The observation that an experimental point has an ordinate less than 1 means that the heterogeneous relaxation frequency has been exceeded, and a considerable deviation from the quarter-circle plot, and from the diffusion form of the $1/\omega R_p$ *vs.* log ω plot, must also be observable. In any case of mixed (or pure reaction) control, the heterogeneous relaxation frequency is that at which $\omega C_p{}^* R_p = 1$.

For the case of pure diffusion-controlled adsorption, it is instructive to investigate further the frequency-dependences of the quantities, C_p and $1/\omega R_p$. Testing whether data follow the form of curve predicted by eqn. (10), is a useful method of examining for any significant deviation from pure diffusion control, and also for obtaining an estimate of τ_D, the diffusion relaxation time. The dependences of C_p, and $1/\omega R_p$ on $\omega^{\frac{1}{2}}$ are illustrated in Fig. 5 for $\tau_D = 10^{-7}$ sec, as in (a) above. From eqns. (9) and (10), it may be shown that as $\omega \to 0$,

$$C_p \rightarrow C_\infty + \Delta C[1 - (\tfrac{1}{2}\omega\tau_D)^{\frac{1}{2}}] \quad (19)$$

$$1/\omega R_p \rightarrow \Delta C(\tfrac{1}{2}\omega\tau_D)^{\frac{1}{2}} \quad (20)$$

Thus, at frequencies much less than that corresponding to τ_D, an extrapolation to zero-frequency of C_p gives accurately the thermodynamic double-layer capacity (C_0). Also, an estimate of τ_D can be made from the slope of the graph. A good test of the applicability of this procedure to any specific data is to test also the dependence of $1/\omega R_p$ on $\omega^{\frac{1}{2}}$; this should also take a linear form, and should extrapolate to zero at zero-frequency. The modulus of the slope should be exactly that of the C_p graph. If the

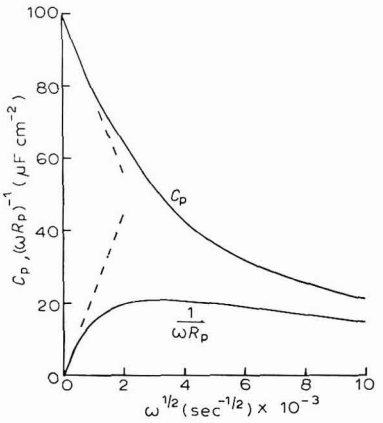

Fig. 5. The extrapolation to zero-frequency of C_p, and $1/\omega R_p$.

$1/\omega R_p$ graph fails to extrapolate through zero, then the capacity data will not extrapolate exactly to C_0. If the frequency range of the data is low enough, the series capacities will extrapolate to C_0 in exactly the same manner as the parallel capacities; but at higher frequencies the series values deviate more rapidly from the linear part of the graph.

Experimentally, this method of obtaining τ_D is limited by the effects of electrolyte penetration, which can considerably alter both C_p and R_p at low frequencies. In situations where τ_D is entirely unknown, it is not safe to use this method to obtain C_0 unless the resistance data are also analysed, and give the same slope, and zero intercept. The capacitance data alone (in series of parallel form) may be analysed when τ_D is known to be considerably removed from the frequencies of the data.

Ideally, as a method of obtaining τ_D, this treatment has the following advantages. An internal test for its applicability exists, in the comparison of the slopes. Also, in cases where there is a heterogeneous relaxation time of the same order as the diffusion time, the latter may be resolved independently from low-frequency measurements.

In connection with Fig. 5, it is emphasised that the frequency range there represented covers several decades, and is not the sort of situation usually found in experimental investigations, in which, when a comparatively small frequency range is used, the respective segments of the Fig. 5 curves could be so expanded that they might be mistaken for straight lines.

It has been claimed[4,5] that finite values ($\sim 10^{-5}$ sec) of τ_H are experimentally detectable from impedance measurements at high frequencies. It was the purpose of this investigation to determine whether τ_H is observable, within our experimental accuracy, for the adsorption of neutral molecules on a mercury electrode, and to illustrate that at the frequencies at which such a process is entirely diffusion-controlled, the relaxation of the adsorption is analogous to a dielectric relaxation process with a particular distribution of relaxation times.

EXPERIMENTAL

Solutions were made up in triply-distilled water using AnalaR KCl and *n*-butyric acid. Mercury was purified by prolonged agitation under dilute nitric acid, and was then distilled twice *in vacuo*. Details of the audio-frequency Wien bridge, and the radio-frequency transformer ratio arm bridge are given elsewhere[6], as is a description of the hanging mercury drop electrode, and the overall cell design. Potentials were measured with respect to a saturated calomel electrode.

RESULTS

Impedance measurements of the interfaces:

Hg (hanging drop)–2 *N* KCl, 0.25 *M* *n*-butyric acid, aq.,

Hg (hanging drop)–2 *N* KCl, 0.05 *M* cyclohexanol, aq.,

were made as follows.

(a) The series capacity was measured on the audio-frequency Wien bridge at frequencies between 100 Hz, and 25 kHz, using electrode areas of approximately 0.04 cm^2; measurements with reduced precision were made at frequencies up to 100 kHz, using drop areas ~ 0.01 cm^2.

(b) The series resistance of the cell was examined at frequencies from 300 Hz – 500 kHz, on the audio-frequency bridge (the use of a Wien bridge to measure resistance at high frequencies is examined in ref. 6).

(c) The impedance was measured as a parallel combination at frequencies between 60 kHz and 1 MHz, using the transformer ratio arm bridge.

Details of the procedure for obtaining accurately the series double-layer capacity from such measurements are given in ref. 6.

The frequency-dependence of the impedances of the interfaces was examined at the potential of the negative peak on the *C–E* curves. The capacity of the interface, Hg/2 *N* KCl aq., was also obtained at these potentials. The capacity of the interfaces was also examined at potentials near the e.c.m.

The first step in the determination of the interfacial impedance is the subtraction from the measured cell resistances of the solution resistance. Previously, four methods have been used to obtain solution resistances, *viz.*:

(1) Calculation from tabulated conductivity data

(2) Direct measurement at very high frequencies

(3) Extrapolation techniques

(4) Measurement of the cell resistance at potentials well removed from the desorption peak potential.

The last method was used in the present work, since by observing the impedance of the same mercury drop at potentials different from that of the peak, even small changes of the resistance can be accurately detected, and the error of the uncertainty of drop area (usually less than 1%) is not reflected in the relative values of the interfacial impedance at different frequencies. Also, any small deviations of the high-frequency resistance due to electrode shielding, or of the low-frequency resistance due to electrolyte penetration, are observed as an apparent frequency-dependence of the impedance at potentials well removed from the peak potential. When direct high-frequency measurement, or extrapolation techniques are employed, there is a possibility that any anomalous frequency dispersion of the impedance is not recognized, and the frequency at which the solution resistance is determined by direct measurement must, in any case, be high enough to be well above the mean relaxation frequency. Calculation of the solution resistance from conductivity data ideally requires the conductivity to be measured *in situ*, to avoid concentration or temperature errors, but even then the interfacial impedance values are subject to considerable error resulting from the electrode area uncertainty. At high frequencies when the interfacial resistance is small, a 1% drop area uncertainty could result in a serious systematic error, which might be interpreted as an apparent deviation from the behaviour of the impedance accompanying purely diffusion-controlled adsorption.

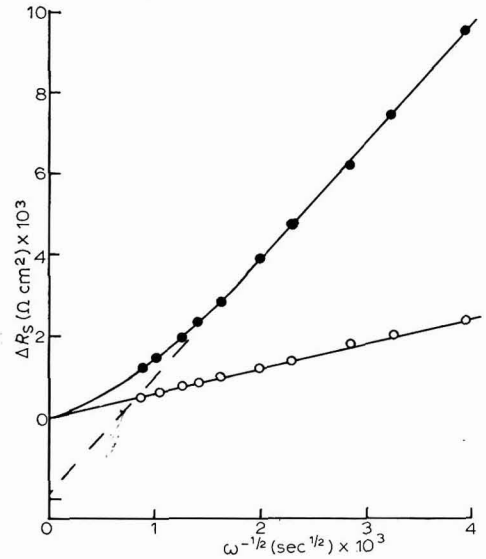

Fig. 6. The experimental extrapolations to infinite frequency of the series interfacial resistance: (●), cyclohexanol; (○), butyric acid.

Calculation of the solution resistance by extrapolating to infinite frequency the measured resistance, *e.g.*, by plotting the measured R_s *vs.* $\omega^{-\frac{1}{2}}$, is a procedure which does in some cases lead to the correct value, but since the limiting slope as $\omega \to \infty$ is 0, then there will exist cases when such a graph "levels out", and an extrapolation from the linear part leads to too low a value of the solution resistance. This procedure was applied as follows to the results reported in the present work. Figure 6

shows the dependence of the interfacial resistance, as obtained from measurements at different potentials, as a function of $\omega^{-\frac{1}{2}}$, for the two interfaces studied. In the case of butyric acid, when the relaxation process had not been completely spanned at the frequencies employed, the extrapolation does give the same value for the solution resistance as that obtained from measurements at different potentials, *i.e.*, the interfacial resistance extrapolates through zero. If this procedure is used to estimate the solution resistance for cyclohexanol results, a considerable over-subtraction arises.

The solution resistance having been subtracted, the remaining components of the impedance are converted to their parallel equivalents. An estimate of the infinite frequency capacity, C_∞, is made by taking the mean of the capacity near the e.c.m., and that in the base electrolyte solution alone, at the potential of the desorption peak. This value is subtracted from the parallel capacity, C_p, to give the capacity, C_p^*, resulting solely from the adsorption process. The somewhat approximate value of C_∞ obtained by this method (which assumes half-coverage at the desorption peak) was not critical in the subsequent analysis.

Figure 7 shows the experimentally-observed variation of the measured C_s with log frequency for the two systems. It may be seen that the measurements for

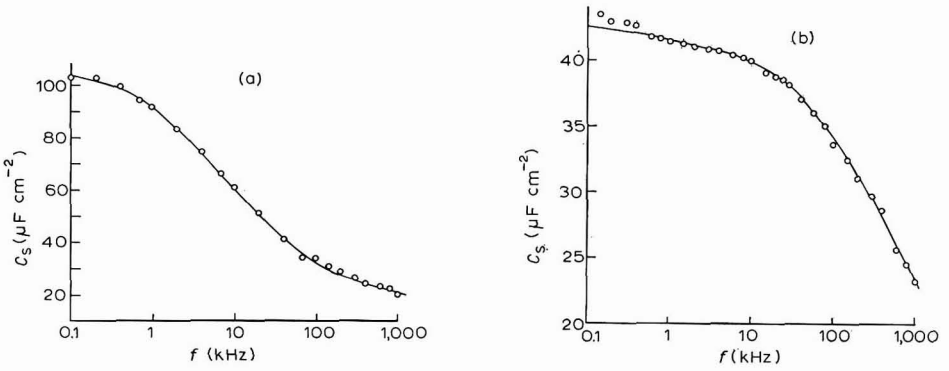

Fig. 7. The frequency-dependence of the observed series double-layer capacity: (a), cyclohexanol; (b), butyric acid.

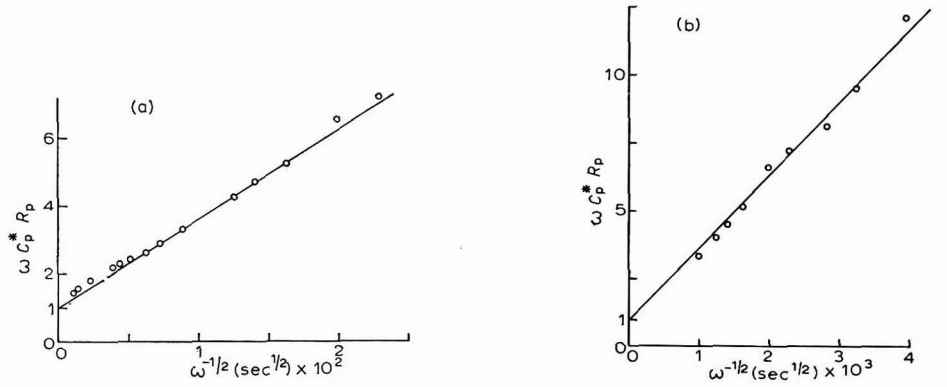

Fig. 8. The dependence of $\omega C_p^* R_p$ on $\omega^{-\frac{1}{2}}$: (a), cyclohexanol; (b), butyric acid.

butyric acid do not show the inflection observed for the cyclohexanol solution, thus illustrating that in the former case the relaxation has not been completely spanned at frequencies approaching 1 MHz.

Figure 8 shows the behaviour of the quantity $\omega C_p^* R_p$ as a function of $\omega^{-\frac{1}{2}}$ at frequencies up to 150 kHz. At no point has $\omega C_p^* R_p$ been observed to be less than 1, and the fact that the extrapolation of the lower frequency results goes through 1 at infinite frequency, within experimental error, shows that there is no significant deviation from diffusion control at the frequencies studied.

In Fig. 9, the analogy of the diffusion-controlled adsorption process with a dielectric relaxation process is tested, plots of the Cole–Cole type taking the form of a quarter-circle, showing that $\alpha = \frac{1}{2}$. The quarter-circles drawn through the experimental points intersect the capacitance axes at values near the estimated infinite frequency capacities, and values near the estimated thermodynamic values (which are shown as closed circles).

Figure 10 shows the dependence of $1/\omega R_p$ on log frequency. The open circles are the experimental points, with the curves drawn through the closed circles at the peaks, according to eqn. (10), corresponding to pure diffusion control. It may be seen that the experimental data closely follow the behaviour for diffusion control.

Figure 11 shows the capacitance extrapolation to zero-frequency for the two systems, the parallel value being used for cyclohexanol, where the relaxation frequency

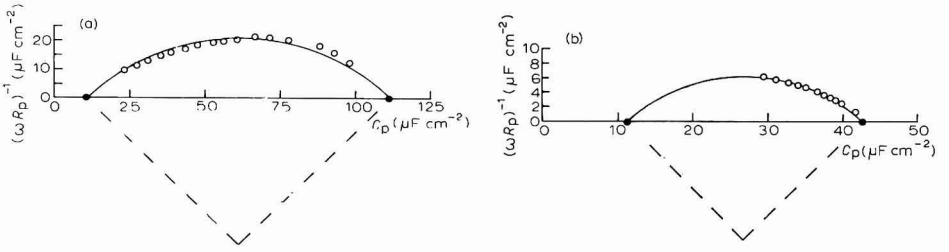

Fig. 9. The dependence of $1/\omega R_p$ on C_p: (a), cyclohexanol; (b), butyric acid.

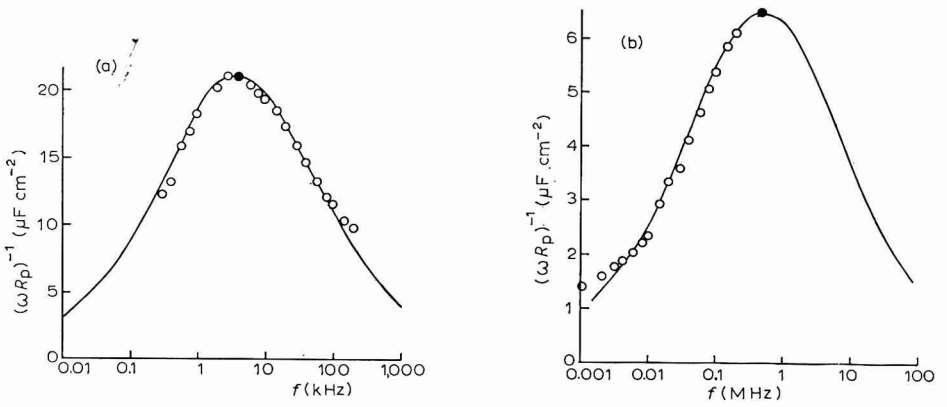

Fig. 10. The frequency-dependence of $1/\omega R_p$: (a), cyclohexanol; (b), butyric acid. (○), exptl. points; curves drawn through closed circles at peaks assuming eqn. (10).

is not far removed from the frequencies shown; in the case of the butyric acid, the series values at these frequencies are almost identical with the parallel capacities, since the relaxation frequency is considerably higher, so the series values are shown. The estimates of C_0 obtained from the intercepts are shown on the Cole–Cole plots (Fig. 9). An estimate of f_D has been made from the slopes of the extrapolations, but owing to the difficulty of avoiding the effects of electrolyte penetration on the measured series resistance and capacitance at low frequencies, this estimate is necessarily less precise than the other estimates discussed in the following section. Also, the fact that for cyclohexanol the estimated relaxation frequency from the slope of Fig. 11 is higher than that obtained from the other treatments, shows that the frequencies used for the C_p extrapolation are too near the relaxation frequency to yield the limiting slope, although, in fact, the slope is only about a factor of 0.7 from the limiting slope predicted from the other estimates of the relaxation frequency made below. The error in the estimation of C_0 is unlikely to be high.

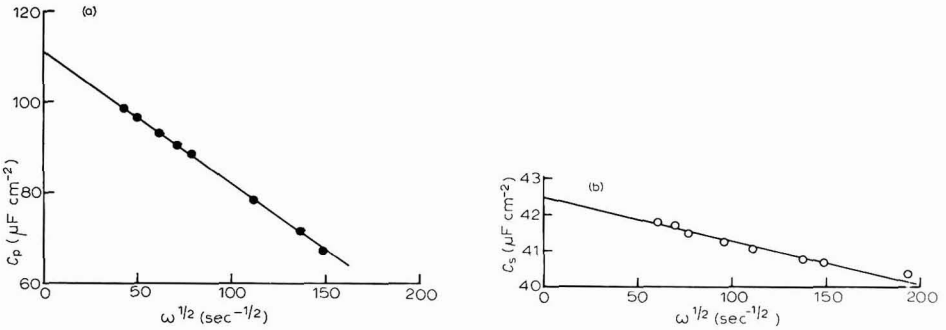

Fig. 11. Extrapolations to zero-frequency of the observed capacities: (●), C_p for cyclohexanol; (○), C_s for butyric acid.

TABLE 1

ESTIMATES OF THE DIFFUSION-CONTROLLED RELAXATION FREQUENCY, f_D

Method of estimation	*0.25 M n-butyric acid 2N KCl, aq., 1135 mV (SCE) 25.9°±0.1° (kHz)*	*0.05 M cyclohexanol 2N KCl, aq., 1213 mV (SCE) 26.3°±0.1° (kHz)*
$\omega C_p^* R_p$ *vs.* $\omega^{-\frac{1}{2}}$ (Fig. 8)	580	5.5
Cole–Cole plots (Fig. 9)	350	6
$1/\omega R_p$ *vs. log f* (Fig. 10)	500	4
C_s, C_p *vs.* $\omega^{+\frac{1}{2}}$ (Fig. 11)	550	9.5
$C_p^* = C/2$	—	6.2
Fig. 12	480	7.3

For a purely diffusion-controlled adsorption process, there are two further methods of analysing the impedance data to obtain estimates of f_D. The parallel capacitance, C_p, falls to a value of $(C_0 - \Delta C/2)$ at f_D. The estimate of f_D thus obtained is included in Table 1. Such an estimate can only be made when the relaxation frequency is actually spanned by the frequencies at which the data are obtained;

any systematic errors in the measurements at these frequencies will be directly reflected in the estimate of f_D.

Secondly, it can be shown that if the function

$$\log\left[\left\{(C_0-C_p)^2+\left(\frac{1}{\omega R_p}\right)^2\right\}\Big/\left\{C_p{}^{*2}+\left(\frac{1}{\omega R_p}\right)^2\right\}\right]$$

is plotted *vs.* log f, a straight line of slope $2(1-\alpha)$ results. Figure 12 shows the results for the two systems treated in this manner; the lines drawn through the experimental points have unit slope, confirming that in this case $\alpha=\frac{1}{2}$. For a completely heterogeneously-controlled process, a straight line of slope 2 would result ($\alpha=0$), and for a case of mixed control, a line of unit slope at low frequencies would

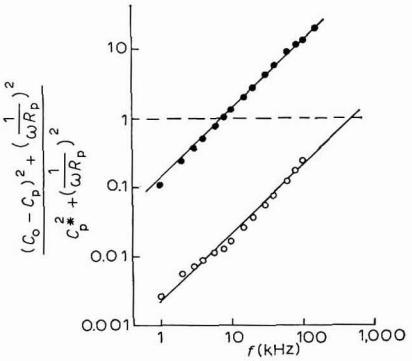

Fig. 12. The dependence of $\log[\{(C_0-C_p)^2+(1/\omega R_p)^2\}/\{C_p{}^{*2}+(1/\omega R_p)^2\}]$ on $\log f$: (●), cyclohexanol; (○), butyric acid.

deviate at higher frequencies, giving ultimately a line of slope 2. A further estimate of f_D may be by noting the frequency at which $(C_0-C_p)=C_p{}^*$, when the function

$$\left\{(C_0-C_p)^2+\left(\frac{1}{\omega R_p}\right)^2\right\}\Big/\left\{C_p{}^{*2}+\left(\frac{1}{\omega R_p}\right)^2\right\}$$

has the value of unity (in a case of pure heterogeneous control, this function would have the value unity at f_H). When measurements at the relaxation frequency are not available, an estimate of f_D may be made by extrapolating low-frequency data; this is done for the butyric acid results in Fig. 12. It is interesting to note that in a case of mixed control, f_D would be obtained by extrapolating low-frequency data, and if measurements could be made at $f \gg f_H, f_D$, an independent estimate of f_H could be made by extrapolating back the high-frequency data.

DISCUSSION

The fact that the plots of Fig. 9 take the form of quarter-circles illustrates that a diffusion-controlled adsorption process is analogous to a dielectric relaxation phenomenon with the particular spread of relaxation times corresponding to a Cole–Cole distribution of relaxation times with $\alpha=\frac{1}{2}$.

The various estimates of the relaxation frequency that can be made from

Figs. 8–12 are listed in Table 1, from which it may be seen that the best general agreement is obtained in the case where the relaxation is completely spanned.

It is thus useful to study adsorption phenomena by measuring the electrode impedance, and treating the results as outlined above; the agreement between the various estimates of the relaxation frequency is a sensitive test of the precision of the data. In the cases examined, there is no evidence for any deviation from pure diffusion control at frequencies up to 150 kHz, thus τ_H must in both cases be less than about 10^{-6} sec. However, since the organic molecule has a particular orientation with respect to the electrode when adsorbed, whereas in solution the orientation is random, τ_H cannot be less than the rotational relaxation time of the molecule, which is probably of the order of 10^{-10} sec.

Finally, some suggestions are made concerning possible causes of the discrepancy between the work of LORENZ[4,5] and the present investigation. The importance of accurate estimation of the solution resistance has already been emphasised. LORENZ[4] regarded the estimation of the solution resistance by extrapolation to infinite frequency of a plot of R_s *vs.* $\omega^{-\frac{1}{2}}$, as superior to a value obtained by measuring the resistance in a potential region where it is frequency-independent. Whilst the latter method may involve errors arising from the potential-dependence of electrolyte penetration effects, these errors are small for aqueous systems at the frequencies involved, and can also be carefully assessed either by comparing the measurements on both sides of the cathodic desorption peak, or by using the potential region between the anodic and cathodic desorption peaks. As we have shown, the extrapolation method must always underestimate the solution resistance, and such an error would explain the form of the discrepancy between the results obtained by LORENZ and our own. It is also possible that errors due to inductive effects[6] at $\sim$100 kHz arose in LORENZ's Wien bridge circuit in view of the relatively large electrode area used.

ACKNOWLEDGEMENTS

R.D.A. thanks I.C.I. Ltd. for a research fellowship, and W.P.R. thanks the S.R.C. for a research studentship, during the tenures of which the present work was undertaken.

SUMMARY

It is shown theoretically, and illustrated experimentally, that an entirely diffusion-controlled adsorption process leads to a frequency-dependence of an electrode impedance which is analogous to that produced by a dielectric relaxation process with a particular spread of relaxation times. The possibility of detecting a finite adsorption rate from impedance measurements is examined experimentally for the adsorption of *n*-butyric acid, and cyclohexanol on a mercury electrode, and it is concluded that the relaxation time of the adsorption step lies between 10^{-6} and 10^{-10} sec in these cases.

NOTATION

c Concn. of species being adsorbed (mole cm^{-3})

C_s Series interfacial capacity (μF cm^{-2})
C_p Parallel interfacial capacity (μF cm^{-2})
C_0 Interfacial capacity as $f \to 0$ (μF cm^{-2})
C_∞ Interfacial capacity as $f \to \infty$ (μF cm^{-2})
ΔC $C_0 - C_\infty$ (μF cm^{-2})
C_p^* $C_p - C_\infty$ (μF cm^{-2})
D Diffusion coefficient (cm^2 sec^{-1})
f Frequency (Hz)
f_D Equivalent relaxation frequency for diffusion-controlled adsorption (kHz)
f_H Equivalent relaxation frequency for heterogeneously-controlled adsorption (kHz)
K Henry's law constant for the adsorption of species at an electrode (cm)
ΔR_s Series interfacial resistance (Ω cm^2)
R_p Parallel interfacial resistance (Ω cm^2)
v Net rate of adsorption due to a departure from equilibrium conditions (mole cm^{-2} sec^{-1})
α Parameter $0 \leqslant \alpha \leqslant 1$ determining the distribution of relaxation times
Γ Surface concentration (moles cm^{-2})
Γ_t Surface concentration at time t (moles cm^{-2})
Γ_e Surface concentration at equilibrium (moles cm^{-2})
ε^* Complex dielectric constant
ε' Real part of ε^*
ε'' Imaginary part of ε^*
ε_0 Static dielectric constant ($f \to 0$)
ε_∞ Infinite frequency dielectric constant ($f \to \infty$)
τ_H Relaxation time for a heterogeneously-controlled adsorption process (sec) $= 1/2\pi f_H$ (equivalent to V_Γ in the notation of LORENZ[4])
τ_D Relaxation time for a diffusion-controlled adsorption process (sec) $= 1/2\pi f_D$
ϕ Potential (V)
ω Angular frequency (radians sec^{-1})

REFERENCES

1 A. N. FRUMKIN AND V. I. MELIK-GAIKAZYAN, *Dokl. Akad. Nauk, SSSR*, 77 (1951) 855.
2 K. S. COLE AND R. H. COLE, *J. Chem. Phys.*, 9 (1941) 341.
3 P. DELAHAY AND I. TRACHTENBERG, *J. Am. Chem. Soc.*, 79 (1957) 2355.
4 W. LORENZ, *Z. Elektrochem.*, 62 (1958) 192.
5 W. LORENZ AND F. MOCKEL, *Z. Elektrochem.*, 60 (1956) 507.
6 R. D. ARMSTRONG, W. P. RACE AND H. R. THIRSK, to be published.

ELECTROANALYTICAL CHEMISTRY AND INTERFACIAL ELECTROCHEMISTRY
Elsevier Sequoia S.A., Lausanne – Printed in The Netherlands

ÜBER DEN CHARAKTER DER KATALYTISCHEN REAKTION, DIE BEI DER KATODISCHEN REDUKTION EINIGER ANORGANISCHER OXO-VERBINDUNGEN AN OXIDBEDECKTER PLATINOBERFLÄCHE BEOBACHTET WIRD

LOTHAR MÜLLER
Physikalisch-Chemisches Institut der Humboldt-Universität, 108 Berlin (DDR)
(Eingegangen am 7 April, 1967; revisioniert am 21 Juli, 1967)

Die beschleunigende Wirkung von Oberflächenoxiden auf die Geschwindigkeit elektrochemischer Reduktionsprozesse an Pt-Elektroden wurde in der Literatur von verschiedenen Autoren beschrieben und diskutiert[1–9]. Dabei nehmen DAVIS[4] und HOARE[8] an, dass die beschleunigende Wirkung von Pt-Sauerstoffchemisorptionsschichten auf elektrochemische Prozesse in der Beschleunigung der Elektronendurchtrittsreaktion über einen sogenannten "Oxidbrückenmechanismus" besteht.

ANSON UND KING[2] vertreten dagegen die Meinung, dass die Beschleunigung elektrochemischer Reduktionsreaktionen durch Pt-Sauerstoffverbindungen auf eine Platinierung der Elektrode infolge Reduktionen der bei der anodischen Vorpolarisation gebildeten Pt-Sauerstoffverbindungen zurückzuführen ist.

In unseren Arbeiten[10,11] konnte gezeigt werden, dass Pt-Sauerstoffchemisorptionsschichten elektrochemische Reduktionsreaktionen sowohl hemmen als auch beschleunigen können. So wird die Reduktion von Co^{3+} zu Co^{2+} [10] und von O_2 zu H_2O_2[11] durch Pt-Sauerstoffchemisorptionsverbindungen gehemmt, während die Reduktionsreaktionen von H_2O_2[11], S_2O_8[10,12], ClO^-[13] in 0.1 *N* KOH und IO_3^-[14] in 0.1 *N* H_2SO_4 durch Pt-Sauerstoffverbindungen gleichzeitig sowohl gehemmt als auch beschleunigt werden. Die Beschleunigung der letztgenannten Reaktionen durch Pt-Sauerstoffchemisorptionsverbindungen drückt sich deutlich in der für sie charakteristischen Form der Polarisationskurve (I–φ-Kurve) aus, wie sie in Abb. 1 (Kurven 1 und 2) für die Jodatreduktion dargestellt ist. Die I–φ-Kurven zeigen im Potentialbereich $\varphi \sim 0.75$–0.4 V* Abfall des Stromes und bei $\varphi < 0.4$ V einen erneuten Anstieg des Reduktionsstromes. Diese Kurvenform ist für alle von uns untersuchten Reduktionsreaktionen, bei denen beschleunigender Einfluss von Pt-Sauerstoffchemisorptionsverbindungen beobachtet wird, typisch (bei der Red. von $S_2O_8^{2-}$ beobachtet man keinen Stromabfall, sondern nur starke Hemmung des Prozesses bei $\varphi < 0.65$ V), obwohl die Potentiale, bei denen der Abfall des Stromes einsetzt, bzw. bei denen erneuter Stromanstieg beobachtet wird, in jedem Fall etwas verschieden sind, bedingt durch Unterschiede in den elektrochemischen und kinetischen Parametern der jeweiligen Reaktion.

Der auftretende Stromabfall ist, wie bereits in der Arbeit von ANSON[1] über die Reduktion von IO_3^- und in unseren Arbeiten über die Reduktion von Sauerstoff in alkalischer Lösung gezeigt wurde[11,15], auf die Reduktion der Sauerstoffchemisorp-

* Alle Potentiale beziehen sich auf die reversible Wasserstoffelektrode in der gleichen Lösung.

tionsverbindungen an der Pt-Oberfläche zurückzuführen. Dieser Schluss folgt aus dem Vergleich mit Ladekurven[16], die zeigen, dass im Potentialbereich $\varphi \sim 1.1$–0.4 V die Sauerstoffchemisorptionsverbindungen reduziert werden, was zur Folge hat, dass sich in diesem Potentialgebiet die physikalisch-chemischen Eigenschaften der Oberfläche der Pt-Elektrode stark ändern. In Abhängigkeit vom Typ der katodischen

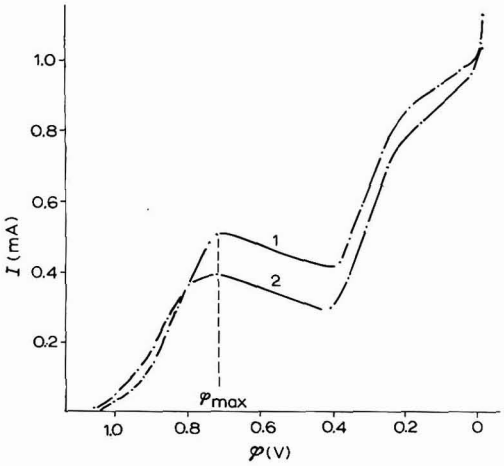

Abb. 1. I–φ-Kurven der Reduktion von Jodat in 0.1 N H_2SO_4 in Abhängigkeit vom Potential der anodischen Endaktivierung. $m = 27$ U/sec. (1), $\varphi_{AE} = +2.0$; (2), $\varphi_{AE} = +1.6$ V.

Reduktionsreaktion kann diese Veränderung der physikalisch-chemischen Eigenschaften der Pt-Oberfläche zu einer Erhöhung oder Erniedrigung der Geschwindigkeit der elektrochemischen Reduktionsreaktion führen. Die Tatsache, dass die Reduktion der Pt-Oberfläche die Geschwindigkeit verschiedener Reaktionen in verschiedener Richtung beeinflusst, lässt die ANSON'sche Ansicht[2] über die beschleunigende Wirkung von Pt-Sauerstoffchemisorptionsverbindungen sehr unwahrscheinlich erscheinen, da Platinierung der Pt-Elektrode in jedem Falle zu einer Beschleunigung des Elektrodenprozesses führen sollte. Ausserdem ist nach ANSON die Hemmung des Reduktionsprozesses bei $\varphi < 0.8$ V für die Reduktion von H_2O_2, ClO^- und $S_2O_8^{2-}$ in alkalischer Lösung nicht erklärbar, denn in dem Masse, wie die Pt-Sauerstoffchemisorptionsverbindungen reduziert werden, sollte es nach ANSON zu einer Erhöhung der katalytischen Aktivität der Elektrodenoberfläche infolge Platinierung kommen und nicht zu einer Erniedrigung derselben. Eine Erniedrigung der katalytischen Aktivität infolge Adsorption des Reaktionsproduktes, wie es bei der Jodatreduktion in 0.1 N H_2SO_4 möglich wäre, trifft für die obengenannten Reduktionen nicht zu, so dass die von ANSON entwickelten Vorstellungen über die Beschleunigung kathodischer Prozesse durch Pt-Sauerstoffchemisorptionsverbindungen für die von uns untersuchten Reaktionen kaum zutreffend sein können.

Betrachten wir deshalb kurz die Anwendbarkeit der erstmals von ANSON[1] für die Reduktion von Jodat ausgesprochenen Idee des Oxidbrückenmechanismus, die in der Folgezeit von ihm verworfen wurde, aber in den Arbeiten von DAVIS[4] und besonders von HOARE[8,17] auch weiterhin diskutiert wird, auf unsere Arbeiten. Dabei zeigt sich, dass zwar der Abfall des Stromes mit Hilfe dieses Mechanismus erklärt

werden könnte, dass aber die neben der beschleunigenden Wirkung gleichzeitig auftretende hemmende Wirkung von Pt-Sauerstoffverbindungen auf die kathodische Reduktion von $S_2O_8^{2-}$ [10], ClO^- [13], IO_3^- [14], eine formale Anwendung des Oxidbrückenmechanismus nicht erlaubt (bei der Reduktion von Jodat z.B. drückt sich die hemmende Wirkung in der Verschiebung der I–φ-Kurve nach negativen Potentialen bei Erhöhung des Oxydationsgrades der Pt-Elektrodenoberfläche aus (vgl. Kurve 1 und 2 in Abb. 1). Die zweifache Wirkung von Pt-Sauerstoffchemisorptionsverbindungen auf die kathodischen Reduktionsprozesse macht deutlich, dass mindestens zwei voneinander verschiedene heterogene Prozesse durch Oberflächensauerstoffverbindungen des Pt beeinflusst werden, wobei der eine von ihnen die elektrochemische Durchtrittsreaktion ist.

Unsere Untersuchungen ergaben, dass die Ströme der Reduktion von ClO^-, IO_3^- und $S_2O_8^{2-}$ bei Potentialen $\varphi > \varphi_{max.}$ kinetischer Natur sind und im Anfangsgebiet der Tafel'schen Beziehung gehorchen, was den Schluss zulässt, dass der geschwindigkeitsbestimmende Schritt in diesem Potentialbereich in allen 3 Fällen die elektrochemische Durchtrittsreaktion ist. Erhöht man den Oxidationsgrad der Pt-Elektrodenoberfläche durch Vorbehandlung bei höheren anodischen Potentialen, erhält man Tafelgeraden, die bei gleichem Potential einen niedrigeren Stromwert haben, d.h. dass Pt-Sauerstoffchemisorptionsverbindungen die elektrochemische Durchtrittsreaktion hemmen.

Bestätigt wurde diese Aussage durch die Untersuchung[10] des Reduktionsprozesses, $Co^{3+} + e \rightarrow Co^{2+}$.

Bei dieser Reaktion handelt es sich um einen einfachen Elektronendurchtritt und heterogen-katalytische Prozesse wie sie bei der Reduktion von Molekülen auftreten können, in deren Verlauf Bindungen gesprengt werden, sind hierbei ausgeschlossen. Der Vergleich der I–φ-Kurven der Co^{3+}-Reduktion mit den unter gleichen Bedingungen erhaltenen Kurven des Sauerstoffbedeckungsgrades an Pt in Abhängigkeit vom Potential zeigt, dass beide Kurven konform gehen, d.h. dass die Geschwindigkeit der Reduktion von Co^{3+} in dem Masse ansteigt, wie die Pt-Elektrode frei von Sauerstoffverbindungen wird.

Die beschleunigende Wirkung von Pt-Sauerstoffchemisorptionsverbindungen auf kathodische Reduktionsprozesse kann demzufolge nicht auf die unmittelbare Beschleunigung des Durchtrittsprozesses zurückgeführt werden, wie das durch den Oxidbrückenmechanismus formuliert wird. Beschleunigt wird eine zweite an der Elektrodenoberfläche ablaufende heterogene Reaktion, die offensichtlich darin bestehen muss, dass in ihrem Verlauf Produkte entstehen, die sich mit geringerer Überspannung reduzieren lassen als das Ausgangsprodukt selbst. Die in Abb. 1 dargestellte Form der Polarisationskurve, die gleichermassen bei der Reduktion von H_2O_2 und ClO^- beobachtet wird, kann hiernach dadurch erklärt werden, dass der polarografischen Stufe der Reduktion des Ausgangsproduktes eine durch Oberflächenoxide katalysierte Stufe vorgelagert ist. Noch eine kurze Bemerkung zu der Annahme von HOARE[17], dass nicht der an der Pt-Oberfläche chemisorbierte Sauerstoff katalytisch aktiv sei, sondern der im Pt gelöste Sauerstoff. Wir meinen, auf Grund unserer Experimente den Schluss ziehen zu können, dass die katalytische Aktivität durch den an der Oberfläche chemisorbierten Sauerstoff bedingt ist, die Stabilität der katalytischen Aktivität der Pt-Oberfläche jedoch durch den im Pt gelösten Sauerstoff. So zeigt sich z.B. bei der Reduktion von O_2 in alkalischer Lösung,

dass der Strom bei $\varphi < 0.6$ V sehr schnell abfällt, wenn die Elektroden nur kurze Zeit bei +1.4 V anodisch vorbehandelt wurden, dass dagegen der Strom nur ganz langsam absinkt, wenn die Elektroden längere Zeit bei +1.4 V vor dem Versuch anodisch vorbehandelt wurden. Nimmt man die polarografische Strom–Spannungskurve in umgekehrter Richtung auf, dann springt der Strom in jedem Falle nach Passieren des Potentials des Stromminimus der I–φ-Kurve augenblicklich auf den maximalen Wert bei $\varphi \sim 0.7$ V, d.h. die Pt-Elektrode erlangt in einer Zeit von weniger als einer Sekunde den maximalen Wert der katalytischen Aktivität zurück. Diese Erscheinung lässt sich nur erklären, wenn man annimmt, dass unmittelbar katalytisch aktiv der an der Pt-Oberfläche chemisorbierte Sauerstoff ist.*

Einen wertvollen Hinweis für die Lösung des Problems der beschleunigenden Wirkung von Oberflächensauerstoffverbindungen auf elektrochemische Reduktionsprozesse an Pt-Elektroden gab die Untersuchung der kathodischen Reduktion von H_2O_2 in 0.1 N KOH[11]. Mit Hilfe der rotierenden Scheibenelektrode mit Ring konnte von uns nachgewiesen werden, dass die beschleunigende Wirkung von Pt-Sauerstoffchemisorptionsverbindungen in der Beschleunigung der Geschwindigkeit des heterogen-katalytischen Zerfalls von H_2O_2 besteht. Über den Chemismus der Zerfallsreaktion konnten auf der Grundlage dieser Messungen allerdings keine Aussagen gemacht werden.

Um in dieser Frage weiterzukommen, untersuchten wir die kathodische Reduktion von $S_2O_8^{2-}$ in alkalischer Lösung, das die gleiche molekulare Struktur wie H_2O_2 besitzt und bei dessen elektrochemischer Reduktion ebenso wie beim H_2O_2 die O–O-Bindung gesprengt wird[12].

Rückschlüsse auf den Reduktionsmechanismus von $S_2O_8^{2-}$ und damit auf die Wirkungsweise der Pt-Sauerstoffchemisorptionsverbindungen ergaben sich aus der Bestimmung der Reaktionsordnung, n. An einer oxidierten Pt-Oberfläche ($\varphi =$ 0.95–0.65 V) erhält man $n = 0.5$, während bei $\varphi < 0.65$ V, d.h. bei Potentialen, bei denen starke Hemmung des Reduktionsprozesses beobachtet wird, n mit steigendem kathodischen Potential anstieg und sich dem Wert 1 näherte. Diese Erscheinung liess sich nur unter der Annahme erklären, dass Pt-Sauerstoffchemisorptionsverbindungen die Einstellung des dissoziativen Chemisorptionsgleichgewichtes

$$S_2O_8^{2-} \rightleftarrows 2\ SO_4^{\dot{-}} \qquad (1)$$

beschleunigen, der die Entladung der entstandenen $SO_4^{\dot{-}}$-Radikale als die geschwindigkeitsbestimmende Reaktion nachgelagert ist. Die Reaktionsordnung dieser Durchtrittsreaktion bezogen auf $S_2O_8^{2-}$ muss dann 0.5 sein. In dem Masse wie sich die Oberfläche reduziert ($\varphi < 0.65$ V) verlangsamt sich die Geschwindigkeit der Einstellung des dissoziativen Chemisorptionsgleichgewichtes und es kommt mehr und mehr zur direkten Entladung von $S_2O_8^{2-}$-Molekülen und demzufolge zu einem Übergang zur Reaktionsordnung 1.

Diese Erkenntnis, angewandt auf den heterogen-katalytischen Zerfall von

* Die im Potentialbereich fallender I–φ-Charakteristik auftretende schnelle Änderung des Potentials und des Stromes in beiden Richtungen (Oszillationen) sind vielfach beschrieben und sind das Ergebnis gleichzeitig auftretender Aktivierungs- und Passivierungsprozesse. Im gegebenen Falle handelt es sich um die gleichzeitig auftretende elektrochemische Reduktion der Pt-Sauerstoffchemisorptionsverbindungen ("Passivierung") und die dieser Erscheinung entgegengerichtete chemische Bildung derselben durch den in der Lösung enthaltenen Sauerstoff (Aktivierung).

H_2O_2 an einer oxidierten Pt-Elektrode, gestattete, diesen Prozess in der Weise zu erklären, dass an einer oxidierten Pt-Elektrode sich das dissoziative Chemisorptionsgleichgewicht

$$H_2O_2 \rightleftarrows 2\ OH^{\cdot}_{Chem.} \tag{2}$$

schnell einstellt. Die sich dabei bildenden $OH^{\cdot}_{Chem.}$-Radikale reagieren mit hinzudiffundierendem H_2O_2 nach einem Mechanismus, wie er für den Zerfall von H_2O_2 in homogener Lösung formuliert wurde[18,19]. An reduzierter Pt-Oberfläche wird kein merklicher Zerfall von H_2O_2 beobachtet[11], da die Initialreaktion des Zerfalls, die in der Bildung von $OH^{\cdot}_{Chem.}$-Radikalen nach Gl. (2) besteht, sehr stark gehemmt ist.

Bei der Untersuchung der Reduktion von Jodat in schwefelsaurer Lösung zeigt sich[14], dass im Potentialgebiet $\varphi = 1.2$–0.4 V eine merkliche Reduktion von Jodat nur an einer anodisch bei $\varphi > 1.2$ V vorbehandelten Pt-Elektrode beobachtet wird, d.h. dass Pt-Oxide den Initialschritt der Reduktion von Jodat beschleunigen. Da die elektrochemische Durchtrittsreaktion der Jodatreduktion durch Pt-Oxide gehemmt wird, muss die durch Pt-Oxide beschleunigte Initialreaktion heterogenkatalytischer Natur sein. Die im Potentialbereich 1.2–0.75 V gefundene Reaktionsordnung $n = 0.5$ für die der heterogen-katalytischen Reaktion nachfolgende geschwindigkeitsbestimmende Durchtrittsreaktion ist nur zu erklären, wenn man annimmt, dass die durch Pt-Sauerstoffchemisorptionsverbindungen beschleunigte katalytische Reaktion in der dissoziativen Chemisorption von Jodat nach

$$IO_2\text{–}OH \rightleftarrows IO^{\cdot}_{2\,Chem.} + OH^{\cdot}_{Chem.} \tag{3}$$

besteht, wobei das entstandene $IO^{\cdot}_2$-Radikal schnell mit Wasser unter Bildung eines zweiten $OH^{\cdot}$-Radikals reagiert

$$IO^{\cdot}_{2\,Chem.} + H_2O \rightleftarrows IO_2^- + H^+ + OH^{\cdot} \tag{4}$$

Da das entstandene IO_2^-, wie aus der Literatur bekannt, schnell in I^- und IO_3^- disproportioniert, besteht die geschwindigkeitsbestimmende Durchtrittsreaktion in der Entladung von $OH^{\cdot}$-Radikalen. Die Bildung von zwei $OH^{\cdot}$-Radikalen aus einem Molekül IO_2-OH erklärt die bezüglich der Jodatkonzentration gefundene Reaktionsordnung, $\vec{n} = 0.5$.

$$i \sim C^{1}_{OH^{\cdot}_{Chem.}} \sim C^{0.5}_{IO_2\text{–}OH}$$

Auch bei der Reduktion von ClO^- in 0.1 *N* KOH[13] zeigte sich, dass der geschwindigkeitsbestimmenden Durchtrittsreaktion an einer oxidierten Pt-Oberfläche eine heterogen-katalytische Initialreaktion vorgelagert ist, denn nur wenn die Oberfläche mit einer bestimmten Menge Oxid bedeckt ist, beobachtet man die Ausbildung der ersten hügelförmigen Stufe (vgl. Abb. 1). Dieses Ergebnis bestätigt, dass das Wesen der beschleunigenden Wirkung von Pt-Sauerstoffchemisorptionsverbindungen darin besteht, dass an einer oxidierten Pt-Oberfläche das Ausgangsprodukt in einer heterogen-katalytischen Reaktion in ein Produkt überführt wird, das sich mit geringerer Überspannung reduzieren lässt, als das Ausgangsprodukt selbst. Da der geschwindigkeitsbestimmende Schritt der Reduktion von ClO^- an einer reduzierten Pt-Elektrode

in der Anlagerung des ersten Elektrons unter Sprengung der Cl–O⁻-Bindung nach

$$ClO^- + e \rightarrow Cl^- + O\doteq$$

besteht[13], muss die katalytische Wirkung von Pt-Oberflächenoxiden auf die Sprengung bzw. Lockerung der kovalenten Bindung Cl–O⁻ zurückgeführt werden.

Summiert man die in den Einzeluntersuchungen der Reduktion von H_2O_2, $S_2O_8^{2-}$, IO_2–OH und ClO^- erhaltenen Ergebnisse, so gelangt man zu dem Ergebnis, dass Pt-Sauerstoffchemisorptionsverbindungen eine der elektrochemischen Durchtrittsreaktion vorgelagerte heterogen-katalytische Reaktion beschleunigen, die im Falle von H_2O_2, IO_2–OH und ClO^- in der Sprengung bzw. Lockerung der bei der elektrochemischen Reduktion zu spaltenden kovalenten X–OH-Bindung besteht (im Falle von $S_2O_8^{2-}$ kommt es zur Abspaltung der –O–$(SO_3)^-$-Gruppe).

Um die zuletzt gemachte sehr wichtige Aussage über den Chemismus der katalytischen Reaktion zu bestätigen, gingen wir davon aus, Stoffe elektrochemisch an aktiven Pt-Elektroden zu reduzieren, die in ihren chemischen Eigenschaften den oben genannten nicht verwandt sind, bei deren katodischer Reduktion aber der erste bzw. einzige Schritt in der Spaltung der vorhandenen kovalenten X–OH-Bindung besteht.

Diese Voraussetzungen sind im Falle der elektrochemischen Reduktion von HNO_2 erfüllt. Das Gleichgewicht, $HNO_2 + H^+ \rightleftarrows NO^+ + H_2O$ liegt in 0.1 *N* H_2SO_4-Lösung ganz auf Seiten der undissoziierten HNO_2[20], so dass die elektrochemische Reaktion in der Entladung von HNO_2[21] und nicht, wie in den Arbeiten von SCHMID[22], in der Entladung des NO^+ besteht.

Der erste Schritt der elektrochemischen Reduktion von salpetriger Säure wäre demnach die Spaltung der ON–OH-Bindung nach der summarischen Reaktion

$$ON\text{–}OH + e \rightarrow NO + OH^- \qquad (5)$$

so dass entsprechend den oben beschriebenen Versuchsergebnissen über die beschleunigende Wirkung von Pt-Sauerstoffchemisorptionsverbindungen auf die Geschwindigkeit elektrochemischer Reaktionsprozesse bei der Reduktion von HNO_2 eine katalytische Vorstufe auftreten sollte.

Einfluss des Zustandes der Elektrodenoberfläche auf die elektrochemische Reduktion von salpetriger Säure zeigt sich auch in den Arbeiten von SCHMID[22], der diese Erscheinung auf die Beeinflussung der NO^+-Nachlieferung bzw. NO-Desorption zurückführte. VETTER[23] fand im System HNO_3/HNO_2 einen kinetischen Grenzstrom, der von ihm jedoch nicht diskutiert wird.

Unsere Versuche wurden in kathodisch vorgereinigter, mit N_2-entlüfteter 0.1 *N* H_2SO_4-Lösung bei 20° durchgeführt. Die Elektrode wurde platiniert, da nur in diesem Falle die vorgelagerte katalytische Stufe gut ausgeprägt war. Vor der Aufnahme jeder I–φ-Kurve wurde die Pt-Elektrode, wie in den Lit.[11] beschrieben, durch wechselseitige kathodische und anodische Polarisation aktiviert. Die HNO_2-Lösungen wurden unmittelbar vor der Messung durch Auflösen von $NaNO_2$ in mit Stickstoff entlüfteter 0.1 *N* H_2SO_4 erhalten. Die Messlösungen waren $4 \cdot 10^{-3}$ *M* an HNO_2.

Die mit Hilfe der rotierenden Scheibenelektrode aufgenommenen I–φ-Kurven (Abb. 2, Kurve a) zeigen tatsächlich im Potentialbereich $\varphi = 0.9$–0.32 V eine Stufe, wie sie für eine durch Pt-Sauerstoffchemisorptionsverbindungen hervorgerufene heterogen-katalytische Reaktion typisch ist.

Eine ausführliche Untersuchung der im Potentialbereich 0.90–0.32 V auftretenden Stufe zeigt, dass die Ströme unabhängig von der Umdrehungsgeschwindigkeit der rotierenden Scheibenelektrode sind und im Potentialbereich 0.90–0.68 V der Tafelbeziehung mit einem Wert für "b" von 0.235 V bzw. $\alpha = 0.25$ genügen (Abb. 3). Die aus der Konzentrationsabhängigkeit der Ströme berechnete Reaktionsordnung "n" beträgt bezüglich $HNO_2 = 1$.

Die Abweichungen von der Tafelbeziehung bei $\varphi < 0.68$ V, die bei $\varphi < 0.55$ V schliesslich in einen Abfall des Stromes übergeht, ist, wie der Vergleich mit Ladekurven zeigt[16], auf die Reduktion der Pt-Oberflächenoxide und dem damit verbundenen Abfall der katalytischen Aktivität der Elektrodenoberfläche zurückzuführen. Da Pt-Sauerstoffchemisorptionsverbindungen elektrochemische Durchtritts-

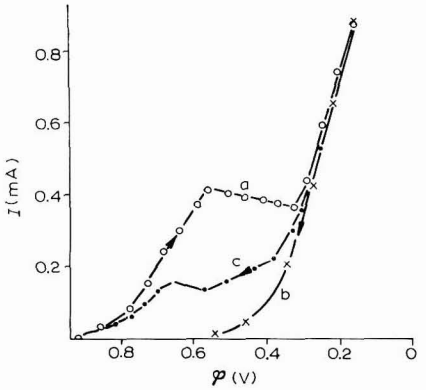

Abb. 2. I–φ-Kurven der Reduktion von HNO_2 an einer plat. Pt-Elektrode in 0.1 N H_2SO_4. (a), Stationäre Strom–Spannung-Kurve; (b), sehr schnell aufgenommene I–φ-Kurve in Richtung sinkender kathodischer polarisation (8–10 sec); (c), stationäre I–φ-Kurve in Richtung sinkender kathodischer Polarisation aufgenommen.

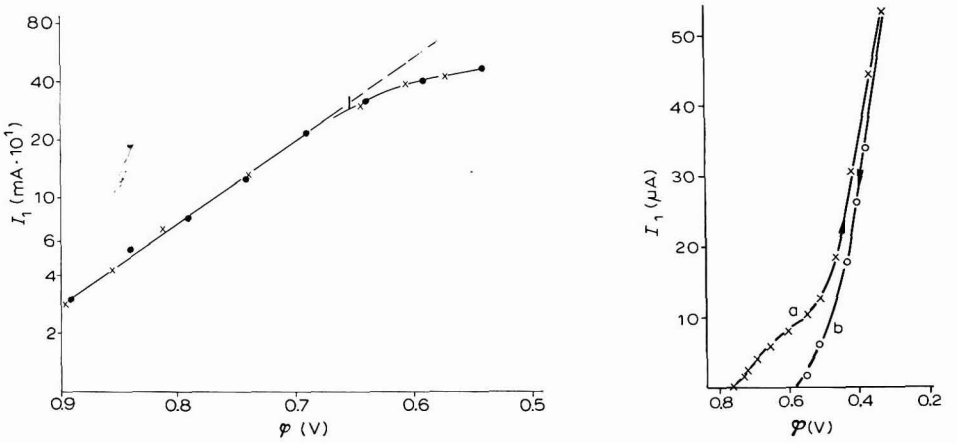

Abb. 3. log I–φ-Abhängigkeit der Ströme der katalytischen Vorstufe der Reduktion von HNO_2 in 0.1 N H_2SO_4 bei verschiedenen Rührgeschwindigkeiten. (●), $m = 76$; (×), $m = 28$ U/sec.

Abb. 4. Polarisationskurven der Reduktion von H_3N^+–OH an einer plat. Pt-Elektrode in 0.1 N H_2SO_4.

reaktionen hemmen, muss die bei der Reduktion von HNO_2 auftretende Vorstufe wie auch in den oben beschriebenen Fällen einer durch Pt-Sauerstoffchemisorptionsverbindungen hervorgerufenen katalytischen Reaktion zugeordnet werden.

Zur Aufklärung der durch Pt-Oberflächenoxide beschleunigte Reaktion war es wichtig, zu untersuchen, ob Pt-Oxide tatsächlich den nach Gl. (5) formulierten Initialschritt der HNO_2-Reduktion beschleunigen, da nur in diesem Falle die katalytische Wirkung von Oberflächenoxiden eindeutig auf die Sprengung bzw. Lockerung der ON–OH-Bindung zurückgeführt werden kann. Die Entscheidung dieser Frage war durch die Aufnahme der I–φ-Kurve an einer oxidfreien Pt-Elektrode möglich. Die Reduktion von HNO_2 an einer oxidfreien Pt-Oberfläche wird bei Potentialen $\varphi < 0.32$ V beobachtet und bedingt den erneut einsetzenden starken Anstieg des Stromes der I–φ-Kurve bei $\varphi < 0.32$ V (Abb. 2). Nimmt man die I–φ-Kurve von negativen Potentialen ausgehend ($\varphi < 0.32$ V) in anodischer Richtung auf, dann lässt sich auch der untere Teil der I–φ-Kurve der Reduktion von HNO_2 an einer oxidfreien Pt-Oberfläche realisieren (Abb. 2, Kurve b). Diese Untersuchungen wurden insoweit erschwert, da HNO_2 selbst ein starkes Oxidationsmittel ist und es zur chemischen Bildung von Pt-Oberflächenoxiden kommt. Die Aufnahme des unteren Teils der I–φ-Kurve an einer reduzierten Pt-Oberfläche musste deshalb schnell geschehen, damit die chemische Oxidation der Oberfläche durch HNO_2 und somit die Aktivierung der Oberfläche gegenüber der vorgelagerten heterogen-katalytischen Reaktion vernachlässigbar war. Die in Abb. 2 dargestellte Kurve C, die der langsamen Aufnahme des unteren Teiles der I–φ-Kurve entspricht, zeigt deutlich den aktivierenden Effekt, der auf die chemische Oxidation der Oberfläche durch HNO_2 zurückzuführen ist. Die oxidative Wirkung der HNO_2 ist auch der Grund dafür, dass die elektrochemische Vorbehandlung der Pt-Elektroden bei verschiedenen anodischen Potentialen keinen Einfluss auf die Lage und Höhe der katalytischen Vorstufe hatte.

Kurve b in Abb. 2 zeigt, dass an einer oxidfreien Pt-Oberfläche keine Vorstufe beobachtet wird, d.h. dass Pt-Oberflächenoxide den Initialschritt der HNO_2-Reduktion beschleunigen und ihre katalytische Wirkung somit in der Sprengung bzw. Lockerung der ON–OH-Bindung besteht.

Des weiteren untersuchten wir die Reduktion von Hydroxylamin unter den gleichen Versuchsbedingungen, wie sie für die HNO_2-Reduktion beschrieben wurden.

Bei der Reduktion von $(NH_3–OH)^+$, die nach der Gleichung

$$(NH_3–OH)^+ + e^- \rightarrow NH_3 + OH^{\cdot} \text{ (geschwindigkeitsbestimmend)}$$

$$OH^{\cdot} + e^- \rightarrow OH^-$$

verläuft, besteht die elektrochemische Reaktion ihrem Wesen nach in der Sprengung der kovalenten Bindung $H_3N^+–OH$, so dass eine etwaige auftretende Beschleunigung des kathodischen Reduktionsprozesses durch Pt-Oberflächenoxide nur auf eine katalytische Sprengung oder Lockerung der $H_3N^+–OH$-Bindung zurückgeführt werden kann. Die an platinierten Pt-Elektroden in 0.1 N H_2SO_4 aufgenommenen I–φ-Kurven zeigen im Potentialbereich 0.74–0.5 V eine Vorstufe (Abb. 4, Kurve a), die verschwindet, wenn die Kurve von negativen Potentialen kommend schnell aufgenommen wurde (Abb. 4, Kurve b). Dass diese Vorstufe durch Oberflächenoxide hervorgerufen wird und damit katalytischer Natur sein muss, ergibt sich aus dem Potentialbereich ihres Auftretens: 0.75–0.5 V und der Tatsache, dass sie an oxidfreier Pt-Oberfläche nicht beobachtet wird (Abb. 4, Kurve b).

Die Ergebnisse dieser gezielt durchgeführten Experimente zeigen, dass sich die auf der Grundlage der Reduktion von H_2O_2, ClO^- und IO_2–OH gemachte Aussage über die heterogen-katalytische Wirkung von Pt-Oberflächenoxiden zu der Aussage verallgemeinern lässt, dass Pt-Oberflächenoxide die katalytische Sprengung bzw. die Lockerung der bei der elektrochemischen Reduktion zu spaltenden X–OH-Bindung bewirken.

Herrn Prof. Dr. R. LANDSBERG möchte ich für seine Hilfe bei der Diskussion der Versuchsergebnisse recht herzlich danken.

ZUSAMMENFASSUNG

Die Ergebnisse der Untersuchungen über die beschleunigende Wirkung von Pt-Oberflächenoxiden auf die Geschwindigkeit der kathodischen Reduktionsprozesse von H_2O_2, IO_2–OH, ClO^- werden zu der Aussage verallgemeinert, dass die heterogen-katalytische Wirkung von Platinoberflächenoxiden in der katalytischen Sprengung bzw. Lockerung der bei der elektrochemischen Reduktion zu spaltenden X–OH-Bindung besteht. Diese Aussage wurde an Hand der Untersuchung der Reduktionsreaktionen von HNO_2 und H_3N^+–OH geprüft und bestätigt gefunden.

SUMMARY

The results of investigations on the accelerating effect of Pt surface oxide on the rate of the cathodic reduction of H_2O_2, IO_2–OH and ClO^- were summarised in the statement that the heterogeneous catalytic effect of platinum surface oxide arises from the catalytic breaking or weakening of the X–OH bond which is ruptured in the electrochemical reaction. This statement was tested and found to hold for the reduction of HNO_2 and H_3N^+–OH.

LITERATUR

1 F. C. ANSON, *J. Am. Chem. Soc.*, 81 (1959) 1554.
2 F. C. ANSON UND D. M. KING, *Anal. Chem.*, 34 (1962) 362.
3 G. BIANCHI, F. MAZZA UND T. MUSSINI, *Electrochim. Acta*, 7 (1962) 457.
4 D. DAVIS, *Talanta*, 3 (1960) 335.
5 M. MOCHIZUKI, *J. Electrochem. Soc. Japan*, 28 (1960) 583.
6 J. J. LINGANE, *J. Electroanal. Chem.*, 2 (1961) 296.
7 D. T. SAWYER UND L. V. INTERRANTE, *J. Electroanal. Chem.*, 2 (1961) 310.
8 J. P. HOARE, *Electrochim. Acta*, 9 (1964) 599.
9 J. M. KOLTHOFF UND E. R. NIGHTINGALE, *Anal. Chim. Acta*, 17 (1957) 329.
10 L. MÜLLER, *Electrochim. Acta*, 12 (1967) 557.
11 L. MÜLLER UND L. N. NEKRASSOW, *J. Electroanal. Chem.*, 9 (1965) 282.
12 L. MÜLLER, *J. Electroanal. Chem.*, 13 (1967) 275.
13 L. MÜLLER, *Elektrokhimija*, im Druck.
14 L. MÜLLER, *J. Electroanal. Chem.*, 16 (1968) 67.
15 L. N. NEKRASSOW UND L. MÜLLER, *Dokl. Akad. Nauk SSSR*, 149 (1963) 1107.
16 W. VIELSTICH, *Z. Instrumentenk.*, 71 (1963) 29.
17 J. P. HOARE, *J. Electroanal. Chem.*, 12 (1966) 29.
18 J. A. KASARNOWSKI UND N. P. LIPICHIN, *Izv. Akad. Nauk SSSR, Ser. Khim.*, (1965) 312.
19 L. MÜLLER, *J. Electroanal. Chem.*, 14 (1967) 193.
20 F. SEEL UND R. WINKLER, *Z. Phys. Chem. N.F.*, 25 (1960) 217.
21 D. T.-W. CHOW UND R. J. ROBINSON, *Anal. Chem.*, 25 (1953) 1493.
22 G. SCHMID UND G. KRIECHEL, *Ber. Bunsengesell. Physikal. Chem.*, 68 (1964) 677.
23 K. J. VETTER, *Z. Elektrochem.*, 55 (1951) 121.

ELECTROANALYTICAL CHEMISTRY AND INTERFACIAL ELECTROCHEMISTRY
Elsevier Sequoia S.A., Lausanne – Printed in The Netherlands

ELECTROCHEMISTRY OF NITRIC OXIDE AND OF NITROUS ACID AT A MERCURY ELECTRODE

DEWAYNE L. EHMAN AND DONALD T. SAWYER
Department of Chemistry, University of California, Riverside, Calif., 92502 (U.S.A.)
(Received July 21st, 1967)

Although the reduction of nitric oxide in aqueous solution has been studied polarographically by several groups, the details of the reduction process have not been established. One group has reported two waves with half-wave potentials of −0.5 and −1.10 V *vs.* S.C.E.[1], while other workers[2] have observed a single wave with an $E_{\frac{1}{2}}$ of −1.16 V *vs.* S.C.E. CORBELLINI AND LANZA[3] have concluded that the reduction is a one-electron process based on the rate of decay of i_d in a drop of solution. In contrast, MAŠEK[4] has observed two completely independent waves for the reduction of NO in acidic solutions. He has concluded that the first wave is due to a two-electron reduction of the dimer, N_2O_2, to $N_2O_2^{2-}$ and that the second wave is due to the direct uptake of three electrons by NO to produce hydroxylamine.

Several workers[1,5-7] have studied the polarographic reduction of nitrous acid alone and in the presence of UO_2^{2+} and MoO_2^{2+}. In all cases, a wave with an $E_{\frac{1}{2}}$ of −1.0 V *vs.* S.C.E. has been observed. MAŠEK[8] has concluded that HNO_2 is reduced by a four-electron process to NH_2OH in unbuffered solutions. He has also observed that two waves are obtained for the reduction of HNO_2 in buffered solutions with half-wave potentials of −1.0 V and −1.6 V *vs.* NCE[9]. The first wave has been attributed to the reduction of HNO_2 to NH_2OH; the second to the reduction of NH_2OH to NH_4OH.

Oxides of nitrogen are subject to a number of decomposition and hydrolysis reactions. This requires that great care be taken if meaningful electrochemical data are to be obtained. Because NO reacts rapidly with O_2 to form NO_2, which reacts with water to form HNO_2 and HNO_3[10], an air-tight cell must be used. Another problem is that cold, dilute solutions of HNO_2 decompose slowly to give NO and HNO_3[10].

Several chemical reactions are known that further complicate electrochemical studies of NO and HNO_2. For example, two-electron reducing agents (such as Sn^{2+}) can reduce HNO_2 to NH_2OH[11]. The mechanism of the reaction is thought to involve an intermediate compound of +1 oxidation state, $NH(OH)_2$, because its formation involves no O–N bond breakage. The reaction

$$HNO_2 + NH_3OH^+ \rightarrow N_2O + 2\ H_2O + H^+ \qquad (1)$$

which has been studied in acetate buffers[12], is an added complication to the electrochemical reduction of HNO_2.

The aims of the present study have been to investigate the electrochemical

reduction of NO and of HNO_2 in aqueous media and to determine the kinetic parameters, the probable mechanisms, and the identity of the products of the reduction.

EXPERIMENTAL

The electrochemical measurements were performed with an instrument constructed from Philbrick operational amplifiers following the design of DEFORD[13]. A three-electrode assembly was used for all electrochemical measurements. A Corning model 12 pH-meter was used for adjustment of solution acidity and for acid–base titrations.

An air-tight glass cell of 50-ml capacity was used for all electrochemical studies. The top of the cell contained a glass tube closed with a fine-porosity glass frit for isolation of the auxiliary electrode; an inlet for the insertion of the mercury working electrode, and an opening covered with a rubber stopper for degassing, sample introduction, and sampling. The bottom of the cell contained a tungsten wire to make contact with a mercury pool electrode. The top and bottom of the cell were fabricated from the two halves of a 40/35 standard taper joint.

The reference electrode consisted of a AgCl-coated wire in a solution of 0.4 F KCl contained in a 13-cm length of glass tubing with a small ball of soft glass sealed in one end to give a cracked tip. The potential of this electrode was 0.000 V *vs.* S.C.E.

The mercury working electrode was prepared by abrading a Beckman Pt-inlay electrode with carborundum paper in a mercury pool until a uniform coverage of mercury was obtained on the Pt surface. The electrode was tapped gently to remove excess mercury and to assure a reproducible area. The area of the mercury electrode, which was determined with a cathetometer, had an average value of 0.245 cm^2.

The pH of the buffered solutions was adjusted with KOH and H_2SO_4. Solutions of HNO_2 were prepared from KNO_2 which was standardized by titration with $KMnO_4$. Mixtures of NO and N_2 containing 3.01, 10.6, 32.1 and 100% NO were obtained from the Matheson Co. Nitric oxide solutions were prepared by saturating the solvent system with the appropriate gaseous mixture at atmospheric pressure.

The concentration of 100% NO at 1 atm in 0.5 F Na_2HPO_4 has an average value of 1.74×10^{-3} F which was determined by chronopotentiometry on 100% NO solutions in steadily decreasing concentrations of Na_2HPO_4, and extrapolating the $i\tau^{\frac{1}{2}}$-values to zero concentration of supporting electrolyte. The value was obtained by using the known solubility of NO in pure water (1.88×10^{-3} F at 25° and 1 atm)[14] and assuming that the diffusion coefficient does not change with electrolyte concentration.

A 6-ft. Porapak Q column at room temperature was used for the gas chromatographic determination of NO, N_2O and N_2. The carrier gas was He. Concentrations of NH_2OH were determined from its chronopotentiometric oxidation wave on a pre-reduced Pt electrode.

RESULTS

Nitric oxide

Well-defined chronopotentiometric waves are observed for the reduction of nitric oxide in 0.5 F Na_2HPO_4 solutions between pH 5 and pH 7 as illustrated in

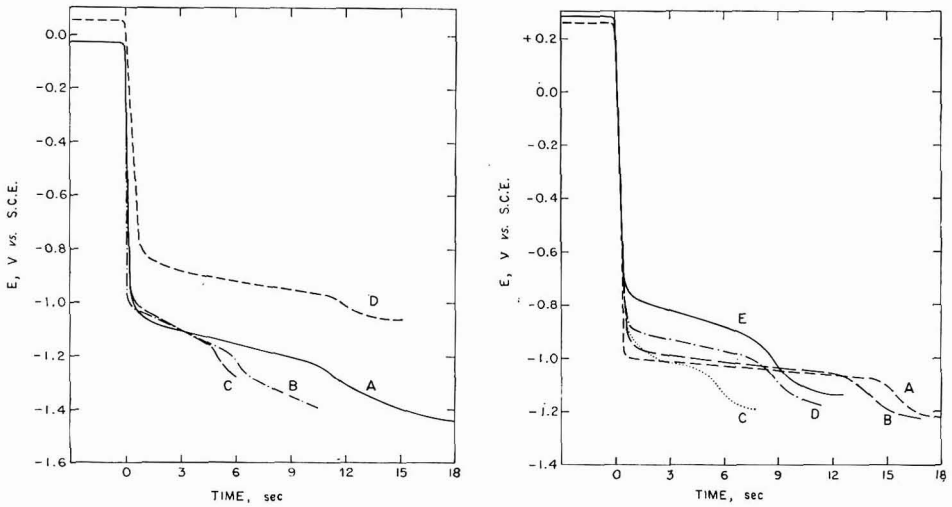

Fig. 1. Chronopotentiograms of NO at a mercury electrode in 0.5 F Na_2HPO_4.
(A), pH 7.0, 1.74×10^{-3} F NO, 60 μA; (B), pH 7.0, 5.58×10^{-4} F NO, 25 μA; (C), pH 7.0, 1.84×10^{-4} F NO, 5 μA; (D), pH 5.0, 1.74×10^{-3} F NO, 60 μA.

Fig. 2. Chronopotentiograms of HNO_2 at a mercury electrode in 0.5 F Na_2SO_4 and 0.5 F NaH_2PO_4.
(A), pH 3.3, 5×10^{-3} F HNO_2, 450 μA; (B), pH 3.3, 3×10^{-3} F HNO_2, 300 μA; (C), pH 3.3, 1×10^{-3} F HNO_2, 150 μA; (D), pH 3.0, 2.5×10^{-3} F HNO_2, 300 μA; (E), pH 2.0, 2.5×10^{-3} F HNO_2, 300 μA.

TABLE 1

CHRONOPOTENTIOMETRIC DATA FOR THE REDUCTION OF NITRIC OXIDE AT A MERCURY ELECTRODE IN A 0.5 F Na_2HPO_4 SOLUTION AT PH 7.0

$[NO]$ (M)	$i_0\tau^{\frac{1}{2}}/C$ $(A\ sec^{\frac{1}{2}}\ cm\ mole^{-1})$
1.74×10^{-3}	473
5.58×10^{-4}	454
1.84×10^{-4}	588
5.23×10^{-5}	683

Fig. 1. At pH 7.0, the value of $E_{\frac{1}{4}}$ is -1.12 V *vs.* S.C.E. A reverse chronopotentiometric wave is not observed under any conditions.

Although the value of $i\tau^{\frac{1}{2}}$ is constant for a given NO concentration for transition times from 2–20 sec, the value of $i\tau^{\frac{1}{2}}/C$ varies with concentration (see Table 1). This type of behaviour is characteristic of a pre-chemical equilibrium[15], $pY \rightleftarrows O$, preceding the electron transfer reaction, $O + ne^- \rightarrow R$. When the rate of attainment of equilibrium is so slow that interconversion of O and Y cannot occur during the time of electrolysis, then

$$C_0 = (pC_t)^p K_e - 2i_0 t^{\frac{1}{2}}/\pi^{\frac{1}{2}} nFD^{\frac{1}{2}} \qquad (2)$$

where C_0 is the concentration at the electrode surface, C_t the bulk concentration, i_0 the current density, t the time of electrolysis, n the number of electrons in the overall

electrode process, F the faraday, D the diffusion coefficient of the electroactive species, and K_e equals $[O]/[Y]^p$. When t equals the transition time, C_0 is zero, and a plot of $i_0\tau^{\frac{1}{2}}$ *vs.* C_t will give a straight line if p equals unity. Such a plot for NO reduction at a mercury electrode gives a straight line with a zero intercept and a slope of 4.8×10^{-2}.

The chronopotentiometric data indicate that the reduction of nitric oxide at a mercury electrode is an irreversible process that is controlled by semi-infinite linear diffusion. However, the electrode process is preceded by a slow chemical equilibrium of the type $Y \rightleftarrows O$. The equilibrium constant, K_e, for the pre-chemical reaction can be evaluated from the slope of the plot of $i_0\tau^{\frac{1}{2}}$ *vs.* C_t if the value of the diffusion coefficient, D, is known. At pH 7, the value for K_e is 1.10, assuming that the value for D is 2.6×10^{-5}, which is the value for O_2[16].

The relationship between potential and time (at constant current) for an irreversible, diffusion-controlled system is given by[17]

$$E = \frac{0.059}{\alpha n_a} \log\left[\frac{nFACk_{f,h}^0}{i}\right] + \frac{0.059}{\alpha n_a} \log\left[1 - \left(\frac{t}{\tau}\right)^{\frac{1}{2}}\right] \qquad (3)$$

where E is the potential of the working electrode *vs.* NHE, α the transfer coefficient, n_a the number of electrons in the rate-determining step, A the electrode area, $k_{f,h}^0$ the heterogeneous rate constant for the reduction reaction, i the current, C the bulk concentration of the electroactive species, F the faraday, τ the transition time, and t the time of electrolysis. This equation can be used to evaluate the quantity, αn_a, by plotting either E_t *vs.* $\log [1-(t/\tau)^{\frac{1}{2}}]$ or $E_{t=0}$ *vs.* $-\log i$. Plots of this type give linear curves for NO reduction at a mercury electrode between pH 5 and pH 7; the average value obtained for αn_a is 0.40 (see Table 2). This value implies that the rate-determining electron transfer reaction is a one-electron process. The values for the kinetic parameters as determined by the two methods for a variety of conditions are summarized in Table 2. Values obtained for $k_{f,h}^0$ are not constant, but vary linearly with the hydrogen ion concentration of the solutions. This implies that the electroactive

TABLE 2

KINETIC PARAMETERS FOR THE REDUCTION OF NITRIC OXIDE AT A MERCURY ELECTRODE IN 0.5 F Na_2HPO_4 SOLUTION AT PH 5 AND PH 7

Method of evaluating αn_a	$[NO] \cdot 10^3$ *(M)*	*pH*	i *(μA)*	αn_a	$E_{t=0}$ *vs. NHE (V)*	$k_{f,h}^0 \cdot 10^9$ *(cm/sec)*	$k_{f,h}^0/[H^+] \cdot 10^2$ *(cm l/mole sec)*
E_t *vs.* $\log [1-(t/\tau)^{\frac{1}{2}}]$							
	174	7	60	0.37	−0.828	10	10
	55.8	7	20	0.40	−0.781	8	8
	18.4	7	8	0.40	−0.755	10	10
	5.23	7	5	0.47	−0.727	6	6
	174	5	60	0.39	−0.587	200	2
	174	5	80	0.35	−0.597	600	6
$E_{t=0}$ *vs.* $-\log i$							
	174	7	60	0.41	−0.806	4	4
	55.8	7	20	0.39	−0.754	20	20
	18.4	7	8	0.43	−0.744	8	8
	5.23	7	5	0.41	−0.766	20	20
	174	5	60	0.39	−0.567	300	3
		Mean value		0.40±0.02			9±4

species is not NO, but rather some intermediate formed by the combination of NO and H^+. Thus, the concentration used in eqn. (3) to calculate $k_{f,h}{}^0$ should be that of the intermediate rather than the concentration of NO. The intermediate concentration can be expressed by the relation

$$[\text{intermediate}] = K_e'[\text{NO}][\text{H}^+] \quad (4)$$

Thus, a more realistic heterogeneous rate constant, $k_{f,h}{}^{0\prime}$, can be evaluated by assuming that

$$k_{f,h}{}^{0\prime} = k_{f,h}{}^0/(\text{H}^+) = (k_{f,h}{}^0)_{\text{intermediate}} \cdot K_e' \quad (5)$$

and by dividing the values of $k_{f,h}{}^0$ in Table 2 by the hydrogen ion concentration. The last column in Table 2 summarizes the calculated values for $k_{f,h}{}^{0\prime}$.

Controlled-potential coulometry of nitric oxide solutions at a potential of -1.20 V *vs.* S.C.E. using a mercury pool electrode establishes that NO is reduced by an overall one-electron process. During the coulometric runs, the concentration of NO decreases and the concentration of N_2O increases, based on gas chromatographic analysis of gaseous samples from above the buffered solution in the coulometric cell. This indicates that N_2O is the final product of the reduction of NO at mercury.

Gold and platinum electrodes behave unsatisfactorily for the reduction of NO in aqueous solutions. Both metals exhibit chronopotentiometric waves that do not disappear entirely on sweeping NO out of the solution with N_2. Also, the lengths of the waves produced on both metals depend greatly on the pre-treatment of the electrode.

Nitrous acid

Chronopotentiometric waves are observed with a mercury electrode for the reduction of nitrous acid in 0.5 *F* Na_2SO_4 solutions that have been acidified with H_2SO_4 (Fig. 2). The transition time for the wave increases up to a limiting value with decreasing pH, which indicates that only HNO_2 is electroactive. Reverse chronopotentiometric waves are not observed for HNO_2 under any conditions. The addition of 0.5 *F* NaH_2PO_4 helps to buffer the solution in the pH-range 1.5–3.5, the most suitable acidity for the chronopotentiometric reduction of HNO_2. At pH 3.0, the value for $E_{\frac{1}{4}}$ is -1.00 *vs.* S.C.E. For transition times from 2–20 sec and for bulk concentrations of HNO_2 from $5 \cdot 10^{-4}$–$5 \cdot 10^{-3}$ *F*, $i_0\tau^{\frac{1}{2}}/C$ has a constant value of 1422 ± 12 A $\text{sec}^{\frac{1}{2}}$ cm mole^{-1} (0.5 *F* Na_2SO_4 and 0.5 *F* NaH_2PO_4, pH 3.3).

The chronopotentiometric data establish that nitrous acid is reduced at a mercury electrode by an irreversible process which is controlled by semi-infinite linear diffusion. Plots of E_t *vs.* $\log[1-(t/\tau)^{\frac{1}{2}}]$ and $E_{t=0}$ *vs.* $-\log i$ yield straight lines which give an average value for αn_a of 0.49. This implies that the rate-determining electron transfer reaction is a one-electron process. The values for the kinetic parameters as determined by the two methods for a variety of conditions are summarized in Table 3. Again, the values obtained for $k_{f,h}{}^0$ are not constant, but vary linearly with the hydrogen ion concentration of the solutions. This implies that the electroactive species is not HNO_2, but rather some intermediate formed rapidly by the combination of HNO_2 and H^+. The concentration of the intermediate species is expressed by a relation similar to eqn. (4) and a more realistic rate constant, $k_{f,h}{}^{0\prime}$, can be determined by eqn. (5). Values for $k_{f,h}{}^0$ divided by the hydrogen ion concentration are summarized in the last column of Table 3.

TABLE 3

KINETIC PARAMETERS FOR THE REDUCTION OF NITROUS ACID AT A MERCURY ELECTRODE IN 0.5 F Na_2SO_4 AND 0.5 F NaH_2PO_4 UNDER VARIOUS CONDITIONS

Method of evaluating αn_a	$[HNO_2]\cdot 10^4$ *(M)*	*pH*	*i* *(μA)*	αn_a	$E_{t=0}$ *(V vs. NHE)*	$k_{f,h}{}^0\cdot 10^{10}$ *(cm/sec)*	$k_{f,h}{}^0/[H^+]\cdot 10^6$ *(cm l/mole sec)*
E_t *vs.* $\log [1-(t/\tau^{\frac{1}{2}})]$							
	50	3.32	650	0.52	−0.736	5	1
	40	3.32	450	0.49	−0.718	10	2
	30	3.32	400	0.50	−0.710	8	2
	20	3.32	300	0.52	−0.701	10	2
	10	3.32	150	0.52	−0.688	10	2
	5	3.32	100	0.49	−0.667	50	10
	25	2.50	200	0.46	−0.561	300	9
	25	3.50	200	0.47	−0.672	40	4
$E_{t=0}$ *vs.* $-\log i$							
	25	3.00	100	0.49	−0.649	20	2
	25	2.50	100	0.51	−0.534	100	3
	25	3.50	100	0.47	−0.690	10	3
	25	2.00	100	0.46	−0.505	500	5
	50	3.32	650	0.51	−0.744	5	1
		Mean value		0.49	± 0.02		4±2

TABLE 4

ANALYSIS OF PRODUCTS FROM THE COULOMETRIC REDUCTION OF NITROUS ACID AT A MERCURY POOL

Soln.: 0.5 F Na_2SO_4 and 0.5 F NaH_2PO_4, pH 3.00, $100\cdot 10^{-6}$ mole HNO_2 originally present.

Product	*Method of analysis*	*Moles found* $\cdot 10^6$
NO	gas chromatography	1.2
N_2O	gas chromatography	25.9
N_2	gas chromatography	1.9
NH_2OH	chronopotentiometry	44.8

Controlled-potential coulometry of HNO_2 at −1.10 V *vs.* S.C.E. with a mercury pool yields values for n which range from 3.2 at pH 3.5 to 2.0 at pH 1.6, with an average value of 3.0 at pH 3.0. The product analysis for the reduction of HNO_2 at pH 3.0 is summarized in Table 4. This is based on the assumption that the gaseous products are in equilibrium between the gas and liquid phases, and that Dalton's Law of Partial Pressures is applicable.

DISCUSSION AND CONCLUSIONS

Nitric oxide

The equilibrium constant, K_e, for the equilibrium step preceding the electron transfer reaction for the electrochemical reduction of NO, is equal to [O]/[Y], where O is the electroactive form of NO and Y is the non-electroactive form of NO. Thus, K_e does not include hydrogen ion which, on the basis of the data of Table 2, has been shown to be involved in the pre-chemical equilibrium. An equilibrium constant which includes hydrogen ion concentration is given by the relation

$$K_e' = K_e/[H^+] = [O]/[Y]\,[H^+] \tag{6}$$

At pH 7.0, the value for K_e is 1.10; thus the value for K_e' is 1.10×10^7.

The heterogeneous rate constant, $(k_{f,h}{}^0)_{\text{intermediate}}$, for the electroactive

species of nitric oxide reduction at a mercury electrode can be evaluated on the basis of eqn. (5), the value for K_e', and the value for $k_{f,h}^0$; the average value for $(k_{f,h}^0)_{\text{intermediate}}$ is $9 \cdot 10^{-9}$ cm sec^{-1}. A more useful parameter is the simple heterogeneous rate constant, $k_{s,h}$, which is the rate constant at the formal potential for the rate-determining couple. This constant is obtained by the relation[18]

$$k_{s,h} = k_{f,h}^0 \exp[(-\alpha n_a F/RT)\, E^{0\prime}] \tag{7}$$

where $E^{0\prime}$ is the formal electrode potential for the rate-determining couple. The rate-determining step for the reduction of NO at a mercury electrode is a one-electron reaction involving one proton. A reduction mechanism for nitric oxide which is consistent with the data can be represented by the reactions

$$NO + H^+ \rightleftarrows NOH^+ \qquad K_e' \text{ slow} \tag{8}$$

$$NOH^+ + e^- \rightarrow NOH \qquad \text{slow} \tag{9}$$

$$2\ NOH \rightarrow N_2O + H_2O \qquad \text{fast} \tag{10}$$

The formal electrode potential is not known for the proposed rate-determining couple (reaction (9)), but it has been estimated to be -0.3 V *vs.* NHE[19] for the reaction represented by the combination of eqns. (8) and (9). If this value is used for $E^{0\prime}$, the value for $k_{s,h}$ is $1 \cdot 10^{-6}$ cm sec^{-1}.

Nitrous acid

The heterogeneous rate constant, $(k_{f,h}^0)_{\text{intermediate}}$, for the electroactive species of nitrous acid reduction at a mercury electrode can be evaluated on the basis of eqn. (5), the galvanostatic data of Table 3, and the value of K_e' for the electroactive species. The rate-determining step is a one-electron process and involves one proton. A reduction mechanism for HNO_2 that is consistent with the data and the reduction products can be represented by the reactions

$$HNO_2 + H^+ \rightleftarrows H_2NO_2^+, \qquad K_e' \quad \text{fast} \tag{11}$$

$$H_2NO_2^+ + e^- \rightarrow H_2NO_2 \qquad \text{slow} \tag{12}$$

$$2\ H_2NO_2 \rightarrow NH(OH)_2 + HNO_2 \qquad \text{fast} \tag{13}$$

$$2\ NH(OH)_2 \rightarrow NH_2OH + HNO_2 + H_2O \quad \text{fast} \tag{14}$$

$$NH_2OH + HNO_2 \rightarrow N_2O + 2\ H_2O \quad \text{slow} \tag{15}$$

The equilibrium constant, K_e', for reaction (11) has a value of $2 \cdot 10^{-7}$ [20] which indicates that the majority of the nitrous acid is in the form of HNO_2 although $H_2NO_2^+$ is the electroactive species. If this value for K_e' is used, the average value for $(k_{f,h}^0)_{\text{intermediate}}$ is $2 \cdot 10^1$ cm sec^{-1}.

The proposed reduction mechanism for HNO_2, reactions (11)–(15), explains the presence of NH_2OH among the products as well as the build-up of N_2O. Thus, the coulometric reduction of HNO_2 gives an overall three-electron process because of the removal of some HNO_2 by NH_2OH. The small amount of NO may come from the decomposition of HNO_2; N_2 may come from the decomposition of NH_2OH. At lower pH-values, HNO_2 decomposes more quickly to cause the coulometric results to indicate fewer electrons/HNO_2 molecule.

Again, the simple heterogeneous rate constant, $k_{s,h}$, is a more useful parameter.

This quantity can be evaluated on the basis of the proposed mechanism and eqn. (7). The formal potential for the proposed rate-determining couple is not known, but the value of $E^{0\prime}$ for the HNO_2/NO couple, which represents the combination of eqns. (11) and (12)[21] is 1.00 V *vs.* NHE. If this value is used in eqn. (7), the value for $k_{s,h}$ is $1 \cdot 10^{-7}$ cm sec^{-1}.

The diffusion coefficient for HNO_2, D, can be calculated from the Sand equation[22].

$$i\tau^{\frac{1}{2}}/C = n\pi^{\frac{1}{2}} FAD^{\frac{1}{2}}/2 \qquad (16)$$

The average value of D for HNO_2 in 0.5 F Na_2SO_4 and 0.5 F NaH_2PO_4 at pH 3.0 is 1.73×10^{-5} cm^2 sec^{-1}.

ACKNOWLEDGEMENT

This work was supported by the National Science Foundation under Grant No. GP-7201. We are grateful to the National Science Foundation for a pre-doctoral fellowship to D.L.E.

SUMMARY

The electrochemistry of nitric oxide and nitrous acid have been studied at a mercury electrode in buffered aqueous solutions using chronopotentiometry and controlled-potential coulometry. The reduction of NO is an irreversible one-electron process with $\alpha n_a = 0.40$ and $k_{s,h} = 10^{-6}$ cm sec^{-1}. Gas chromatographic analyses establish that the only product is N_2O. The electroactive species appears to be a slowly formed intermediate, HNO^+, with a formation constant of 10^7. Nitrous acid is irreversibly reduced at a mercury electrode by a one-electron process, the kinetic parameters for the rate-controlling electron transfer step having the values $\alpha n_a = 0.49$ and $k_{s,h} = 10^{-7}$ cm sec^{-1}. The electroactive species appears to be a rapidly formed intermediate, $H_2NO_2^+$. Controlled-potential coulometry for the reduction of nitrous acid indicates an overall three-electron process (at pH 3.00). Gas chromatography establishes that the major products are equivalent amounts of NH_2OH and N_2O. The actual electrochemical reduction of HNO_2 is an overall four-electron process to give NH_2OH which reacts with HNO_2 to give N_2O. Mechanisms consistent with the experimental data are proposed for the reduction of NO and of HNO_2.

REFERENCES

1 L. Riccoboni and P. Lanza, *Ric. Sci.*, 18 (1948) 1055.
2 K. Namba and T. Yamashita, *J. Ind. Explosives Soc., Japan*, 13 (1952) 151.
3 A. Corbellini and P. Lanza, *Atti Accad. Naz. Lincei, Rend., Classe Sci. Fis. Mat. Nat.*, 14 (1953) 294.
4 J. Mašek, *Z. Anal. Chem.*, 224 (1) (1967) 99.
5 K. Schwartz, *Z. Anal. Chem.*, 115 (1939) 161.
6 B. Keilin and J. W. Otvos, *J. Am. Chem. Soc.*, 68 (1946) 2665.
7 D. T. Chow and R. J. Robinson, *Anal. Chem.*, 25 (1953) 1493.
8 J. Mašek, *Collection Czech. Chem. Commun.*, 21 (1956) 1214.
9 J. Mašek, *ibid.*, 21 (1956) 1347.
10 W. M. Latimer, *The Oxidation States of the Elements and Their Potentials in Aqueous Solutions*, Prentice-Hall, New York, 2nd ed., 1953, p. 92.
11 W. M. Latimer, *ibid.*, p. 94

12 V. C. DÖRING AND H. GEHLEN, *Z. Anorg. Allgem. Chem.*, 312 (1961) 32.
13 D. D. DEFORD, Private Communication, presented at the 133rd National Meeting ACS, San Francisco, California, 1958.
14 A. SEIDELL, *Solubilities of Inorganic and Metal Organic Compounds*, Vol. 1, D. Van Nostrand Co., New York, 3rd ed., 1940, p. 1142.
15 W. H. REINMUTH, *Anal. Chem.*, 33 (1961) 322.
16 L. MEITES, *Polarographic Techniques*, Interscience Publishers, Inc., New York, 1955, p. 277.
17 P. DELAHAY, *New Instrumental Methods in Electrochemistry*, Interscience Publishers Inc., New York, 1954, p. 187.
18 P. DELAHAY, *ibid.*, p. 35.
19 W. M. LATIMER, op. cit., p. 101.
20 T. A. TURNEY AND G. A. WRIGHT, *J. Chem. Soc.*, (1958) 2415.
21 W. M. LATIMER, *op. cit.*, p. 94.
22 P. DELAHAY, *op. cit.*, p. 194.

ELECTROANALYTICAL CHEMISTRY AND INTERFACIAL ELECTROCHEMISTRY
Elsevier Sequoia S.A., Lausanne – Printed in The Netherlands

POTENTIOMETRIC ACID–BASE TITRATIONS IN MOLTEN SALTS. THE ACID CHARACTER OF Li^+, Na^+, K^+, Ca^{2+}, Sr^{2+}, Ba^{2+} AND Pb^{2+} AS INFERRED FROM THE REACTION OF THEIR CARBONATES WITH $K_2Cr_2O_7$ IN MOLTEN KNO_3

A. M. SHAMS EL DIN AND A. A. EL HOSARY
Laboratory of Electrochemistry and Corrosion, National Research Centre, Dokki, Cairo (U.A.R.)
(Received August 9th, 1967)

In a recent communication we reported on the potentiometric titration of the acid, $NaPO_3$, with the carbonates of the alkali and alkaline-earth metals, in molten KNO_3 at 350°[1]. Both "forward" and "backward" neutralization curves showed marked potential inflexions at simple acid : oxide-ion donor relations. The P:O and P:e (e is negative charge) ratios of the primary-formed phosphates were proposed as measures for the acidity of the cations. On this basis, the six cations studied were arranged in decreasing order of acidity as: $Ca^{2+} > Li^+ > Sr^{2+} > Ba^{2+} > Na^+$, K^+. The differences between the acid character of the various cations were resolved, and emphasized by the large number of possible P–O compounds that can be formed, as well as by the glass-forming properties of the phosphates[2].

It was therefore, of interest to establish whether such differences can be demonstrated by reactions with simpler acids. The present paper reports on the results of "forward" and "backward" titrations of the acid $K_2Cr_2O_7$, with the carbonates of Li^+, Na^+, K^+, Ca^{2+}, Sr^{2+}, Ba^{2+} and Pb^{2+} in fused KNO_3 at 350°. Previous experience has shown that the forward neutralization curves of this acid with KOH[3], $NaHCO_3$[4], K_2CO_3[4] or Na_2O_2[4,5] consist of a single step corresponding to the reaction:

$$Cr_2O_7^{2-} + O^{2-} \rightarrow 2\ CrO_4^{2-} \qquad (1)$$

The equilibrium constant of this reaction, *viz.*, $K = [CrO_4^{2-}]^2/[Cr_2O_7^{2-}][O^{2-}]$, was found[6] to be 1.8×10^{12} at 350°, which indicates that $Cr_2O_7^{2-}$ is a relatively strong Lux acid[7].

EXPERIMENTAL

"Forward" neutralization experiments (in which the oxide-ion donors were added to the acid in fused KNO_3) and "backward" experiments (in which the procedure was reversed) were carried out with the seven carbonates. The technique of *in situ* potentiometric titration in fused salts has already been described[3]. 50.000 g of pre-melted and dehydrated KNO_3 were used as diluent in all cases. An oxygen (Pt) electrode was used as indicator electrode and its potential was measured relative to an Ag/Ag(I), melt/glass reference half-cell[8]. All chemicals were of analytical grade. Corrections were made for the water contents of NaOH and KOH. Unless otherwise stated, experiments were conducted at 350°.

RESULTS AND DISCUSSION

The curves given in Fig. 1,A represent the neutralization of different amounts of $K_2Cr_2O_7$ with Li_2CO_3 in molten KNO_3 at 350°. Curves B of the same figure are the corresponding backward titration curves. Both sets of curves show a single potential inflexion of *ca.* 350 mV at a molar ratio $Cr_2O_7^{2-}:CO_3^{2-}$ of 1:1 (insert of Fig. 1). Neutralization can be represented as:

$$Cr_2O_7^{2-} + CO_3^{2-} \rightarrow 2\ CrO_4^{2-} + CO_2 \qquad (2)$$

Almost the same behaviour was observed when Na_2CO_3 or K_2CO_3 were used as oxide-ion donors. Differentiation between the acid character of the three cations on the basis of the reaction of their carbonates with $K_2Cr_2O_7$ is, therefore, impossible.

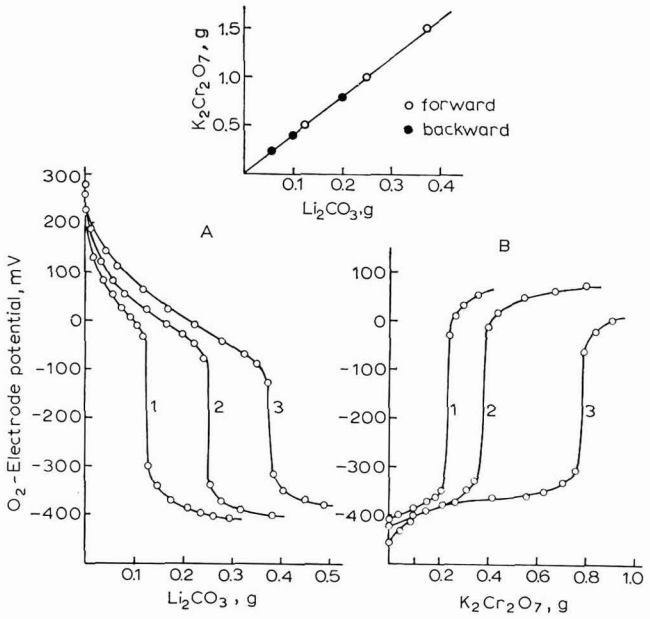

Fig. 1. Forward (A) and backward (B) titration curves of $K_2Cr_2O_7$ with Li_2CO_3 in KNO_3 at 350°. (A,1), 0.500; (A,2), 1.000; (A,3), 1.500 g $K_2Cr_2O_7$. (B,1), 0.058; (B,2), 0.100; (B,3), 0.200 g Li_2CO_3. Insert: relation between the quantitites of $K_2Cr_2O_7$ and Li_2CO_3; line drawn theoretically.

In the reaction with $NaPO_3$, however, Li^+ was shown to be acid with respect to Na^+ and K^+. The two latter cations behaved similarly and did not allow any distinction to be made between their acid properties. That K^+ is more basic than Na^+ was proved in the present study by carrying out "cyclic" neutralization experiments with the hydroxides of the two elements as oxide-ion donors. For a better appreciation of these results, the titration characteristics of $K_2Cr_2O_7$ with NaOH and KOH are first summarized: Forward neutralization of the acid with either compound produces curves with a single step accompanied by a drop in the O_2-electrode potential of *ca.* 700 mV, Figs. 2A and 3A. At the inflexion points of these curves, the molar ratio,

$Cr_2O_7^{2-}$:O^{2-} (O^{2-}=2 OH^-) is 1:1 and neutralization leads to the formation of CrO_4^{2-}. In the backward titration experiments, however, the curves are formed of two equal steps associated with potential rises of 250 and 300 mV. These take place

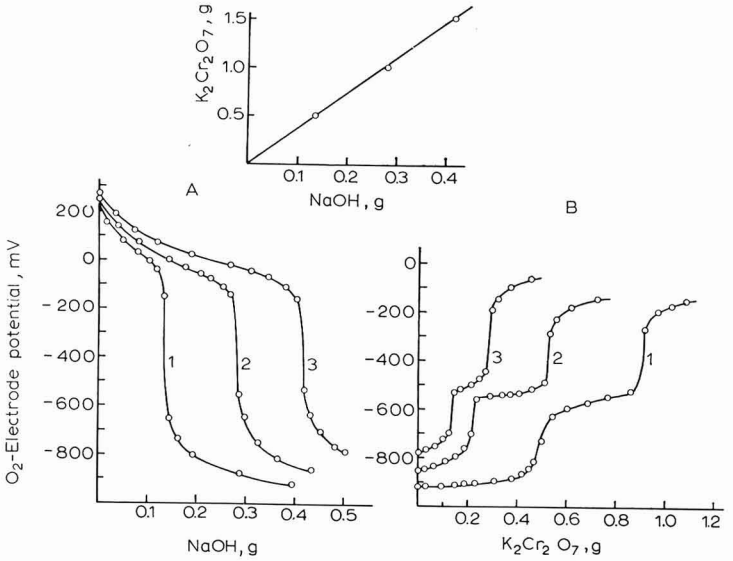

Fig. 2. Forward (A) and cyclic (B) titration curves of $K_2Cr_2O_7$ with NaOH in KNO_3 at 350°. (A,1), 0.500; (A,2), 1.000; (A,3), 1.500 g $K_2Cr_2O_7$. (B) backward neutralization of excess NaOH in expt. (A). Insert: relation between the quantities of $K_2Cr_2O_7$ and NaOH (expt. A); line drawn theoretically.

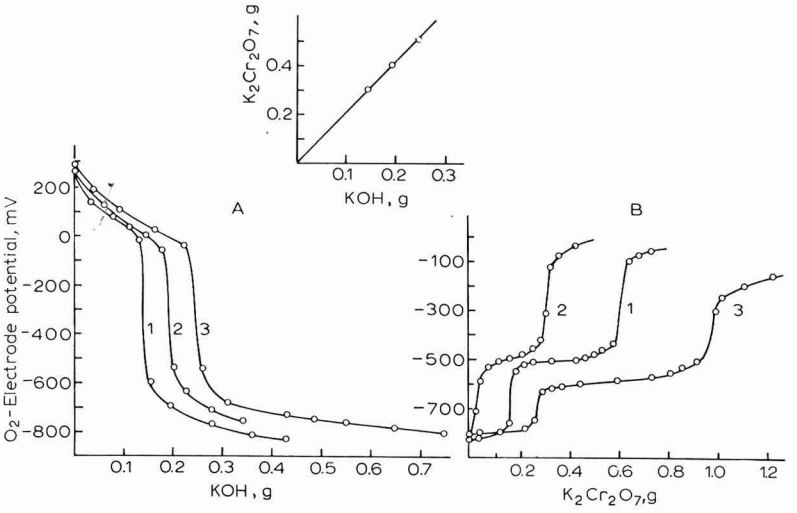

Fig. 3. Forward (A) and cyclic (B) titration curves of $K_2Cr_2O_7$ with KOH in KNO_3 at 350°. (A,1), 0.300; (A,2), 0.400; (A,3), 0.500 g $K_2Cr_2O_7$. (B) backward neutralization of excess KOH in expt. (A). Insert: relation between the quantities of $K_2Cr_2O_7$ and KOH (expt. A); line drawn theoretically.

at the molar relations, $Cr_2O_7^{2-}$: 2 O^{2-} and $Cr_2O_7^{2-}$:O^{2-}, respectively. Reaction with the two oxide-ion donors is as follows[2]:

$$Cr_2O_7^{2-} + 2\ O^{2-} \rightarrow 2\ CrO_4^{2-}\cdot O^{2-} \quad (3)$$

and

$$Cr_2O_7^{2-} + 2\ CrO_4^{2-}\cdot O^{2-} \rightarrow 4\ CrO_4^{2-} \quad (4)$$

which—in contrast to weak oxide-ion donors, *e.g.*, carbonate[2]—allows the formation of the basic chromate 2 $CrO_4^{2-}\cdot O^{2-}$ as an intermediate neutralization product.

The behaviour of $K_2Cr_2O_7$ upon "cyclic" neutralization with the two hydroxides is different from that described above, and enables the acid character of the cations to be differentiated. In these experiments, the acid is first titrated with either of the two oxide-ion donors and a certain excess is added after the equivalence point. This is then titrated with the acid. When using NaOH, neutralization of the extra oxide takes place in two equal steps, corresponding to reactions (3) and (4), Fig. 2,B. With KOH, on the other hand, cyclic titration curves exhibit two steps only when the amount of the oxide-ion donor in the melt is larger than that consumed in the forward titration experiment (curves 1 and 3, Fig. 3 B). Also, under these conditions the consumption of acid along the two neutralization steps is not equal, the second step consuming more acid than the first. When, however, KOH is present in amounts less than those taken in forward experiments, cyclic neutralization curves show only the second step (curve 2, Fig. 3B). These observations indicate that, in contrast to NaOH, KOH readily adds to CrO_4^{2-} present in the melt to form the basic structure 2 $CrO_4^{2-}\cdot O^{2-}$:

$$2\ CrO_4^{2-} + O^{2-} \rightarrow 2\ CrO_4^{2-}\cdot O^{2-} \quad (5)$$

Free O^{2-}-ion, which neutralizes in two equal steps, would accordingly be present in the melt only when all the chromate has been transformed into the basic structure. The acidification of such melts would therefore produce curves with two unequal steps, the first being due to the reaction of free O^{2-} (reaction 3), while the second —consuming more acid—represents the conversion of the originally-present and the newly-formed 2 $CrO_4^{2-}\cdot O^{2-}$ into CrO_4^{2-} (reaction 4). When, on the other hand, the amount of KOH added after the inflexion point is less than that already consumed, free O^{2-} would not be present in the melt and acidification would show only reaction (4). The fact that KOH adds to CrO_4^{2-} to give 2 $CrO_4^{2-}\cdot O^{2-}$ while NaOH under similar conditions does not, indicates clearly that the two cations differ in their acid character, K^+ being apparently less acid (more basic).

The three alkaline-earth carbonates also react with $K_2Cr_2O_7$ in the forward direction to yield CrO_4^{2-}, *i.e.*, the molar ratios $Cr_2O_7^{2-}$:CO_3^{2-} at the points of inflexion are 1:1, Figs. 4–6,A. At the equivalence points, potential drops of *ca.* 250, 300 and 450 mV are measured with $CaCO_3$, $SrCO_3$ and $BaCO_3$, respectively. For the first two compounds, the drop in potential is considerably smaller than that for $BaCO_3$ or for the alkali carbonates, and suggests that the $CaCrO_4$ and $SrCrO_4$ formed are more acid than the other chromates. That this is actually the case was proved by experiments in which, after reaching the inflexion points, the titration was continued with Na_2CO_3. Curves A', Figs. 4 and 5 show clearly that under these conditions the melts continue to consume the new oxide-ion donor, and that one equivalent of it is needed to bring about a second inflexion of *ca.* 200 mV in the case of Ca^{2+}, and

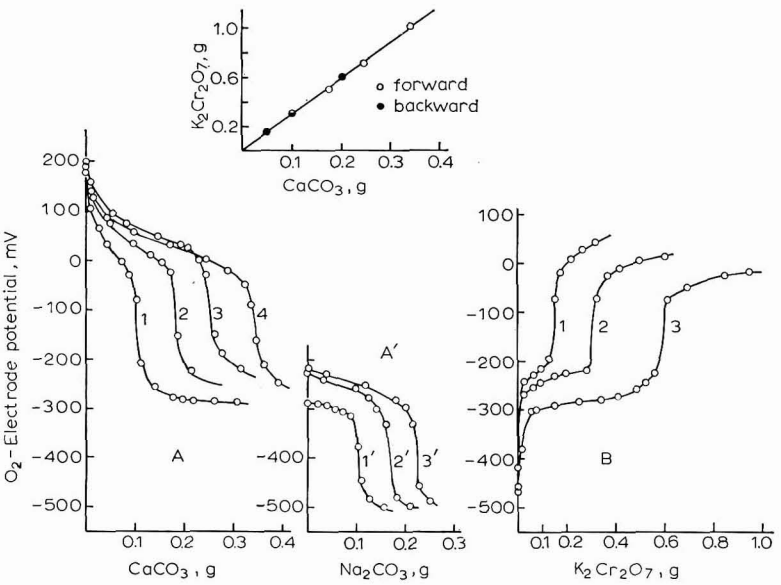

Fig. 4. Forward (A) and backward (B) titration curves of $K_2Cr_2O_7$ with $CaCO_3$ in KNO_3 at 350°. (A,1), 0.300; (A,2), 0.500; (A,3), 0.700; (A,4), 1.000 g $K_2Cr_2O_7$. (A′) further titration of products in (A) with Na_2CO_3. (B,1), 0.050; (B,2), 0.100; (B,3), 0.200 g $CaCO_3$. Insert: relation between the quantities of $K_2Cr_2O_7$ and $CaCO_3$; line drawn theoretically.

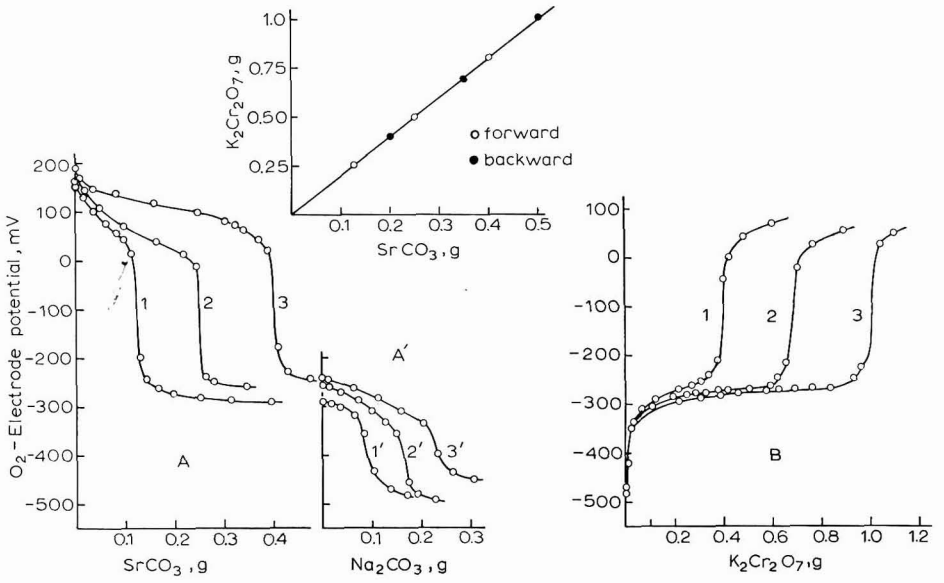

Fig. 5. Forward (A) and backward (B) titration curves of $K_2Cr_2O_7$ with $SrCO_3$ in KNO_3 at 350°. (A,1), 0.250; (A,2), 0.500; (A,3), 0.800 g $K_2Cr_2O_7$. (A′) further titration of products in (A) with Na_2CO_3. (B,1), 0.200; (B,2), 0.350; (B,3), 0.500 g $SrCO_3$. Insert: relation between the quantities of $K_2Cr_2O_7$ and $SrCO_3$; line drawn theoretically.

150 mV in the case of Sr^{2+}. Curves similar to those of Figs. 4A′ and 5A′ were also obtained when $CaCrO_4$ and $SrCrO_4$ were titrated with Na_2CO_3 in molten KNO_3 at 350°. It was therefore of interest to establish the nature of the basic chromates thus formed. The solidified and pulverized reaction products (corresponding to the inflexion points of curves A′, Figs. 4 and 5) were treated with HCl, whereby CO_2 was evolved. The collected gas volumes indicated the presence of 1 mole of carbonate/mole

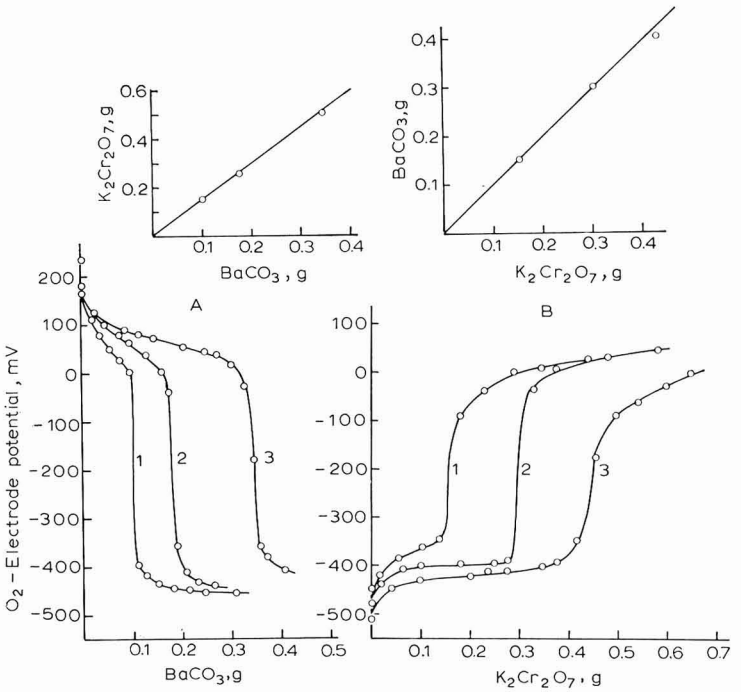

Fig. 6. Forward (A) and backward (B) titration curves of $K_2Cr_2O_7$ with $BaCO_3$ in KNO_3 at 350°. (A,1), 0.150; (A,2), 0.250; (A,3), 0.500 g $K_2Cr_2O_7$. (B,1), 0.150; (B,2), 0.300; (B,3), 0.400 g $BaCO_3$. Inserts: relations between the quantities of $K_2Cr_2O_7$ and $BaCO_3$; lines drawn theoretically.

chromate. It can be concluded from this that the reaction of Na_2CO_3 with the chromates of Ca^{2+} and Sr^{2+} leads to the formation of an addition product of formula $CaCrO_4 \cdot Na_2CO_3$ ($SrCrO_4 \cdot Na_2CO_3$). It was of further interest to determine whether the acid chromates of Ca^{2+} and Sr^{2+}, formed under the conditions of the potentiometric titration, are simple or mixed chromates. The neutralization reaction of $CaCO_3$, can be written as:

$$K_2Cr_2O_7 + CaCO_3 \rightarrow K_2Ca(CrO_4)_2 + CO_2 \quad (6)$$

or

$$K_2Cr_2O_7 + CaCO_3 \rightarrow K_2CrO_4 + CaCrO_4 + CO_2 \quad (7)$$

Therefore, $CaCO_3$ ($SrCO_3$) was added to the acid-nitrate melts just to the point of equivalence. The melts were then cooled, crushed and dissolved in water. The solutions were coloured yellow and contained an insoluble residue. The precipitate was filtered and the clear solutions were analyzed quantitatively for chromate

(precipitation as mercurous chromate); the presence of one equivalent of soluble chromate/equivalent $CaCO_3$ ($SrCO_3$) added to the melt was proved. If it is assumed that water does not hydrolytically attack a structure like $K_2Ca(CrO_4)_2$, the above result indicates that reaction (7) is the one most probably taking place. This conclusion is also supported by the fact that the chromates formed behave—upon further neutralization with Na_2CO_3—in a manner similar to that of the pure compounds.

The reaction product of $BaCO_3$ and $K_2Cr_2O_7$, *i.e.*, $BaCrO_4$, does not add an extra equivalent of Na_2CO_3 as do the reaction products of Ca^{2+} and Sr^{2+}. The Ba^{2+}-ion is, accordingly, less acid than Ca^{2+} or Sr^{2+}. The acid properties of the last two cations cannot be differentiated on the basis of the reaction of their carbonates with $K_2Cr_2O_7$. However, the potentials of the O_2-electrode in melts of equivalent quantities of $CaCrO_4$ and $SrCrO_4$ in fused KNO_3, show that Ca^{2+} is more acid than Sr^{2+}. The study of the reaction of the two carbonates with $NaPO_3$[1] led to the same conclusion.

Backward titration curves of the carbonates of Ca^{2+}, Sr^{2+} and Ba^{2+} are shown in Figs. 4–6,B. These curves are characterized by a single neutralization step accompanied by a potential rise of *ca.* 200, 250 and 350 mV, respectively. The molar ratios $Cr_2O_7^{2-}$:CO_3^{2-} at the inflexion points are 1:1 for Ca^{2+} and Sr^{2+}, and 2:3 for Ba^{2+}. Both $CaCO_3$ and $SrCO_3$ react with $K_2Cr_2O_7$ to yield the normal chromate, CrO_4^{2-}, upon forward or backward neutralization. $BaCO_3$, in backward titration experiments, however, behaves differently. First, the reaction with the acid is exceedingly slow and the O_2-electrode requires relatively long times to establish steady-state potentials. After each dichromate addition, the potential changes momentarily towards positive values (acid melts) and then drifts slowly back to more negative potentials. This behaviour is apparently related to the fact that both $BaCO_3$ and its reaction product with the acid are insoluble in the melt. Nevertheless, when enough time is given for steady-state potentials to establish, reproducible titration curves are obtained with inflexions at the molar ratio, 2 $Cr_2O_7^{2-}$: 3 CO_3^{2-}. Neutralization leads, most probably, to the formation of 2 $BaCrO_4 \cdot BaCO_3$.

The reactions between $PbCO_3$ and $K_2Cr_2O_7$ and $PbCO_3$ and KNO_3 are of particular interest and were studied in some detail. Forward neutralization of the acid gives rise to curves with two inflexions of 200 mV each, Fig. 7,A. At the first potential drop, the ratio $K_2Cr_2O_7$:$PbCO_3$ is 1:1, and thus the reaction is:

$$K_2Cr_2O_7 + PbCO_3 \rightarrow PbCrO_4 + K_2CrO_4 + CO_2 \qquad (8)$$

This has been confirmed by analyzing the reaction products in the manner described above for Ca^{2+} and Sr^{2+} carbonates. The consumption of $PbCO_3$ along the second neutralization step is equal to that with the first step. That this step does not represent a precipitation reaction of the form:

$$K_2CrO_4 + PbCO_3 \rightarrow PbCrO_4\downarrow + K_2CO_3 \qquad (9)$$

was established by analyzing aqueous solutions of solidified melts after this stage; it was found that the filtrate contained no K_2CO_3, but K_2CrO_4 in quantities corresponding to that required from an acid–base reaction. Further, the addition of extra K_2CrO_4 to the melt after the first neutralization stage did not affect the consumption of $PbCO_3$ along the subsequent step. It may therefore be concluded that $PbCrO_4$ formed along the first step of the titration curves adds an equivalent of $PbCO_3$ along the second to give the compound $PbCrO_4 \cdot PbCO_3$. Analysis of the cooled

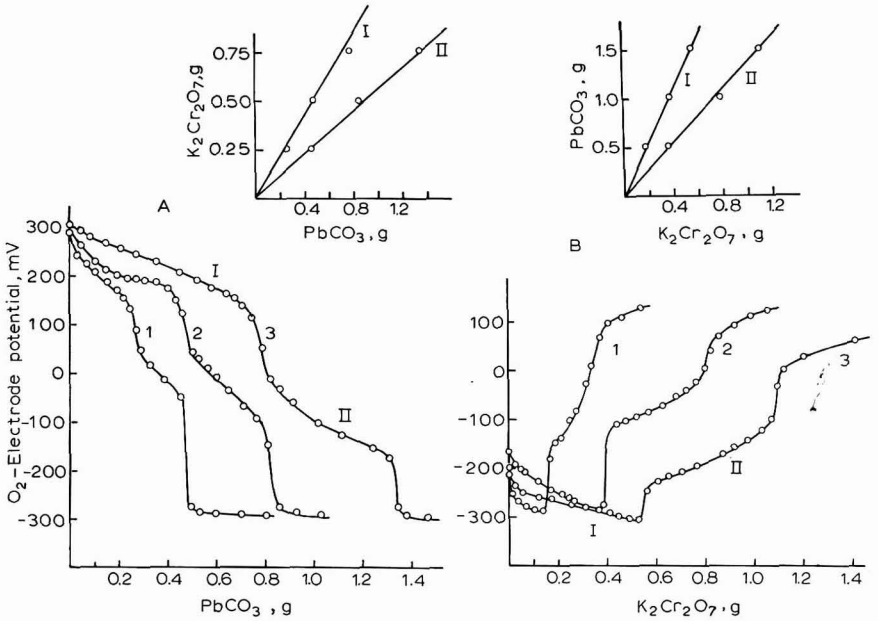

Fig. 7. Forward (A) and backward (B) titration curves of $K_2Cr_2O_7$ with $PbCO_3$ in KNO_3 at 350°. (A,1), 0.250; (A,2), 0.500; (A,3), 0.750 g $K_2Cr_2O_7$. (B,1), 0.500; (B,2), 1.000; (B,3), 1.500 g $PbCO_3$. Inserts: relations between the quantities of $K_2Cr_2O_7$ and $PbCO_3$; lines drawn theoretically.

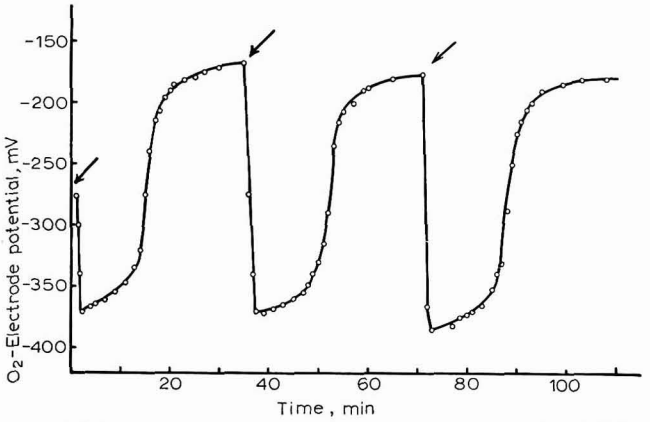

Fig. 8. Variation with time, of the O_2-electrode potential in KNO_3 at 350° on addition of 1.000-g quantities of $PbCO_3$. Arrows indicate time of addition.

salts confirmed this conclusion. The fact that $PbCrO_4$ can add another molecule of the titrant ($PbCO_3$) indicates that it is more acid than either $CaCrO_4$ or $SrCrO_4$ and Pb^{2+} can therefore be regarded as the most acid cation among those studied in the present investigation.

Before the results of the backward titration experiments with $PbCO_3$ are discussed, the reaction between this compound and molten KNO_3 has first to be resolved. Thus, in contrast to the carbonates of the alkali and alkaline-earth metals,

which are both chemically and thermally stable in the melt under consideration, $PbCO_3$ when added to fused KNO_3 evolves CO_2. At the same time, the potential of the O_2-electrode drops first to negative values, remains constant for a certain period and then changes to a constant, positive value. Time–potential curves representing this behaviour are given in Fig. 8, where successive charges of 1.000 g $PbCO_3$ were added to 50.000 g KNO_3 at 350°. The shape of these curves indicates clearly that the carbonate changes, through reaction with the melt, into a less basic compound. To determine the reaction of $PbCO_3$, the melts, after the establishment of steady-state potentials, were cooled, crushed and treated with excess dilute HNO_3; the CO_2 evolved was collected in a gas-burette. The volumes of gas thus obtained (corrected to N.T.P.) were found to be two-thirds of those obtained from similar KNO_3–$PbCO_3$ mixtures not subjected to fusion. This shows that one-third of the carbonate has changed during fusion into a form that does not evolve CO_2 and does not react readily with $K_2Cr_2O_7$ (see later). It was further established that the addition of PbO to KNO_3–$PbCO_3$ mixtures which had not been subjected to fusion had no effect on the volumes of CO_2 collected upon treatment with acid. It is, therefore, reasonable to assume that the fusion of $PbCO_3$ with KNO_3 leads to the formation of white lead[8], $2\,PbCO_3 \cdot PbO$, according to:

$$3\,PbCO_3 \rightarrow 2\,PbCO_3 \cdot PbO + CO_2 \qquad (10)$$

The kinetics of this transformation were examined in some detail. Thus,if the time, τ, taken by the oxygen electrode to establish steady-state potentials is considered as the reaction time, the suitable rate equation for decomposition can be derived. The curves of Fig. 9 represent the variation with time of the O_2-electrode potential in nitrate melts at 350, 370, 390 and 415°, to which different amounts of

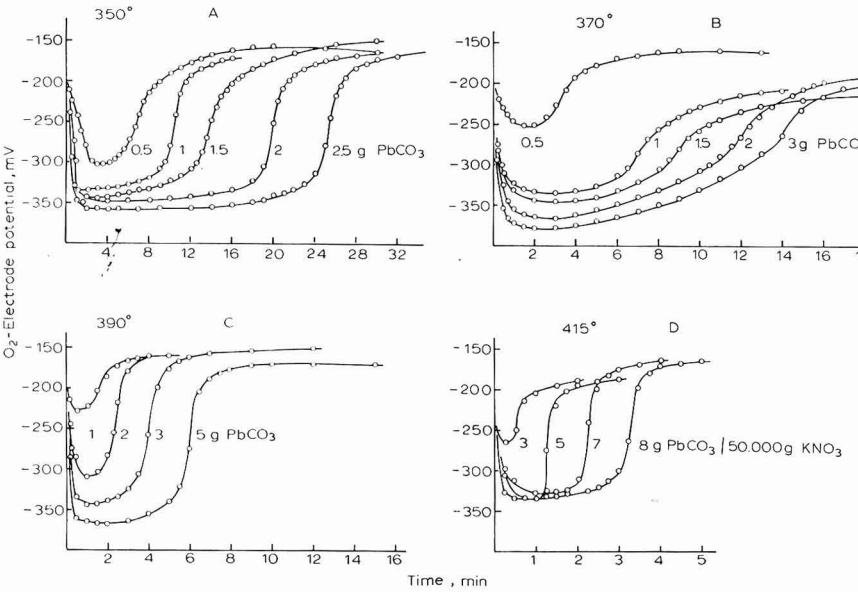

Fig. 9. Variation with time of the O_2-electrode potential during the reaction of $PbCO_3$ with KNO_3 at various temps.

$PbCO_3$ were added. At any one temperature, τ increases with the $PbCO_3$-content of the melt. On the other hand, for melts of comparable composition, τ decreases as the temperature is raised. From the weights of carbonate, the corresponding molarities were calculated according to:

$$M = 1000\ W_s d / M_s w \tag{11}$$

where W_s is the weight of $PbCO_3$, M_s its molecular weight, w the weight of KNO_3 (50.000 g) and d the density of molten KNO_3 at temperature t (°C) computed from the relation[9]:

$$d = 2.044 - 0.0006\ t\ \text{g cm}^{-3} \tag{12}$$

The molarities thus calculated are plotted as function of the reaction time, τ, in Fig. 10,A. Straight lines are invariably obtained which supports the conclusion

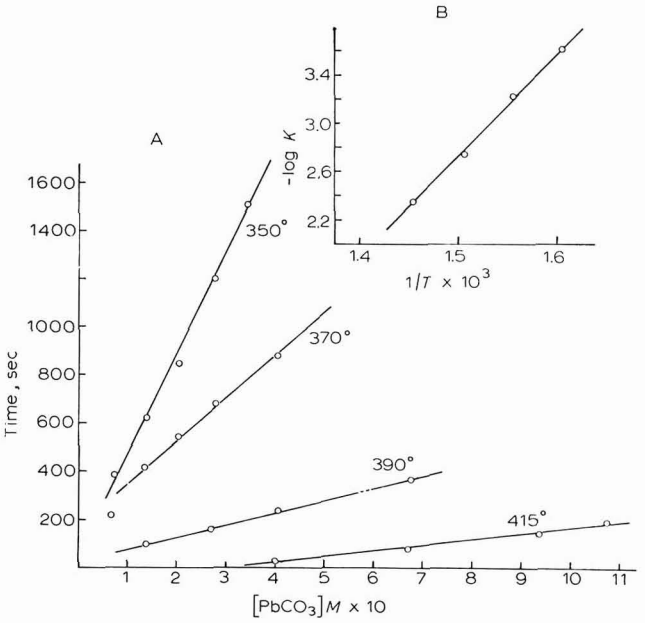

Fig. 10. (A), relation between reaction time and molarity of $PbCO_3$ at different temps.; (B), log k–$1/T$ plot for the decomposition of $PbCO_3$ in molten KNO_3.

that the conversion of $PbCO_3$ into $2PbCO_3 \cdot PbO$ is a zero-order reaction with respect to carbonate. From the slopes of the lines of Fig. 10,A, the rate constants are calculated as 2.33, 5.71, 19.05 and 44.70×10^{-4} mole l^{-1} sec^{-1} at 350, 370, 390 and 415°, respectively. A plot of the logarithm of these constants as a function of $1/T$ is shown in Fig. 10,B; the slope of this line gives the activation energy of transformation as 38.2 kcal $mole^{-1}$.

It is of interest to note before the results of the backward titration of $PbCO_3$ with $K_2Cr_2O_7$ are presented that attempts to titrate the acid with PbO were unsuccessful. The O_2-electrode did not respond to acid- or oxide-ion donor additions

in backward or forward titration experiments, respectively. The reason for this behaviour is not fully understood, but the strong oxidizing properties of molten nitrate which make possible the conversion of PbO into higher, acid oxides may be significant.

When $K_2Cr_2O_7$ is added to KNO_3–$PbCO_3$ mixtures that have been equilibrated, titration curves similar to those shown in Fig. 7,B are obtained. The curves have two inflexions of *ca.* 150 mV each. Up to the end of the first step, the molar quantity of $K_2Cr_2O_7$ corresponds to one-third of the *original* $PbCO_3$ of the melt. Double this quantity is needed to affect the second inflexion. If it is taken into consideration, however, that during equilibration the carbonate has changed into white lead, $2PbCO_3 \cdot PbO$, and that PbO does not react with $K_2Cr_2O_7$ under the experimental conditions, the *actual* molar ratios are 1 : 2 and 1 : 1, respectively. Backward neutralization can therefore be represented as:

$$K_2Cr_2O_7 + 2\ PbCO_3 \cdot PbO \rightarrow K_2CrO_4 + PbCrO_4 \cdot PbCO_3 + PbO + CO_2 \qquad (13)$$

and

$$K_2Cr_2O_7 + PbCrO_4 \cdot PbCO_3 \rightarrow K_2CrO_4 + 2\ PbCrO_4 + CO_2 \qquad (14)$$

which is the reverse of the reaction taking place during forward titration. Analysis of the melt after the first inflexion (treatment of the solidified masses with dilute HNO_3 and collection of the CO_2 evolved) proved the existence of one-third of the added $PbCO_3$ in the mixture.

The present investigation on the titration of the acid, $K_2Cr_2O_7$, with different carbonates results in an arrangement of their cations in decreasing order of acidity as Li^+, $Na^+ > K^+$ and $Pb^{2+} > Ca^{2+} > Sr^{2+} > Ba^{2+}$. This series is the same as that established in a previous study on the basis of the reaction of the same carbonates with $NaPO_3$.

SUMMARY

The acid, $K_2Cr_2O_7$, has been titrated potentiometrically with the carbonates of Li, Na, K, Ca, Sr, Ba and Pb in fused KNO_3 at 350°. Both "forward" and "backward" neutralization curves (except for the case of Pb) consist of a single step corresponding usually to formation of CrO_4^{2-}. "Cyclic" neutralization curves with NaOH and KOH suggest that Na^+ is acid with respect to K^+. The acidity of Ca^{2+}, Sr^{2+} and Ba^{2+} decreases in the order given. $CaCrO_4$ and $SrCrO_4$ add an extra molecule of Na_2CO_3 to give $CaCrO_4 \cdot Na_2CO_3$ ($SrCrO_4 \cdot Na_2CO_3$); $BaCrO_4$ does not. Pb^{2+} is the most acid cation studied. $PbCrO_4$ adds another molecule of $PbCO_3$ and gives a second inflexion in the titration curves, corresponding to the formation of $PbCrO_4 \cdot PbCO_3$.

$PbCO_3$ decomposes thermally in fused KNO_3 to give white lead, $2PbCO_3 \cdot PbO$. The reaction is zero-order with respect ot $PbCO_3$ and has an activation energy of 38.2 kcal $mole^{-1}$.

REFERENCES

1 A. M. Shams El Din, H. D. Taki El Din and A. A. El Hosary, *Electrochim. Acta*, in press.
2 A. M. Shams El Din and A. A. El Hosary, *Electrochim. Acta*, in press.
3 A. M. Shams El Din, *Electrochim. Acta*, 7 (1962) 278.
4 A. M. Shams El Din and A. A. A. Gerges, *J. Electroanal. Chem.*, 4 (1962) 309.

5 A. M. SHAMS EL DIN AND A. A. EL HOSARY, *J. Electroanal. Chem.*, 9 (1965) 349.
6 A. M. SHAMS EL DIN AND A. A. A. GERGES, *Electrochim. Acta*, 9 (1964) 613.
7 H. LUX, *Z. Elektrochem.*, 45 (1939) 303.
8 A. M. SHAMS EL DIN, A. A. EL HOSARY AND A. A. A. GERGES, *J. Electroanal. Chem.*, 6 (1963) 131.
9 J. M. MELLOR, *A Comprehensive Treatise on Inorganic and Theoretical Chemistry*, Vol. VII, Longman, Green and Co., London, 1947, p. 836.
10 R. LORENZ, H. FREI AND A. JABS, *Z. Physik. Chem., Leipzig*, 61 (1908) 468.

ELECTROANALYTICAL CHEMISTRY AND INTERFACIAL ELECTROCHEMISTRY
Elsevier Sequoia S.A., Lausanne – Printed in The Netherlands

POLAROGRAPHISCHES VERHALTEN DES ARSENS UND PHOSPHORS IV. POLAROGRAPHIE DER CARBOXYALKYLPHOSPHINE*

K. ISSLEIB, H. MATSCHINER UND S. NAUMANN
Institut für Anorganische Chemie der Universität Halle (Saale)
(Eingegangen am 7. April 1967; revisioniert am 24. Juli 1967)

P,P-disubstituierte Carboxyalkylphosphine setzen die Wasserstoffüberspannung an der Hg-Kathode herab[2]. In Fortführung der Untersuchung galt es, den Einfluss des dreibindigen Phosphors bei diesem Elektrodenvorgang zu studieren, was eine Ausdehnung der Untersuchungen auch auf Verbindungen des Typs I–IV voraussetzt.

I: $RP(H)CH(R')COOH$ $R = C_6H_5, C_6H_{11}, H$; $R' = H, CH_3, C_2H_5$

II: $RP(H)(CH_2)_nCOOH$ $R = C_6H_5, C_6H_{11}$,

III: 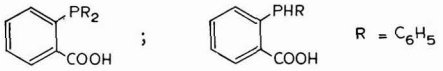

IV: R_3P, R_2PH, RPH_2, PH_3 $R = C_6H_5$

Ausserdem sollte der Einfluss der Schwermetallionen, besonders der Kobalt(II)- und Kobalt(III)-ionen auf die katalytischen Effekte der Organophosphorverbindungen, wie sie durch analoge schwefelhaltige Verbindungen bekannt geworden sind[3,4], untersucht werden.

ERGEBNISSE

In dem Umfang wie die Phenylsubstituenten am Phosphor durch Wasserstoffatome ersetzt werden, verringert sich die katalytische Aktivität. Triphenylphosphin ist beispielsweise wesentlich aktiver als Diphenylphosphin, Monophenylphosphin und PH_3 sind hingegen inaktiv.

Bei den Carboxyalkylphosphinen ist ferner noch der Einfluss der Carboxylgruppe zu berücksichtigen. Verbindungen mit β-ständigen Phosphinsubstituenten sind im Gegensatz zu α-ständigen (II, $n=2$) inaktiv.

Der Einfluss von Kobaltionen ist am deutlichsten im Falle der unsubstituierten Carboxyalkylphosphine $H_2PCHRCOOH$ zu erkennen. Bereits 10^{-8} M $CoCl_2$ oder $[Co(NH_3)_6]Cl_3$ in einer schwach salzsauren Alkalichloridlösung genügen, um eine gut ausgebildete katalytische Welle hervorzurufen. Die katalytische Stufe (i_k) wächst

* Für die III. Mitteilung, siehe Ref. 1.

bei Kobaltzugabe bis zur Höhe der normalen Wasserstoffwelle (i_H). Gleichzeitig verschiebt sich das Halbstufenpotential zu positiveren Potentialen wie aus Tabelle 1 ersichtlich ist. Solange i_k im Verhältnis zu i_H klein ist, erfolgt eine Vergrösserung sowohl mit sinkender Behälterhöhe als auch nach Zugabe von Gelatine. Höhere Gelatinekonzentrationen als 0.006% wirken dann dämpfend auf den Elektrodenvorgang.

TABELLE 1

EINFLUSS DER KOBALT(II)IONEN AUF DIE KATALYTISCHE STUFE (i_k) VON H_2PCH_2COOH IN SALZSAUREN KALIUMCHLORIDLÖSUNGEN

$[H_2PCH_2COOH] = 1.78 \times 10^{-4}\ M$, $[H^+] = 8.9 \times 10^{-4}\ M$

$[Co^{2+}]$ (M)	i_k/i_H	$E_{\frac{1}{2}}(mV)$	i_k/i_H*	$E_{\frac{1}{2}}(mV)$*
8.85×10^{-8}	0.204	−1290	0.573	−1290
1.77×10^{-7}	0.366	−1285	0.815	−1290
2.63×10^{-7}	0.505	−1280	0.93	−1270
3.5×10^{-7}	0.725	−1280	0.965	−1265
4.4×10^{-5}	—	—	1.0	−1025

i_k/i_H = Verhältnis der katalytischen Welle i_k zur normalen Wasserstoffwelle; i_k/i_H* bzw. $E_{\frac{1}{2}}$*, Ergebnisse in Gegenwart von 0.0022% Gelatine.

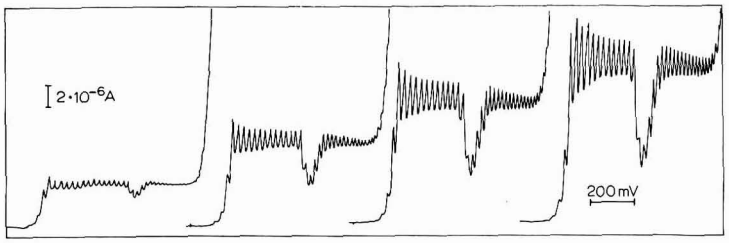

Abb. 1. Abhängigkeit der katalytischen Stufe von der HCl-Konzentration. 0.1 M KCl; $4.2 \times 10^{-5}\ M$ $C_6H_{11}P(H)CH_2COOH$; $4 \cdot 10^{-5}\ M$ $CoCl_2$. HCl-Konz.: 2.3; 4.5; 7.0 und $9.1 \times 10^{-4}\ M$. Startpotential = −0.75 mV.

Erreicht die katalytische Stufe die Höhe der Wasserstoffstufe, so ist sie rein diffusionsbedingt und proportional der Protonenkonzentration (vgl. Abb. 1).

Die durch Kobaltsalze verursachte Vergrösserung der katalytischen Stufe der Carboxyalkylphosphine eignet sich für den Ultramikronachweis von Kobaltionen. Auch in Pufferlösungen vergrössern sich die katalytischen Wellen der Carboxyalkylphosphine nach Zugabe von Kobaltionen (Abb. 2). Dies trifft nicht nur für saure Lösungen zu, sondern auch in kobalthaltigen NH_3–NH_4Cl-Puffern können gut ausgebildete katalytische Wellen beobachtet werden. Besonders bemerkenswert ist in diesem Zusammenhang, dass ebenfalls PH_3 und $PH_2C_6H_5$ in Gegenwart von $[Co(NH_3)_6]Cl_3$ katalytisch aktiv sind, während die katalytischen Wellen des $P(C_6H_5)_3$ durch Kobaltionen nicht beeinflusst werden. Konzentrationen von $10^{-7}\ M$ PH_3 können in sauren Pufferlösungen (pH = 3–5), die $[Co(NH_3)_6]Cl_3$ enthalten, noch erfasst werden.

Die katalytischen Wellen in Gegenwart von Kobaltionen vergrössern sich mit

sinkendem pH-Wert (Abb. 3) und mit der Phosphinkonzentration. Im Falle relativ niedriger Phosphinkonzentrationen ($<5\times10^{-4}$ *M*) wachsen die katalytischen Wellen mit sinkender Behälterhöhe. Treten zwei katalytische Wellen auf, z.B., unter bestimmten Bedingungen für III, so ist die erste Welle diffusionsbedingt, während sich

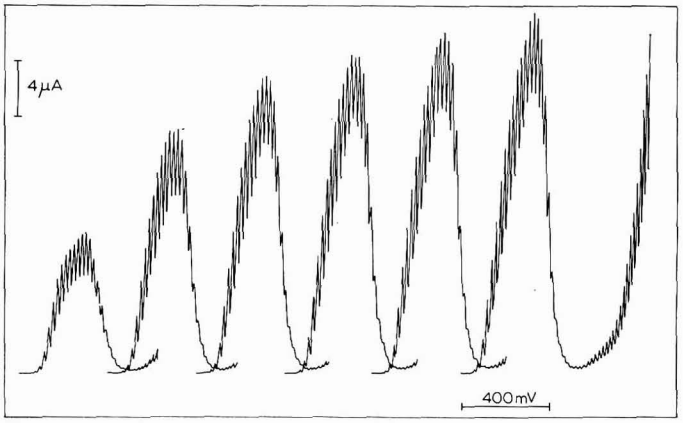

Abb. 2. Einfluss von $CoCl_2$ auf die katalytische Welle der *o*-Diphenylphosphinobenzoesäure. B.R.-Puffer pH = 5.5; 2×10^{-5} *M* *o*-$P(C_6H_5)_2C_6H_4COOH$; 0.005% Gelatine. $CoCl_2$-Konz. von links nach rechts: 2.44×10^{-6}; 4.76×10^{-6}; 9.62×10^{-6}; 1.18×10^{-5}; 1.43×10^{-5}; 1.66×10^{-5} *M*. Spannungsbeginn: −0.9 V.

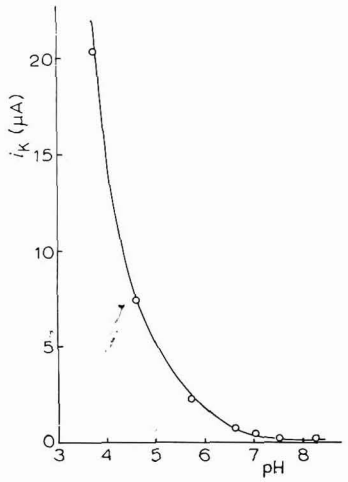

Abb. 3. Abhängigkeit der katalytischen Wellen vom pH-Wert des Grundelektrolyten B.R.-Puffer. 2.4×10^{-6} *M* $[Co(NH_3)_6]Cl_3$; 1.05×10^{-4} *M* $C_6H_5P(H)CH_2\cdot CH_2COOH$.

die zweite Welle mit sinkender Behälterhöhe vergrössert (Abb. 4). In der Lösung ist beim Potential der katalytischen Wasserstoffabscheidung ein starkes Strömen in Richtung zur Kapillarmündung zu beobachten. Indifferente Salze verringern die katalytische Wirksamkeit, ihr Einfluss wächst in der Reihenfolge $Li^+ < Na^+ < K^+$.

Die Tropfzeitkurven lassen für die Phosphine I–IV eine starke Adsorption

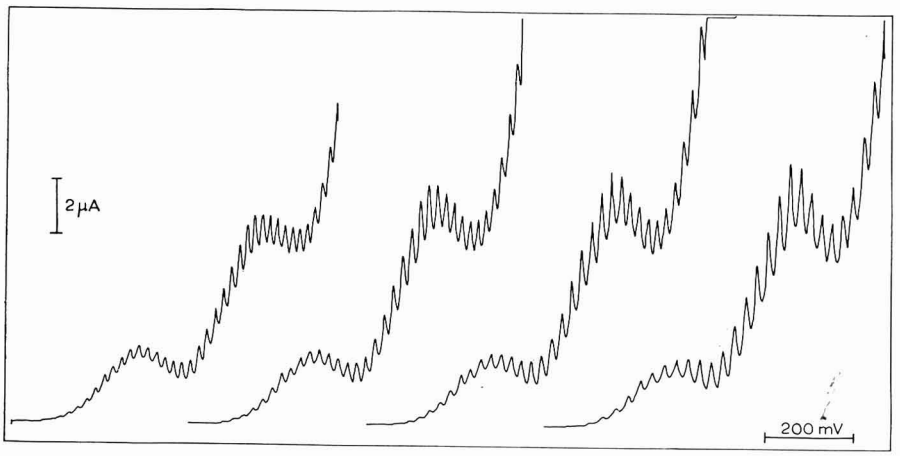

Abb. 4. Abhängigkeit von der Behälterhöhe B.R.-Puffer pH = 3.7; $2 \cdot 10^{-6}$ *M* $CoCl_2$; $5 \cdot 10^{-6}$ *M* *o*-$P(C_6H_5)_2C_6H_4COOH$. Behälterhöhen: 100, 90, 80 und 70 cm. Spannungsbegin: −0.9 V.

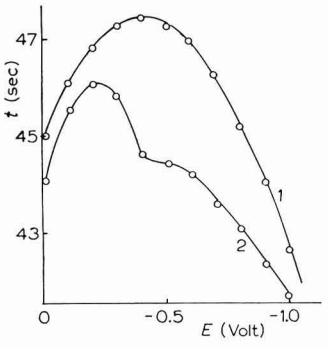

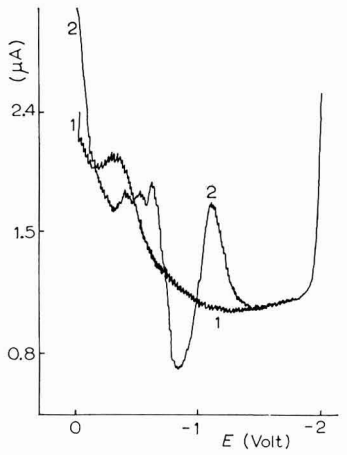

Abb. 5. Tropfzeitkurven. (1), B.R.-Puffer pH = 5.02; (2), 8.7×10^{-5} *M* *o*-$P(C_6H_5)_2C_6H_4COOH$ und nach Zugabe von 4.35×10^{-5} *M* $CoCl_2$.

Abb. 6. Tensammetrische Kurven der *o*-Monophenylphosphinobenzoesäure. (1), 1 *M* KCl; (2), 1 *M* KCl und $1 \cdot 10^{-4}$ *M* *o*-$P(H)C_6H_5C_6H_4COOH$.

auf der Elektrodenoberfläche erkennen. Die Deformation der Tropfzeitkurve wird durch Kobaltsalze nicht verstärkt (vgl. Abb. 5). Auf den tensammetrischen Kurven ist eine relativ hohe Grundstromerniedrigung, ein kleiner Adsorptions- und ein grösserer Desorptions-peak zu erkennen (vgl. Abb. 6.). Gleichfalls treten Kapazitätseinschnitte auf den $dE/dT = f(E)$-Kurven auf.

EXPERIMENTELLES

Für die Aufnahme der Stromspannungskurven dient der Polarograph OH-101,

während die tensammetrischen Untersuchungen mit dem Polarographen GWP 563 durchgeführt werden. Als Hg-Elektroden werden mehrere stumpfe Jenaer Kapillaren mit Tropfzeiten zwischen 2–4 sec und Ausflussgeschwindigkeiten von 2 bis 2.5 mg/sec bei einer Behälterhöhe von 75 cm verwendet. Als Messzelle dient ein modifiziertes Kalousek-Gefäss mit gesättigter Kalomelelektrode als Vergleichselektrode. Sämtliche Messungen erfolgen unter Luftausschluss in Argonatmosphäre.

DISKUSSION

Die vorliegenden Ergebnisse bestätigen den in früheren Arbeiten diskutierten Mechanismus der katalytischen Wasserstoffabscheidung unter dem Einfluss von Organo-Phosphorverbindungen[2,5]. Offensichtlich ist die Protonisierung von I–IV als wichtigster Teilschritt des gesamten Elektrodenvorganges anzusehen. Ausserdem spielt auch die Adsorption des Depolarisators auf der Elektrodenoberfläche eine Rolle. So werden die Elektrokapillarkurven in Pufferlösungen mit pH = 6 auf dem negativ geladenen Teil deformiert, während der potentiometrisch ermittelte pK_a-Wert z.B., der Diphenylphosphinogruppe in III, unter 2 liegt[6]. Es ist hier, wenn auch nur teilweise, die Existenz eines inneren Salzes[7] nicht auszuschliessen. Im Sinne der Theorie von CALUSARU UND KŮTA wäre dadurch ein Elektronenübergang von der auf der Elektrodenoberfläche adsorbierten Phosphinogruppe auf die protonisierte Carboxylgruppe[8] möglich. Diese Annahme würde den starken Abfall der katalytischen Aktivität, der nicht allgemein auf Basizitätsunterschiede zurückzuführen ist, von $C_6H_5P(H)CH_2COOH$ gegenüber $C_6H_5P(H)CH_2 \cdot CH_2COOH$ erklären. Auf Grund der ^{31}P-NMR-Spektren ist aber für $H_2PCHRCOOH$ eine derartige teilweise Betainstruktur auszuschliessen[9].

Die Untersuchungsergebnisse lassen eindeutig erkennen, dass koordinativ einzählige Liganden wie PH_3, $PH_2C_6H_5$ und $PH(C_6H_5)_2$ in Gegenwart von Schwermetallionen die Überspannung des Wasserstoffs an der Hg-Elektrode ebenfalls herabsetzen. Somit ist für das Auftreten katalytischer Wasserstoffwellen in Gegenwart von Kobaltionen eine Chelatkomplexbildung[10] keineswegs Voraussetzung. Der Einfluss von Schwermetallionen auf die katalytischen Wellen lässt einen Zusammenhang komplexchemischer Reaktionen schwefel-[11] und phosphor-haltiger Liganden erkennen.

Die hohe katalytische Aktivität in Anwesenheit äusserst geringer Kobaltionen-Konzentrationen ist offensichtlich nicht mit der Ansicht zu vereinbaren, dass Kobalt während des Elektrodenvorganges abgeschieden wird[12]. Es ist wahrscheinlicher, dass der katalytisch aktive Komplex durch eine dem Elektrodenvorgang nachgelagerte Reaktion regeneriert wird. Auf diese Weise können die Cyanokomplexe des Kobalts unter gewissen Vorbehalten als Modellsubstanzen betrachtet werden[13]. Während der Pentacyanokobalt(II)-Komplex an der Hg-Tropfelektrode zu einem stabilen Kobalt(III)-hydridokomplex gemäss

$$[Co^{II}(CN)_5]^{3-} + e + H_2O \rightarrow [Co^{III}(CN)_5H]^{3-} + OH^-$$

reduziert wird, reagieren die Reduktionsprodukte des Tetracyanokobalt(II)-Komplexes mit Protonen unter Wasserstoffabscheidung. Über die durch Kobalt-cyanokomplexe verursachte katalytische Wasserstoffabscheidung soll an anderer Stelle berichtet werden[14].

ZUSAMMENFASSUNG

Es wird über die katalytische Wasserstoffabscheidung durch Carboxyalkylphosphine, *o*-Phosphinobenzoesäure, Phosphorwasserstoff und prim. sowie sek. Phosphine berichtet. Die katalytischen Wellen wachsen mit steigender Kobaltionenkonzentration, was nicht nur einen Ultramikronachweis der Kobaltionen, sondern auch eine qualitative und quantitative Bestimmung des Phosphorwasserstoffs ermöglicht. Die katalytische Aktivität koordinativ einzähliger P-Liganden beweist, dass für eine Wasserstoffabscheidung die bisher angenommene Voraussetzung einer Chelatkomplexbildung nicht generell zutrifft.

SUMMARY

Some details on the catalytic activity of carboxyalkylphosphines in acid buffer solutions are reported. The investigations on the effect of heavy-metal ions, as for instance cobalt(II)- and cobalt(III)-ions, on the catalytic waves were also extended to the compounds PH_3, H_2PR, HPR_2, PR_3. The results show that compounds with one functional group can also lower the hydrogen-overvoltage.

LITERATUR

1 H. MATSCHINER UND K. ISSLEIB, *Z. Anorg. Allgem. Chem.*, 354 (1967) 60.
2 K. ISSLEIB UND H. MATSCHINER, *Z. Anorg. Allgem. Chem.*, 240 (1965) 34.
3 M. VON STACKELBERG, W. HANS UND W. JENSCH, *Z. Elektrochem.*, 62 (1958) 839.
4 M. SHINAGAWA, H. NEZU, A. MUROMATSU UND B. SHIOTANI, *Z. Anal. Chem.*, 224 (1967) 226.
5 K. ISSLEIB, H. MATSCHINER UND M. HOPPE, *Z. Anorg. Allgem. Chem.*, im Druck.
6 P. KNOP, *Diplomarbeit*, Universität Halle, 1966.
7 K. ISSLEIB UND G. THOMAS, *Z. Anorg. Allgem. Chem.*, 330 (1964) 295.
8 A. CALUSARU UND J. KŮTA, *Abhandl. Deut. Akad. Wiss. Berlin (Kl. Med.)*, 4 (1966) 443.
9 R. KÜMMEL, *Dissertation*, Universität Halle, 1967.
10 A. CALUSARU UND J. KŮTA, *Collection Czech. Chem. Commun.*, 31 (1966) 814.
11 S. G. MAIRANOVSKII, *Katalytische und kinetische Wellen in der Polarographie*, Nauka, Moskau, 1966.
12 P. S. SHETTY UND A. FERNANDO, *J. Inorg. Nucl. Chem.*, 28 (1966) 2873.
13 H. MATSCHINER, *Dissertation*, Universität Halle, 1963.
14 A. A. VLČEK UND H. MATSCHINER, *Collection Czech. Chem. Commun.*, Publikation in Vorbereitung.

ELECTROANALYTICAL CHEMISTRY AND INTERFACIAL ELECTROCHEMISTRY
Elsevier Sequoia S.A., Lausanne – Printed in The Netherlands

VOLTAMMETRY OF THE AQUODIETHYLTIN(IV) CATION–POLYDIETHYLTIN(II) SYSTEM

MICHAEL D. MORRIS
Department of Chemistry, The Pennsylvania State University, University Park, Pa. 16802 (U.S.A.)
(Received August 14th, 1967)

The reduction of the aquodiethyltin(IV) cation at the dropping mercury electrode has been studied by several groups. RICCOBONI AND POPOFF[1] describe the essential features of the system: that the reaction is a reversible, two-electron change the stoichiometry of which corresponds to eqn. (1).

$$(C_2H_5)_2Sn^{2+} + 2\,e^- \rightarrow (1/n)\,[(C_2H_5)_2Sn]_n \qquad (1)$$

We have[2] investigated the effect of hydrolytic and complex formation equilibria on the polarographic system and have demonstrated that the polarographic method can be used to study the equilibrium properties of dialkyltin(IV) complexes. DEVAUD[3] has explained the effects of adsorption of the parent ions and the polymeric products on the morphology of the polarographic waves of the aquodiethyltin(IV) system. As all investigators have noted, these waves become increasingly distorted as the bulk concentration of the depolarizer is increased above about $1 \cdot 10^{-4}\,M$.

Although the electrochemistry of the parent ion has been thoroughly investigated, little work has been done on the electrochemistry of the reduced species. We have observed that greenish-yellow polymers are the ultimate products of coulometric reduction of the aquodiethyltin(IV) cation and its complexes, but we have not attempted to characterize these. NEUMANN AND PEDAIN[4] have shown that various linear and cyclic polymers of approximate composition, $[(C_2H_5)_2Sn]_n$, can be prepared chemically. The structure of the polymer or polymers obtained depends on the method of synthesis.

We have investigated the electrochemistry of the aquodiethyltin(IV)–polydiethyltin(II) system at a hanging mercury drop electrode. Linear potential sweep chronoamperometry has been employed to verify the diffusion-controlled nature of the reduction of aquodiethyltin(IV), and cyclic voltammetry has been employed to observe the electrochemical behavior of the electro-generated polydiethyltin(II) polymers.

EXPERIMENTAL

The polarograph and cell employed have been previously described[2]. A Hewlett-Packard 202A function generator was used in place of the conventional integrator scan input to obtain triangular waves for cyclic voltammetry. Current–potential curves were recorded on a Honeywell X–Y recorder or a Tektronix 514D oscilloscope, equipped with camera, as appropriate. The charge consumed during

the electrode process corresponding to a given peak, was estimated by planimeter integration of the pen tracing obtained with the X–Y recorder.

A micrometer-type hanging mercury drop electrode assembly (Metrohm, Ltd., Herisau, Switzerland) was used as the working electrode. The extruded drops had areas of $1.38 \pm 0.05 \times 10^{-2}$ cm^2.

Diethyltin dichloride (City Chemical Corp., mp.. 84°–85°) was used as received. Diethyltin oxide, $(C_2H_5)_2SnO$, was precipitated from aqueous solutions of diethyltin dichloride by neutralization with sodium hydroxide[5]. The oxide was collected, washed to remove chloride and dried at 115°. Known amounts of diethyltin oxide were dissolved in perchloric acid to give solutions of aquodiethyltin(IV) perchlorate.

All other reagents were of ACS reagent-grade. Distilled water was used to prepare all solutions.

LINEAR POTENTIAL SWEEP CHRONOAMPEROMETRY

Solutions of $1 \cdot 10^{-4}$ *F* aquodiethyltin(IV) cation in 0.1 *F* perchloric acid give a single peak ($E_p = -0.66$ V *vs.* SCE). The peak height is proportional to the square root of scan rate, confirming the diffusion-control well known from polarographic studies. At $2 \cdot 10^{-4}$ *F* and more concentrated, multiple waves appear. Such behaviour is typical of systems in which an insoluble film of reduction product is formed at the electrode surface[6]. At $1 \cdot 10^{-3}$ *F* aquodiethyltin(IV) cation, the height of the main wave is proportional to $V^{0.66}$, where V is the potential scan rate (V sec^{-1}). LAVIRON has shown[6] that the peak current should increase with the two-thirds power of the potential scan rate when the current is limited by coverage of the electrode with an insoluble film.

Thus, the results of linear potential sweep chronoamperometry confirm the well-established conclusions of classical polarographic studies of this system[1-3]: that the reduction is diffusion-controlled at low concentrations and limited by formation of a polymeric film at higher concentrations.

CYCLIC VOLTAMMETRY

A typical cyclic voltammogram of $1 \cdot 10^{-4}$ *F* aquodiethyltin(IV) in an acetic acid–sodium acetate buffer, pH = 4.5, is shown in Fig. 1. Similar curves are obtained in 0.1 *F* perchloric acid solution. Cyclic voltammetric data are summarized in Table 1.

Two cathodic peaks (1C and 2C in Fig. 1) are clearly distinguishable in this system. Two anodic peak systems, 1A and 2A, are present.

Peak 2C is the main cathodic peak and corresponds to the polarographic reduction wave of the aquodiethyltin(IV) cation to polymeric diethyltin(II). This peak is broken into two or three closely spaced peaks, clearly separated at higher concentrations, as observed in single voltage scans.

Peak 1C is actually an anodic current and is capacitative in nature. The data in Table 1 show that the quantity of electricity consumed during the scanning of this peak is relatively constant and does not vary systematically with scan rate. Because of the small charges involved, these measurements are highly imprecise.

Peak 1C is absent on the first scan of a cyclic voltammagram or on a single cathodic sweep. Thus, this peak corresponds to the absorption of material produced

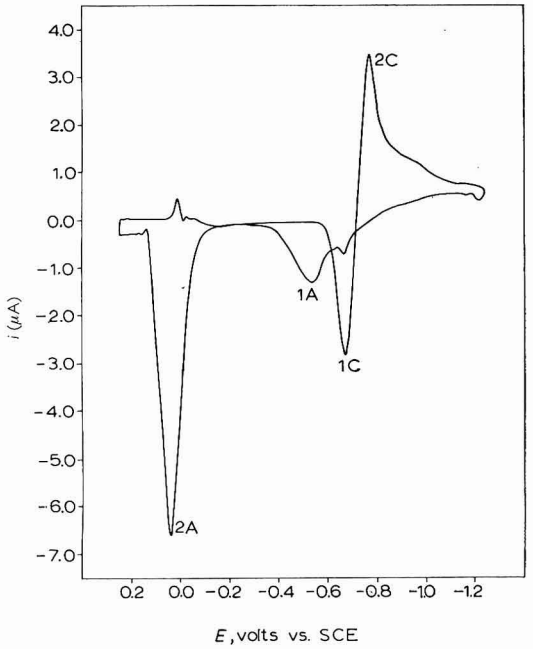

Fig. 1. Cyclic voltammagram of 1.01×10^{-4} F $(C_2H_5)_2Sn(H_2O)_4^{2+}$ in 0.05 F acetic acid, 0.05 F sodium acetate, 0.05 F sodium nitrate buffer (pH = 4.5). Scan rate, 0.24 V sec^{-1} (0.1 Hz).

TABLE 1

CYCLIC VOLTAMMETRY OF THE AQUODIETHYLTIN(IV)–POLYDIETHYLTIN(II) SYSTEM

V (V sec^{-1})	*Sweep frequency (Hz)*	Q_{1C} (μC)	Q_{2C} (μC)	Q_{1A} (μC)	Q_{2A} (μC)
A. $[(C_2H_5)_2Sn(H_2O)_4^{2+}] = 2.07 \times 10^{-4}$ F; 0.1 F $HClO_4$					
0.48	0.2	-0.12_7	0.60	−0.50	-0.37_4
0.24_1	0.1	−0.140	1.11	−0.93	−0.75
0.17_0	0.07	−0.193	1.42	−1.48	−1.18
0.12	0.05	-0.19_0	2.28	−1.71	−0.85
0.048	0.02	[a]	3.2_2	-3.3_3	−1.11
B. $[(C_2H_5)_2Sn(H_2O)_4^{2+}] = 5.18 \times 10^{-4}$ F; 0.1 F $HClO_4$					
0.52	0.2	−0.25	0.76	−0.59	−0.65
0.25_5	0.1	−0.25	2.13	−1.78	−1.41
0.183	0.07	−0.37	2.47	−2.36	−1.50
0.132	0.05	−0.34	2.70	−2.49	−2.11
C. $[(C_2H_5)_2Sn(H_2O)_4^{2+}] = 1.01 \times 10^{-3}$ F; 0.1 F $HClO_4$					
0.45	0.2	-0.28_0	1.52	−1.30	−1.38
0.23_0	0.1	−0.24	1.65	−1.71	−0.77
0.16_0	0.07	−0.21	2.55	−2.11	−0.55
D. $[(C_2H_5)_2Sn(H_2O)_4^{2+}] = 1.01 \times 10^{-4}$ F; $CH_3COOH = 0.05$ F; $KOOCCH_3 = 0.05$ F; $KNO_3 = 0.1$ F; pH = 4.5					
0.48	0.2	−0.263	0.46	−0.49	−1.06
0.24_0	0.1	−0.32	0.63	−0.56	−0.99
0.17_0	0.07	-0.22_2	0.75	−0.81	−0.89
0.121	0.05	[a]	0.87	−0.59	−0.62
0.048	0.02	[a]	1.29	−1.24	−1.09

[a] Current too small to allow reliable integration.

during the electrolysis. Peak 1C and peak 2A are linked and both disappear when the cycling rate is increased above about 10 Hz (26 V sec^{-1}). Peak 1C must be due to the adsorption of a product of the reaction occurring during peak 2A. This product is probably a partially oxidized, polymeric diethyltin, such as $^{+}Et_2Sn–(Et_2Sn)_n–Et_2Sn^{+}$

Anodic peak 1A corresponds to the re-oxidation of most of the diethyltin polymers formed. As the data in Table 1 show, the charge passed during peak 1A (Q_{1A}) accounts for 80–100% of the charge passed during the reduction of the aquodiethyltin(IV) species (Q_{2C}). At all sweep rates within the range of our instrumentation (0.01 Hz–1 kHz) this peak consisted of two or three components. Thus, some polymerization of diethyltin radicals generated by the cathodic process occurs at times as short as 1 msec. We have been unable to assign the different peaks to particular polymers and it is not certain whether appreciable concentrations of monomer exist even at times as short as 1 msec.

Because most of the diethyltin(II) polymers have been reoxidized during the course of peak 1A, only a small amount of diethyltin(II) remains on the electrode surface for oxidation at the potentials of peak 2A. However, the magnitude of the charge consumed during peak 2A is similar to that of the charge consumed during peak 1A or during the cathodic peak, 2C. Thus peak 2A cannot be a simple two-electron reoxidation, the reverse of eqn. (1), but must correspond to a multi-electron process. Peak 2A cannot be purely capacitative, although it may contain a capacitative component, since the charge passed during the course of the peak is not constant, but decreases with increasing potential scan rate. That this peak is absent at scan rates much above 26 V sec^{-1} (10 Hz), is evidence that it is due to the oxidation of a relatively highly polymerized diethyltin(II). One would expect that the difficulty of oxidation would increase with chain length and that the average degree of polymerization (*i.e.*, the amount of highly polymerized diethyltin(II)) would decrease with increasing sweep rate.

Reaction 2 is consistent with the experimental observations.

$$[(C_2H_5)_2Sn]_x–Sn(C_2H_5)_2 + 4\ H_2O \rightarrow 2\ CH_3COOH + Sn^{4+} + [(C_2H_5)_2Sn]_x + 10\ H^{+} + 14\ e^{-} \quad (2)$$

Because this reaction involves fourteen electrons, only a small amount of the polymer is necessary to give rise to a large anodic wave. Aquodiethyltin(IV) cation itself, although thermodynamically unstable, does not show an anodic wave at the dropping mercury electrode. However, a water-insoluble polymer, localized at the electrode surface, might be more easily oxidizable.

An attempt was made to isolate inorganic tin(IV) by carrying out continuous cyclic voltammetry on a slow (drop time, 10 sec) dropping mercury electrode for a period of about 100 h. A small amount of white solid, insoluble in the 0.1 *F* perchloric acid supporting electrolyte but soluble in hydrochloric acid, was obtained. Insufficient product was obtained to allow positive identification. Tin dioxide, SnO_2, is soluble in chloride-containing media, but not in non-complexing mineral acids[7]. Diethyltin(IV) oxide, the expected oxidation product of polymeric diethyltin(II)[4], is soluble in most mineral acids, including perchloric[5]. Thus, the presence of trace amounts of tin dioxide, the expected product of reaction (2), is indicated, but not confirmed.

The present study has shown that the electrochemistry of the aquodiethyltin(IV)–diethyltin(II) system is complicated by the presence at the electrode surface

of several polymers of unknown degrees of polymerization. Polydiethyltin(II) produced coulometrically at a mercury pool electrode over a period of several hours is not reoxidizable[2]. Thus, the polymers formed by the initial reduction of the aquodiethyltin(IV) cation must undergo slow rearrangements to give more stable products. This slow step may be cyclization. The initial steps of the polymerization are doubtless simple agglomerations to form linear polymers of varying length. These polymers would have an unpaired electron on each chain-terminating tin atom. In the absence of other radicals to combine with the polymeric diethyltin radicals, formation of cyclic polymers is the most likely route for the termination of the polymerization[2,4]. Since the stable cyclic polymers contain six to nine diethyltin(II) units, rearrangement of the various linear and cyclic polymers formed on the electrode surface to cyclic hexamers–nonamers, may be slow.

ACKNOWLEDGEMENT

This work was supported in part by National Science Foundation Grant GP-6164.

SUMMARY

Cyclic voltammetric studies of the aquodiethyltin(IV) reduction on mercury show that several polymers are formed. The monomeric diethyltin(II) diradical is very short-lived. Extensive polymerization occurs at times as short as 1 msec. Short-chain polymers are reoxidized to the parent species, but long-chain polymers are oxidized with some loss of organic groups.

REFERENCES

1 L. Riccoboni and P. Popoff, *Atti. Ist. Veneto Sci., Pt. II*, 107 (1949) 123; *C.A.*, 44 (1950) 6752a.
2 M. D. Morris, *Anal. Chem.*, 39 (1967) 476.
3 M. Devaud, *Compt. Rend.*, 263 (1966) 1269.
4 W. P. Neumann and J. Pedain, *Ann. Chem.*, 672 (1964) 34.
5 R. S. Tobias, I. Ogrins and B. A. Nevett, *Inorg. Chem.*, 1 (1962) 638.
6 E. Laviron, *J. Electroanal. Chem.*, 12 (1966) 516.
7 J. J. Lingane, *Analytical Chemistry of Selected Metallic Elements*, Reinhold Publishing Corp., New York, 1966.

ELECTROANALYTICAL CHEMISTRY AND INTERFACIAL ELECTROCHEMISTRY
Elsevier Sequoia S.A., Lausanne – Printed in The Netherlands

POLAROGRAPHIC REDUCTION OF CINNAMALDEHYDE; COMPARISON WITH 3-PHENYLPROPIONALDEHYDE AND PHENYLPROPARGYLALDEHYDE

D. BARNES AND P. ZUMAN*
Department of Chemistry, University of Birmingham (Great Britain)
(Received July 10th, 1967)

For the polarographic reduction of α,β-unsaturated ketones, it was established fairly early[1] that the first two-electron step corresponds to the hydrogenation of the C=C bond in contrast with the rather vague ideas proposed to explain the reduction of α,β-unsaturated aldehydes, especially cinnamaldehyde.

Cinnamaldehyde is reduced in a two-electron process, followed by a further reduction step at more negative potentials which was either not recorded or missed by previous investigators who concentrated their attention on the first two-electron process; this led them to make erroneous deductions. In the early papers[2,3], the waves of the first two-electron process were compared with those of benzaldehyde and because of the formal resemblance observed, the first two-electron process was attributed to the reduction of the carbonyl group.

In later studies[4], the waves of cinnamaldehyde were compared with those of phenylpropargylaldehyde. Because these authors[4] restricted their study to the lower pH-region and to the more positive potential range, they again concluded that the product of the two-electron reduction is an unsaturated alcohol.

Controlled-potential electrolysis at pH 7.75 in the potential range corresponding to the limiting current of the two-electron process is said[5] to yield cinnamic alcohol. Only SATŌ[6] considered the possibility of reduction in the side chain C=C bond, and this was based on circumstantial evidence.

Polarography has been used in the determination of cinnamaldehyde in a variety of mixtures[7–9], and it is therefore of interest to have a better understanding of the reduction sequence.

In connection with the study of reactions of nucleophilic reagents with unsaturated carbonyl compounds[10–12] (which is to be extended to the reactions of cinnamaldehyde) it was of importance to have a detailed knowledge of the course of the reduction of cinnamaldehyde. This type of information was also needed for an extension of our studies on the reduction of α,β-unsaturated carbonyl compounds[12–14].

* On leave from J. Heyrovský Institute of Polarography, Czechoslovak Academy of Sciences, Prague.

EXPERIMENTAL

Apparatus

The polarographic curves were recorded on a Cambridge pen-recording polarograph. A Kalousek vessel with a separated calomel electrode (SCE) was used: The capillary used had, at the potential of the SCE, an outflow velocity $m=2.96$ mg sec^{-1} and drop-time $t_1=3.1$ sec for a mercury pressure, $h=60$ cm. The pH of the buffer solutions were measured using a Pye Dynacap pH-meter with a general purpose glass electrode.

Controlled-potential electrolysis using a mercury dropping electrode was carried out as recommended by MANOUŠEK[15], using the potentiostatted three-electrode system of a Beckman Electroscan 30 instrument.

Ultraviolet measurements were made using a Unicam S.P. 800, the electrolysis product being diluted to produce approximately $5\cdot10^{-5}$ M solutions.

Gas-liquid chromatography (G.L.C.) was carried out as described previously[16], using a polyethyleneglycol adipate column at 180° and a flow rate of 10 ml sec^{-1} using the Pye 104 chromatograph with a flame ionization detector.

Solutions

All buffer solutions were prepared from AnalaR chemicals.

Organic compounds were redistilled under reduced pressure and then used for preparing stock 0.01 M solutions in spectroscopic ethanol.

Techniques

9.8 ml of the appropriate buffer were mixed with 0.2 ml of the 0.01 M stock solution; the solutions were de-aerated and the polarographic curves recorded and then checked to determine whether the curves changed with time. Most of the experiments were carried out in buffers containing 2% ethanol in the final solutions. When it was necessary to avoid adsorption waves, curves were recorded in buffer solutions containing 25% ethanol.

For controlled-potential electrolysis, 10^{-3} M solutions were prepared in the appropriate buffer so that the final solution contained 5% ethanol. Usually, 2.5 ml of this solution were electrolysed to 60–70% completion during 8–12 h. For the electrolysis in alkaline media, 0.5 ml were electrolysed at 0° during 4 h.

The numbers of electrons transferred were estimated by comparison with the known two-electron wave of benzophenone, and were determined coulometrically from the decrease of limiting current during the electrolysis, using a dropping mercury electrode in a small volume which was stirred by the falling of the drops.

RESULTS AND DISCUSSION

The reduction of cinnamaldehyde in aqueous solutions containing a small amount of ethanol, proceeds principally in two steps (Figs. 1 and 2). The first step, i_I, is a two-electron reduction and is followed by a further reduction step, i_{II}.

In the elucidation of the electrode process, the nature of the more negative wave, i_{II}, is of primary importance. It has been shown that the half-wave potential of wave i_{II}, its shift with pH and the pH-dependence of its height, are identical with

those observed for 3-phenylpropionaldehyde. Additional proof was obtained after controlled-potential electrolysis at the limiting current of wave i_I, using a normal dropping mercury electrode as the working electrode[15]. The u.v. spectra and G.L.C. retention times[16] of the product were identical with those of 3-phenylpropionaldehyde. Submicro-titration of the electrolysed solution[16] with bromine monochloride indicated no C=C bond in the product. Finally, a solution of the electrolysis product was studied polarographically at various pH-values in the presence of lithium ions.

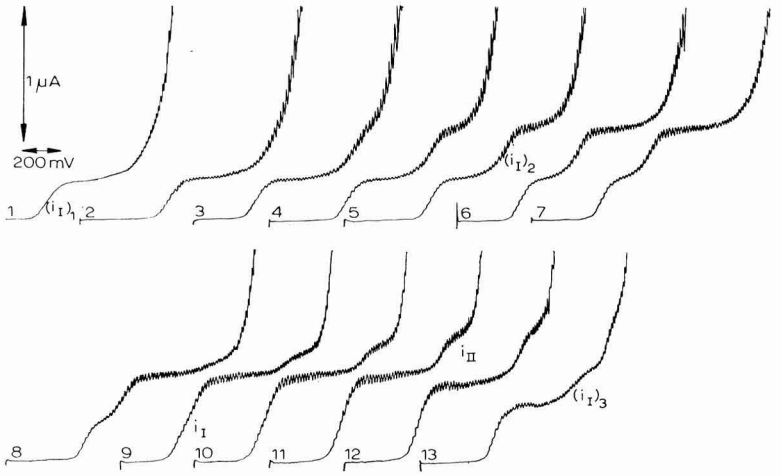

Fig. 1. Dependence of reduction waves of cinnamaldehyde on pH; $2 \cdot 10^{-4}$ *M* cinnamaldehyde in Britton-Robinson buffers containing 25% ethanol. pH-values: (1), 2.3; (2), 2.7; (3), 3.55; (4), 4.6; (5), 5.3; (6), 6.5; (7), 7.0; (8), 7.7; (9), 8.85; (10), 9.5; (11), 9.9; (12), 10.4; (13), 11.8. Curves starting at: (1), −0.4; (2), −0.2; (3–5), −0.4; (6–8), −0.6; (9–13), −0.8 V SCE.

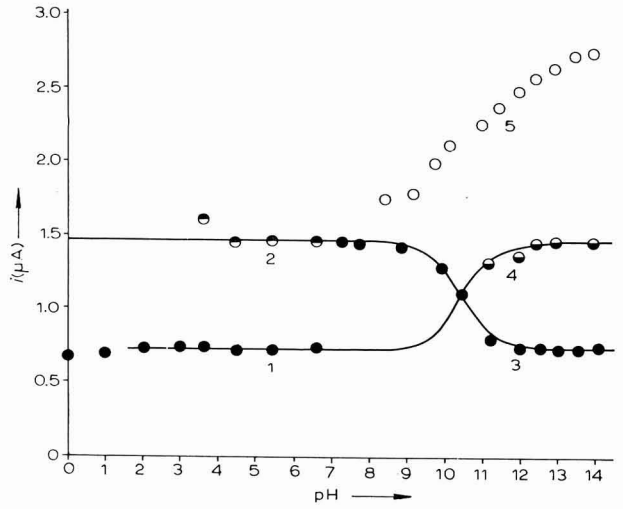

Fig. 2. Dependence of limiting current on pH; $2 \cdot 10^{-4}$ *M* cinnamaldehyde in Britton-Robinson buffers (pH 2–12), sulphuric acid (pH 0–2) and lithium hydroxide (pH 12–14), containing 2% ethanol. (1, ●), wave $(i_I)_1$; (2, ◓), wave $(i_I)_2$; (3, ●), wave i_I; (4, ◒), wave $(i_I)_3$; (5, ○), wave i_{II}.

Over a wide pH-range, the waves obtained for the product had half-wave potentials identical with 3-phenylpropionaldehyde and showed a similar dependence of wave height on pH.

The waves of 3-phenylpropionaldehyde increase with increasing pH, until at pH > 12, they reach a limiting value* corresponding to a two-electron process. The exponent, p, of the dependence of the instantaneous current on time ($i \sim t^p$) increases with decreasing pH. Thus, the wave which at pH 12 is diffusion-controlled, at lower pH-values is partly governed by the rate of a chemical reaction. In the rising part of the current–pH dependence, the current depends on buffer type and concentration, as with formaldehyde[17]. It is assumed that the chemical reaction that precedes the electrode process proper is a general base-catalysed dehydration of the methylene glycol form of 3-phenylpropionaldehyde.

$$RCHO + H_2O \rightleftharpoons RCH(OH)_2$$

The essential difference, compared with formaldehyde, is the position of the hydration–dehydration equilibria which with 3-phenylpropionaldehyde is shifted towards the non-hydrated form. The sensitivity to bases other than hydroxyl ions is considerably smaller for 3-phenylpropionaldehyde than for formaldehyde.

The half-wave potentials of the 3-phenylpropionaldehyde wave depend on the nature and concentration of the cations present in the solution. For a given concentration, lithium and caesium ions cause the greatest shifts toward more positive potentials, anions having little or no effect. Apparently, two antagonistic effects govern the effect of cations on the half-wave potential**.

Confirmation of the course of the reduction of cinnamaldehyde is given by a comparison of its waves with those of phenylpropargylaldehyde (Fig. 3). Under suitable conditions, phenylpropargylaldehyde is reduced at pH 9.3 in two two-electron steps, followed by a wave of 3-phenylpropionaldehyde. The second wave has a half-wave potential identical with that of cinnamaldehyde. Hence, under these conditions, where phenylpropargylaldehyde is reduced in the unprotonated form, the reduction follows the sequence $-C\equiv C-$, $>C=C<$, CHO according to scheme (1–3)

$$C_6H_5C\equiv CCHO + 2\,e^- + 2\,H^+ \rightarrow C_6H_5CH=CHCHO \quad (1)$$

$$C_6H_5CH=CHCHO + 2\,e^- + 2\,H^+ \rightarrow C_6H_5CH_2CH_2CHO \quad (2)$$

$$C_6H_5CH_2CH_2CHO + 2\,e^- + 2\,H^+ \rightarrow C_6H_5CH_2CH_2CH_2OH \quad (3)$$

At lower pH-values, the reduction of phenylpropargylaldehyde follows a more complex pattern which will be discussed elsewhere.

---

* No decrease in the current was observed up to pH 14, provided that in alkaline solutions the values are obtained either by extrapolation to zero-time or by working at 0° to exclude the effect of aldolisation. As $RCH(OH)_2$ for formaldehyde, and 3-phenylpropionaldehyde are acids of comparable strength, the decrease of current at pH > 13 observed for formaldehyde is probably caused by a phenomenon other than the proposed[17] position of the acid–base equilibria.

** Both the change in the value of the capacity current in d.c. polarography, and the tensammetric peaks in a.c. polarography indicate a strong adsorption at a potential of −0.2 V and desorption at −1.4 V; the desorption therefore occurs at potentials more positive than that of the reduction process[18].

Behaviour in acid media

The first two-electron wave, i_I, of cinnamaldehyde at pH < 8 is split into two one-electron steps, $(i_I)_1$ and $(i_I)_2$. The coalescence of the one-electron waves $(i_I)_1$ and $(i_I)_2$, with increasing pH, is due to the shifting of the half-wave potential of wave $(i_I)_1$ to more negative potentials, while wave $(i_I)_2$ is practically pH-independent (Fig. 4). In agreement with previous deductions[2-4] and the results of controlled-

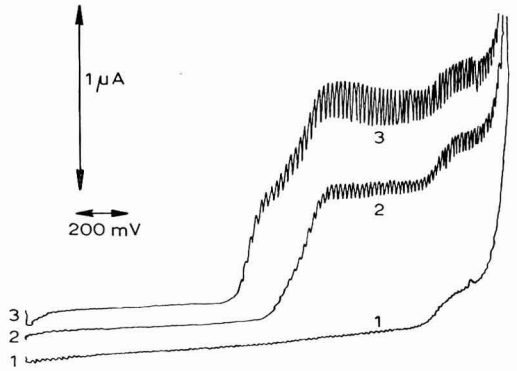

Fig. 3. Comparison of the reduction waves of unsaturated and saturated aldehydes; $2 \cdot 10^{-4}$ *M* aldehyde in borate buffer pH 9.2. (1), 3-Phenylpropionaldehyde; (2), cinnamaldehyde; (3), phenylpropargylaldehyde. Curves starting at 0.0 V SCE.

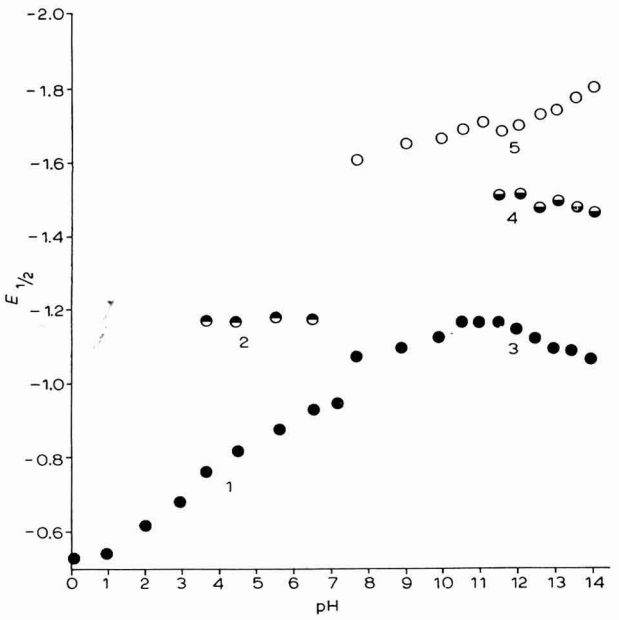

Fig. 4. Effect of pH on half-wave potentials for cinnamaldehyde; $2 \cdot 10^{-4}$ *M* cinnamaldehyde in Britton-Robinson buffers (pH 2–12), sulphuric acid (pH 0–2) and lithium hydroxide (pH 12–14), containing 2% ethanol. (1, ●), wave $(i_I)_1$; (2, ◓), wave $(i_I)_2$; (3, ●), wave i_I; (4, ◒), wave $(i_I)_3$; (5, ○), wave (i_{II}).

potential electrolysis[3], the predominating product in the first wave was proved to be a dimer.

In acid media, scheme (4)–(10) can therefore be suggested for the polarographic reduction of cinnamaldehyde:

$$C_6H_5CH{=}CHCHO + H^+ \rightleftharpoons C_6H_5\underbrace{CH{=}CHCHO}_{H^{(+)}} \quad (4)$$

$$C_6H_5\underbrace{CH{=}CHCHO}_{H^{(+)}} + e^- \overset{(i_I)_1}{\rightleftharpoons} C_6H_5\underbrace{\overset{\cdot}{C}H{=}CHCHO}_{H^{(+)}} \quad (5)$$

$$2\ C_6H_5\underbrace{\overset{\cdot}{C}H{=}CHCHO}_{H^{(+)}} \longrightarrow \text{dimer} \quad (6)$$

$$C_6H_5\underbrace{\overset{\cdot}{C}H{=}CHCHO}_{H^{(+)}} + e^- \xrightarrow{(i_I)_2} C_6H_5\overset{(-)}{C}H_2CHCHO \quad (7)$$

$$C_6H_5\overset{(-)}{C}H_2CHCHO + H_2O \rightleftharpoons C_6H_5CH_2CH_2CHO + OH^- \quad (8)$$

$$C_6H_5CH_2CH_2CHO + H_2O \rightleftharpoons C_6H_5CH_2CH_2CH(OH)_2 \quad (9)$$

$$C_6H_5CH_2CH_2CHO + 2\ e^- + 2\ H^+ \xrightarrow{i_{II}} C_6H_5CH_2CH_2CH_2OH \quad (10)$$

Behaviour in alkaline media

In alkaline media*, wave i_I decreases with increasing pH in the form of a dissociation curve with pK' 10.5, until it reaches a height corresponding to a one-electron transfer. Simultaneously, at more negative potentials, another wave appears, $(i_I)_3$; the sum of these two waves remains sensibly constant. This behaviour formally resembles that of benzaldehyde, but does not correspond to a change in mechanism. Even at pH > 12, when two one-electron waves, i_I and $(i_I)_3$, are observed, the height and half-wave potential of wave i_{II} corresponds to the reduction of 3-phenylpropionaldehyde. Moreover, controlled-potential electrolysis on the two-electron limiting current of $(i_I)_3$ produced a product similar to 3-phenylpropionaldehyde regarding u.v. spectra, G.L.C. retention time, and polarographic behaviour.

In alkaline media, at pH-values greater than about 9, where the half-wave potentials are practically pH-independent (Fig. 4), the following scheme, (11)–(15), can therefore be proposed:

$$C_6H_5CH{=}CHCHO + e^- \overset{i_I}{\rightleftharpoons} C_6H_5\underbrace{CH{=}CHCHO}_{(-)} \quad (11)$$

$$C_6H_5\underbrace{CH{=}CHCHO}_{(-)} + H^+ \rightleftharpoons C_6H_5\underbrace{\overset{\cdot}{C}H{=}CHCHO}_{H^{(+)}} \quad (12)$$

* Values at pH > 12 were extrapolated to zero-time to eliminate the effect of hydration of the double bond[12].

$$\underbrace{\overbrace{C_6H_5\dot{C}H=CHCHO}}_{H^{(+)}} + e^- \xrightarrow{i_I} \overset{(-)}{C_6H_5CH_2\dot{C}HCHO} \qquad (13)$$

$$\overset{(-)}{C_6H_5CH_2\dot{C}HCHO} + H_2O \rightleftharpoons C_6H_5CH_2CH_2CHO + OH^- \qquad (14)$$

$$C_6H_5CH_2CH_2CHO + H_2O \rightleftharpoons C_6H_5CH_2CH_2CH(OH)_2 \qquad (15)$$

$$C_6H_5CH_2CH_2CHO + 2\,e^- + 2\,H^+ \xrightarrow{i_{II}} C_6H_5CH_2CH_2CH_2OH \qquad (16)$$

$$\underbrace{C_6H_5CH=CHCHO}_{(-)} + e^- \xrightarrow{(i_I)_3} \underbrace{C_6H_5CHCHCHO}_{2^{(-)}} \qquad (17)$$

$$\underbrace{C_6H_5CH\text{–}CHCHO}_{2^{(-)}} + 2\,H_2O \rightleftharpoons C_6H_5CH_2CH_2CHO + 2\,OH^- \qquad (18)$$

The half-wave potential of process (13) is either not too different from that of process (11) or is more positive than that of process (11); hence only one two-electron wave (i_I) is observed at pH-values where reaction (12) is fast enough to transfer most of the radical anion $\underbrace{C_6H_5CH=CHCHO}_{(-)}$ into the radical $\underbrace{\overbrace{C_6H_5\dot{C}H=\dot{C}HCHO}}_{H^{(+)}}$.

With increasing pH, the rate of reaction (12) is decreased and the height of wave i_I decreases. The radical anion that was not transformed into the radical, undergoes reduction in wave $(i_I)_3$ according to eqn. (17), followed by protonation (18). The reduction of 3-phenylpropionaldehyde given by (16) is affected by hydration (15).

Hence, in the polarographic reduction of cinnamaldehyde, the product of the two-electron reduction over the entire pH-range, is the saturated aldehyde, even when the product of the dimerisation following the one-electron process may be a pinacol. In the reduction of the system C=C–CO, the carbon–carbon double bond is hydrogenated first, whether the system concerned is an aldehyde or a ketone. The separation of two one-electron waves in acid or alkali cannot be taken as proof of the reduction of a carbonyl group.

ACKNOWLEDGEMENTS

We thank Professor R. BELCHER for his interest and support.

One of us (P.Z.) expresses his thanks to the Scientific Research Council and the other (D.B.) to J. Lyons and Co. Ltd., for the grants which made this study possible.

We would both like to thank Dr. W. BOARDMAN of Hatfield College of Technology for his measurements of the *i–t* curves of 3-phenylpropionaldehyde, Dr. P. C.

UDEN for his advice on the G.L.C. experiments, Dr. P. L. COE and his colleagues for the use of the G.L.C. apparatus, Esso Research for the loan of the Cambridge Polarograph, and Beckman Instruments for the use of the Electroscan 30.

SUMMARY

Cinnamaldehyde is reduced at the dropping mercury electrode in a two-electron step which leads to the formation of 3-phenylpropionaldehyde. This has been proved by controlled-potential electrolysis and identification of the products using u.v. spectra, gas-liquid chromatography, submicro-methods, and electrochemical techniques. The reduction wave of 3-phenylpropionaldehyde occurs at potentials where the compound is desorbed and the wave height is limited by an antecedent dehydration reaction. In acid media, the reduction of the protonated form of cinnamaldehyde occurs in two one-electron steps. Dimer is formed at the potentials of the first step. At sufficiently high pH-values, the unprotonated form of cinnamaldehyde is reduced in a one-electron step to a radical anion that dimerizes and reduces only at more negative potentials. At pH 9.3, the carbon–carbon triple bond in phenylpropargylaldehyde is first reduced to a double bond; in subsequent steps the C=C bond and then the CHO group are reduced. Even in α,β-unsaturated aldehydes the hydrogenation of the double bond takes place prior to the reduction of the carbonyl group.

NOTE ADDED IN PROOF

After the manuscript of this paper was submitted, the paper by G. CAPOBIANCO, E. VIANELLO AND G. GIACOMETTI (*Gazz. Chim. Ital.*, 97 (1967) 243) on the reduction of phenylpropargylaldehyde came to our attention. We agree with the views on the triple bond reduction, a difference exists in the interpretation of the cinnamaldehyde reduction.

REFERENCES

1 R. PASTERNAK, *Helv. Chim. Acta*, 31 (1948) 753.
2 G. SEMERANO AND A. CHISINI, *Gazz. Chim. Ital.*, 66 (1936) 510.
3 A. KORSHUNOV, Z. B. KUZNETSOVA, L. N. SAZANOVA AND A. S. KIRILLOVA, *Zavodsk. Lab.*, 16 (1950) 144.
4 CH. PRÉVOST, P. SOUCHAY AND J. CHAUVELIER, *Bull. Soc. Chim. France*, 18 (1951) 715.
5 S. ONO, *Nippon Kagaku Zasshi*, 76 (1955) 631.
6 H. SATO, *Eisei Shikenjo Hokoku*, 77 (1959) 51.
7 M. SHIKATA AND K. SHOJI, *Mem. Coll. Agr. Kyoto Univ.*, 4 (1927) 75.
8 B. BITTER, O. HANČ AND F. ŠANTAVÝ, *Chem. Listy*, 43 (1949) 137.
9 G. DUŠINSKÝ, M. TYLLOVÁ AND Z. GRUNTOVÁ, *Česk. Farm.*, 6 (1957) 87.
10 V. HORÁK AND P. ZUMAN, *Collection Czech. Chem. Commun.*, 26 (1961) 173.
11 I. ŠESTÁKOVÁ, V. HORÁK AND P. ZUMAN, *Collection Czech. Chem. Commun.*, 31 (1966) 3889.
12 P. ČÁRSKY, P. ZUMAN AND V. HORÁK, *Collection Czech. Chem. Commun.*, 30 (1965) 4316.
13 P. ZUMAN AND J. MICHL, *Nature*, 192 (1961) 655.
14 A. RYVOLOVÁ-KEJHAROVÁ, unpublished results.
15 O. MANOUŠEK, unpublished results.
16 D. BARNES, R. BELCHER AND P. ZUMAN, *Talanta*, 14 (1967) 1197.
17 R. BRDIČKA AND K. VESELÝ, *Collection Czech. Chem. Commun.*, 12 (1947) 313.
18 P. ZUMAN AND D. BARNES, *Nature*, 215 (1967) 1269.

ELECTROANALYTICAL CHEMISTRY AND INTERFACIAL ELECTROCHEMISTRY
Elsevier Sequoia S.A., Lausanne – Printed in The Netherlands

SHORT COMMUNICATION

Stabilisation of the pentavalent state of uranium by hydrazine

The kinetics of the disproportionation of U(V) in the presence of different complexing agents has been the subject of a number of papers[1-5]. In all these investigations, the rate of disproportionation has been found to increase in the presence of complexing reagents, which complex either the U(VI) or the U(IV) ion and hence shift the equilibrium to the right in the following equation.

$$2\ U(V) \rightarrow U(VI) + U(IV)$$

Since reducing agents have been reported to stabilise the lower unstable valence states[6] *e.g.*, the Cr(II)–hydrazine complex[7], it was of interest to study the disproportionation rate of U(V) in the presence of hydrazine.

Polarography was used for this study.

Experimental

The polarograms were taken on a Du Bellay polarograph.

Reagents

Uranyl perchlorate (0.1 *M*). 2.8075 g of high purity U_3O_8 was dissolved in 10 ml of 1:1 nitric acid; the solution was fumed twice with 5 ml of perchloric acid and then diluted to 100 ml with water.

Hydrazine hydrate. BDH Laboratory Reagent.

All other reagents used were of AnalaR grade.

Pentavalent U(V) was prepared by electrolytic reduction of uranyl perchlorate at a controlled potential of − 0.50 V *vs.* SCE at pH 3.0. Different quantities of oxygen-free perchloric acid were added to aliquots of the electrolysed solution to give solutions of different H^+ ion concentration; the anodic wave heights were measured at intervals of 60 sec.

In another set of experiments, hydrazine hydrate was added prior to electrolytic reduction and the measurements were then carried out as above.

Since the disproportionation of U(V) is a bimolecular reaction, a plot of U(V) concentration (which can be computed directly from the anodic wave heights) against time gives the rate of disproportionation at the particular H^+ concentration. The rate constant can be obtained by dividing the rate obtained, by the corresponding H^+ concentrations. In the pH-range 1.0–2.0, the rate constant decreases from 112 $(moles/l)^{-2}\ sec^{-1}$ to 59 $(moles/l)^{-2}\ sec^{-1}$ on the addition of 0.25 *M* hydrazine, the ionic strength being 0.5 *M*.

The effect of ionic strength on the disproportionation reaction was studied and rate constant calculated for various ionic strenghts at a hydrazine concentration of 0.25 *M*, and pH 1.50. The rate constant decreases from 65 $(moles/l)^{-2}\ sec^{-1}$ to 41 $(moles/l)^{-2}\ sec^{-1}$ at 0.20 *M*, from 235 $(moles/l)^{-2}\ sec^{-1}$ to 136 $(moles/l)^{-2}\ sec^{-1}$ at 1.0 *M* and from 341 $(moles/l)^{-2}\ sec^{-1}$ to 187 $(moles/l)^{-2}\ sec^{-1}$ to 187 $(moles/l)^{-2}\ sec^{-1}$ at 2.0 *M* ionic strengths. The concentration of hydrazine was varied and the half-wave poten-

tials were measured in order to see whether there was any complexing of U(V) with hydrazine. The half-wave potential shifts from −0.175 V to −0.160 V *vs.* SCE when the hydrazine concentration is varied from 0 to 1.0 *M*.

Results and discussion

The perceptible decrease in the disporportionation rate in the presence of hydrazine shows that hydrazine stabilises the pentavalent state of uranium. The shift in the half-wave potential to the positive side from −0.175 V to −0.160 V on varying the concentration of hydrazine indicates a definite though weak complexing of U(V) by hydrazine.

The rate constants are considerably lower when hydrazine is present, at various ionic strengths, although there is an increase in the rate with and without hydrazine with increase in ionic strength.

It is clearly indicated that the pentavalent state of uranium can be stabilized by the use of reducing agents such as hydrazine.

Bhabha Atomic Research Centre,
Analytical Division,
Trombay, Bombay 74 (India)

V. T. ATHAVALE
C. S. P. IYER

1 D. M. H. KERN AND E. F. ORLEMANN, *J. Am. Chem. Soc.*, 71 (1949) 2102.
2 H. G. HEAL AND J. G. N. THOMAS, *Trans. Faraday Soc.*, 45 (1949) 11.
3 J. KORYTA AND J. KOUTECKÝ, *Collection Czech. Chem. Commun.*, 20 (1955) 423.
4 D. J. MCEWEN AND T. DE VRIES, *Can. J. Chem.*, 35 (1957) 1225.
5 H. IMAI, *Bull. Chem. Soc. Japan*, 30 (1957) 873.
6 J. C. BAILAR, *Chemistry of Co-ordination Compounds*, Reinhold, New York, 1956.
7 W. TRAUBE AND W. PASSARGE, *Ber.*, 46 (1913) 1505.

Received April 10th, 1967; in revised form, September 28th, 1967

J. Electroanal. Chem., 16 (1968) 583–584

CALENDAR OF FUTURE SCIENTIFIC MEETINGS

Date	*Place*	*Subject*	*Secretary*
9–13 September 1968	Barcelona, Spain	5th International Conference on Surface Active Substances	Secretaria del V. Congreso International de la Detergencia; Apartado 9.180, Barcelona, Spain.

JOURNAL OF ELECTROANALYTICAL CHEMISTRY AND INTERFACIAL ELECTROCHEMISTRY, VOL. 16 (1968)

AUTHOR INDEX

JOURNAL OF ELECTROANALYTICAL CHEMISTRY AND INTERFACIAL ELECTROCHEMISTRY, VOL. 16 (1968)

SUBJECT INDEX

Vol. 16 No. 4 JOURNAL OF ELECTROANALYTICAL CHEMISTRY AND INTERFACIAL ELECTROCHEMISTRY APRIL 1968

CONTENTS

COPYRIGHT © 1968 BY ELSEVIER SEQUOIA S.A., LAUSANNE

PRINTED IN THE NETHERLANDS

Elsevier Titles in Chemistry

INORGANIC CHEMISTRY

A Guide to Advanced Study
Third, completely revised edition

by **R. B. Heslop** and **P. L. Robinson**

6×9″, viii+774 pages, 155 tables, 400 illus., 227 lit. ref., 1967, Dfl. 32.50, 65s., US$11.00

Contents: Modern inorganic chemistry. The atomic nucleus: genesis of the elements. Radiochemistry. Electronic structures of atoms. The periodic table. Valency; nature and classification of chemical bonding. Structure and shape of molecules. Bonding and structure in compounds of non-transition elements. Bonding in transition-metal complexes. The solid state. Oxidation-reduction: redox reactions. Acids and bases. Hydrogen. The hydrides. The noble gases. The alkali metals. Beryllium, magnesium and the alkaline earth metals. Boron and aluminium. Gallium, indium and thallium. Carbon and silicon. Organometallic compounds. Germanium, tin and lead. Nitrogen and phosphorus. Arsenic, antimony and bismuth. Oxygen, sulphur, selenium, tellurium and polonium. The oxides. Peroxides and peroxo-compounds. The halogens. The halides and pseudohalides. The transition metals. Complex or co-ordination compounds and ions. Substitution reactions of metal complexes. The lanthanides, scandium and yttrium The actinides. Titanium, zirconium and hafnium. Vanadium, niobium and tantalum. Chromium, molybdenum and tungsten. Manganese, technetium and rhenium. Iron, cobalt and nickel. The platinum metals. Copper, silver and gold. Zinc, cadmium and mercury. Index.

INTRODUCTION TO THE ATOMIC NUCLEUS

Volume 3 in a collection of monographs on "*Topics in Inorganic and General Chemistry*" edited by P. L. Robinson

by **J. G. Cuninghame**

5½×8½, xi+220 pages, 3 tables, 58 illus., 170 lit. refs., 1964, Dfl. 15.00, 35s., US$4.75

Contents: Historical introduction. General definitions and properties. Nuclear forces. Stable nuclides. Radioactivity. Nuclear models. Nuclear reactions. Fission. Alpha-decay. Beta-decay. Gamma-emission. Interaction of particles and rays with matter. Index.

INTRODUCTION TO NUCLEAR CHEMISTRY

by **D. J. Carswell**

5½×8½″, ix+279 pages, 23 tables, 69 illus., 1967, Dfl. 32.50, 70s., US$11.00

Contents: The development of nuclear chemistry. Fundamental particles and nuclear structure. Nuclear reactions and radioactivity. Properties of nuclear radiations. The detection and measurement of nuclear radiation. Nuclear instrumentation. Radiation chemistry. Isotope measurement and separation methods. Charged particle accelerators, neutron sources, production and properties of the actinide elements. Uses of isotopes. Experimental nuclear chemistry. Index.

RADIOCHEMICAL SURVEY OF THE ELEMENTS

Principal Characteristics and Applications of the Elements and their Isotopes

by **M. Haïssinsky** and **J.-P. Adloff**

6×9″, ix+177 pages, 1965, Dfl. 32.50, 75s., US$12.00

Contents: Introduction. The elements in alphabetical order. Element 102. Element 104.

THE STRUCTURE OF INORGANIC RADICALS

An Application of Electron Spin Resonance to the Study of Molecular Structure

by **P. W. Atkins** and **M. C. R. Symons**

6×9″, x+280 pages, 57 tables, 74 illus., 357 lit. refs., 1967, Dfl. 60.00, £7.0.0, US$21.75

Contents: Introduction. An introduction to electron spin resonance. Formation and trapping of radicals. Trapped and solvated electrons. Atoms and monatomic ions. Diatomic radicals. Triatomic radicals. Tetra-atomic radicals. Penta-atomic radicals. Summary and conclusions.
Appendices: The language of group theory. The spin hamiltonian. Calculation of *g*-values. Determination of spin-density distribution and bond angles. Analysis of electron spin resonance spectra. Index.

Elsevier Publishing Company **Amsterdam London New York**